Reprogramming the Extracellular Matrix to Create a Proinflammatory Microenvironment

Flurin Caviezel

Lincoln College

University of Oxford



A thesis submitted for the degree of Doctor of Philosophy to the Department of Oncology, University of Oxford, Trinity Term 2023

Supervisors: Professor Len Seymour, Professor Kim Midwood

Per mes geniturs

E per quei che vus veis adina schau esser mei sco jeu sun

A statement addressing the impact of the COVID-19 pandemic on the progress of my thesis

I was unable to enter the laboratory from March 2020 until late August 2020, and until May 2021, we were only allowed to work for approximately 30% of the time. This has not only impacted on my experimental work, but also taken a mental toll. Additionally, the main delay was due to the lack of clinical samples provided in the time just after the pandemic, which is also one of the reasons why some graphs shown in this thesis contain lower numbers of patients than was initially hoped.

However, I was still able to conduct most experiments with the time extensions. I especially used the time to start writing the introduction of this thesis.

Declaration of Authentication

The material presented in this thesis was performed under the supervision of Professor Leonard Seymour, Department of Oncology, Medical Sciences Division, University of Oxford. This work is entirely my own and any contribution made by others has been acknowledged. The work submitted does not form part of another thesis in this or any other university.

Flurin Caviezel

September 2023

Abstract:

The extracellular matrix (ECM) is an often-overlooked component of cancer pathology, playing important roles in tumour immune suppression, survival and regrowth, but also offering unique opportunities for therapeutic intervention. Matrix-based immunosuppression is mediated by key players such as TGF-β, which is stored long-term on the matrix, and also directly by ECM components including glycosaminoglycans and collagen. Due to the longevity of the ECM, these immunosuppressive signals can persist even after the cancer cells have been eliminated, posing a potential seeding ground for re-lapsing tumours.

This thesis explores strategies to exploit the longevity of the ECM, by tethering therapeutic agents to it and effectively reversing its immunosuppressive effects. Self-tethering bispecific agents are explored that can agonise CD3 and elicit T cell-mediated, antigen-independent and local bystander cytotoxicity, eliminating neighbouring tumour cells and also tumour associated cells.

Initially, we explored the positive charge interactions used by many growth factor and cytokine motifs to bind to highly negatively charged glycosaminoglycans (GAGs). A 21 amino acid motif derived from PlGF-2 or a synthetically created polyarginine motif were fused to an anti-CD3 scFv and tested in *in vitro* and on *ex vivo* samples. GAG-targeting resulted in T cell activation and bystander cytotoxicity towards cancer cell lines, and led to an IFN-γ production of activated T cells in slices of freshly isolated human colorectal liver metastases.

Secondly, the ECM-mediated immune checkpoint LAIR-1 – collagen I axis was targeted utilising LAIR-2, which has high affinity binding to collagen I, fused to an anti-CD3 scFv (LAIR-2xaCD3). LAIR-2xaCD3 treatment also led to collagen-dependent T cell cytotoxicity towards neighbouring tumour cells and fibroblasts and was sufficiently durable to activate multiple T cells extended over several days. It also induces cytotoxicity in colorectal liver metastasis slices mediated by the endogenous T cell population.

To enable systemic delivery as well as tumour selectivity, the LAIR-2xaCD3 bispecific was encoded into an oncolytic adenovirus (EnAd) for *in situ* production. The bispecific armed oncolytic virus led to the induction of cytotoxicity and upregulation of key cytokines including IFN-γ, IL-17a and effector T cell markers, although in this setting the dependence on collagen was diminished.

In conclusion, the studies reported in this thesis illustrate an important therapeutic use of ECM and simultaneously show that, especially with in situ expression through oncolytic viruses, the ECM has potential as a durable reservoir of therapeutic agents.

Acknowledgements

First and foremost, I would like to thank Prof Len Seymour for his mentorship, guidance and kindness during my DPhil, and for giving the occasional motivational boost when things did not go as planned. Similarly, I'd also like to thank Prof Kerry Fisher for his uncountable insightful ideas and for all the helpful meetings with invaluable input. Thank you both!

A big thank you goes to Prof Kim Midwood, who helped me a lot during the pandemic and always offered her support and guidance.

However, none of the following would probably have happened if I it wasn't for Len's Angels! Thank you all for all the emotional support, laughter, motivational speeches, shared food and shared memories! Therefore, a big thank you to all the alumni Dr Arthur Dyer, Dr Richard Baugh, Dr Tzveta Prokovska, Dr Eleanor Scott, Dr Sally Frost, Dr Egon Jacobus and Dr Will Taverner! A special thank you goes to Dr Arthur Dyer, who was/is never too busy to help with science and who organised countless of the lab socials throughout all the years. You're incredible Arthur and thank you for all your help! To Dr Richard Baugh, thank you very much for sharing the experience of a DPhil with me, I am very lucky to have spent a big chunk of my DPhil time alongside such a great scientist.

I'd also like to thank all the Post Docs in the Seymour lab, Dr Hena Khalique, Dr Janet Lei, Dr Brian Lyons, Dr Sarah Larkin, Dr Ahmet Hazini and Dr Gulsah Albayrak and Gkentiana Zavalani.

Hena, I am unsure how exactly I can express enough thanks for everything you have done for me, for all your scientific input and for all your generosity! I could not have wished for a better supervisor in the lab, and I want to thank you for always being there for me.

And of course, I also want to thank to all the current students in the lab, Peter Wan, Mahnoor Nadeem, Emma Page, Kate Friesen, Fernando Jimenez-Gallardo, Henry Bridgen, Alex Stephens, Yuqian Ou, Sichen Liu, Constantinos Demetriou. You made every day in the last

stretch of my DPhil worth coming in to work, and made lab work (and eating) infinitely more fun. Thanks, Mahnoor, for all the Biryani and all the fun times we shared during my DPhil. Thank you, Emma, for your help with the virus work and all the (late night) shared skepastis and thank you Kate for helping with clinical samples and being THE entertainment. Thank you to Peter and Fernando for your inputs and hopefully a great collaboration in the future. I also want to thank Alex and Yuqian for the countless chats and moral support!

Additionally, I could not forget everyone who helped me to get clinical samples (Katy Gordon Quayle, Martin Pirkl and Prof Simon Buczacki), and Pachtyana Zyar (Pash) for the countless chats and all your help with facilities!

To everyone who shared my journey in Oxford and supported me during this time in one way or another, Arnau, Baptiste, Jan, Anna, Violaine, Heather, Ana, Amanda, Ludwig and many more, thank you!

And to Sarah, thank you very much for all your emotional support, the many delicious Thanks Givings and just for bringing your positive attitude in my life during this time!

I also want to thank my family and especially my grandparents and parents, Marzela and Angelo, for always believing in me and for supporting me along my entire journey. This thesis is dedicated to you, engraziel fetg per tut!

And finally, Marius, although we've lived apart for the past years, I could always count on your unwavering support and love. There are no words to describe how lucky I am to have you by my side and how much this has helped me throughout this time! Thank you for everything!

When everything goes wrong and all my gels are empty
The Westerns don't look fancy
No matter how hard I try
The only thing that grows is a bad contamination
My soul fills with frustration
When I tell my cells goodbye
Science won't break me
I love Len's Angels instead

Table of contents

A statement addressing the impact of the COVID-19 pandemic on the progress of my thesis III
Declaration of Authentication IV
Abstract: V
Acknowledgements VII
Table of Figures 6
List of tables 8
List of Abbreviations 9
1 Introduction 13
1.1 Cancer 13
1.2 Structure and importance of the ECM in physiology 14
1.2.1 The ECM in cancer 15
1.2.2 The effect of ECM on conventional cancer therapies 21
1.3 The interplay of the cancer ECM with the immune system and immunotherapy 23
1.3.1 Cancer-immunity cycle 23
1.3.2 Immune Checkpoints 25
1.3.3 Effector T cell therapies and Bispecific T cell Engagers (BiTEs) 27
1.4 ECM mediated immunosuppression 28
1.5 LAIR-1, an ECM-mediated immune checkpoint 31
1.5.1 LAIR 1 in physiology 32
1.5.2 LAIR-1 signalling 32
1.5.3 The ECM-mediated IC LAIR-1 in cancer 33
1.5.4 LAIR-2 as inhibitor of LAIR-1 34
1.5.5 Conventional and Immunotherapeutic targeting of the ECM 35
1.6 Oncolytic virotherapy 40
1.6.1 Design of oncolytic viruses 42
1.6.2 Arming oncolytic viruses 44
1.6.3 Adenoviruses 45
1.6.4 Oncolytic adenoviruses 48
1.7 Conclusions and hypothesis 50
2 Materials and methods 52
2.1 Tissue culture 52
2.1.1 Cell lines and maintenance 52
2.1.2 Transfections 53

2.1.3 Protein production in HEK293a 54
2.1.4 XTT viability assays 54
2.2 Cellular assays 55
2.2.1 xCELLigence 55
2.2.2 IncuCyte analysis of bispecific and viral cytotoxicity 55
2.3 Molecular biology 56
2.3.1 Cloning and Polymerase Chain Reaction (PCR) 56
2.3.2 Agarose Gels and Gel extraction 56
2.3.3 Colony PCR 57
2.3.4 Colony PCR reaction 58
2.3.5 HiFi Gibson assembly 58
2.3.6 HIFI Reaction 58
2.3.7 Bacterial transformation 58
2.3.8 Plasmid preparation 59
2.3.9 Sanger sequencing 59
2.3.10 Cell lysate and BCA 59
2.3.11 Western Blot 60
2.4 Immunological methods and staining 61
2.4.1 FLAG ELISA 61
2.4.2 Fow cytometry 62
2.4.3 IFN-γ ELISA 64
2.4.4 LegendPlex 64
2.4.5 General T cell activation assay 64
2.5 Virus cloning and virology 65
2.5.1 EnAd cloning and DNA 65
2.5.2 Clonal selection of EnAd 66
2.5.3 Titration of EnAd 66
2.5.4 Viruses used in this thesis 67
2.5.5 EnAd T cell activation assay on collagen I coated plates 67
2.6 Clinical samples 68
2.6.1 Human blood processing 68
2.6.2 Lymphocyte recovery and T cell isolation 69
2.6.3 Malignant Ascites fluid and cells 69
2.6.4 Primary human colorectal samples 69
2.6.5 Gentle MACS dissociation 70
2.6.6 Colorectal liver metastasis 70

2.6.7 Vibratome slicing of liver metastases.....71
2.6.8 Tumour slice and free protein treatment.....71
2.6.9 Tumour slice virus infection and imaging.....72
2.7 Imaging.....72
2.7.1 Microscopy.....72
2.7.2 Confocal microscopy.....72
2.7.3 Celigo.....72
2.8 Statistics.....73
2.9 Chapter specific methods.....73
2.9.1 Chapter 3.....73
2.9.2 Chapter 4.....74
2.9.3 Chapter 5.....75
2.9.4 Chapter 6.....76
3 Exploration of T cell-mediated and antigen-independent bystander killing upon anti-CD3 scFv activation.....77
3.1 Introduction.....77
3.2 Hypothesis.....80
3.3 Results.....81
3.3.1 Graphical abstract.....81
3.3.2 Bystander killing occurs upon specific as well as non-specific T cell activation.....81
3.3.3 Bystander killing is mainly mediated by CD8 T cells, however, CD4 T cells also contribute considerably when activated with a BiTE or Dynabeads.....84
3.3.4 The majority of bystander cytotoxicity occurs via cell-cell contact, with CD8 T cells possessing the ability to secrete mediators capable of inducing cell death as well.....86
3.4 Discussion.....88
4 Targeting extracellular glycosaminoglycans using positively charged bispecifics to elicit bystander cytotoxicity.....92
4.1 Introduction.....92
4.2 Hypothesis.....95
4.3 Results.....95
4.3.1 Graphical abstract.....95
4.3.2 Construct design and production in HEK293a cells.....95
4.3.3 Binding of the constructs to cell lines and ECM-components.....99
4.3.4 Polarginine and PlGF-2 bispecific mediated T cell activation and bystander cytotoxicity 102
4.3.5 Colorectal liver metastases slices show an increased IFN-γ production upon treatment with positively charged bispecifics.....104
4.4 Discussion.....106

5 Targeting collagen I to harness bystander cytotoxicity using a LAIR-2xanti-CD3 bispecific 110
5.1 Introduction: 110
5.2 Hypothesis 112
5.3 Results 113
5.3.1 Graphical abstract 113
5.3.2 LAIR-1 Expression on T cells and construct design 115
5.3.3 Preliminary results using LAIR-2xaCD3 show higher T cell activation compared to aCD3xLAIR-2 117
5.3.4 CD4 and CD8 T cells activation upon challenge with LAIR-2xaCD3 117
5.3.5 LAIR-2xaCD3 binds specifically and strongly to collagen I, however, not to fibronectin 118
5.3.6 LAIR-2xaCD3 activated T cells mediate bystander cytotoxicity 119
5.3.7 LAIR-2xaCD3 bound to collagen is durable in activating multiple generations of T cells 124
5.3.8 Exhausted T cells derived from human ascites fluid can be activated upon treatment with LAIR-2xaCD3 125
5.3.9 Tumour infiltrating T cells from primary human colorectal tumours can be activated with LAIR-2xaCD3. 128
5.3.10 Endogenous immune cells in slices from colorectal liver metastases are activated and mediate cytotoxicity upon treatment with LAIR-2xaCD3 129
5.4 Discussion 132
6 Targeted expression of LAIR-2xaCD3 bispecific through the oncolytic adenovirus Enadenotucirev (EnAd) 138
6.1 Introduction 138
6.2 Hypothesis 141
6.3 Results 141
6.3.1 Graphical abstract 141
6.3.2 Cloning, validation and titrating of EnAd encoding the LAIR-3xaCD3 bispecific agent 142
6.3.3 EnAd encoding LAIR-2xaCD3 activates T cells and mediates cytotoxicity 145
6.3.4 T cells can be robustly activated upon stimulation with EnAd encoding LAIR-2xaCD3 147
6.3.5 “Traffic light” EnAd can be used to study *in vivo* and *ex vivo* infection and replication 149
6.3.6 EnAd encoding LAIR-2xaCD3 bispecific potentially activates endogenous T cells in human biopsies and primes them for bystander killing 153
6.4 Discussion 155
7 Final discussion 161
7.1 CD4 and CD8 involvement in bystander cytotoxicity 161

7.2 Potentiation of bystander killing 162
7.3 Clinically relevant cancer model systems 164
7.4 Exploiting the ECM for a long-term anchoring of therapeutic 166
7.5 Harnessing bystander killing as novel approach 167
7.6 Future challenges 169
7.7 Future directions 171
7.8 Concluding remarks 172
Bibliography 173
Appendix 219
DNA sequences 219
Antibody list 223
Buffer list 224

Table of Figures

Figure 1.1: The extracellular matrix (ECM) in physiology and cancer. 16
Figure 1.2: The tumour immunity cycle. 24
Figure 1.3: Capacity of the ECM to locally sequester (immunosuppressive) mediators. 29
Figure 1.4: Intracellular signalling pathway of the ECM-mediated immune checkpoint LAIR-1.. 33
Figure 1.5: Principle of oncolytic viruses. 42
Figure 1.6: EnAd genome compared to the genome of Ad11p. 49
Figure 2.1: Isotype controls for T cell activation assays. 63
Figure 2.2: Gating strategy for T cell assays. 65
Figure 2.3: Gating strategy for bystander killing experiment. 74
Figure 3.1: Schematic depiction of the hypothesis and aims to assess bystander killing in the context of BiTEs and non-specific CD3/CD28 Dynabeads activation. 82
Figure 3.2: Dynabeads and EpCAM activated T cells show strong tendencies to exert bystander killing. A 83
Figure 3.3: Bystander killing is mostly mediated by CD8 T cells but also involves CD4 T cells. 85
Figure 3.4: Bystander killing is mostly mediated via cell-cell contact whereby CD8 T cells in high concentrations can kill via soluble mediators *in vitro*. 87
Figure 4.1: Positively charged bispecifics binding to the ECM and to CD3 on T cells can activate and prime T cells for bystander cytotoxicity. 96
Figure 4.2: Design and expression of the bispecifics in HEK293a cells. 97
Figure 4.3: Constructs are not cytotoxic after transfection of host cells even at day five post transfection. 97
Figure 4.4: Transfection efficiency in HEK293, Panc-1, DLD-1 and PSN-1 cells. 98
Figure 4.5: Binding of the bispecifics to different host cells after transfection. 100
Figure 4.6: ECM binding capability of the different constructs.. 101
Figure 4.7: Human PBMC T cell activation 16h post transfection. 102
Figure 4.8: T cells mediated bystander cytotoxicity upon activation with positively charged bispecifics. 103
Figure 4.9: Treatment of colorectal liver metastasis slices with the different positively charged bispecifics leads to IFN-γ production of endogenous T cells.. 105
Figure 5.1: Graphical abstract for Chapter 5. 113
Figure 5.2: Patient-derived T cells from various model systems express LAIR-1. 114
Figure 5.3: Design and expression of the different bispecifics and controls.. 115
Figure 5.4: Preliminary data showing LAIR-2xaCD3 bispecific induced more potent T cell activation compared to the other orientation. 116
Figure 5.5: CD4 and CD8 T cell are activated upon interaction with bispecific bound to collagen I. 118
Figure 5.6: LAIR-2 containing constructs bind to human collagen I, however, not to fibronectin. . 119
Figure 5.7: No difference in cytotoxic kinetics is seen when washing or not washing after challenge with the bispecific or control.. 120
Figure 5.8: Visualisation of T cell-mediated cytotoxicity towards DLD-1 cells. 120
Figure 5.9: T cells exert strong bystander cytotoxicity towards Panc-1 cells upon incubation with LAIR-2xaCD3 bispecific. 122
Figure 5.10: LAIR-2xaCD3 bispecific activated T cells exert bystander killing towards normal fibroblasts.. 123
Figure 5.11: LAIR-2xaCD3 bispecific bound to collagen I activates multiple generations of T cells. 124

Figure 5.12: Ascites derived T cells show an exhausted phenotype, displayed an upregulation of several immune checkpoints. 125
Figure 5.13: Ascites-derived T cells can be activated upon incubation with LAIR-2xaCD3 bispecific. 126
Figure 5.14: Exhausted ascites-derived T cells mediate collagen I dependent bystander killing of DLD-1 cells upon LAIR-2xaCD3 treatment. 127
Figure 5.15: Primary colorectal tumour T cells can be activated by LAIR-2xaCD3 bispecific bound to a collagen I coated plate. 128
Figure 5.16: LAIR-2xaCD3 bispecific induces T cell activation in colorectal liver metastases slices. 129
Figure 5.17: Endogenous T cells in colorectal liver metastasis slices are robustly activated and exert cytotoxicity upon activation with the LAIR-2xaCD3 bispecific. 130
Figure 6.1: Graphical abstract of the aims in chapter 6. 141
Figure 6.2: Validation and characterisation of parental EnAd, EnAd encoding LAIR-2 only, anti-CD3 scFv only and LAIR-2xaCD3 bispecific. 142
Figure 6.3: MOI comparison between A549, DLD-1, PSN1 and Panc-1 using a CMV-GFP EnAd 143
Figure 6.4: DLD-1 and Panc-1 killing potency of parental EnAd and EnAd encoding the different constructs. 145
Figure 6.5: Oncolytic adenovirus encoding LAIR-2xaCD3 activates T cells and mediates cytotoxicity, but shows less collagen-dependence. 146
Figure 6.6: LAIR-2xaCD3 expressing OV is able to induce several activation and cytotoxicity markers in CD4 and CD8 T cells upon infection of target cells. 147
Figure 6.7: T cell-dependent and collagen I dependent killing of Panc-1 cells upon LAIR-2xaCD3 EnAd infection can be seen. 148
Figure 6.8: Plaque formation using EnAd encoding an UnaG tagged E1A (early genes, infection) and an mCherry (late genes, major late promotor SA). 150
Figure 6.9: Colorectal liver metastases slices can be infected with EnAd and show upregulated IFN-γ production when infected with EnAd expressing LAIR-2xaCD3 bispecific. 152
Figure 6.10: Responders and poor-responder colorectal liver metastases slices show clear signs of endogenous T cell activation and cytotoxicity upon infection with LAIR-2xaCD3 expressing EnAd. 154

List of tables

Table 1.1: Table listing combination therapies of ECM-targeting agents and ICIs. 37
Table 1.2: Adenovirus serotypes 46
Table 2.1: Cell lines used in this thesis. 52
Table 2.2: Common tissue culture reagents. 53
Table 2.3: Transfection set-up. 54
Table 2.4: Colony PCR reaction 56
Table 2.5: Steps of a PCR. 56
Table 2.6: Colony PCR reaction. 57
Table 2.7: Colony PCR steps 57
Table 2.8: HiFi Reaction. 58
Table 2.9: Sanger sequencing reaction 59
Table 2.10: Viruses used for experiments. 67

List of Abbreviations

Ad – Adenovirus

Akt – Protein kinase B

ALL – Acute lymphoblastic lymphoma

AML – Acute myeloid lymphoma

ATP – Adenosine triphosphate

BiTE – Bispecific T cell engager

B7H3 – B7 homolog 3 protein

CAF – Cancer associated fibroblast

CAR – Coxackie adenovirus receptor

CAR T cell – Chimeric antigen receptor T cell

CD – Cluster of differentiation

cGMP – Current good manufacturing practice

CLL – Chronic lymphocytic lymphoma

CTL – Cytotoxic T lymphocyte

CTLA-4 – Cytotoxic T lymphocyte associated protein 4

CS – Chondroitin sulphate

DAMP – Danger associated molecular pattern

DC – Dendritic cell

DS – Dermatan sulphate

ECM – Extracellular matrix

EDB-FN – Extra domain B fibronectin

EGFR – Epidermal growth factor receptor

EnAd – Enadenotucirev

EpCAM – Epithelial cell adhesion molecule

FAK – Focal adhesion kinase

FAP – Fibroblast activation protein alpha

Fas/FasL – Fas and Fas ligand

FBG – Fibrinogen

FDA – Food and drug administration (USA)

FOXP-3 – Forkhead box P3

GAG – Glycosaminoglycan

GM-CSF – Granulocyte-macrophage colony-stimulating factor

HA – Hyaluronan

HLA – Human leukocyte antigen

HMEC – Human mammary epithelial cells

HMW-HA – High molecular weight hyaluronan

HPSE – Heparinase

HS – Heparan sulphate

HSV – Herpes simplex virus

HUVEC – Human umbilical vein endothelial cells

IT – Intratumoural

IV – Intravenous

IC – Immune checkpoint

ICAM 1 and 2 – Intracellular adhesion molecule 1

ICI – Immune checkpoint inhibitor

ICP – Infected cell protein

IFN-γ – Interferon gamma

IL – Interleukin

ITAM – Immunoreceptor tyrosine-based activation motif

ITIM – Immunoreceptor tyrosine-based inhibitory motif

ITSM – Immunoreceptor tyrosine-based switching motif

JNK – c-Jun N-terminal kinase

KS – Keratan sulphate

LAG-3 – Lymphocyte-activation gene 3

LAIR-1/2 – Leukocyte associated immunoglobulin like receptor 1

LAP – Latency-associated protein

LAT – Linker for activation of T cells

LMW-HA – Low molecular weight hyaluronan

LOX -Lysyl oxidase

LTBP – Latent TGF-beta binding protein

MAPK – Mitogen-activated protein kinase

MHC I and II – Major histocompatibility complex I and II

MICA/B – MHC class I polypeptide-related sequence A/B

MLP – Major late promotor

MMP – Matrix metalloproteinase

MMW-HA – Medium molecular weight hyaluronan

MOI – Multiplicity of infection

NK – Natural killer cell

NKG2D – Natural killer group 2 member D

NMIBC – Non-muscle invasive bladder cancer

NO – Nitric oxide

oHSV – Oncolytic herpes simplex virus

OV – Oncolytic virus

PAMP – Pathogen associated molecular pattern

PDAC – Pancreatic ductal adenocarcinoma

PD-1/PD-L1/2 – Programmed cell death (ligand) 1 and 2

PlGF-2 – Placental growth factor 2

PI3K – Phosphoinositide 3-kinase

PKC – Protein kinase C

PP2A – Protein phosphatase 2A

pTP – Precursor terminal protein

Rb – Retinoblastoma

ROS – Reactive oxygen species

scFv – Single chain variable fragment

SHP-1/2 – Src homology region 2 domain-containing phosphatase-1/2

SP-D – Surface protein D

TAA – Tumour associated antigen

TACS – Tumour associated collagen signature

TAM – Tumour associated macrophage

TCR – T cell receptor

TP – Terminal protein

TGF-β – Transforming growth factor beta

TIGIT – T cell immunoreceptor with Ig and ITIM domains

TIM-3 – T cell immunoglobulin and mucin domain-containing protein 3

TLR-4 – Toll like receptor 4

TME – Tumour microenvironment

TNFα – Tumour necrosis factor alpha

TPL – Tripartite leader

TRAIL - TNF-alpha-related apoptosis-inducing ligand

TTG II – Tissue transglutaminase II

T-Vec – Talimogene laherparepvec

VEGF – Vascular endothelial growth factor

vHMW-HA – Very high molecular weight hyaluronan

VISTA – V-domain immunoglobulin suppressor of T cell activation

ZAP-70 – Zeta-chain-associated protein kinase-70

1 Introduction

1.1 Cancer

Cancer is the term used for a myriad of different diseases which relate to uncontrollable cell division and invasion of different tissues. Essentially, this happens due to the accumulation of several mutations in the DNA, which can be induced, spontaneous or genetically inherited. Factors relating to lifestyle can also greatly influence and shape the development of cancer. Ultimately, mutations leading to dysregulation in important, well-controlled physiological mechanisms result in the development of a tumour. The establishment of cancer can take several years, if not decades, and therefore is statistically more likely to manifest in the elderly population. When looking at current cancer incidence statistics, there are approximately 375,000 new cases each year in the UK, with approximately 167,000 deaths (Cancer Research UK (CRUK) 2023; Sung et al. 2021).

Hannahan and Weinberg have laid out the key characteristics, or ‘hallmarks’, that commonly define cancer cells. These hallmarks originally included: Resisting cell death, sustaining proliferation, evading growth suppression, angiogenesis, immortalisation and metastasis and invasion (Hanahan and Weinberg 2000). Further hallmarks have since been identified such as genome instability, phenotypic plasticity, metabolic hijacking and immune evasion (Hanahan and Weinberg 2011).

Although 24.5 billion US $ have been invested in cancer research and development between 2016-2020 globally (public and philanthropic awards only), the overall mortality for most cancers has not fundamentally changed (Mcintosh et al. 2023). This modest success despite many proclaimed “scientific breakthroughs” may have many causes, including the possibility that factors important to tumour survival may have been overlooked.

One of these key factors could be the extracellular matrix (ECM), which has historically attracted little attention in cancer research. As will be elaborated in more detail in this first

chapter, the ECM is directly and indirectly involved in several of the cancer hallmarks mentioned above. Given this fundamental role of the ECM, the main focus of this thesis is to explore ECM targeting strategies in cancer that can potentially improve cancer therapies.

1.2 Structure and importance of the ECM in physiology

The extracellular matrix (ECM) is a network of a myriad of macromolecules, ranging from monomers to multimers, that can be assembled in fibrils and complex structures in order to form a scaffold for cells and tissues to be organised in. Broadly, the ECM is divided into the interstitial ECM surrounding cells, and the basement membrane separating cells of different origins (Hussell et al. 2018).

In physiology, the main three functions of the ECM are to (1) provide a mechanical scaffold for cells and tissues to form and adhere to (for example collagens), (2) control and organise various cellular processes such as proliferation, migration, polarity and differentiation (for example collagen, fibronectin and proteoglycans) and (3) form a reservoir for different mediators and growth factors (proteoglycans and glycosaminoglycans (GAGs), see **Figure 1.1**) (Yue 2014). Collagen is the most abundant protein in the ECM, with 46 different collagen chains forming 28 distinct known collagen types (Mecham 2012; Ricard-blum 2011), in which three alpha chains form a triple helical structure as base protein. Thereafter, collagens can be assembled into fibril-forming collagen (e.g, type I, II, III), basement network-forming (type IV), membrane bound collagens (type XVII) and others. The assembly of collagens happens for the most part in the extracellular space, whereby lysyl oxidases (LOX) play an important role in their crosslinking (Tenti and Vannucci 2020).

Another important component of the ECM is fibronectin (FN), a large multidomain glycoprotein, broadly consisting of three regions: The N-terminal domain, the central binding domain and the heparin-binding domain (To and Midwood 2011). Once secreted as dimers, assembly into fibrils is mediated by the binding of integrins to FN and a subsequent complex assembly process (Garrison, Schwarzbauer, and Weaver 2021; Singh, Carraher, and Schwarzenbauer

2010). When assembled, FN plays an important role in for the migration and attachment of different cells and is also crucial in the process of wound healing (To and Midwood 2011; Yue 2014). Proteoglycans form another important part of the ECM, which consist of a core protein with attached GAG chains. The GAGs themselves are highly negatively charged repeats of disaccharides. In contrast to collagen and fibronectin, proteoglycans can bind water due to their many negative charges in their GAG side chains, allowing them to act as lubricants of the ECM (Bełdowski et al. 2019). Additionally, the negative charge also acts to sequester many different growth factors containing positive motifs and other mediators, which have evolved mechanisms to exploit charge-based binding. This retention is very important for paracrine and autocrine signalling, which is desired in situations such as wound healing. Further components of the ECM include elastins and laminins alongside many other proteins ensuring the proper function of the ECM.

The ECM is a dynamic structure which undergoes constant remodelling. This is achieved by the selective expression of several enzymes such as LOX interacting with collagens and elastins or matrix metalloproteinases (MMPs), which can release different sequestered factors from the ECM through cleavage (e.g. vascular endothelial growth factor (VEGF) (Bergers et al. 2000)). Additionally, MMPs cleave proteins such as perlecan (Grindel et al. 2014) or pro-collagen to collagen for assembly (Broder et al. 2013; Canty and Kadler 2005). These enzymes have also been heavily studied in the context of cancer, especially because their overexpression or constant activation can lead to cancer cell invasion and metastasis (Quintero-fabián et al. 2019).

1.2.1 The ECM in cancer

In cancer, the ECM undergoes massive structural and biochemical changes and is actively shaped to support and sustain the progression and invasion of cancer cells into new tissues, as can be seen in **Figure 1.1** (Popova and Jücker 2022). Although many of the proteins are the same compared to physiological conditions, their relative quantities and post-translational

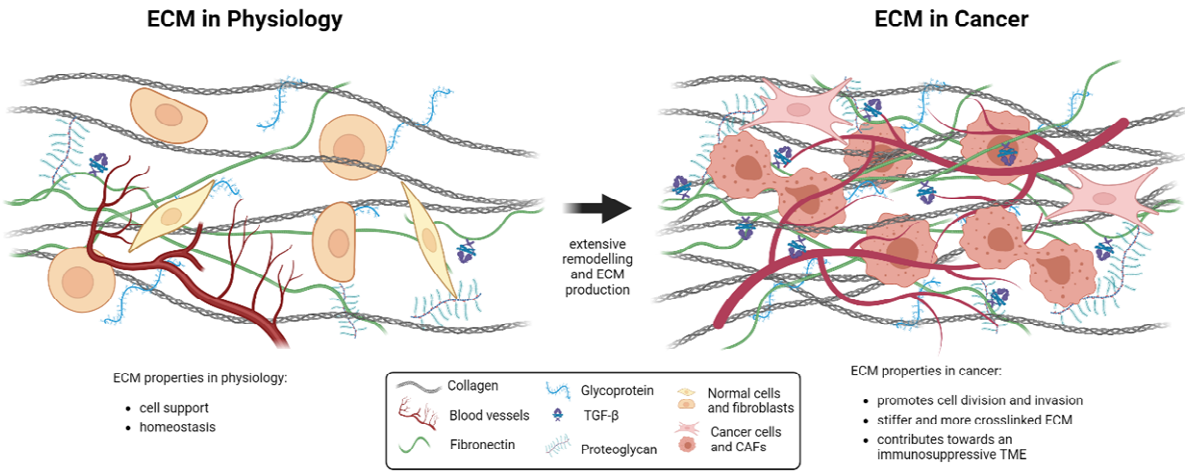

Figure 1.1: The extracellular matrix (ECM) in physiology and cancer. In physiology, the ECM has important functions contributing towards a homeostasis and support of cells, including facilitating paracrine signalling. Upon cancer development, the ECM undergoes extensive remodelling through the deposition of newly produced ECM proteins and through the function of matrix metalloproteinases and other enzymes. Once the cancer has established, the ECM's functions support and maintain a pro-cancer environment, and influences several classical "hallmarks" of cancer. This includes the promotion of cell proliferation through ECM stiffness, invasion of healthy tissues thorough migration of tumour cells on the cancerous ECM fibres, and capturing of immunosuppressive mediators, and thus maintaining an immunosuppressive microenvironment. This figure was created using BioRender.

modifications are altered heavily. In cancer, ECM is mainly produced by two types of cells: The cancer cells themselves and cancer associated fibroblasts (CAF). CAFs can arise from various residing fibroblasts and other local cells such as endothelial cells (Zeisberg et al. 2007) and adipocytes (Bochet et al. 2013), resulting in high CAF heterogeneity. The transition into CAFs is often regulated by transforming growth factor beta (TGF-β) (Popova and Jücker 2022; Yoon et al. 2021).

In the following paragraphs, different ECM components and their involvement to promote and sustain a pro-cancer microenvironment are described in more detail.

1.2.1.1 Collagen and type I collagen in cancer

Collagen expression is often upregulated in cancer and is associated with a poor prognosis (Necula et al. 2022; Sun et al. 2023). This can be demonstrated by looking at collagen I mRNA levels in different cancer patients, where many types of cancer, including liver hepatocellular carcinoma, metastatic lung cancer and others, showed higher expression of collagen I in comparison to their normal tissues (Hou et al. 2021; H. Ma et al. 2019). Additionally, when

correlated in Kaplan-Meier survival curves, it was evident that patients with upregulated collagen I genes faced a worse prognosis (Sun et al. 2023). In cancer, collagen fibres generally re-organise from a wavy phenotype in healthy ECM to a more straightened organisation in tumours. Different tumour-associated collagen signatures (TACS) have been initially identified in breast cancer but have since been observed in other cancer types such as pancreatic ductal cancer (PDAC) (Ray et al. 2022) or glioblastoma (Brett et al. 2020; Provenzano et al. 2006). TACS-1 features increased collagen deposition on the margins of tumours, while TACS-2 features straightened collagen fibres around the tumour and, TACS-3 consists of perpendicular collagen fibres to the margin of the tumour, reaching out into the normal tissue (Brett et al. 2020). These TACS can in the future potentially be used to predict cancer patients' outcomes and decide about therapeutic interventions, as has already been looked at for TACS-3 in breast carcinoma (Conklin et al. 2011). CAFs have also been observed to align collagens in a linear fashion, further promoting tumour invasion, as these aligned fibres are often a preferred means for cancer cells to migrate along (Conklin et al. 2011).

Collagen I also plays a crucial role in the development of cancer. In PDAC, for example, it has been shown that pancreatic stellate cells are responsible for collagen I deposition, which then, in turn, leads to pancreatic cancer cells displaying higher invasion properties and viability (Mekapogu et al. 2019). Furthermore, collagen I has been observed to evoke the formation of invadopodia and thus promote the migration of tumour cells and other cell types (Artym et al. 2015). It has also been demonstrated that in non-muscle invasive bladder cancer (NMIBC, normally linked to a better patient outcome), collagen I is an important player in mediating the switch into muscular invasive bladder cancer (associated with a poorer patient survival) (Brooks et al. 2016).

In conclusion, collagen and specifically type I collagen has been shown to impact several different hallmarks including metastasis and invasion of tumour cells. In a later paragraph, the effect of collagen I towards immunosuppression will be considered in more detail.

1.2.1.2 Glycosaminoglycans in cancer

GAGs are unbranched, linear polysaccharides which consist of repeating disaccharide units and are highly negatively charged (Wieboldt and Läubli 2022). The disaccharide repeat is made up of an acidic sugar (D-Glucuronic acid or L-Iduronic acid) and an amino sugar (N-Acetylgalactosamine or N-Acetylglucosamine). Keratan sulphate (KS) additionally contains D-Galactose instead of the acidic sugars mentioned above. There are five main classes of GAGs: On the one hand GAGs which are covalently linked to proteoglycans and are synthesised in the Golgi including chondroitin sulphate (CS), keratan sulphate (KS), dermatan sulphate (DS) and heparan sulphate (HS). Hyaluronan (HA), on the other hand, is non-sulphated and binds to proteoglycans via binding motifs and is synthesised in the cytoplasm by the hyaluronan synthases (Vigetti et al. 2014). There are over 500 identified proteins which interact with GAGs, illustrating the critical role GAGs play in the ECM and also the potential effect they might have in different hallmarks of cancer by retaining growth factors and cytokines in the tumour microenvironment (TME) (Sarkar and Desai 2015; Wieboldt and Läubli 2022).

Several different GAGs are overexpressed in cancer compared to normal tissues. Therefore, HA has been found to be upregulated in breast, lung and genitourinary cancer (Auvinen et al. 2000; Pirinen et al. 2001; Simpson and Lokeshwar 2009); CS in renal cell and neuroendocrine cancer (García-suárez et al. 2014; Ucakturk et al. 2016) and KS in pancreatic and ovarian cancer (Leiphrakpam et al. 2019; Miyamoto et al. 2011). Additionally, the covalently bound GAGs often correlate with the upregulation of certain proteoglycans, such as KS and lumican (Cappellesso et al. 2015; Nikitovic et al. 2014), and CS and versican (Ghosh et al. 2011). In most instances, the upregulation of these GAGs is linked to increased cancer progression, metastasis and poor prognosis (Wieboldt and Läubli 2022). General GAGs in the tumour ECM have also been linked to poorer penetration of antibodies and therapies, therefore potentially impeding their *in vivo* efficacy (Jacobetz et al. 2013; Kohli et al. 2014).

The function of HA, however, differs slightly from the function of other GAGs reflecting its non-covalent binding to proteins. HA molecules can be characterized depending on their molecular weight: Molecules below 250 kDa are described as low molecular weight hyaluronans (LMW-HA), between 250-1000 kDa are classed as medium molecular weight (MMW-HA), and greater than 1000 kDa are classed as high molecular weight (HMW-HA). The main cellular receptor for HA is CD44 (Misra and Ghatak 2015).

HMW-HA are predominantly found in normal tissue and are associated with homeostasis, anti-inflammatory and anti-proliferative properties. In contrast, LMW-HA are nearly absent in normal tissue and mostly arise in areas with high hyaluronidase, reactive oxygen species (ROS) or nitric oxide (NO) activity, for example, in areas of injury or wound healing (Cowman et al. 2015; Tavianatou et al. 2019)(Cowman et al. 2015). The link between cancer and hyaluronan has been made in several studies, including its effects on cancer cells and chemotherapy resistance (Mueller et al. 2011; Price, Lokman, and Ricciardelli 2018; Tian et al. 2013).

Very high molecular weight hyaluronan (vHMW-HA) is reported to be important in anti-cancer mechanisms at initial development of the disease, as has been demonstrated in the naked mole rat, a species that uniquely possesses very high molecular weight HA (>6000 kDa), and have an extremely low cancer incidence (Boehm 2017). In theory, the very long HA chains bind to CD44 and cover a large proportion of the cell surface, shielding other receptors and the cell from stress signals. This process puts the cells in a mode called cytoprotection and can be exploited by the cancer to cause immunosuppression in the later stages. This can maintain and/or promote cancer progression. In contrast, low molecular weight HA is too short to promote the same effect. On another note, a correlation between the expression of different length of HA and the polarisation of monocytes to tumour associated macrophages (TAMs) has been reported in several studies (Kuang et al. 2007; Zhang et al. 2016). In breast cancer, a correlation was found between the amount of expressed hyaluronan and the amount of

TAMs, furthermore it could be shown that the HA-CD44 signalling axis was involved in TAM polarisation through ERK1/2 pathway (Zhang et al. 2016), which could also be seen *in vivo*.

1.2.1.3 Fibronectin and Extradomain B Fibronectin in cancer

Fibronectin is another ECM protein type that is altered in cancer. Similarly to collagens, fibronectin is re-organised in the tumour ECM and aligned to form paths for cancer cells to migrate and invade tissues. This re-organisation is in part orchestrated by CAFs present in the tumour (Erdogan et al. 2017).

Besides its role in structural re-organisation, fibronectin is important in promoting cell proliferation and angiogenesis in the newly forming tumour. Firstly, cell proliferation can be triggered and sustained by fibronectin though the engagement of integrins and the subsequent activation of the focal adhesion kinase (FAK) and Src pathway, as was shown in a study looking at ovarian cancer (Mitra et al. 2011). Secondly, fibronectin and especially extra domain B Fibronectin (EDB-FN) play an important role in angiogenesis. EDB-FN is a cancer ECM-specific marker and is highly expressed in breast cancer, head and neck cancer, pancreatic cancer and ovarian cancer (Hooper et al. 2022). EDB-FN is considered an oncofetal protein and therefore expressed in foetal tissue, whereas it is nearly completely lost in adult tissues (Carnemolla et al. 1989; Oyama et al. 1990). In cancer, EDB-FN is often associated with angiogenesis and can be found during new vessel development, whereas in mature blood vessels, it is absent (Castellani et al. 1994). EDB-FN expression has been demonstrated in a variety of cancers including breast cancer, lung cancer, colorectal cancer and liver cancer (Kaczmarek, Castellani, and Nicolo 1994; Oyama et al. 1989, 1990; Pujuguet et al. 1996), and has been identified as a potential maker for progression in breast cancer (Vaidya et al. 2020).

1.2.2 The effect of ECM on conventional cancer therapies

After having discussed the role of the major ECM components in cancer, it is important to highlight the impact of the ECM on the activities of conventional cancer therapies such as chemotherapy and radiation.

Chemotherapy and ECM: Chemotherapy is a type of cancer treatment which uses chemical compounds in order to achieve regression of the tumour. Commonly used agents include for example antimetabolites, alkylating agents and topoisomerase inhibitors. This approach allows the treatment of both solid and liquid cancers and reaches circulating cancer cells or potential small, undetected metastases. Chemotherapies are often given orally or systemically via intravenous (IV) administration. However, the majority of agents target any rapidly dividing cell and are not specifically targeted towards cancer cells. This often leads to severe side effects, especially in epithelial regions with rapid turnover such as the gastrointestinal tract and hair follicles (Altun and Sonkaya 2018). They can also damage the immune system through bone marrow toxicity. In general, tumours can acquire resistance to chemotherapies following extended selective pressure leading to outgrowth of resistant tumour clones.

Dense and highly crosslinked ECM in solid tumours may decrease the distance of drug convection from the blood vessel, limiting efficacy of systemically-administered chemotherapies (Dewhirst, Secomb, and Carolina 2019). Additionally, fibroblasts can often be found next to the vessels in solid tumours, potentially further shielding tumour cells from any drug convecting from the blood vessels (Sewell-loftin et al. 2017; Zeine et al. 2009). In another study it has been shown that a dense and crosslinked ECM plays a role in chemoresistance in triple negative breast cancer (Saatci et al. 2020). The study also went on to show that by targeting LOX and effectively reducing collagen cross-linking and fibronectin assembly, tumours showed increased drug penetration and were re-sensitised to the chemotherapy.

Secondly, integrin mediated focal adhesion kinase (FAK) signalling plays an important role in cancer cell survival and can play a crucial role in resistance mechanisms. FAK is activated

through ECM stiffness and subsequently leads to the induction of pro-survival signals through the phosphoinositide 3-kinase/protein kinase B (PI3K/AKT) pathway (Hastings et al. 2019). This can in turn lead to the development of resistances, as for example in 5-FU treatment of colorectal cells (Chen et al. 2010) or resistance to rapamycin (Henke, Nandigama, and Ergün 2020; Yoon et al. 2017).

Radiotherapy and ECM: In cases of solid tumours and/or localised tumours, radiotherapy is often used to locally administer high doses of radiation and therefore leads to double stranded DNA breaks in cancer cells, which ultimately leads to cancer cell death. Currently, approximately half of all cancer patients receive radiation as mono- or combination therapy (Baskar et al. 2012). Especially combination therapies involving radiation have in the past decades proven to be effective. The main limitations of radiotherapy are (1) the fast resistance mechanisms which often arise in cancers, (2) the off-target effects on normal cells and (3) the limited possibility to use radiation for cellular cancers which do not form discreet, solid tumours.

It has been known since 1992, that the adhesion of cells to the ECM plays a role in the response to radiation, especially when adhered to a dense ECM (Onoda, Piechocki, and Honn 1992). Additionally, similarly to chemotherapeutic resistance, FAK signalling has also been shown to play an important role. FAK and other integrin signalling pathways have been shown to affect the sensitivity of tumour cells to radiotherapy by increasing cell survival and proliferation. It has been observed that A549 cells which bind to fibronectin show resistance towards radiotherapy, which is likely to be mediated via the α5β1 integrin (Cordes and Beinke 2004; Eke et al. 2013). Another study has shown an upregulation of α5β3 integrin post radiation, and that an antagonist blocking binding of the integrin increased radiosensitivity (Abdollahi et al. 2005). MMPs can also influence the outcome of radiotherapy greatly. MMPs are upregulated in many cancers and associated with poor survival (Henke et al. 2020; Noël et al. 2012). They further play a significant role in ECM remodelling and turnover of different ECM components.

In addition to chemo- and radiotherapy, immunotherapy has established as a therapeutic approach throughout the past decades. The following paragraphs will therefore focus on the interplay of the immune system and the tumour, followed by the involvement and effect of the ECM in immunotherapy.

1.3 The interplay of the cancer ECM with the immune system and immunotherapy

Immunotherapy is an important therapeutic approach in oncology, by which the host's immune system is re-activated and directed towards the tumour. Although several observations and connections between the immune system and tumours even before 1900s have been made, it was not until the individual components were discovered and their mechanisms elucidated throughout the second half of the 20th century, that the importance of immunology in cancer was further explored. Especially the proposition of the immunosurveillance theory and cancer development by Thomas and Burnet in 1957 (Burnet 1957; Kim, Emi, and Tanabe 2007) paved the way for understanding cancer in an immunological context. It was only in the late 20th century that Schreiber, Dunn and Old managed to definitely prove the involvement of T cells in preventing the development of cancer (Dunn et al. 2004). At the same time, the immune evasive capacities of cancer were discovered, which would later translate into an important new cancer hallmark (Hanahan and Weinberg 2011). It was also later shown that cancer development, progression and metastasis are all processes associated with a dysfunctional immune system (Kobayashi, Lim, and Yamaguchi 2020).

1.3.1 Cancer-immunity cycle

Tumour immunology is a complex interplay between different segments of the immune system and the developing tumour. A theory of the cancer-immunity cycle has been published based on findings by Dunn et al. (Dunn et al. 2002), and the different steps of the cycle are shown in **Figure 1.2** (Chen and Mellman 2013). Firstly, the innate immune response is initiated through

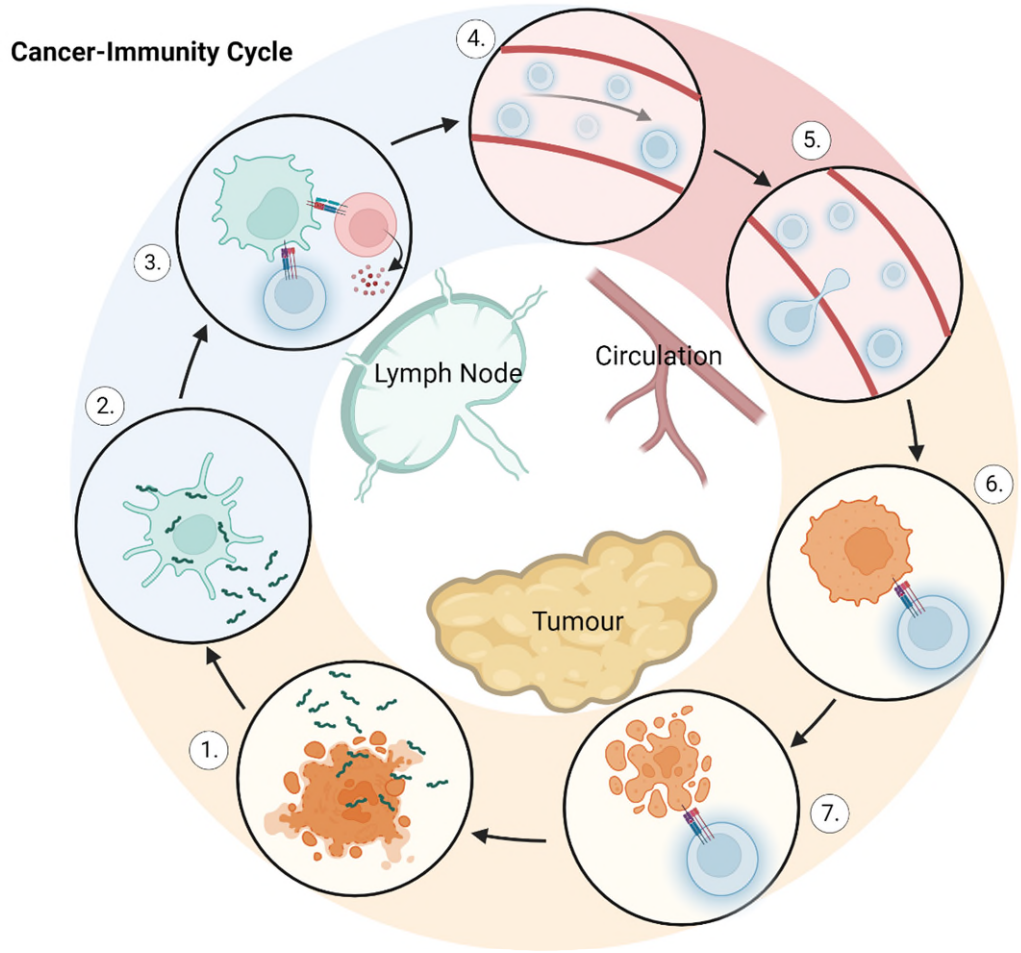

Figure 1.2: The tumour immunity cycle. (1) Cancer cell death leads to the release of tumour associated antigens (TAAs). (2) TAAs are up taken by antigen presenting cells (APCs) such as dendritic cells (DCs), processed and (cross-)presented in the lymph nodes to T cells. (3) T cells (CD4 and CD8) in the lymph nodes are activated via MHC I and MHC II presentation pf the TAAs by the DCs. (4) Activated T cells migrate into the blood stream, (5) where they extravasate into the tumour site and TME. (6) The activated T cells recognise the cancer cells via MHC I and (7) exert cytotoxicity towards them, leading to the release of TAAs and the cycle begins again. Modified from Chen and Mellman 2013. This Figure was created using BioRender.

the release of tumour associated antigens (TAAs) by cancer cells, which are subsequently taken up by antigen presenting cells (APCs), a process enhanced in the presence of proinflammatory factors such as tumour necrosis factor alpha (TNFα), type I interferons and adenosine triphosphate (ATP). The APCs then migrate to the tumour-draining lymph node, where they present and cross-present the TAAs via major histocompatibility complex I and II (MHC I/II in mice or human leukocyte antigen (HLA) I and II in humans) in order to activate CD4/CD8 T cells and B cells. Antigen-specific B cells are activated by the peptide presented on MHC II on the APCs and mature into plasma cells, which in turn secrete antibodies as a humoral response. Antigen-specific CD8 T cells are activated via the peptide presented via MHC I on APCs, which together with antigen-specific activated CD4 T cells producing IL-2 and

co-stimulation, induces a robust CD8 T cell activation and proliferation. The activated T cells, mainly CD8 cytotoxic T lymphocytes (CTLs), then relocate through the blood stream to the tumour, where they extravasate and infiltrate into the TME. Upon recognition of TAAs in the context of MHC I on the surface of cancer cells, CTLs kill cancer cells either by secreting cytotoxic granules including granzyme and perforin, or by interacting with membrane bound receptors, such as Fas/Fas ligand (FasL) (Chen and Mellman 2013; Kim and Cho 2022). This tumour cell cytotoxicity then enables APCs to once again take up TAA and the cycle is re-initiated. In patients suitable for immunotherapy, this cycle is dysfunctional and can be blocked at one or several steps to various extents by the tumour, which is coined as immune evasion (Hanahan and Weinberg 2011).

Through extensive research and with the help of different scoring systems, tumours are often categorised as immunologically “cold”, “altered” or “hot”. Although some definitions in the literature vary, “cold” tumours are defined by a poor T cell infiltration, low inflammation and a low expression of key players for a functional tumour-immunity cycle, such as HLA class I and neoantigens. “Hot” tumours, however, show a higher degree of T cell infiltration throughout the tumour in the presence of inflammation. Altered tumours are often classified in between “cold” and “hot” tumours, either exhibiting immune cell infiltration on the margins but not in the core (“altered excluded” phenotype), or immunosuppressed when the tumours are infiltrated to a low degree but hindered in the recruitment of novel immune cells. Immunotherapies have highest chances to respond in immunologically “hot” tumours, which are often limited by immunosuppression mediated through immune checkpoints due to effector cell exhaustion (Galon 2019).

1.3.2 Immune Checkpoints

Immune checkpoints (ICs) are signalling proteins mainly found on T cells, which negatively regulate the helper and effector functions of CD4 and CD8 T cells. Physiologically, these proteins are very important in order to prevent excessive tissue damage and out-of-control T

cell activation, or to preserve self-tolerance. Therefore, many ICs are upregulated upon T cell activation, an effect which is exacerbated in chronic infection or long-term inflammation such as cancer.

Cytotoxic T lymphocyte-associated protein 4 (CTLA-4), an important immune checkpoint, binds competitively to CD80/86 and thereby outcompetes co-stimulatory CD28 (Jansson et al. 2020). This lack of co-stimulation can eventually lead to the functional intrinsic inactivation of the T cell, called anergy. Although the mechanisms are still subject of intense debate, the suppression appears mediated, at least in part, by intracellular tyrosine rich motifs (Schneider et al. 1995) leading to the indirect interference of zeta-chain-associated protein kinase-70 (ZAP70) and T cell receptor (TCR) recruitment and the phosphorylation of linker for activation of T cells (LAT), eventually resulting in an interruption of mediator expression such as interleukin (IL)-2. Molecules such as Src homology region 2 domain-containing phosphatase 2 (SHP-2) and protein phosphatase 2A (PP2A) are also recruited, interfering with protein kinase B (AKT) activation and further inhibiting vital T cell activation pathways and cytokine production (Parry et al. 2005). This collectively leads to a decrease of T cell activation and proliferation (Pisibon et al. 2021; Schneider et al. 1995).

Programmed cell death 1 and programmed cell death ligand 1 (PD-1/PD-L1) is another IC axis often used by the tumours to dampen T cell effector functions. PD-1 belongs to the family of CD28 receptors and contains a cytoplasmic immunoreceptor tyrosine-based inhibitory motif (ITIM) and immunoreceptor tyrosine-based switching motif (ITSM). The ligands include PD-L1, mainly expressed on cancer cells, fibroblasts and macrophages (Khalique et al. 2021; Zou, Wolchok, and Chen 2016) and programmed cell death ligand 2 (PD-L2), which binds with a higher affinity and is expressed on DCs, monocytes and macrophages (Youngnak et al. 2003). Upon binding, the intracellular motifs become phosphorylated and recruit SHP-1 and SHP-2, which interfere with the main TCR co-stimulation pathways by dephosphorylating crucial players such as CD3ε, ZAP70, PI3K and protein kinase C (PKC), leading to the suppression of T cell activation (Parry et al. 2005; Sheppard et al. 2004). The disruption of the PD-1 and

PD-L1 axis has been shown to be effective in restoring the functional ability of exhausted CD8 T cells within the tumour, and therefore, PD-1 and PD-L1 blocking antibodies are used in state of art immunotherapeutic administrations in patients with melanoma and Hodgkin's lymphoma, but also as combination therapies with other approaches (R. Chen et al. 2019; Gong et al. 2018).

Other immune checkpoints include lymphocyte-activation gene 3 (LAG-3), T cell immunoglobulin and mucin domain-containing protein 3 (TIM-3), T cell immunoreceptor with Ig and ITIM domains (TIGIT), V-domain immunoglobulin suppressor of T cell activation (VISTA) and B7 homolog 3 protein (B7H3). However, this is not an exhaustive list and novel emerging immune checkpoints are a matter of ongoing research. Although immune checkpoint therapy sounds promising, the main objective is to remove the inhibitory signals and to restore the natural activity of dysfunctional T cells, rather than directly activate or redirect engagement of T cell effector functions.

1.3.3 Effector T cell therapies and Bispecific T cell Engagers (BiTEs)

Several of the clinically effective immunotherapies target one or multiple effector cells, including chimeric antigen receptor (CAR)-T cells, immune checkpoint inhibitors (ICIs) and bispecific T cell engagers (BiTEs). For the purposes of this thesis, the focus will mainly be set on BiTEs and their function. BiTEs consist of two single chain variable fragment (scFvs) fused together, whereby one targets an antigen on a tumour or target cell and the other one binds and activates T cells, usually via CD3. Upon binding to the target cell and T cell, BiTE-mediated clustering of CD3 within the newly formed immunological synapse activates both CD4 and CD8 T cells robustly (Freedman et al. 2017; Khalique et al. 2021). The use of nanobodies instead of scFvs has also been explored, reducing the size of BiTEs and potentially decreasing the depth of the synapse (Khalique et al. 2021; Maali, Gholizadeh, and Seyed-motahari 2023).

A prominent BiTE used in the clinic is Blinatumomab, targeting CD19 on cancer cells and CD3 on T cells. It is used to treat acute lymphoblastic leukaemia (ALL) (Franquiz and Short 2020).

BiTEs have also been combined with other therapies such as oncolytic viruses (OVs), examples include epithelial cell adhesion molecule (EpCAM) or fibroblast activation protein α (FAP)-targeting BiTEs, which have been encoded in OVs (with the latter currently being investigated in clinical trial (NCT04053283)).

BiTEs have a relatively small molecular size (50-60 kDa) and therefore show enhanced penetration in solid tumours compared to full length antibodies (Bates and Power 2019; Li et al. 2016). At the same time, their small size also contributes towards a short half-life in the body due to a fast clearance through the kidneys, particularly if given IV. Therefore Blinatumomab is continuously administered over the course for the treatment (Klinger et al. 2012).

1.4 ECM mediated immunosuppression

Effector cell targeting therapies often face immunosuppressive conditions within the tumour, probably mediated largely by tumour cells and associated cytokines and chemokines. The ECM, however, is another key player in maintaining and perpetuating immunosuppression. ECM has three main ways to mediate local immunosuppression, including though covalent binding and storage of immunosuppressive cytokines (for example TGF-β), non-covalent association of cytokines (through interactions with GAGs), and through ECM components themselves (as seen in **Figure 1.3**). Although many immunosuppressive cytokines and mediators possess ECM-binding domains and contribute towards the immunosuppression mediated through the ECM (IL-10, IL-6 and others), the following section will focus on the main players which are covalently linked or mediated directly by ECM molecules.

1.4.1.1 TGF-β

The most notorious immunosuppressive mediator trapped by the ECM is TGF-β. TGF-β1 (hereafter referred to as TGF-β) is a multifunctional, secreted protein which is involved in the regulation of cell growth and immune response modulation. The latent TGF-β complex is made

up of inactive TGF-β, which is non-covalently associated to the latency-associated protein (LAP). This complex, in turn, dimerises and is connected through disulphide bonds to the latent TGF-β binding protein 1 (LTBP-1 protein) (Robertson et al. 2016). These disulphide associations are crucial for the functionality, as mutagenesis studies showed that by abrogating these interactions in mice, they exhibited tumorigenic and inflammatory phenotypes, similar to TGF-β null mice (Yoshinaga et al. 2008). Upon secretion, the entire complex is covalently fixed onto multiple ECM proteins including fibrillin and (indirectly) fibronectins (Robertson et al. 2016), a process mediated through tissue transglutaminase II (TTGII) (Lockhart-Cairns et al. 2022). As long as TGF-β is associated with LAP and LTBP-1, it remains inactive and is only capable of acting upon liberation (Buscemi et al. 2011; Shi et al. 2011; Wipff et al. 2007). TGF-β can be activated through extreme pH, deglycosidases and cell-surface integrins such as α5β6 and α5β8, and other members of the α5 family by interaction with LAP (Robertson and Rifkin 2016). These integrins are able to release the

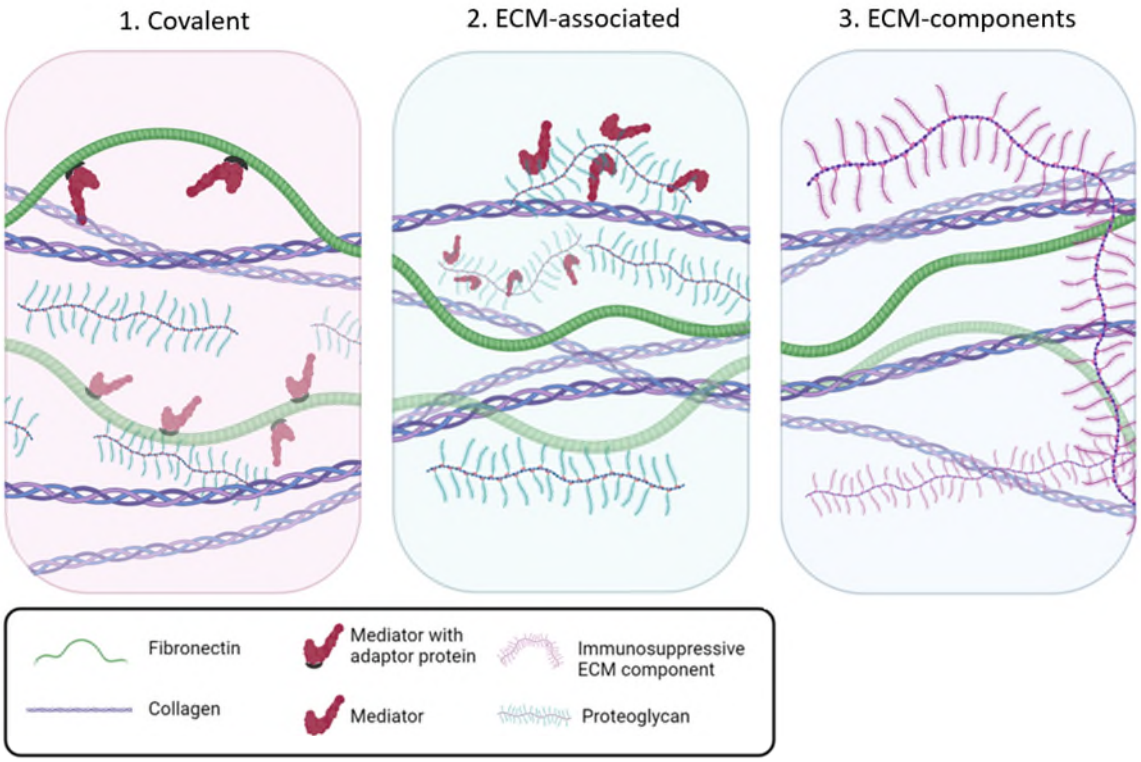

Figure 1.3: Capacity of the ECM to locally sequester (immunosuppressive) mediators. (1) The ECM can covalently sequester mediators through adaptor proteins. One example for this is TGF-β, which is attached through the LAP and LTBP protein to fibrillin and fibronectin. (2) Mediators can also be sequestered by the ECM through charge-charge or non-covalent interactions. Prominent examples include IL-10 and IL-6, which both interact with glycosaminoglycans. (3) Thirdly, ECM components themselves can be immunosuppressive and have a direct effect on immune cells. This includes vHMW-HA and collagen I interacting with LAIR-1 on immune cells (described in 1.5). This Figure was created using BioRender.

active form of TGF-β by mechanical traction forces formed between the cells and the LAP protein. A second possibility is the liberation of TGF-β through proteases after integrin binding (Robertson and Rifkin 2016).

In the TME, the bulk of TGF-β is produced by stroma and cancer cells (Colak and ten Dijke 2017). Initially, TGF-β is thought to be a tumour-suppressor and only becomes a malignant factor in later stages of cancer (Fessler et al. 2014). Interestingly, TGF-β is involved in altering both the adaptive and innate immune cells at different stages. Effector cells are directly suppressed by TGF-β, with CD8 T cells for example showing downregulated granzyme and perforin content and a decrease in interferon gamma (IFN-γ) release, which could all be restored upon TGF-β blockade (Thomas and Massagué 2005). Additionally, TGF-β is able to suppress and influence CD4 T cells, neutrophils, macrophages and DCs (Fessler et al. 2014) and can also induce regulatory T cells (T_{reg}) differentiation, thus maintaining an immunotolerant environment in the tumour (Fessler et al. 2014).

1.4.1.2 Exclusion of Immune cells

Immunotherapies are only effective if the appropriate immune cells are present in the TME. When looking at T cells, for example, the ECM has been attributed a significant role in excluding T cells from migrating into the tumour. One of the reasons might be linked to hypoxia, whereby the consequent high level of VEGF leads to the activation of endothelial cells, which then again downregulate important proteins such as intracellular adhesion molecule (ICAM)-1 or ICAM-2, which are pivotal in T cell extravasation (Dirkx et al. 2003).

Additionally, it has been shown that collagen and matrix density play a crucial role in T cell infiltration in mammary tumours (Kuczek et al. 2019). It was observed that higher matrix density led to a higher CD4/CD8 T cell ratio. Interestingly, they could also show a significant downregulation in multiple key cytotoxicity mediators and T cell activation genes such as granzyme B and perforin when cultured in a high density-matrix. This was accompanied by an upregulation of forkhead box P3 (FOXP3) and TGF-β.

These findings suggest that the degree of tumour infiltration is highly dependent on the ECM properties and is also influenced by the degree of matrix density.

1.4.1.3 Collagen I

Another important immunosuppressive ECM-component is collagen I. Although some of the pro-cancer properties have been described in previous sections, collagen I also binds to the inhibitory leukocyte-associated immunoglobulin-like receptor-1 (LAIR-1) present on many immune cells and especially T effector cells, mediating local immunosuppression. This is detailed in the next paragraph.

1.5 LAIR-1, an ECM-mediated immune checkpoint

LAIR-1 (CD305) is an inhibitory surface receptor with a molecular weight of approximately 32 kDa and consists of 286 amino acids (Guo et al. 2020). It is composed of a single extracellular C2-type-Ig-like domain and two intracellular immuno-receptor inhibitory tyrosine-based motifs (ITIMs) and is classed as a type I transmembrane glycoprotein (Meyaard 2008). The inhibitory capacity of LAIR-1 has been demonstrated in many different cells and will be considered carefully. LAIR-1 is widely expressed on immune cells (Meyaard et al. 1997). The main importance in cancer immunotherapy is the high expression on T cells (CD8 T cells in particular), macrophages, dendritic cells, NK cells and B cells (Van Laethem et al. 2022). However, recent studies have also explored the expression of LAIR-1 on non-haematopoietic cancer cells and have revealed that it can be highly expressed on tumour cells, and even reported a positive correlation between LAIR-1 expression and malignancy of the tumour (Wu et al. 2019). The two main ligands, collagen I (and III) and C1q have been well documented to bind LAIR-1 with high affinity, however MBL, surface protein-D (SP-D), Rifins and Colectin-12 (Colec12) have also been shown to bind to LAIR-1 (Lebbink et al. 2006; Nordkamp et al. 2014; Saito et al. 2017; Son et al. 2012; Xie et al. 2022).

1.5.1 LAIR 1 in physiology

The main function of LAIR-1 in physiology can be attributed to the developmental stages of haematopoietic cells. Therefore, LAIR-1 is expressed higher in naïve and poorly differentiated cells, whereby its expression decreases with the degree of cell differentiation and changes after stimulation threshold of T cell activation, whereas the higher LAIR-1 expression on naïve T cells is important to prevent the formation of reactive T cells against self-antigens (Guo et al. 2020). It has been shown that the activation of naïve T cells has been inhibited by the crosslinking of their surface LAIR-1 (Maasho et al. 2005).

1.5.2 LAIR-1 signalling

The LAIR-1 inhibitory function requires phosphorylation of conserved tyrosine residues inside both intracellular ITIMs. This phosphorylation is generally carried out by Src family kinases (Verbrugge et al. 2003), followed by SHP-1 and SHP-2 recruitment, which in turn leads to the dephosphorylation of many important proteins and kinases involved in downstream activation pathways such as T cell activation (Meyaard et al. 1997).

Figure 1.4 shows the signalling pathway of LAIR-1 and its interference with the T cell activation pathway. It was observed in human T cell lines that pre-treatment with collagen before CD3/CD28 stimulation showed reduced phosphorylation of ZAP-70 and the MAP kinases extracellular signal-regulated kinases 1 and 2 (ERK1/2), c-Jun N-terminal kinase 2 (JNK 2) and p38 (Park et al. 2020). They further determined that tyrosine residues at positions 251 and 281, one in each ITIM, were involved in the TCR inhibitory downstream signalling, with tyrosine 251 (tyr-251) being crucial for the suppression. Tyr-251 was determined to be the residue recruiting C-terminal Src kinase, which was further demonstrated to be crucial in the process to inhibit TCR signalling (Park et al. 2020). These inhibitory signals collectively lead to the direct inhibition of T cell activation (Van Laethem et al. 2022).

1.5.3 The ECM-mediated IC LAIR-1 in cancer

The role of LAIR-1 in cancer can either be examined from the standpoint of the immune system or the tumour cells themselves. When considering the tumour cells, the loss of LAIR-1 can lead to the rise of malignancies. A study has shown that loss of LAIR-1 increased B cell activation with increased JNK and p38 signalling, which eventually lead to the uncontrolled proliferation of B cells in chronic lymphocytic lymphoma (CLL) (Poggi et al. 2008). Other studies on CLL patients have also reasoned that LAIR-1 may be responsible for halting the progression of the cancer (Perbellini et al. 2014; Rawstron et al. 2010). In acute myeloid leukaemia (AML) however, the function of LAIR-1 is more ambiguous. Different leukaemia cell lines showed less proliferation and increased cell death via apoptosis when LAIR-1 was knocked down, which could also be seen when cells without LAIR-1 were transplanted *in vivo* (Kang et al. 2015). Similarly, another study showed that a high expression of ITIM containing receptors such as LAIR-1 expression correlated with a worse prognosis in patients with acute

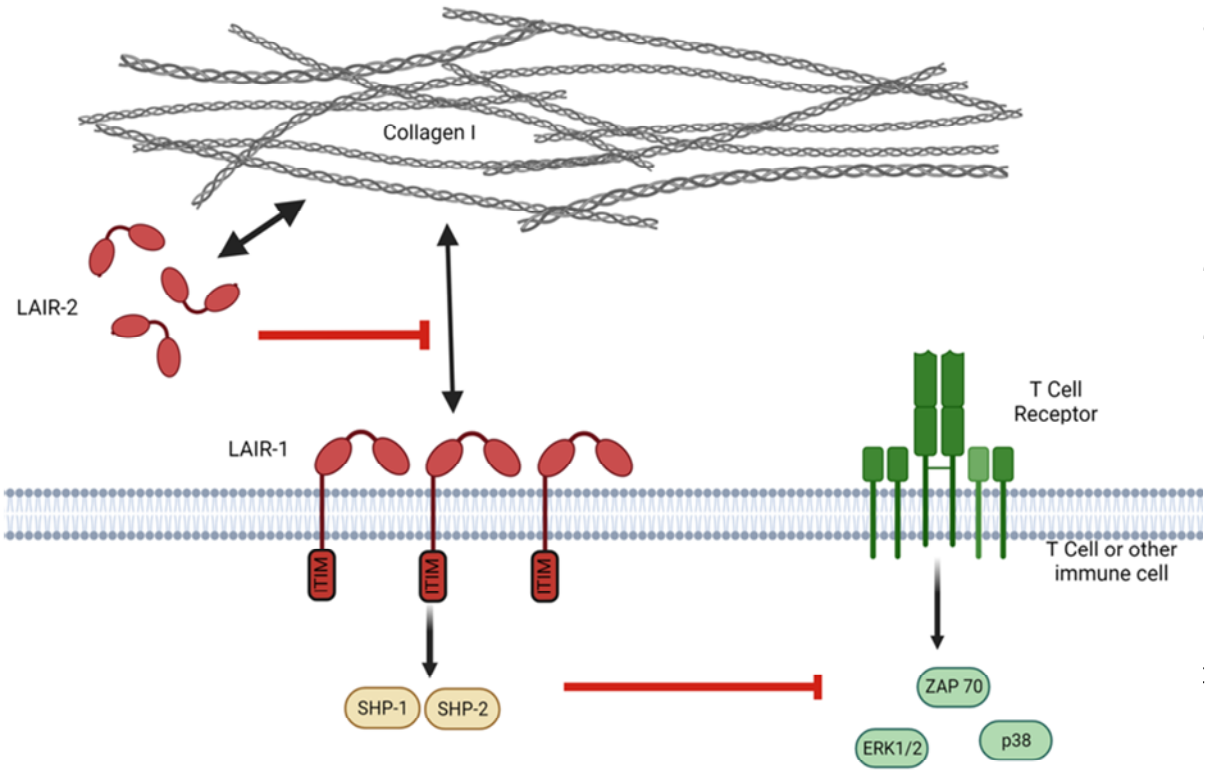

Figure 1.4: Intracellular signalling pathway of the ECM-mediated immune checkpoint LAIR-1. Upon binding to collagen I, LAIR-1 recruits SHP-1 and 2 through their intracellular motifs, which in turn dephosphorylate key kinases in the T cell activation pathway (ERK1/2. p38, ZAP 70). However, soluble LAIR-2 can outcompete LAIR-1 for collagen I binding and thus abrogate the inhibitory signal. This Figure was created using BioRender.

different cell types negatively (Van Laethem et al. 2022; Vijver et al. 2021). Although the bulk of the studies looking at LAIR-1 so far are not focused on cancer but rather on autoimmune diseases, there are still important points which can be made on how LAIR-1 affects immune cells. It has been shown that LAIR-1 crosslinking was able to reduce natural killer cell (NK) cytotoxicity (Meyaard et al. 1997) and reduce DC function including cytokine production (Omiya et al. 2009). However, several recent studies have looked at the effect of LAIR-1 on effector T cells (Meyaard et al. 1999; Peng et al. 2020). Peng et al. have seen that LAIR-1 contributed towards the resistance against PD-1/PD-L1 through SHP-1 signalling in CD8 T cells, probably forming a redundant pathway. They also identified that CD18, which is generally expressed on leukocytes and is important for extravasation, can further upregulate LAIR-1 upon binding to collagen, thus exacerbating the inhibitory effects of LAIR-1 mediated through collagen. Additionally, the analysis of patient datasets revealed that LAIR-1 could not only be used as a marker to look at general T cell exhaustion, but also as a predictive marker for sensitivity and potential success of immunotherapy in melanoma patients (Peng et al. 2020).

1.5.4 LAIR-2 as inhibitor of LAIR-1

LAIR-2 is a soluble protein and shared 83% identity with LAIR-1. Hence, it binds to similar ligands, including collagen I. The small differences in the proteins result in LAIR-2 binding with higher affinity to collagen I, therefore outcompeting and interrupting the inhibitory LAIR-1 – collagen I axis (Lebbink et al. 2008). The role of LAIR-2 in physiology is probably linked to the modulation of the immune landscape and immune response at inflammation sites, as it has previously been detected in elevated levels in patients suffering from the chronic inflammation rheumatoid arthritis or with autoimmune thyroid disease (Simone et al. 2013). Although soluble LAIR-1 has been observed, LAIR-2 remains a more potent inhibitor of membrane bound LAIR-1 (Nordkamp, Van Roon, et al. 2011). In fact, LAIR-2 has been used as an inhibitor of LAIR-1 in order to rescue exhausted CD8 T cells, which was demonstrated to counteract inhibition

mediated by LAIR-1. However, in order to fully eliminate the LAIR-1-mediated inhibition, a SHP-1 inhibitor had to be used alongside LAIR-2 *in vivo*. Furthermore, a reduction of primary tumours and metastasis could be seen when used in combination with an anti-PD-1 antibody (Peng et al. 2020).

The use of LAIR-2 as a possible inhibitor of LAIR-1 has also been explored in other studies, including as a dimer with an Fc portion (NC410) demonstrating that it can lead to an enhanced effector cell function and expansion in mice (Ramos et al. 2021). The most recent of the two clinical trials involving NC410 is a Phase 1b/2 study in combination with Pembrolizumab in order to treat unresectable and ICI refractory solid tumours (NCT05572684). Unfortunately, no updates about the ongoing clinical trials have been posted yet, with the first trial ending in December 2023 (NCT04408599 and NCT05572684). However, both of the trials involve systemic IV delivery of the NC410, with the potential of NC410 binding to C1q in the blood stream and therefore dampen the therapeutic effect.

1.5.5 Conventional and Immunotherapeutic targeting of the ECM

Although targeting the ECM directly in cancer is a difficult task, there have been several more or less effective attempts to tackle the ECM in several different ways.

1.5.5.1 Conventional ECM targeting

Due to the partly large size of ECM proteins and structures, conventional ECM therapies have focussed on targeting ECM components on a transcriptional level or ECM-modifying enzymes rather than ECM components directly. Collagen I, for example, has been targeted on a transcriptional level through drugs such as Phenylbutyrate. Phenylbutyrate is a histone deacetylase inhibitor, which limits collagen I mRNA production (Rishikof et al. 2004). Similarly, Baicalein has been shown to decrease TGF-β induced collagen I mRNA (Sun et al. 2020). However, therapeutics blocking collagen transcription are very difficult to justify, as normal

tissue relies on a functioning collagen I regulation and thus could result severe toxicity if administered systemically (Shi et al. 2022).

Another approach to target collagen I is by blocking LOX or MMPs, both involved in modifying and crosslinking collagens. However, results particularly for MMPs have been disappointing, possibly due to their vast role in healthy tissues and the high toxicity resulting from systemic administration of the inhibitors (Shi et al. 2022; Winer, Adams, and Mignatti 2019). Furthermore, transcriptional approaches are very difficult to use, as normal tissue rely on a functioning collagen I regulation and thus could result in many side effects should the inhibitors reach the tissues in too high concentrations (Shi et al. 2022).

Similarly, GAGs have been explored for targeted cancer therapy using a range of strategies such as synthetic or semi-synthetic HS in order to block heparinase (HPSE) and other GAG-binding partners (Wieboldt and Läubli 2022). Pixatimod is a HS that has been shown to inhibit the activity of HPSE in this way and in addition to this has an effect on several immune cells, including the activation of NK cells and suppression of TAMs (Hammond et al. 2018).

Hyaluronidases such as PEGPH20, on the other hand, have been used to increase intratumoural spread of several therapies such as monoclonal antibodies or chemotherapy in mice by degrading hyaluronan within the TME and increasing fluid convection (Beckenlehner et al. 1992). Unfortunately, a clinical trial involving PEGPH20 was largely abandoned after a phase III clinical trial for failing to meet the primary endpoints (Hakim et al. 2020). In a more sophisticated strategy, hyaluronidases have been expressed by an oncolytic adenovirus (Guedan et al. 2009), aiming to achieve large amounts of enzyme produced actually within the tumour itself and thereby obviating the delivery issue. In murine studies this approach led to the regression of approximately 60% of tumours compared to the parental adenovirus by presumably increasing intratumoural spread of the oncolytic virus.

1.5.5.2 Immunotherapeutic targeting of the ECM

Immunotherapies targeting the ECM have thus far only scarcely been explored. However, there are four main ways in which approaches have been designed.

Firstly, monoclonal antibodies such as ICIs have been used in combination with enzymes modifying or degrading the ECM. A comprehensive list of these approaches can be found in **Table 1.1**. The main goal of these approaches includes the improved penetration of the antibodies through solid tumour ECM and therefore potentially leads to a higher efficacy of the therapeutic (He et al. 2021).

Secondly, the main ECM-producing cells such as CAFs could be targeted in order to reduce further ECM production. This approach includes for example the expression of a FAP-specific BiTE in oncolytic viruses, or “normalising” the function of CAFs to reduce ECM deposition (Ford et al. 2021; Freedman et al. 2018; Hanley and Thomas 2021). Some of these approaches have also been taken into clinical trials (for example NCT04826003 or NCT04053283). Although their primary goal is the elimination of stromal cells and CAFs, their abrogation simultaneously will also lead to a reduction in ECM production and therefore also

Table 1.1: Table listing combination therapies of ECM-targeting agents and ICIs. Modified from He et al. 2021

ECM target	Agent targeting the ECM	Combination with immunotherapy target and compound	Cancer type	NIH number
Collagen	Losartan	Nivolumab, PD-1	Pancreatic cancer	NCT03563248
Collagen	Cetuximab	Monalizumab, NKG2A	SCC of HNC	NCT04590963
Collagen	Cetuximab	Pembrolizumab, PD-1	Recurrent SCC of HNC	NCT03082534
Hyaluronan	PEGPH20	Pembrolizumab, PD-1	NSCLC and gastric cancer	NCT02563548
Hyaluronan	PEGPH20	Atezolizumab, PD-L1	Gallbladder adenocarcinoma	NCT03267940
Hyaluronan	PEGPH20	Atezolizumab, PD-L1	Resectable PDAC	NCT03979066
Hyaluronan	PEGPH20	Avelumab, PD-L1	Chemotherapy resistant pancreatic cancer	NCT03481920

indirectly target the ECM. The main problem these approaches face, however, is that cancer cells themselves also produce considerable amounts of ECM (Hebert et al. 2020) and that fibroblasts can arise from varying cells making it difficult to find one common marker to target all of them.

Thirdly, ECM components themselves have been targeted to modulate the immune landscape within the TME. One such approach involves tenascin C, a multimeric glycoprotein mostly expressed in cancer ECM and absent in human tissue. Tenascin C has previously been shown to be linked to poorer prognosis in breast cancer (Oskarsson et al. 2011). Although involved in several cancer hallmarks, the role of tenascin C in polarising macrophages has been of particular interest (Deligne et al. 2020). This polarisation has been shown to be mediated via the engagement of toll-like receptor 4 (TLR-4) on macrophages by binding of the fibrinogen (FBG) domain in tenascin C. Interestingly, the phenotypic change in macrophages could be abrogated and reversed with a monoclonal antibody blocking the toll-like receptor 4 binding site on tenascin C, leading to a reduction in tumour size *in vivo*, especially in combination with anti-PD-L1 therapy (Deligne et al. 2020).

Similarly, Hongu et al have demonstrated that the TLR-4 induction on macrophages through tenascin C in lung cancer played an important role in the formation of a premetastatic niche together with metastasis associated endothelial cells (Hongu et al. 2022). Therefore, tenascin C might pose an alternative therapeutic target in order to create a more pro-inflammatory and anti-cancer microenvironment by targeting an ECM component.

In a different study, the inhibitory collagen I – LAIR-1 axis was targeted using two LAIR-2 motifs fused to an Fc-portion (Ramos et al. 2021). In pre-clinical testing, Ramos et al. were able to show that NC410 interfered and block the LAIR-1 – collagen I axis, effectively slowing down tumour growth and enhancing effector cell function and expansion in mice. Additionally, this reduction in tumour growth could be shown to be T cell dependent and was especially effective in collagen-rich areas of the tumour (Ramos et al. 2021). The most recent of the two clinical trials (NCT04408599 and NCT05572684) involving NC410 is a Phase 1b/2 study in

combination with Pembrolizumab to treat unresectable and ICI refractory solid tumours (NCT05572684). Unfortunately, no updates about the ongoing clinical trials have been posted yet, with the first trial ending in December 2023.

Lastly, ECM proteins can also be used to anchor and retain therapeutics within the ECM. One example further discussed in Chapter 4 involves GAG targeting. Ishihara et al. together with Hubbell et al. identified a 21 amino acid motif in placental growth factor 2 (PlGF-2) binding strongly to several ECM components (Ishihara et al. 2017; Martino et al. 2014). In a therapeutic approach, they coupled the motif to different ICIs (anti-PD-L1 and anti-CTLA4). Upon peritumoural injections in mice, an increased retention time of the antibody could be observed, including a prolonged survival and a diminished tumour growth rate could be observed in breast cancer and melanoma mouse models. In addition to this, the constructs also increased CD8 and CD4 T cells in the tumour and promoted T cell activation. However, no crucial experiments were done using human tissues or patient derived tumour samples, and no further updates or new studies on this approach have been published since. In a similar study, Ishihara et al. fused a collagen binding domain to ICIs and IL-2, yielding similar results as above in mice, but lacking relevant human clinical data (Ishihara et al. 2019).

In another approach, EDB-FN has been used to target IL-12 to tumours (huBC1-IL-12) (Yan et al. 2007). HuBC1-IL-12 is a hexameric protein of approximately 300 kDa, aimed to be targeted to EDB-FN in order to reduce IL-12 toxicity. Due to model system limitations, this study only looked at mouse models using a murine version of IL-12, whereas no experiments involving human cells were performed. The compound was then assessed in a clinical trial phase 1 in melanoma or renal cell carcinoma patients, concluding with a recommended phase 2 dose (15 µg/kg/week) and some efficacy evidence (Rudman et al. 2012). No further work has since been published on this compound. However, another similar IL-12-armed antibody binding to EDB-FN with the L-19 antibody (Ongaro et al. 2019) is currently being investigated in a phase one clinical trial (NCT04471987), although no results have been posted yet. Besides IL-12, L19 has also been used in various clinical trials (in some instances together

with radiotherapy) delivering therapeutic agents IV as fusion proteins, such as IL-2, TNFα, IFN-γ and more (Dakhel et al. 2019; Ebbinghaus et al. 2005; Rekers et al. 2018). Unfortunately, the results from the L19-TNFα fusion protein clinical trial were modest, given that many side effects were found and no measurable objective tumour response could be seen (Berardi and Pas 2013).

LAIR-2 has also been used to directly tether cytokines to the ECM in one prior approach. This novel approach is being explored by Cullinan Oncology, a BioTech company based in the US, who have only published as an abstract with limited data. In short, a LAIR-2 is fused together with a human serum albumin, IL-2 and IL-12 (CLN-617) is injected IT in B16F10 and MC38 syngeneic mice. Upon injection, all tumours in the group showed a response and 50% of the mice showed no re-growth of the tumour after a second challenge. Additionally, when two tumour lesions were present, the non-injected lesion also showed an increase in CD8 T cell numbers. This approach was then further tested in combination with an anti-PD-1 antibody, leading to the elimination of 100% of the treated and 90% of the non-treated tumours in mice (Naveen et al. 2022). Although encouraging, the published data only used the mouse equivalent of CLN-617 and completely lacked any human work.

Although many of these approaches are feasible and the results obtained are promising, they often struggle to harness their full potential due to the low specificity of cancer ECM-markers. Despite tumour specific expression of tenascin C and EDB-FN, their abundance within the tumour ECM is relatively low compared to other targets such as general fibronectin or collagens. Additionally, the preferred delivery method (IV) can often not be applied. Therefore, a superior delivery vector such as an oncolytic virus, could make an impactful difference in enhancing the effectiveness of ECM-targeting immunotherapies.

1.6 Oncolytic virotherapy

One of the possible reasons why therapies are not efficacious in patients and therefore do not succeed in clinical trials might lay in the difficulty of delivering the drug in high enough

concentrations at the tumour site. Therefore, a more elegant method of delivery might be considered, such as encoding and expressing the immunotherapeutic *in situ* using an OV.

Oncolytic virotherapy is the therapeutic approach to treat cancer by using replicating viruses. In principle, the viruses are injected into the patient and replicate selectively in tumour cells only, lysing and killing the cancer cells whilst sparing normal cells (see **Figure 1.5**). This way of treatment has several benefits besides the active cytotoxicity of the virus against the tumour cells: Firstly, the lysis of the tumour cells releases both danger associated molecular pattern (DAMPs) and pathogen associated molecular pattern (PAMPs) into the TME, helping to turn the TME from immunologically “cold” to “hot”. Secondly, the lysis also promotes the release of new TAAs, which in turn can be taken up by DCs and fed into the cancer-immunity cycle. And thirdly, the virus amplifies itself within the tumour and can subsequently be released into the circulation, potentially infecting secondary tumours or metastases. This potential secondary infection or induction of a systemic immune response has been demonstrated in several different studies, including against melanoma where the abscopal effect shows a reduction in size of the non-injected tumour lesion (Havunen et al. 2018; Kaufman et al. 2016; Kuryk and Møller 2019). Lastly, OVs can also be used as gene therapy vectors encoding payloads such as immunotherapeutics (BiTEs and cytokines), leading to a localised *in situ* expression leading to high concentrations of the therapeutic within the tumour without severe on-target, off tumour side effects.

Although not evident at first sight, viruses in general have a natural affinity for cancer cells, reflecting overlap between the hallmarks of cancer and the ‘hallmarks of virus infection’ (Seymour and Fisher 2016). One major factor contributing to this is the high anabolic rate of cancer cells, ensuring ample supply of amino acids and nucleotides for the virus to reproduce. Furthermore, cancers often naturally have upregulated viral entry receptors such as CD46 for group B adenoviruses, which leads to cancer cells being more permissive for the OV.

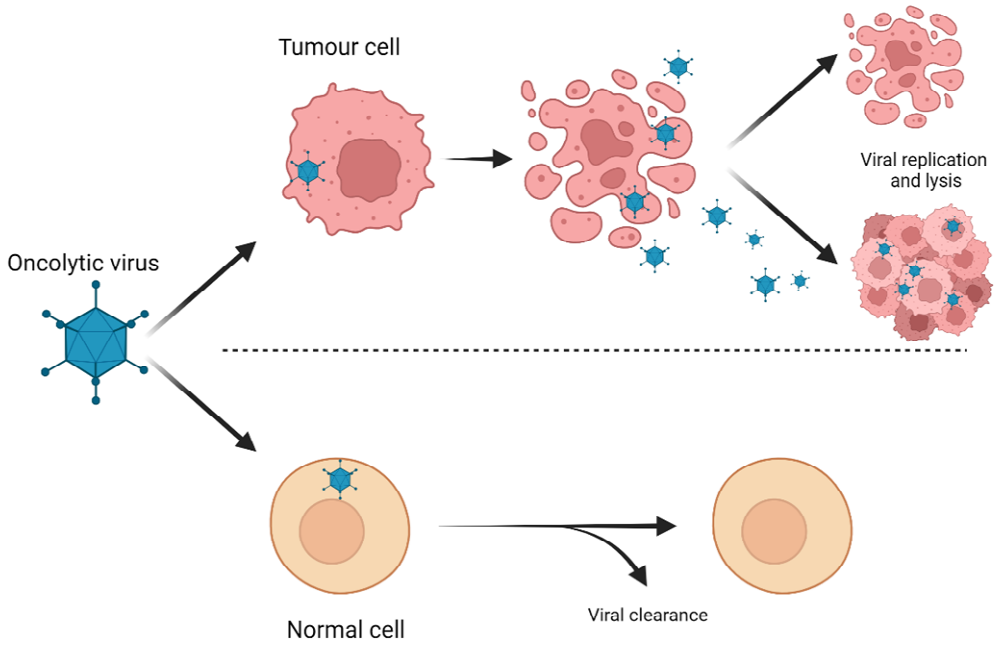

Figure 1.5: Principle of oncolytic viruses. Upon infection of a tumour cell, the virus can replicate, leading to the lysis of the host cell and the release of PAMPs and DAMPs in the TME. However, the oncolytic virus cannot replicate in normal cells, which inevitably leads to the viral clearance and leaves the normal cells unharmed. This Figure was created using BioRender.

Many different virus types have thus far been explored as oncolytic viruses, with approximately 80% of the viruses which enter clinical studies being DNA viruses (Li et al. 2022). Furthermore, about 40% of the OVs used in clinical trials are based on adenoviruses, 25% herpes simplex viruses (HSV) and 15% on vaccinia virus (Li et al. 2022).

1.6.1 Design of oncolytic viruses

There are several ways in which OVs can be designed in order to ensure tumour cell selectivity as well as potency. In the following paragraphs, some of the most common approaches will be outlined.

Deletion of specific genes: Amongst the most common and empirical strategies is the deletion of important viral genes. Through targeted deletions, the virulence or important replication genes which are potentially redundant in tumour cells (due to functional

complementation by transformation) can be deleted for a more successful OV design (Liu et al. 2022).

One of the most prominent examples is Talimogene laherparepvec (T-VEC or Imlygic™), the first Food and Drug Administration (FDA) approved oncolytic virus for clinical use. In order to achieve cancer cell selectivity for the herpes simplex 1 based OV (oHSV1), the infected cell protein 34.5 (ICP34.5) gene was deleted, leading to a loss of pathogenicity and introducing tumour selective replication (Ferrucci et al. 2021; Liu et al. 2003). T-VEC additionally has an ICP47 deletion, which allows for a potentiated viral growth in tumour cells without impacting selectivity through HSV US11 expression. Additionally, deletion of ICP47 inhibits the virally-induced suppression of antigen presentation and therefore enhances the immunogenicity of the virus (Ferrucci et al. 2021).

Tumour selective promotors: Vital genes involved in the viral life cycle can be placed under transcriptional control of cancer or tissue specific promotors, such as telomerase reverse transcriptase or hypoxia-related genes, which only allows the virus to fully replicate within cells with the required phenotype (Bommareddy et al. 2017).

One example is adenovirus, which can be engineered to be tumour selective by placing the essential E1A gene under expression of the E2F-1 promotor. This promotor is only active in cancer cells which display an aberrant retinoblastoma (Rb) pathway (Tsukuda et al. 2002). Another example is herpes virus, which was made selective for the liver and hepatocellular carcinoma by placing the ICP4 gene under transcriptional control of the albumin-enhancer-promotor (Miyatake, Iyer, and Martuza 1997).

Targeted surface proteins: Additionally, oncolytic viruses can further be enhanced to target tumour cells by directly altering their capsid or membrane proteins in order to re-target them towards cancer cells (Maroun et al. 2017).

One example of this strategy includes the capsid modification of an adenovirus type 5 to include TNFα-related apoptosis-inducing ligand (TRAIL). This ensures that the virus is mostly

targeted towards tumour cells, which generally have a higher expression of TRAIL receptors compared to normal cells (Wang et al. 2016).

Directed evolution: Another way of achieving OV cancer selectivity is by directed evolution. In this instance, a pool of viruses are subjected to several rounds of infection in tumour cells at high multiplicity of infection (MOI) to encourage recombination. The infection can be done in cancer cells lines *in vitro* or theoretically could also be done *in vivo* or *ex vivo* to more closely resemble the conditions similar to the *in vivo* tumour. The resulting enriched pools are then challenged with cancer and normal cells, whereby a virus clone is selected which selectively and potently kills cancer cells, while leaving normal cells unharmed. One of the main advantages of this approaches is the lack of human bias based on the current understanding of cancer molecular biology and virology towards the design of the final candidate, but rather the 'agnostic' selection of a robust OV by functional bio selection.

An example of a virus designed with this strategy is Enadenotucirev (EnAd), the oncolytic adenovirus used in this thesis. Details of the directed evolution of EnAd will be described in

1.6.2 Arming oncolytic viruses

Arming OVs with a payload is a potentially effective way of expressing a selected protein in the TME, which could give an added benefit on top of all the strengths of the virotherapy alone. Arming of OVs is especially common with DNA viruses, as they are less prone to mutations during the manufacturing process and therefore are more reliable vectors to deliver payloads. Especially adenoviruses and herpes simplex viruses are well suited to encode a payload, given that both contain genetic deletions when used as OVs and have medium-large DNA genomes. Although enzymes and other proteins have been encoded in OVs in the past, often to potentiate the virotherapy or improve spread, more recent payloads have been related to stimulation of immunotherapies.

Amongst the most popular payloads are cytokines. T-VEC, the first OV to be approved by the FDA, is an oHSV expressing granulocyte-macrophage colony-stimulating factor (GM-CSF) and has shown some success in patients (Ferrucci et al. 2021). Additionally, cytokines such as IL-2 (Carew et al. 2001), IL-15 (Niu et al. 2015) and IFN-γ (Roy et al. 2016) have also been expressed by various oncolytic viruses. Alternatively, IC inhibitors such as anti-PD-1 (Du et al. 2014; Ju et al. 2022) have also been tested for treatment of melanoma, however due to ease, ICIs are nowadays often administered IV alongside oncolytic virus therapies rather than encoded within the virus (Wan, Fernandes, and Seymour 2023). More recently, arming OVs with bispecific proteins and expressing them selectively *in situ* has shown to be promising, with examples including EpCAM BiTEs (Freedman et al. 2017; Wei et al. 2022), PD-L1 BiTEs (Khalique et al. 2021) and epidermal growth factor receptor (EGFR) BiTEs (Fajardo et al. 2017; Graaf et al. 2020).

Arming OVs can potentially add a valuable component of powerful immunotherapies or proteins expressed locally in situ, working together and ideally synergising with the lytic activity of the OVs to eradicate the tumour.

1.6.3 Adenoviruses

Adenoviruses are icosahedral, non-enveloped viruses measuring approximately 90 nm in diameter. Their capsid is mainly made up of 240 hexon proteins with a penton protein at the corner of each icosahedron, which forms the base for the attachment of the trimeric fibre proteins (Wodrich 2019). The genomes of adenoviruses are approximately 36 kbp of double stranded, highly condensed, linear DNA encoding for over 40 proteins with a terminal protein (TP) covalently attached at each 5’ end (Wodrich 2019). Currently some 103 different types or serotypes of adenovirus have been identified, commonly divided into seven groups on the basis of genome homology (A-G, **Table 1.2**). Most adenovirus infections happen between birth and reaching five years (Lion 2014). A high prevalence of certain adenoviral types lead to over 50% of the population showing preexisting adenovirus immunity, in particular against

adenovirus type 5 (Yu et al. 2012). However, certain serotypes such as Ad11 show a very low seroprevalence and therefore potentially make better gene delivery vectors (D'Ambrosio et al. 1982; Stone et al. 2005).

1.6.3.1 Life cycle of adenoviruses

The lifecycle begins with the entry of the adenovirus into an epithelial cell, which generally is mediated through receptors such as Coxsackie and Adenovirus receptor (CAR), CD46 or others depending on the serotype. Upon endosome escape and entry into the cytosol, the viruses accumulate at the nuclear pore complex (NPC) after approximately 45 minutes (Wodrich 2019), where the genome enters the nucleus via the nuclear pore complex (NPC) (Greber et al. 1993) and terminal protein docks it on to the chromatin. E1A is the first protein to be expressed 1-2 hours post infection (Nevins et al. 1979), followed by the expression of the other early proteins encoded in the E1B, E2, E3 and E4 transcription units. These proteins take control of the cell and use its resources to replicate the viral DNA. Subsequently, the transcription of the major late promotor (MLP) is initiated, which consist of one large transcriptional unit with five alternatively spliced subunits encoding the main virion structural proteins, followed by virion packaging and cell lysis.

Table 1.2: Adenovirus serotypes. Modified from Zhao et al. 2021.

Group	Adenovirus Types	Main Entry Receptor
A	12, 18, 31, 61	CAR
B	3, 7, 11, 14, 16, 21, 34, 35, 50, 55, 66, 68, 76-79	CD46
C	1, 2, 5, 6, 57, 89	CAR
D	8, 9, 10, 13, 15, 17, 19, 20, 22-30, 32, 33, 36-39, 42-49, 51, 53, 54, 56, 58-60, 62-65, 67, 69-75, 80-88, 90-103	Sialic acid, CAR, CD46
E	4	CAR
F	40, 41	CAR
G	52	CAR

1.6.3.1.1 Early gene expression

The very first genes to be expressed are E1A and E1B, which have the function to prime the host cell and re-program it towards autophagy and inhibition of apoptosis in order to allow for an optimal viral replication (Rodriguez-Rocha et al. 2011). E1A is heavily involved in controlling the cell cycle through direct binding and sequestration of retinoblastoma, mediating E2F gene expression (Decaprio 2009; Frisch and Mymryk 2002). Therefore, E1A can be expressed in primary cells as a method to immortalise cell lines, such as the widely used HEK293 cell line (Frisch and Mymryk 2002; Ruley 1983). E1B, expressed immediately after E1A, encodes for two proteins (19k and 55k) involved in modifying the cell environment and skew it towards DNA replication, viral protein production and avoidance of apoptosis. Subsequently, the E2 and E3 regions are expressed, whereby E2 encodes proteins essential for the viral DNA replication including the precursor terminal protein (pTP), which binds to the viral DNA and forms a complex with the adenoviral DNA polymerase to create a pre-initiation complex for replication (Charman, Herrmann, and Weitzman 2020; Mysiak, Holthuizen, and Vliet 2004). Meanwhile, the E3 region encodes for proteins involved in the modulation of the immune system of the host, which includes evasion of apoptosis through E3 6.5K interfering in the TRAIL pathway or through E3 19K forming a complex with MHC I to prevent antigen presentation on the cell surface. Additionally, it is responsible for supressing the expression of natural killer group 2 member D (NKG2D) ligands MHC class I polypeptide-related sequence A/B (MICA and MICB), allowing cells to evade NK cell mediated killing (Lichtenstein et al. 2009; Mcsharry et al. 2008). The last of the early genes to be expressed are encoded in the E4 region, whereby the proteins have several different functions ranging from DNA replication, mRNA processing and the regulation of transcription regulation. E4ORF4 for example, binds and activates the protein phosphatase 2A (PP2A) and thus dephosphorylates different target proteins, which includes the inactivation of different transcription factors (Branton and Roopchand 2001; Kleinberger 2015).

1.6.3.1.2 Late gene expression

Following the viral genome replication in the early phase, the major late promotor controlling the late gene transcription is turned on. The late genes are all transcribed as one long mRNA, which is subsequently spliced into the different mRNAs for translation of individual proteins. The genes encoded under the MLP are mainly structural proteins (penton, hexon, fibre and others), but also three non-structural proteins. All of the mature mRNA derived from the MLP contain a tripartite leader sequence (TPL) which enables cap-independent translation and modulates processes such as mRNA stability and nuclear export, resulting in the efficient production of the viral proteins. Subsequently, the capsids self-assemble and are then loaded with the genomes, eventually leading to the lysis of the cells and the release of the progeny virus into the extracellular space.

1.6.4 Oncolytic adenoviruses

As mentioned above, oncolytic adenoviruses are the most commonly used OV in clinical trials. One reason for this could be the relative ease and efficiency of current good manufacturing practice (cGMP): Adenoviruses are double stranded DNA viruses and thus relatively stable for production, and their lack of a membrane means that each packaging cell can produce many thousands of copies. Secondly, with the common deletions of the E3 and E4 regions, they allow for the genetic insertion of genes encoding relatively large or multiple smaller proteins as payloads. Additionally, wildtype adenoviruses often only show only limited replication-related pathology when given IV, making them more attractive as an OV platform. As such, several genetic modifications to adenoviruses were explored in the past in order to obtain a highly cancer selective OV.

1.6.4.1 EnAd development

ColoAd1, clincially known as Enadenotucirev (EnAd), was the first oncolytic virus to be designed using the approach of directed evolution. Briefly, a pool of various adenovirus serotypes (Ad3, Ad11p and Ad16 from group B, Ad5 (group C), Ad9 (group D), Ad4 (group E) and Ad40 (group F)) were mixed for infection at a high viral particle:cell ratio (200:1) in HT29 colorectal cancer cells, in order to provide an environment which encourages viral recombination among the different serotypes. After two passages, the output viruses were incubated with fresh HT29 cells and serially passaged, being harvested at the first signs of the cytopathic effect. Thereafter, the resulting viral pools were compared in potency to the input viral pool and Ad5. From these results, the most potent viral pool was subjected to plaque purification, whereby the most potent virus by MTS assay (defined in the list of abbreviations) was established to be ColoAd1 (EnAd). In order to further characterise EnAd, its replication was evaluated on the human colorectal carcinoma cell lines DLD-1 and HCT116, and also primary human umbilical vein endothelial cells (HUVEC) and human mammary epithelial cells (HMEC), as well as using human *ex vivo* colon cancer and normal tissues from patients. The data showed high selectivity for virus replication within tumour cells in both cell lines and primary cultures with little to no replication found in normal colorectal tissue or normal cell lines (Kuhn et al. 2008a).

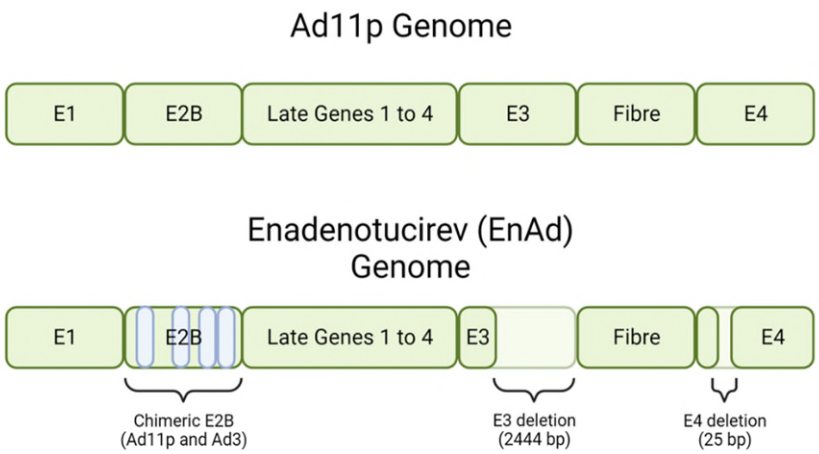

Figure 1.6: EnAd genome compared to the genome of Ad11p. As can be seen, most of the EnAd genome is identical to the Ad11p genome, with exception of the chimeric E3B (containing regions from Ad3), the big E3 deletion (2444 bp) and a smaller E4 deletion (25 bp). This Figure was created using BioRender.

1.6.4.2 EnAd genome

The genome of EnAd has a total length of 32,235 base pairs and is a chimera between Ad3 and Ad11p. As seen **Figure 1.6**, the majority of the genome is derived from Ad11p, with a Ad11p/Ad3 chimeric E2B region. Additionally, there is a large deletion in the E3 region of 2444 bp and a smaller deletion of 25 bp in the E4 region (E4ORF4). Conveniently, this rather large 2444 bp deletion allows for a payload to be added.

Due to EnAd not being designed rationally by targeted deletions but rather bioselected by directed evolution, it is difficult to exactly know why the deletions and chimeric proteins that occurred makes the virus oncolytic. EnAd, alongside many other viruses, shares a natural preference for cancer cells, as aberrant cells often already exhibit overlapping hallmarks with viral infections, such as evasion of apoptosis and a deregulated metabolism (Seymour and Fisher 2016). It is thought that particularly the metabolic aspect is important for the cancer specificity of EnAd. As cancer cells naturally use glutamine as a source for intermediary metabolites and biosynthetic precursors, it has been shown that it also enhances the viral activity of EnAd (Dyer et al. 2019). It is possible that the genetic changes in EnAd render it unable to activate glutaminolytic metabolism and therefore the virus only replicate in cells with a pre-existing high glutamine metabolism, although this is not yet proven.

1.7 Conclusions and hypothesis

In conclusion, the ECM is a vital player in the development, growth and invasion of cancer. Efforts to target the ECM in tumours have so far been few in number and relatively unsuccessful, not least due to the lack of tumour specific markers.

Most attempts targeting ECM components directly (such as EDB-FN) were thus far faced with a trade-off between minimising side effects and the abundance of the ECM target present in the tumour (i.e. the number of binding sites). This low abundance might also influence the low clinical efficacies observed using these therapies. Therefore, we hypothesise that a locally

expressed bispecific consisting of an anti-CD3 scFv and an ECM-binding domain can be immobilised in the TME and activate T cells to exert cytotoxicity towards cancer and stromal cell. Thus in Chapter 3, the ability of an anti-CD3 motif to induce T cell activation is explored, together with its ability to induce ‘bystander cytotoxicity’ against cells to which the T cell has not formed an immunological synapse. In the subsequent Chapter 4 and 5, bispecifics containing anti-CD3 motifs and targeting glycosaminoglycans and collagen I were produced and validated *in vitro* and with *ex vivo* patient samples. Finally, the specific and local expression of said bispecifics though an adenoviral OV was evaluated in Chapter 6.

The specific and local expression though an OV eliminates the aforementioned trade-off and allows the targeting of abundant ECM components, potentially leading to a higher efficacy.

2 Materials and methods

2.1 Tissue culture

2.1.1 Cell lines and maintenance

General product codes for cell culture items can be found in the table below. Cell lines were obtained from the sources mentioned in the table below and frozen down in freezing medium (10% DMSO (Merck Group, Germany), 90% FBS (Thermo Fisher Scientific, USA)), and kept in liquid nitrogen storage or at -80°C for short term storage. Cells were revived swiftly by putting the tubes in a 37°C water bath and then washed generously with pre-warmed corresponding medium. Revived cells were kept in a humidified incubator at 37°C with 5% CO_2. Cells were split at confluencey several times per week as indicated below by washing 1x with PBS (Thermo Fisher Scientific, USA) and adding trypsin to remove adherent cells. Cells were then re-suspended in the appropriate medium containin FBS and added to a new flask. After two-three months of using, cells were thrown away and a new, low passage vial was thawed for further experiments.

Table 2.1: Cell lines used in this thesis.

Cell Line	Culture Condition	Source	Splitting frequency	Mycoplasma Test
HEK293a	DMEM 10% FBS	Gifted from Oxgene	1/10 every two days	Periodically, negative
DLD-1	DMEM 10% FBS	Liquid Nitrogen stock Seymour Lab, ATCC	1/10 every two days	Periodically, negative
PANC-1	DMEM 10% FBS	Kindly provided by the Cornelissen Lab	1/10 every two days	Periodically, negative
PSN-1	RPMI 10% FBS	Kindly provided by the O'Neill Lab	1/10 every two days	Periodically, negative
NHDF	DMEM 10% FBS	Liquid Nitrogen stock Seymour Lab, ATCC	1/5 every five-seven days	Periodically, negative
A549	DMEM 10% FBS	Liquid Nitrogen stock Seymour Lab, ATCC	1/10 every two days	Periodically, negative

Table 2.2: Common tissue culture reagents.

Name	Company	Product code
Dulbecco's Modified Eagle's Medium - high glucose	Merck Group, Germany	D5796-500ML
RPMI 1640 Medium, Gibco	Thermo Fisher Scientific, USA	11875093
PBS, pH 7.4, Gibco	Thermo Fisher Scientific, USA	10010023
Trypsin-EDTA (0.25%), phenol red, Gibco	Thermo Fisher Scientific, USA	25200056
GlutaMAX™ Supplement, Gibco	Thermo Fisher Scientific, USA	35050061
Penicillin-Streptomycin (10,000 U/mL), Gibco	Thermo Fisher Scientific, USA	15140122
Insulin-Transferrin-Selenium (ITS -G) (100X)	Thermo Fisher Scientific, USA	41400045
Fetal Bovine Serum, Gibco	Thermo Fisher Scientific, USA	10500064
OptiMEM, Gibco	Thermo Fisher Scientific, USA	31985062
Lipofectamine 2000	Thermo Fisher Scientific, USA	11668019
Cell Dissociation Buffer, enzyme-free, PBS, Gibco	Thermo Fisher Scientific, USA	13151014

2.1.2 Transfections

Product codes are listed in the table above. Mammalian cell transfections were conducted with the reagent conditions as shown below. In short, two tubes with OptiMEM (Thermo Fisher Scientific, USA) were set up, one was mixed with the DNA and the other one with the Lipofectamine 2000 (Thermo Fisher Scientific, USA) and then left at room temperature (RT) for 5 minutes. Thereafter, the tubes were mixed and left at RT for 20 minutes. In the meantime,

the cells were washed carefully 2x with OptiMEM, before the DNA-Lipofectamine mixture was added. Transfections were incubated for 4-6h in the cell incubator before the supernatant was removed and FBS free medium was added to the cells. If proteins were not harvested, medium containing 10% FBS was added instead.

Table 2.3: Transfection set-up.

Format	DNA (ng/well)	Lipofectamine 2000 (µl), 1:3 ratio	Total OptiMEM (DNA+Lipofectamine)
96-well plate	130	0.4	80 µl (40 µl + 40 µl)
24-well plate	770	2.31	500 µl (250 µl + 250 µl)
6-well plate	2'500	7.5	1000 µl (500 µl + 500 µl)
T75 flask	20'000	60	10 ml (5 ml + 5 ml)

2.1.3 Protein production in HEK293a

Protein production was carried out with HEK293a cells in 6-well plates or in T75 flasks. After transfection, a minimal amount of serum free medium was added and incubated for 2-3 days. Supernatant was harvested and spun down to remove any debris or cells at 500g for 10 minutes at 4°C. Subsequently, the supernatant was concentrated using appropriate Amicon spin columns (Merck Group, Germany, #UFC905008), making sure that the cutoff was at least two times as big as the protein for 40 minutes at 4000g at 4°C. The concentrated supernatant was aliquoted into smaller tubes and kept at -20°C or -80°C for long-term storage.

2.1.4 XTT viability assays

XTT viability assay was performed using the kit provided by (Roche Switzerland, #11465015001). In short, the cells were washed with PBS once before adding the XTT solution. XTT solution for a 96-well plate was prepared by mixing 100 µl of solution A with 5 ml of solution B in 10 ml of PBS, resulting to 150 µl/well. The cells were then incubated for up to 4h in the cell incubator. Plates were read at 450 nm absorbance using a VarioScan (Thermo

Fisher Scientific, USA, #VL0000D0). Results were normalised to the untreated control unless indicated otherwise.

2.2 Cellular assays

2.2.1 xCELLigence

The xCELLigence (Agilent, USA) machine is used to measure impedance over time and thus allows for a quantification of live cells adhering to the plate. For all experiments in this thesis, treatment and cells were added to the plate before putting the plate in the xCELLigence machine and immediately taking the first timepoint. Subsequently, the machine was left to run for up to six days measuring the impedance, before analysing the data using GraphPad Prism.

2.2.2 IncuCyte analysis of bispecific and viral cytotoxicity

For the bispecific cytotoxicity, a 24-well plate was coated with collagen I and incubated with bspecific and controls at 10 nM, as mentioned in section below. Subsequently, 50,000 DLD-1 cells and 250,000 T cells were added, alongside with a 1:400 dilution of the CellEvent™ Caspase-3/7 Green Detection Reagent (in DMSO, Thermo Fisher Scientific, USA, #C10723). The experiment was incubated for five days in the machine and analysed with the supplied software.

For the traffic light virus plaque assay, a 24-well palate was seeded with 120,000 cells A549 and infected the subsequent day with 10 virus particles per cell for 5h. After that, the supernatant was removed and overlayed with 1.4% of low melting point agarose (Thermo Fisher Scientific, USA, #16520-050) mixed with 2x DMEM (DMEM powder, Thermo Fischer Scientific, USA, # 12800082) and 2% FBS (1:1 mixture, total of 0.7% of agarose concentration in the end). The plates were left to dry and moved to the IncuCyte for five-day analysis. Images were analysed with the supplied software.

2.3 Molecular biology

2.3.1 Cloning and Polymerase Chain Reaction (PCR)

PCRs were performed with the cycles and reactions showed below. In short, primers were designed using the NEB Builder Website for Gibson Assembly and ordered from IDT (USA). Phusion 2x Mastermix (Thermo Fisher Scientific, #F531L) was used.

Table 2.4: Colony PCR reaction.

Reagent	µl
2x Mastermix Phusion Thermo Fisher	25
Primer Forward (10 µM)	3
Primer Reverse (10 µM)	3
Input DNA (1 ng)	1
H_2O	18
Total	50 µl

2.3.2 Agarose Gels and Gel extraction

Table 2.5: Steps of a PCR.

Step	Function	Temeprature in °C	Time in mm:ss
Step 1	Denaturation	98	00:30
Steps 2-4, Repeat	Denaturation	98	00:20
30x	Annealing	45-72	00:20
	Elongation	72	30 sec/kb
Step 5	Final Elongation	72	07:00
Step 6	Hold	4	For ever

Prior to gel extractions, the PCRs were run on an agarose gel. The agarose gel was cast by dissolving 0.8% of agarose powder (Sigma Aldrich, USA, #A9539-500G) in 1x TAE buffer including 1:10’000 gelred (Biotium, USA, #41003) for visualisation. The gel was then subsequently left to cool and harden in a mould. DNA samples were then mixed with 6x loading buffer (New England Biolabs (NEB), USA, #B7025) and loaded in the wells. The gel was run

for 40-60 minutes at 100 V in 1x TAE buffer. For visualisation, the gel was transferred to the BioRad imager (BioRad, USA) and the gel red signal was acquired.

Table 2.6: Colony PCR reaction.

Reagent	µl
2x OneTaq NEB Polymerase	5
Primer Forward (10 µM)	1.5
Primer Reverse (10 µM)	1.5
Input DNA (bacterial colony)	-
H_2O	2
Total	10

If proceeding with gel extraction, the gel was transferred onto the imaging tray with a protective cover, whereby the bands could still be visualised. The bands were then cut using a scalpel and transferred into a 2 ml tube. Thereafter, the protocol for a gel extraction kit by NEB (NEB, USA, #T1020S) was followed according to manufacturer's instructions.

2.3.3 Colony PCR

Colony PCRs were performed by pipetting the 2x mastermix from NEB OneTaq (NEB, #M0480) shown below and by picking a colony from a plate with a pipet tip and then dab it in the tube containing the mastermix.

Table 2.7: Colony PCR steps.

Step	Function	Temeprature in °C	Time in mm:ss
Step 1	Denaturation	94	00:30
Steps 2-4, Repeat 30x	Denaturation	94	00:20
	Annealing	45-72	00:20
	Elongation	68	1 min/kb
Step 5	Final Elongation	68	05:00
Step 6	Hold	4	For ever

2.3.4 Colony PCR reaction

2.3.5 HiFi Gibson assembly

HiFi assembly was performed using the NEB 2x HiFi Assembly Master mix (NEB, #E2621L), by pipetting as indicated below and incubation for 15 min-1h at 50°C.

2.3.6 HIFI Reaction

Table 2.8: HiFi Reaction.

Reagent	µl
HiFi DNA Assembly NEB	5
DNA Fragment Ratio 3 (molar ratio to backbone)	1.5
DNA Backbone Ratio 1 (plasmid approx. 100 ng)	1.5
H_2O	-
Total	10

2.3.7 Bacterial transformation

Bacterial transformation was done using 10β competent *E. coli* bacteria (NEB, USA, #C3019H). Approximately 2 µl of the HiFi reaction was incubated for 20 minutes on ice with 50 µl of the competent bacteria before heat shock. Heat shock was performed at 42°C for 42 seconds, before the cells were incubated for 5 minutes on ice immediately afterwards for recovery. 450 µl of SOC (Thermo Fisher Scientific, USA, #15544034) medium was then added to the tubes and the tubes were incubated at 37°C for 1h. Afterwards, the bacteria were spread on LB Agar plates containing either ampicillin (Sigma Aldrich, USA, #59349-100MG, 50 µg/ml working concentration) or kanamycin (Merck Group, Germany, #K1377-1G, 50 µg/ml working concentration). The plates were then incubated at 37°C overnight before colonies could be picked for colony PCR or plasmid minipreps.

Table 2.9: Sanger sequencing reaction.

Reagent	µl
Primer 5 nM	5
DNA 500 ng	x
H_2O	x
Total	10

2.3.8 Plasmid preparation

Mini- (NEB, USA, #T1010L), Midi- and Maxipreps (Qiagen, Germany, #12145) were performed according to manufacturer's protocol. Prior to each Miniprep, 400 µl of the bacteria culture was mixed with 400 µl of 50% gluycerol (Merck Group, Germany, #G5516) in ddH_2O (sterile) and kept at -80°C for long term storage.

2.3.9 Sanger sequencing

Sanger sequencing was conducted by Genewiz (Azenta, USA) after pipetting and submitting reactions as shown below.

2.3.10 Cell lysate and BCA

Supernatant for western blot (WB) were processed as described before. After supernatant harvesting, RIPA buffer (Thermo Fisher Scientific, #89900) with protease inhibitors (Thermo Fisher Scientific, USA, #78430) was added to the cells in the well and incubated for 5 minutes at RT. The mixture was added into a tube and spun at 10,000 RPM on a tabletop centrifuge at 4°C. The clear supernatant was then transferred into a new tube.

A BCA (Pierce BCA Protein Assay Reagent A, Thermo Fisher Scientific, USA, #23221) was performed for the lysates to normalise protein loading. Therefore, the manufacturers protocol of the Pierce BCA (Thermo Fisher, #23225). In short, the BSA standard was made up to concentrations starting at 1000 µg/ml down to 50 µg/ml and several sample dilutions were made in water. Subsequently, 25 µl of each sample and standard were added to a flat bottom

96-well plate. A working solution of 50:1 ration of reagent A and B was prepared and 200 µl was added to each well, including blanks containing water only. All wells were mixed quickly and the plate was wrapped in aluminium foil and protected from light at 37°C for 30 minutes. The plate was removed and left to cool down to RT for 5-10 minutes, before the reading at 562 nm absorbance was performed on the VarioScan (Thermo Fisher Scientific). All results were blank-absorbed and plotted in Excell in order to interpolate the unknowns.

2.3.11 Western Blot

Prior to western blotting, an SDS PAGE was performed using the BioRad Gel chambers BioRad, USA) and pre-cast SDS Gels from BioRad, 4%-20% (BioRad, USA, #4568093EDU) unless stated otherwise. 8 µl of the prestained protein ladder PageRuler™ (Thermo Fisher Scientific, USA, #26616) and approximately 20 µg of protein per lane of lysate and 10 µl of concentrated supernatant. Samples were mixed with 6x Laemmli buffer (Thermo Fisher Scientific, USA, #J61337-AD) to achieve 1x. Subsequently, samples were boiled at 98°C for 10 minutes to denature the proteins, before they were loaded onto the gel and run in the chamber containing SDS running buffer for 60-90 minutes at 80 V for the first 20 minutes and then at 120 V for the remainder of the time.

After running, the gel was removed from the cassette and transferred onto a pre-packed transfer pack (BioRad, USA, #1704158) using the Transblot system (BioRad, USA) with the 7 minute quick transfer setting. Equal loading was confirmed using ponceau staining and then the membranes were blocked for 30 minutes at RT using the blocking buffer from BioRad (BioRad, USA, #12010020). The FLAG detection antibody (Direct Blot FLAG Biolegend as indicated in the antibody list at the end of this section) was added in 1:15,000 dilution and incubated with the membrane overnight under movement. The next day, the membrane was thoroughly washed using PBST (0.1%) for 3x for 10 minutes at RT before visualisation. Visualisation was done using the Super Signal West Dura (Thermo Fisher Scientific, USA, #34075) for a maximum of 2 minutes, before the solution was washed away and the

membrane was imaged for chemiluminescence, and a picture of the ladder was taken on the BioRad imager.

2.4 Immunological methods and staining

2.4.1 FLAG ELISA

Quantification of the produced protein was conducted with a FLAG ELISA. For this, an ELISA plate was coated over night with the FLAG antibody (Genscript, USA, #A00187) at 2.5 µg/ml, 50 µl per well in PBS. The next day, the plate was washed 2x with PBST (0.1%) and then the plate was incubated with 100 µl/well of blocking buffer containing PBS with 1% BSA (Sigma Aldrich, USA, #MFCD00130384) for 1h at RT on a shaker. The plate was again washed 2x with PBST (0.1%) and the samples were added in different dilutions in blocking solution. As standard, the C-terminal FLAG BAP (Sigma Aldrich, USA, #P7582-100UG) was added in various dilutions for 1h at RT on a rocker. The plate was washed for 3x with PBST (0.1%). As last step, the FLAG-HRP directblot antibody was added 1:15,000 dilution in blocking buffer at 100 µl per well for 1h at RT on the shaker. The plate was subsequently thoroughly washed 6x with PBST (0.1%), before 100 µl of TMB substrate (Thermo Fisher Scientific, USA, #N301) was added. The plate was then incubated in the dark for 2-20 minutes and stopped when the top standard wells reached a dark-blue colour. Reactions were stopped by addition of 50 µl of 0.18 M sulphuric acid (Sigma Aldrich, USA, #339741). The values were immediately measured at 450 nm absorption in a plate reader. Blanks were subtracted from all the wells in order to obtain the proper interpolated values using Microsoft Excell and GraphPad Prism.

2.4.2 Fow cytometry

2.4.2.1 Cell staining

Cell staining was performed in a sterile cell culture hood an in 96-well plates with a U-bottom. Therefore, cells were harvested and washed once with PBS buffer (200 µl/well) and centrifuged at 450g for five minutes (same for the rest of the spins in this protocol). Subsequently, the supernatant was removed by quickly but firmly turning the plate upside down in a bucket filled with tissues and virkon or chemgene. The cells were then re-suspended in MACS buffer (50 µl/well) containing 1:100 FcR blocking solution (Miltenyi, USA, #130-059-901) and incubated for ten minutes at RT. In this time, half of the contents of the live/dead control well was removed and incubated for three minutes at 98°C, before adding it back to the well after it had cooled slightly. The cells were then topped up to 200 µl/well with MACS buffer and centrifuged. The cells were then incubated with the antibody solution and, containing MACS buffer and the indicated dilution of staining antibody (appendix), 50 µl/well for 15 minutes in the dark at RT. Thereafter, the wells were topped up to 200 µl/well with MACS buffer and centrifuged. The samples were then washed once more by adding 200 µl/well MACS buffer, resuspending the cells followed by centrifugation. The cells were then incubated in 100 µl/well of 10% formalin (Sigma Aldrich, USA, #HT501128-4L) for fixation for ten minutes at RT in the dark. The wells were then topped up to 200 µl/well and centrifuged one last time. Finally, the cells were re-suspended in 205 µl/well of MACS buffer before measurement at the flow cytometer. Results were analysed using Flow Jo software.

2.4.2.2 Intracellular staining for flow cytometry

Prior to the intracellular staining, an extracellular staining was performed, however, instead of blocking with 10% formalin, the step was carried out using 4% PFA (Sigma Aldrich, USA). Subsequently, the cells were washed twice with 1x Perm/Wash (Biolegend, USA, #421002) diluted to 1x in ddH_2O, 200 µl per well. Then, the antibodies were diluted in Perm/Wash

solution and stained for 15 minutes at room temperature in the dark (50 µl per well). The cells were washed 2x with Perm/Wash and re-suspended in 205 µl of MACS buffer for measurement.

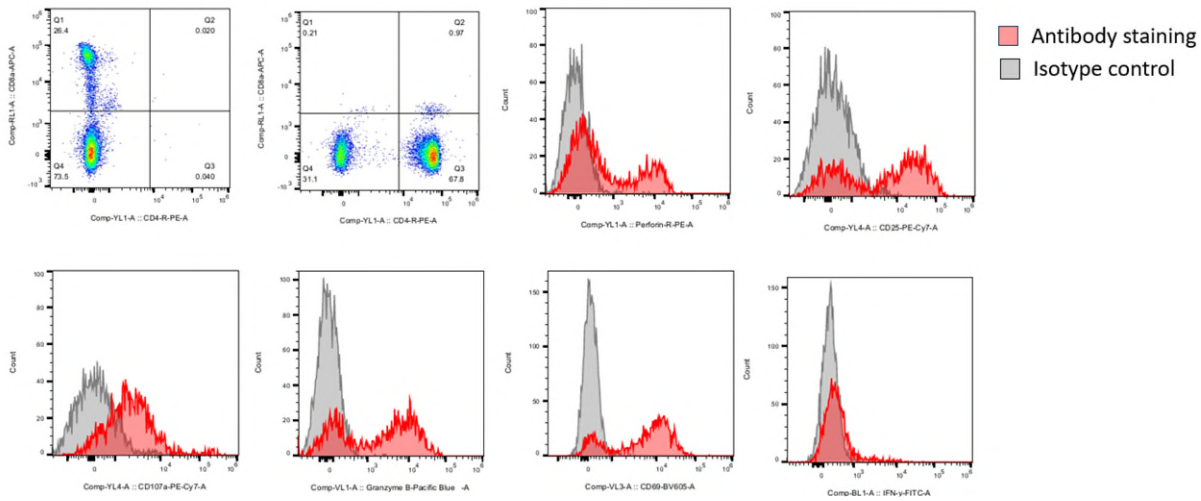

Figure 2.1: Isotype controls for T cell activation assays.

2.4.2.3 Flow cytometry measurement

All flow cytometry in this thesis was performed using the NxT Attune™ with four lasers (Thermo Fisher Scientific, USA). The machine was daily calibrated and tested using the performance beads provided. Compensation was performed using single stains of either cells or compensation beads (Thermo Fischer Scientific, USA, #01-222-42) with the dilutions provided in the appendix.

As controls, either isotype control antibodies in the same dilutions were added to the sample or an FMO containing the isotype of the antibody in the proper concentration was prepared. The different relevant isotype controls are shown below. Analysis was conducted on FlowJo (Becton Dickinson, USA).

2.4.3 IFN-γ ELISA

IFN-γ ELISA was conducted using the ELISA MAX kit (BioLegend) according to manufacturer's conditions. For the tumour slices, the samples were collected at days 0, 2, 3 and 5 and frozen at -20C until analysis. The samples were then thawed and spun down for 10 minutes at 450g, before being added to the pre-coated ELISA plates. After detection, samples were measured at 450 nm and at 570 nm, whereas the latter was subtracted from the first value for correction. Virus samples were diluted approximately 1:20-1:25, free protein samples were diluted 1:3-1:5.

When measuring IFN-γ release from primary colorectal samples, the supernatant after 5 days was collected, spun down (450g for ten minutes) and frozen at -20°C until needed. Upon thawing, the supernatant was spun at 450g for 10 minutes and proceeded similarly to above. Samples were diluted between 1:5-1:30.

2.4.4 LegendPlex

LegendPlex assay (Human CD8/NK panel, BioLegend, USA, #741187) was performed according to manufacturer's specifications. In short, collected supernatants from slices were kept at -20°C until analysed. Samples were thawed and spun down at 450g for 10 minutes, before the supernatant was transferred to a new plate. Then the samples and standard of the kit were mixed and prepared as described in the protocol. The beads were measured using the NxT Attune (Thermo Fisher Scientific) and analysed using the LegendPlex Software provided in the kit.

2.4.5 General T cell activation assay

T cell activation assays were performed using PBMC-derived T cells. Therefore, frozen lymphocytes were thawed the night before and cultured at 6 million cells/ml overnight in RPMI-1640 10% FBS. Prior to the experiment, the cells were isolated using the pan T cell isolation

kit (Miltenyi, USA, #130-096-535) or CD4 T cell isolation kit (Miltenyi, USA, #130-096-533) according to manufacturer's instructions. T cells were always added in a 5:1 ratio to target cells for activation assays. Assays were performed in RPMI-1640 with 2% FBS and incubated for one to five days before harvesting and analysis.

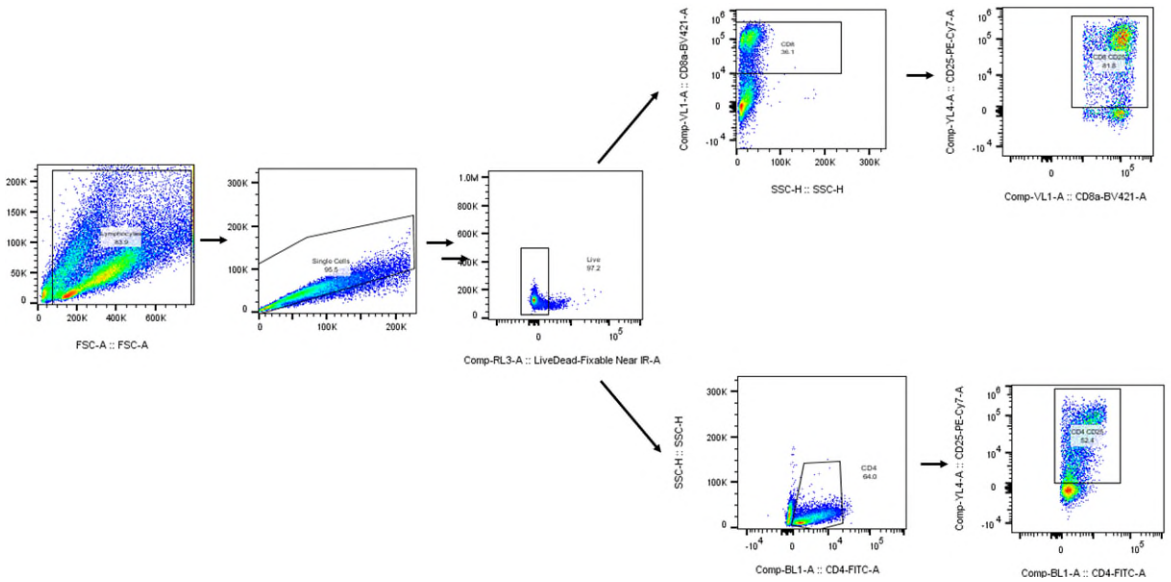

Figure 2.2: Gating strategy for T cell assays.

2.5 Virus cloning and virology

2.5.1 EnAd cloning and DNA

The EnAd backbone was first produced in bacteria and a Maxiprep was done according to manufacturer's recommendations (Quiagen, Germany). Subsequently, 15 µg of the DNA was digested with SbfI and AsisI (NEB, USA) for 16h over night at 37°C in Cutsmart buffer, leaving a linearised backbone. The backbone was then purified and used for HiFi assembly (NEB, USA). Prior to the HiFi assembly, the insert was amplified using the primers indicated in the appendix. Thereafter, the products were run on a gel and gelpurified, before mixing it with the backbone at a 15:1 (insert:backbone) ratio and incubated for 1h. Subsequently, 2 µl of the reaction was transferred into a tube containing 10β *E coli* and transformed as described above.

Once plated and grown over night on kanamycin plates, a colony PCR was performed and the positive colony was grown in a miniprep, sequenced and then a maxiprep with the same colony was set up. The plasmid was then harvested the next day according to manufacturer's recommendations. Thereafter, the plasmid was linearised with Asc I (NEB, USA) over night at 37°C, before a transfection was performed. Because of the large size of the viral backbone, a T25 flask with HEK293a (1.2 Mio seeded cells) was transfected according to the protocol above, but with a 1:4 ratio of DNA to Lipofectamine 2000. After approximately 5-12 days, plaques formed and the cytopathic effect could be observed, and another 5 days later the entire flask had plaqued and was therefore harvested (cells and supernatant together).

2.5.2 Clonal selection of EnAd

For each construct, the collected virus mixture was freeze-thawed three times, then spun down at 500g for ten minutes and the supernatant was removed and frozen down. Then, a $TCID_{50}$ (described in the next paragraph) was performed two times in a row in a 96 well plate containing A549 (20'000 per well), with dilutions allowing for wells containing only one plaque. The well containing only one plaque was collected five days post infection, whereby it served as the starting point for a second $TCID_{50}$ which was carried out similarly to the first one. Subsequently, the well containing a single plaque were collected and a T25 flask (1.2 Mio A549) was infected with each well. After five days, the flasks were collected (cells and supernatant), freeze thawed 3x and spun at 500g for ten minutes and aliquoted.

2.5.3 Titration of EnAd

OVs were titred in a 96-well plate seeded with 20,000 A549 cells per well. The next day, the virus was diluted 1:100,000 as initial dilution before doing eight further 1:10 dilutions for each row of the 96-well plate. Ten wells were used for the calculation, whereas the last two wells were uninfected controls. After five days, the number of wells containing at least one plaque were counted and the multiplicity of infection (MOI) could be calculated using:

$$\text{Titre (TCID50/mL)} = 10^{1 + D(S - 0.5)}$$

D = log(dilution factor)

S = sum of the ratios of wells with infection to infection-free wells

2.5.4 Viruses used in this thesis

Table 2.10: Viruses used for experiments.

Name	Insert	Promoter	Titre (in A549)	Source
EnAd Parental	-	-	$1.27x10^9$	Emma Page, Seymour lab
EnAd LAIR-2 (L)	LAIR-2 full length	CMV	$3.94x10^9$	Selfmade
EnAd aCD3 (N)	Anti-CD3 scFv	CMV	$1.2x10^9$	Selfmade
EnAd LAIR-2xaCD3 (K)	LAIR-2xaCD3 bispecific	CMV	$5.74x10^8$	Selfmade
EnAd CMV GFP	GFP	CMV	$5.15x10^9$	Emma Page, Seymour lab
Traffic light virus	UnaG, mCherry	CMV, SA (MLP)	Concentration in VP/ml $6.27x10^{12}$	Egon Jacobus, Seymour lab

2.5.5 EnAd T cell activation assay on collagen I coated plates

96-well plates were coated with collagen I as described in the next section (96-well plate). Subsequently, target cells (10,000) and 1:5 ratio T cells (50,000) were added to the wells together with the appropriate amount of virus. T cell activation was measured after 2 days, whereas T cell cytotoxicity was measured after three days.

2.6 Clinical samples

Several different clinical samples were collected and processed in this thesis in order to use the cells in *in vitro* or *ex vivo* model systems.

2.6.1 Human blood processing

Leukocyte cones were ordered and collected from NHSBT (NHS, Oxford) under the ethics number REC: 19/LO/1848, Start: 01/10/2019, End: 01/11/2024. Once in the lab, the cone was opened and drained in a tube. Subsequently, the blood was diluted with PBS containing 2% FBS to 30 ml, which is then added into two SepMate tubes (Stemcell Technologies, Canada), 15 ml in each containing 15 ml Ficoll (Cytivia, Sweden, #17544203) in the bottom of each. Centrifuge at 1200g for ten minutes with full acceleration and brakes. Collect the PBMC layers and wash it once with 2% FBS PBS in two 50 ml falcons and spin at 500g for five minutes. Perform an RBC lysis (Qiagen, Germany, #158904) by resuspending the pellet in 10 ml RBC solution by combining the two tubes of PBS and leave for ten minutes in the fridge. Fill up the tube with 2% FBS PBS and spin for 500g for five minutes. Then resuspend in PBS and continue with Percoll steps.

An osmolarised 46% of 285 mOsm Percoll was created by adding 11.1 ml of Percoll (Cytivia, Sweden, #17544501) and 0.9 ml of 10x PBS to make up Percoll/PBS solution, which is then mixed by adding 115 ml with 13.5 ml of exact 10%FBS RPMI-1640 medium. 6 ml of this solution was then added to four separate 15 ml falcons, where a 5 ml solution of PBMCs in exact 10% FBS RPMI was overlayed, very carefully. The tubes were then spun at 950g for 30 minutes with acceleration on 5, deceleration on 0. Collect the monocyte layer (middle) and lymphocyte pellet (bottom pellet) and proceed. The lymphocytes were washed once more with PBS before being re-suspended in freezing medium (10% DMSO and 90% FBS, 30 million per tube) and frozen in the -80°C using a cryo-container for later use.

2.6.2 Lymphocyte recovery and T cell isolation

Lymphocytes were revived by thawing the tubes quickly in the hands and washing once generously with RPMI 10% FBS (pre-warmed). Cells were then kept overnight in a T25 flask upright, at a concentration of approximately 5 million cells per ml in 10% FBS RPMI. Cells were revived at least 16 hours prior to isolation and experiment, as DMSO might impact on T cell activation (Holthaus et al. 2018).

2.6.3 Malignant Ascites fluid and cells

Malignant ascites fluids and cells was obtained from Churchill hospital Oxford under the ethics number: REC: 19/SC/0173 ORB, Ascites – ORB 20/A013, Start: 11/12/2018, End: 11/12/2023. Drainage bags containing the fluid were collected and brought to the laboratory for further processing. The fluid was collected by spinning twice at 400g at RT for ten minutes to make sure there are no cells in the fluid and stored at -20°C. The cells were obtained by spinning and combining all the fluid in 500 ml tubes. The supernatant was discarded and the cells were collected in PBS and spun down at 400g for ten minutes. Then, an RBC lysis step was performed by adding 10 ml of RBC lysis buffer to the cells and incubate them for ten minutes at 4°C. The tube is then topped up with PBS and centrifuged as before. Should there still be erythrocytes visible, the steps from the RBC lysis can be repeated up to two more times. Thereafter, the cells are washed two more times with PBS, before counting with trypan blue and freezing them down similar to lymphocytes described above, 20 million per tube. The samples used in this thesis were processed by Dr Sarah Larkin and Gkentiana Zavalani.

2.6.4 Primary human colorectal samples

Primary human colorectal cancers were kindly receive in collaboration with Prof Dr Simon Buczacki under ethics number: REC: 16/YH/0247, Start: 11/11/2021, End: 11/11/2026. Consenting of patients was done prior to surgery. Samples were collected freshly from surgery

and washed several times in tubes containing PBS and PBS with 1x Penicilin/Sterptomycin with a single use Pasteur pipette in a sterile hood.

2.6.5 Gentle MACS dissociation

Subsequently, tumour samples were transferred to a petri dish containing 5 ml of RPMI-1640 medium without FBS. The sample was then cut into very small pieces using plyers and a sharp scalpel. For the dissociation, the MACS cell dissociation kit (Miltenyi, USA, #130-095-929) was used. Therefore, a MACS C-tube (Miltenyi, USA) was opened and 200 µl enzyme H, 100 µl enzyme R and 25 µl enzyme A were added. Additionally, all the small tumour pieves were added to the tube along with 4.7ml of RPMI-1640. The tube was then closed and inverted before adding to the machine, making sure that the contents are not caught in the top of the tube. Then the tube was placed in the GentleMACS dissociator (Miltenyi, USA) and the program for soft tissue disruption (1h) was selected (37_h_TDK_1). After the completion, the cells wre strained in the 70 µm strainer (Thermo Fisher Scientific, USA, #352350) before washing 1x with PBS and centrifuged at 400g for 5 minutes. In case there are RBCs, an RBC lysis step for ten minutes in the fridge can be performed followed by a wash. Cells were washed with PBS and counted before centrifugation using trypan blue. The cells were in the end be re-suspended in slice medium (RPMI-1640 containing 1x Glutamax, 1xP/S, 1x ITS and 10% FBS).

2.6.6 Colorectal liver metastasis

Colorectal liver metastases were collected from the theatre just after surgeries at the Churchill Hospital in Oxford under ethics number: EC: 21/YH/0206– 17/LS/PJ, Start: 11/11/2021, End: 11/11/2026. Consenting was done by Katy Gordon-Quayle and Martin Pirkl. Samples were subsequently brought to Pathology in the John Radcliff Hospital, Oxford, for assessment by pathologists. Thereafter, the sample was taken back to the lab, where the tumour and adjacent liver tissue were further processed in a sterile hood in RPMI-1640 medium on a petri dish.

Especially normal liver tissue was removed from the tumour to avoid cross-contamination of normal liver immune cells.

2.6.7 Vibratome slicing of liver metastases

In order to cut the liver metastases into slices, the tumour and normal adjacent tissue were cut into 5 mm x 5 mm pieces and mounted on a flat piece of thin plastic using super glue. After mounting, the tissue blocks were embedded in 4% of low melting point agarose (LMP) and left to harden for ten minutes at RT. Subsequently, the tissue blocks were fixed using super glue to the stage, and the stage was placed in the holder. The holder was then filled with cold RPMI (no FBS), whereas the outside of the stage was filled with ice to keep the cutting process as cold as possible. The stage was then moved into the vibratome, whereas the blade was mounted after the stage is installed. After adjusting the height, the slices were cut in 250 µm thickness and collected in a 24-well plate containing 500 µl of RPMI-1640 with 1x P/S. The slices originating from the same block were numbered in order to be able to trace them back. Subsequently, the plate was moved in a sterile hood, where the medium was replaced with slice medium (RPMI-1640 containing 1x Glutamax, 1xP/S, 1x ITS and 10% FBS), and the slices were stored in the cell incubator for further experiments.

2.6.8 Tumour slice and free protein treatment

Tumour slices were added to a 24 well plate with 500 µl of slice medium after slicing and kept overnight in the incubator. The next day, the first sample of supernatant was taken in order to measure the background activity (day 0). Thereafter, the samples were incubated with the appropriate amount of protein as indicated, in 1 ml of medium per well. Day 2, day 3 and day 5 samples were taken, 250 µl each (120 µl for IFN-γ ELISA and 120 µl for LegendPlex analysis). Results in the end were adjusted for the loss of volume, as it was not replenished after each sample was taken in order to keep the treatment the same. Samples were then analysed using ELISA and LegendPlex.

2.6.9 Tumour slice virus infection and imaging

See above for the method. It was assumed that each slice contained approximately 1 million cells, whereas each slice was infected with an MOI of 10. For the traffic light virus, 100 virus particles (vp)/cell were treated as MOI of 1, so 1000 vp/cell were used for infection. Images were taken with Zeiss 780 confocal microscope and the 10x objective.

2.7 Imaging

2.7.1 Microscopy

General microscopy regarding cell culture to check on morphology on a day-to-day basis, and rudimentary fluorescent protein assessment (no pictures) was conducted on two light microscopes. More detailed microscopy such as confocal and fluorescence microscopy was done at the Microscopy Facility in the Department of Oncology.

2.7.2 Confocal microscopy

Tumour slices were imaged using the Zeiss 780 (Carl Zeiss AG, Germany) microscope on either the 10x objective or as indicated. Therefore, slices were not fixed in order to preserve fluorescence of the proteins and samples were imaged in a 24-well plate.

2.7.3 Celigo

Depending on the plate size, the appropriate amount of cells were seeded prior to conducting the experiment. Thereafter, the images were captured using the Celigo software and processed using ImageJ.

2.8 Statistics

Throughout the different experiments, different statistical tests were conducted in order to analyse if any of the datapoints were significantly changed to the corresponding controls. All statistics was dons using Graphpad Prism (UK). For the most experiments comparing more than two groups, a two-way ANOVA with either a Bonferroni, Tukey's or Dunnett's post hoc analysis was conducted. Significances are indicated underneath each graph including star values p=0.01-0.05 (*), 0.001-0.01 (**), 0.0001-0.001 (***) and <0.0001 (****). The n of each experiment is indicated underneath each Figure.

2.9 Chapter specific methods

2.9.1 Chapter 3

2.9.1.1 Co-culture for bystander cytotoxicity

Bystander killing co-culture experiments were performed in a 48-well plate by seeding 15,000 NHDF (stained using cytopainter deep red (Abcam, UK, #138894) cells and 25,000 DLD-1 cells (stained using cytopainter blue (Abcam, UK, #ab138890) the day prior to the experiment. EpCAM bispecific was kindly gifted by Hena Khalique for the use in this thesis. T cells were added in a ratio of 5:1 to DLD-1 cells (125,000), and BiTEs or Dynabeads (Thermo Fisher Scientific, USA, #11161D) were added in the appropriate concentrations in RPMI-1640 containing 2% FBS. Cells were harvested after 48h by addition of trypsin for the adherence cells and analysed on flow cytometry. Results were analysed using FlowJo software.

2.9.1.2 Cellular versus mediator T cell bystander cytotoxicity

20,000 DLD-1 cells were seeded in a 96-well plate the day prior to the experiment. Then, 100,000 T cells with the indicated EpCAM BiTE concentration were added the next day and

incubated in RPMI-1640 with 2% FBS supplementation for 48h. Subsequently, the T cells and supernatants were collected and separated by 450g centrifugation for 10 minutes. Ratios of the T cells used: CD4=100,000 CD4 T cells, CD8= 100,000 CD8 T cells and CD4+CD8=50,000CD4 and 50,000 CD8 T cells.

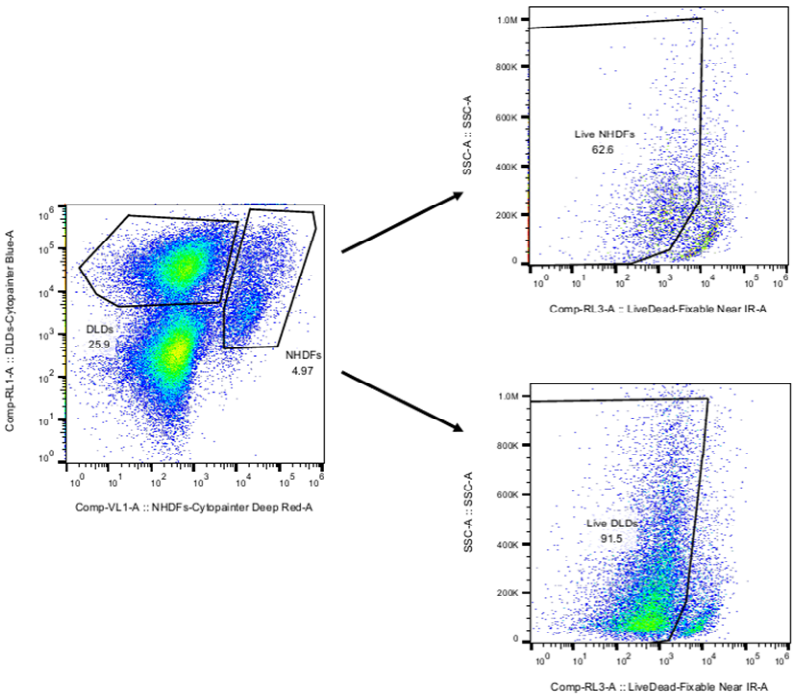

Figure 2.3: Gating strategy for bystander killing experiment.

The day prior to the experiment, NHDF cells were seeded at 10,000 cells per well in a 96-well plate. Conditioned supernatant and pre-activated T cells (50,000) from above were then transferred onto the cells and incubated for 48h before dissociating the NHDF cells with trypsin and measurement on flow cytometry.

2.9.2 Chapter 4

2.9.2.1 ECM ELISA

ECM ELISA was conducted similar to the ELISA described above. In short, the ELISA plate was coated with the ECM proteins (collagen I (Corning, USA), fibronectin from Abcam, UK,

#ab80021) at 50 nM for 1h, before vigorous washing and blocking. Then, the constructs were added in blocking buffer at 50 nM and incubate for 1h at RT, before washing and detection using 1:15,000 of the Direct Blot FLAG-HRP. After washing, TMB solution was added and incubated for 20 minutes before stopping with 0.18 M of sulphuric acid and reading at 450 nm absorbance using the VarioScan plate reader (Thermo Fisher Scientific, USA).

2.9.2.2 Polyarginine and PlGF-2 T cell activation and cytotoxicity assays

T cell activation and T cell cytotoxicity assays were performed by transfecting target cells in a 96-well plate as described above. Cells were left over night to recover. T cells were added (100,000 per well) the next day and incubated for 24h. Cells were then harvested and stained for flow cytometry. For cytotoxicity, cells were incubated for five days and measured using an XTT endpoint assay.

2.9.3 Chapter 5

2.9.3.1 Collagen I-coating of plates

A human collagen I (Corning, USA, #354265) solution was prepared on ice in order to prevent premature polymerisation. An end concentration of 100 µg/ml of the collagen I was added to cold 0.2 mM acetic acid in ddH_2O, before 50 µl/well were added to a 96-well plate. Thereafter, the plate was incubated at RT for 1h in the tissue culture hood, before the wells were washed with warmed PBS 2x. The plate was directly used for experiments.

2.9.3.2 LAIR-2 ELISA

For the LAIR-2 ELISA, 100 µg/ml of human collagen I (Corning) was coated on an ELISA plate and incubated for 1h at RT. Subsequently, the plate was washed 2x and blocked with ELISA blocking buffer as mentioned above. The samples were incubated at 10 nM for 1h at RT on a shaker before being washed 3x. Detection was done using an anti-FLAG HRP direct blot,

before TMB solution (Thermo Fisher Scientific) was added. The ELISA was stopped after 60 seconds-5 minutes with stop solution (0.18 M sulphuric acid) and measured using the plate reader at 450 nm.

2.9.3.3 LAIR-2 T cell activation assay

Every free LAIR-2 bispecific experiment was conducted in a similar way. The plate was coated as mentioned above with human collagen I and washed 3x using warmed PBS. Subsequently, the plate was incubated with 10 nM (or as indicated) of the bispecific or control in RPMI-1640 with 2% FBS. Wells were washed 1x after incubation and cancer cells and/or T cells were added. A total of 10,000 target cells were added to avoid overcrowding of the well.

2.9.4 Chapter 6

2.9.4.1 LAIR-2 Virus activation assay

Every EnAd LAIR-2 bispecific experiment was conducted in a similar way. The plate was coated as mentioned above with human collagen I and washed 3x using warmed PBS. Subsequently, 10,000 target cells, EnAd virus and T cells (5:1 effector to target ratio) were added at the same time and incubated for the indicated amount of time before harvest and analysis. MOIs were all measured on A549 cells and used as follows for the experiments unless indicated otherwise: A549, DLD-1 MOI 0.2, Panc-1 MOI 10. T cell activation and cytotoxicity was measured on day 3 either by flow cytometry or XTT assay.

3 Exploration of T cell-mediated and antigen-independent bystander killing upon anti-CD3 scFv activation

3.1 Introduction

T cell mediated cytotoxicity is one of the most exploited effector functions of the immune system in immunotherapy. This is to a large extent important in approaches such as bispecific T cell engagers (BiTEs), CAR T cells and even cancer vaccines. In these therapies, the final goal is the antigen-specific eradication of cancer cells, which all rely on the cytotoxic T cell mechanisms.

The ‘canonical’ T cell killing mechanism is mediated by perforin and granzyme (Barry and Bleackley 2002; Kägi et al. 1994). Upon T cell binding to the target cell, the T cell is activated and perforin and granzymes (amongst others) are released into the immune synapse. These mediators are stored within secretory granules in the T cells. Initially, an immunological synapse has to form with the engagement of LFA-1 on T cells, and ICAM-1 on target cells (Dustin and Long 2011; Somersalo et al. 2004). This stabilisation is then followed by the secretion of the several mediators. Upon secretion, perforin binds to the available calcium and docks to the plasma membrane of the target cell via phospholipids, where it polymerises to channels (Andrin et al. 1998). Subsequently, granzymes can enter the cytoplasm of the target cell, either through the channels formed by perforin or through endocytosis (Boivin et al. 2009). Once in the cytoplasm of the target cell, granzymes can directly activate the effector caspase 3, and also interact with Bid, which then activates the mitochondrial cell death pathway through Bax-Bak and cytochrome c release. Both mechanisms eventually lead to the induction of programmed cell death in the target cell (Boivin et al. 2009; Osińska, Popko, and Demkow 2014). This pathway is also generally assumed to be harnessed by BiTEs and CAR T cells (Gruen et al. 2004).

The second major way in which T cells mediate cytotoxicity is through cell surface receptors. Although often overlooked, this pathway is crucial in the process of clearance of tumour cells (Schro et al. 2000). The most prominent members of this family are Fas and FasL, whereby FasL expressed on T cells leads to a trimerisation of Fas on the tumour cell surface. The clustering of engaged Fas leads to a close association of their intracellular death domains (DD), which recruit the Fas-associated death domain (FADD) adapter proteins and pro-caspase 8, leading to the cleavage and activation of caspase 8 in the death-inducing signalling complex (DISC). Caspase 8 is in turn able to activate the main effector caspase 3, which then induces apoptosis in the target cells (Benmebarek et al. 2019).

Fas and FasL killing also plays an important role in CAR T cell and BiTE mediated cytotoxicity. Upadhyay et al. have visualised and compared the two therapies and dependency on Fas/FasL-mediated killing, whereby both therapies showed involvement of Fas/FasL, especially when it came to non-antigen-specific killing as discussed in this chapter (Upadhyay et al. 2021). Additionally, the involvement of Fas-mediated killing has also been observed in CD4 CTLs, where the secretory killing pathway was blocked (Malyshkina et al. 2017).

However, there have been multiple studies shedding light on alternative and novel mechanisms of T cell cytotoxicity. Firstly, although traditionally attributed only to CD8 T cells, CD4 T cells themselves possess the ability to induce target cell killing. Initially considered an *in vitro* artefact, CD4 CTLs have also been shown to arise in *in vivo* experiments (Xie et al. 2010). On top of this, it is believed that at least a large part of their cytotoxic mechanism is mediated though perforin and granzyme, and that CD4 CTLs kill directly through MHC II molecules (HLA-DS, HLA-DP and HLA-DQ), which are sometimes overexpressed by cancer cells (Lin et al. 2023). In the case of BiTEs, where T cell activation is HLA independent and where the anti-CD3 of the BiTE can re-direct and activate both CD4 and CD8 T cells, CD4 CTLs can exert directed cytotoxicity towards target cells (Freedman et al. 2017; Khalique et al. 2021; Scott et al. 2019).

Secondly, cytotoxicity is generally assumed to imply the formation of a mature immunological synapse. However, recent studies have shown that there is no need to create a mature immunological synapse and that a rudimentary synapse is already sufficient in order to induce cytotoxicity (Bálint et al. 2020; Mayya et al. 2018). It was observed that virus infected cells, for example, are killed through the formation of kinetic synapses (‘kinapses’) which allowed cytotoxic T cells to remain motile while killing (Halle et al. 2016). They further also observed a cooperation of T cells, where the target cell was more likely to be eliminated by more than two cytotoxic T cells. Additionally, it was shown that the secretion of the cytotoxic granules already takes place within one minute after cell-to-cell contact (Bertrand et al. 2013). A combination of these mechanisms probably enables T cells to kill in a sequential way and up to 20 target cells in a day (Ganusov and Boer 2008). Sequential killing has also been observed for CAR-T cells (Davenport et al. 2018). Furthermore, a recent study by the Dustin group suggests that CD8 T cells are able to secrete supramolecular attack particles (SMAPs), which themselves possess the autonomous ability to induce cytotoxicity (Bálint et al. 2020). They also found that these particles were approximately 120 nm in diameter, stored in multicore granules and their delivery target was dependent on the components of their outer shell.

Thirdly, the concept of antigenic specificity has recently been contested in several studies showcasing another mechanism of T cell mediated cytotoxicity, coined bystander killing. In this instance, antigen negative cells which happen to be geographically close to antigen specific cells will also be eliminated through T cell cytotoxicity. The pathway through which the antigen negative cells are killed is to this day still highly debated, however, attributed and researched predominantly only in CD8 T cells.

Only a few studies have thus far looked into the mechanism of bystander cytotoxicity. A recent study by Upadhyay et al. showed the clearance of antigen negative cells *in vitro* and *in vivo* by T cells. They further demonstrated that this was mainly mediated by Fas and FasL involvement, rather than the traditional granzyme/perforin pathway. They further hypothesise that secreted IFN-γ enhances the expression of Fas on the tumour cell surface and, which

could potentiate bystander killing mediated via Fas/FasL pathway (Upadhyay et al. 2021). In another study, Schietinger et al. aimed to take advantage of bystander killing in a therapeutic approach by targeting stromal cells and at the same time rely on bystander killing leading to elimination of tumour cells. They concluded that CD8 as well as CD4 T cells were required to cooperate in order for bystander killing to occur (Schietinger et al. 2010).

In a related study by Ross et al., the mechanism behind BiTE activated T cell bystander cytotoxicity in particular has been looked at in more detail (Ross et al. 2015). Their experiments suggest that BiTE activated T cells locally secrete IFN-γ and TNFα, which both upregulate ICAM-1 and Fas expression on cancer cells. This subsequently primes the bystander cancer cells to engage with activated T cells via LFA-1 – ICAM-1 and facilitates Fas/FasL- mediated cell death. Blocking either Fas or ICAM-1 led to a partial abrogation of the cytotoxicity towards bystander cells, suggesting that, at least to a certain extent, bystander killing is driven by this mechanism (Ross et al. 2015).

Given the fact that BiTEs engage both CD4 and CD8 T cells alike (Freedman et al. 2017; Khalique et al. 2021; Ross et al. 2015; Scott et al. 2019), it remains elusive whether both cell types mediate bystander killing and/or to what extent they contribute. Therefore, the objective of this chapter is to test the amount both CD4 and CD8 T cell contribute towards bystander killing and whether this killing is cell-contact mediated or mediated through secreted proteins. In therapeutic approaches designed to exploit antigen-specific T cell cytotoxicity, the involvement of bystander killing could pose a novel angle and possibly bring forth unwanted toxicities. Conversely, in our case we are particularly keen to determine whether bystander killing is sufficiently potent and robust to be relied upon as the primary cytotoxic mechanism in therapeutic strategies to be developed later in this thesis.

3.2 Hypothesis

In this chapter, we hypothesise that activated T cells are able to (1) mediate significant antigen-independent local cytotoxicity through CD4 and CD8 T cells, (2) eliminate antigen-negative

stromal cells as well as antigen-positive cancer cells and (3) kill cells upon cell-to-cell contact and also via supernatant components, independent of cell-to-cell contact.

3.3 Results

3.3.1 Graphical abstract

As bystander T cell killing has been observed by other studies in different contexts (Ross et al. 2015; Schietinger et al. 2010; Upadhyay et al. 2021), it was important to elucidate the general significance of bystander killing in the *in vitro* systems used in this thesis. **Figure 3.1** shows a graphical depiction of the approaches prioritised in this chapter to further elucidate the cells involved in bystander killing. T cell killing is assessed in an experimental setting involving EpCAM positive DLD-1 cells and EpCAM negative NHDF cells, whereby human-derived T cells will either be activated with an EpCAM BiTE (antigen-dependent activation), or CD3/CD28 Dynabeads (antigen-independent activation). The EpCAM BiTE is a fusion protein consisting of an scFv recognising human EpCAM and an scFv against the epsilon portion of the CD3 within the TCR complex (derived from clone OKT3). This system should therefore shed more light onto CD4 and/or CD8 T cell involvement in bystander killing in the presence (BiTE) and absence (Dynabeads) of an antigen-dependent T cell activation mechanism.

3.3.2 Bystander killing occurs upon specific as well as non-specific T cell activation.

In order to assess and quantify bystander killing, a test system shown in **Figure 3.2** A was set up. Accordingly, EpCAM expressing DLD-1 and EpCAM negative NHDF cells were co-cultured and mixed with T cells. The T cells were then either activated using an EpCAM BiTE or CD3/CD28 Dynabeads. T cell activation and DLD-1/NHDF cell viability could subsequently be measured using flow cytometry and a live dead dye. The EpCAM BiTE for this chapter was kindly provided by Hena Khalique.

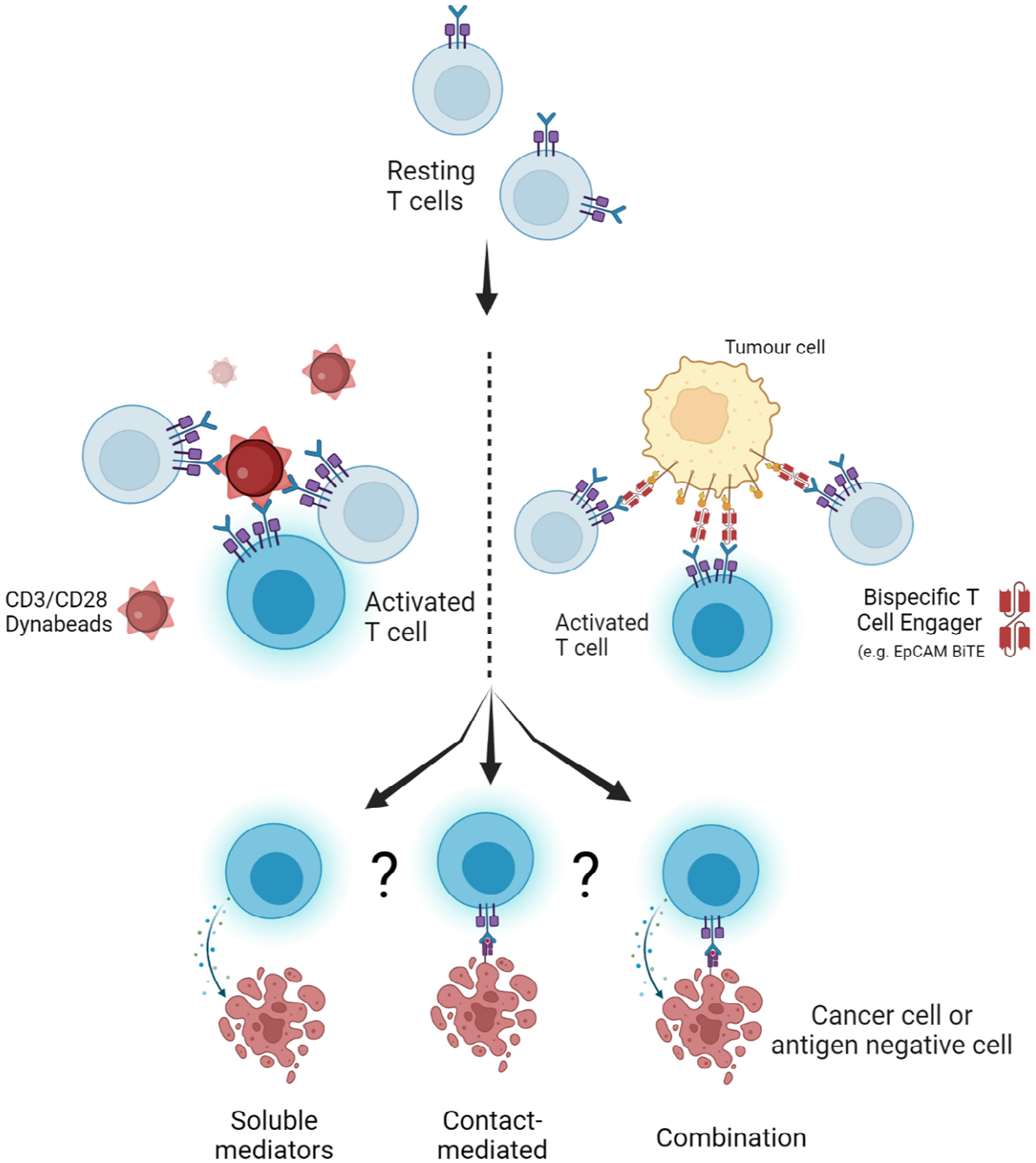

Figure 3.1: Schematic depiction of the hypothesis and aims to assess bystander killing in the context of BiTEs and non-specific CD3/CD28 Dynabeads activation. Resting T cells will either be specifically activated with the EpCAM BiTE in the presence of EpCAM positive cells (DLD-1) and bystander killing will be measured on EpCAM negative cells (NHDFs), or activated using antigen-independent CD3/CD28 Dynabeads, whereas bystander killing can be measured on both, DLD-1 and NHDF cells. It is important to assess in this chapter if both CD8 and CD4 are involved in bystander killing and additionally, if bystander killing is mostly mediated through cell-cell contact or if cytotoxicity can also be induced by soluble mediators released into the supernatant.

Figure 3.2 B shows the general timeline for the experiments in this chapter, DLD-1 (25'000 cells) and NHDF cells (15'000 cells) were seeded on day -1 (D-1) and T cells (125'000 cells, 1:5 to DLD1 cells) and Dynabeads or EpCAM BiTE were added the following day (D0). All cells were harvested on day 2 (48h post activation) for analysis by flow cytometry.

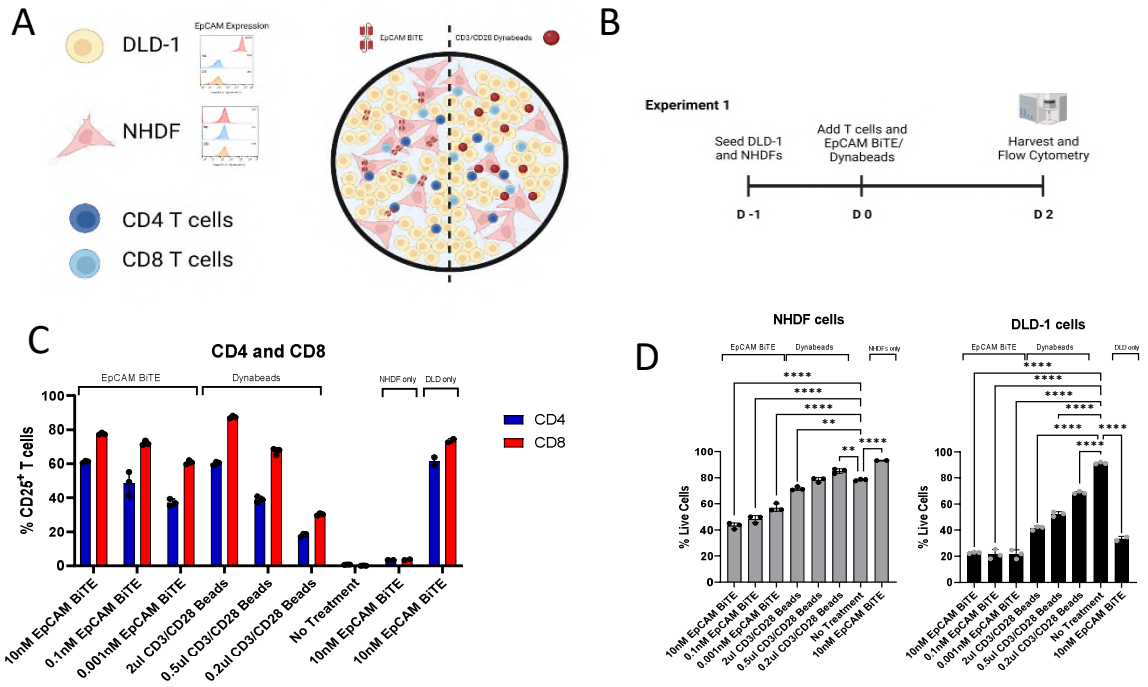

Figure 3.2: Dynabeads and EpCAM activated T cells show strong tendencies to exert bystander killing. A: Schematic representation of the experimental set up: DLD-1 (EpCAM positive) and NHDF (EpCAM negative) cells were co-cultured together with T cells and either the EpCAM BiTE (only killing EpCAM positive DLD-1 cells) or Dynabeads (killing DLD-1 and NHDF cells independent of an antigen). B: All experiments were conducted with seeding of the DLD-1 and NHDF cells on D-1 (25'000:15'000 ratio), T cells and activation treatment was added on D0 in the indicated amounts. All cells were harvested on D2 after 48h incubation and stained for viability and T cell activation markers for further analysis. C: T cell activation after 48h incubation, measured by the surface expression of CD25. n=3 shown. D: Viability of NHDF and DLD-1 cells after 48h incubation. Viability was assessed via flow cytometry using a fixable live dead staining. n=3, one-way ANOVA with Dunnett's multiple comparisons test to no treatment, p<0.05 *, p<0.01 **, p<0.001 ***, p<0.0001 ****. This figure was created using BioRender.

As shown in **Figure 3.2** C, T cells could be activated to high extent (about 85%) using the EpCAM BiTE or Dynabeads in the presence of EpCAM-positive DLD-1 cells, and CD8 T cell activation was consistently approximately 20% higher than CD4 T cell activation. Moreover, there was no T cell activation observed with just NHDF cells and EpCAM BiTE, validating the assay and potentially indicating that T cell activation by the EpCAM BiTE could be dependent on crosslinking T cells to EpCAM-positive target cells, allowing for the formation of a pseudo immune synapse and clustering of CD3. It was notable that the greatest activation of CD8 cells was achieved using Dynabeads (2 µl/well).

Figure 3.2 D shows cell viability of DLD-1 and NHDF cells after 48h co-culture with T cells and EpCAM BiTE or Dynabeads. Specific T cell killing can be seen in the first three bars of the DLD-1 graph and the corresponding bystander killing of NHDF cells in the adjacent graph. At the highest BiTE concentration (10 nM), approximately 80% of antigen-positive DLD-1 cells

were killed, and so were over 50% of the antigen-negative fibroblasts. This validates the concept of bystander killing by EpCAM BiTE-activated T cells and suggests it can be a potent mechanism of cytotoxicity. At lower BiTE concentrations, although a similar amount of DLD-1 cells are killed, a decreasing amount of bystander killing reflected in fewer NHDF cells being killed. This assay was validated by the DLD-1 cells alone being killed by T cells in the presence of BiTE, whereas NHDF cells alone in the presence of T cells and EpCAM BiTE were not killed. In turn, when assessing Dynabead-mediated T cell cytotoxicity, which is antigen-independent and occurs entirely through bystander killing, the highest concentration achieved only about 60% killing of DLD-1 cells and about 30% killing of fibroblasts. This suggests that DLD-1 cells may be more susceptible to T cell cytotoxicity than NHDF cells, which might also impact on the observation (above) that EpCAM BiTE-activated T cells can kill more EpCAM$^+$ DLD-1 cells than EpCAM- NHDF, notwithstanding there is a different cytotoxic mechanism involved. In addition, the observation that EpCAM BiTE (at all concentrations) can kill more NHDF cells than even the highest concentration of beads (**Figure 3.2** D) is unexpected, since the latter mediated the greatest level of T cell activation, assessed by CD25 expression (**Figure 3.2** C). It is conceivable that the BiTE mechanism, which requires formation of a pseudo synapse with DLD-1 target cells before T cells are fully activated (whereas beads can activate T cells in solution) may endow a geometric advantage to bystander killing of NHDF cells in close proximity to the DLD-1 cells.

3.3.3 Bystander killing is mainly mediated by CD8 T cells, however, CD4 T cells also contribute considerably when activated with a BiTE or Dynabeads.

In a next step, we investigated whether the bystander killing is CD4 and/or CD8 T cell mediated. Therefore, CD4 and CD8 T cells were isolated from the same donor and subsequently added to DLD-1 and NHDF cells. T cells were activated using either EpCAM BiTE or CD3/CD28 Dynabeads. **Figure 3.3** shows T cell activation and resulting cell viability for one experiment. As can be seen in **Figure 3.3** A, T cells were activated by the EpCAM BiTE as

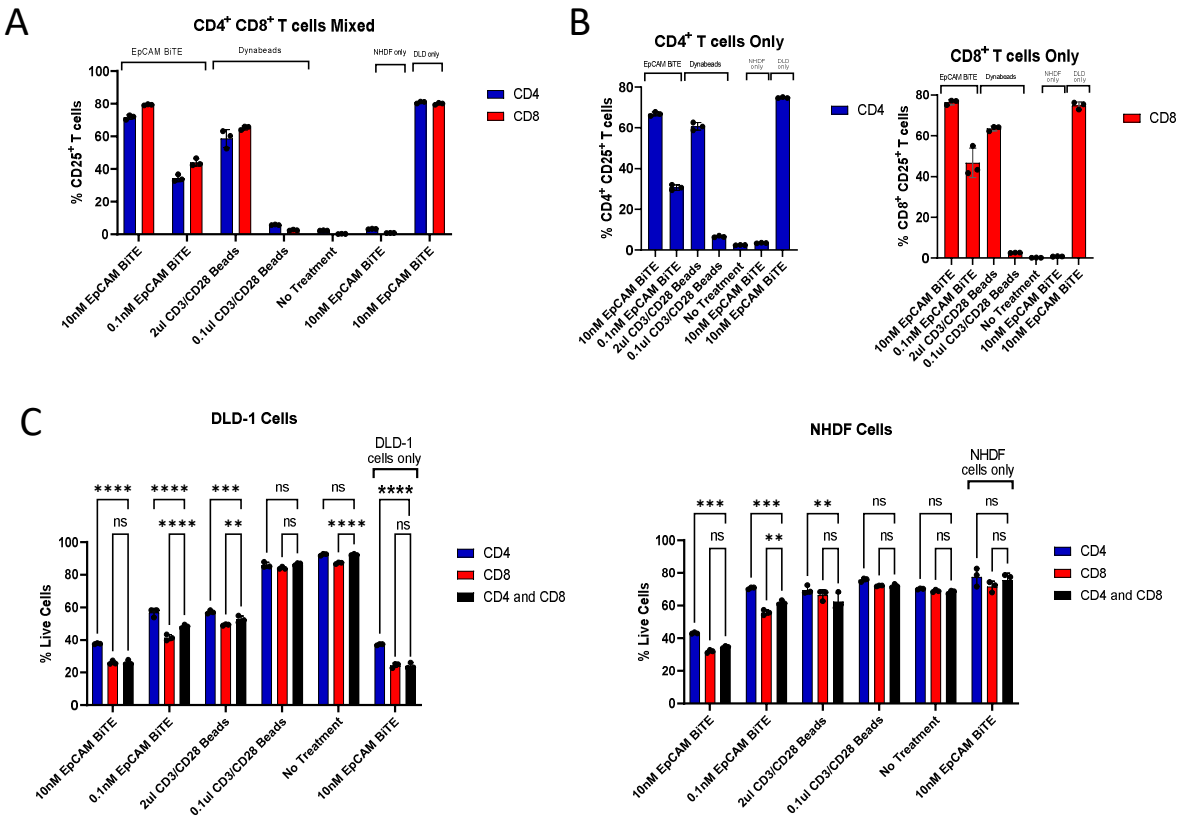

Figure 3.3: Bystander killing is mostly mediated by CD8 T cells but also involves CD4 T cells. All data shown in the graph is from the same experiment following a similar set up as shown in **Figure 3.2Figure 2.3** B. A: and B: show the different T cell activation levels, whereby T cells were activated as a 50%/50% CD4 and CD8 in A and separated into CD4 or CD8 T cells in B. In both graphs, T cells were harvested after 48h and stained for flow cytometry for surface expression of CD25. n=3 shown. C: The graphs show the viability of DLD-1 and NHDF cells respectively. The cells were harvested together with the T cells and gated in a similar fashion as shown in **Figure 2.3**. n=3, two-way ANOVA with Dunnett's multiple comparisons test to CD4 and CD8, p<0.05 *, p<0.01 **, p<0.001 ***, p<0.0001 ****.

a mixture of CD4 and CD8 T cells, whereas in **Figure 3.3** B, CD4 and CD8 T cells were activated separately by the EpCAM BiTE. The extent of activation of CD4 and CD8 T cells (assessed by expression of CD25) is comparable no matter whether they were activated in a mixture of both T cells or separately. Consistent with the previous experiment, CD8 T cells show a slightly higher level of activation than CD4 T cells, and NHDF cells incubated with T cells and EpCAM BiTE shows no T cell activation.

In **Figure 3.3** C, the viability of DLD-1 and NHDF cells is plotted. Generally, CD4 T cells mediate marginally less cytotoxicity than CD8 T cells when they are studied in isolation, whereas when they are both present, the cytotoxicity is intermediate. It follows that the cytotoxicity is in different cases mediated slightly more by CD8 T cells compared to CD4 T cells, although both

show significant cytotoxicity. Additionally, there is a general dose dependency, with more cells being killed at higher concentration of BiTE and Dynabeads, consistent with the T cell activation levels seen in **Figure 3.3** A and B. The BiTE-induced T cells killed more DLD-1 cells than the beads, most likely reflecting their ability to direct T cells to bind EpCAM on the DLD-1 cell surface. High concentrations of BiTE also mediated greater bystander killing of antigen negative NHDF cells than beads, and the low concentration of BiTE (0.1 nM) mediated similar cytotoxicity to NHDF cells as the high concentration of Dynabeads (2 µl), despite mediating less activation of T cells (**Figure 3.3** A, B). This echoes the results discussed in the previous section.

3.3.4 The majority of bystander cytotoxicity occurs via cell-cell contact, with CD8 T cells possessing the ability to secrete mediators capable of inducing cell death as well.

Having shown that CD8 T cells mediate more bystander killing than CD4 T cells, it was important to investigate in more detail how exactly bystander killing is mediated. We already had a clue, from the greater bystander cytotoxicity mediated by BiTEs than Dynabeads, despite similar levels of T cell activation, that cellular proximity was important. Therefore, T cells were co-cultured with DLD-1 cells and activated using the EpCAM BiTE at different concentrations. After 48h, the T cells were harvested and separated from the conditioned supernatant. Both were added to freshly seeded NHDF cells and incubated for 48h before harvesting and measurement using flow cytometry, exemplified in **Figure 3.4** A.

Figure 3.4 B shows the activation level of the T cells after 48h pre-activation on DLD-1 cells before they were added to the NHDF cells. The graph shows a strong CD4 and CD8 T cell activation independently if the cells were activated separately or as a CD4/CD8 T cell mixture (similar to **Figure 3.3** A and B).

In **Figure 3.4** C the viability of NHDF cells can be seen after a 48h incubation with only the T cells that were pre-activated on DLD-1 cells with EpCAM BiTE. Again, CD4 T cells mediated less bystander cytotoxicity than CD8 T cells, with the mixture of both T cells showing similar bystander killing to CD8 T cells alone or in between CD4 and CD8 T cell killing. There was also a BiTE dose dependent drop of NHDF cell viability, corresponding to the T cell activation seen in **Figure 3.4** B.

In **Figure 3.4** D, it can be appreciated that the conditioned supernatants of pre-activated CD4 T cells mediated very little cytotoxicity. In contrast, the supernatants harvested from pre-activated CD8 T cells showed a clear drop in viability of NHDF cells. However, with conditioned supernatants from a mixture of co-cultured and pre-activated CD4 and CD8 T cells (each at half the previous density to maintain the same total cell number), there was again no drop in viability of NHDF cells. This might suggest that cytotoxicity mediated by supernatants from

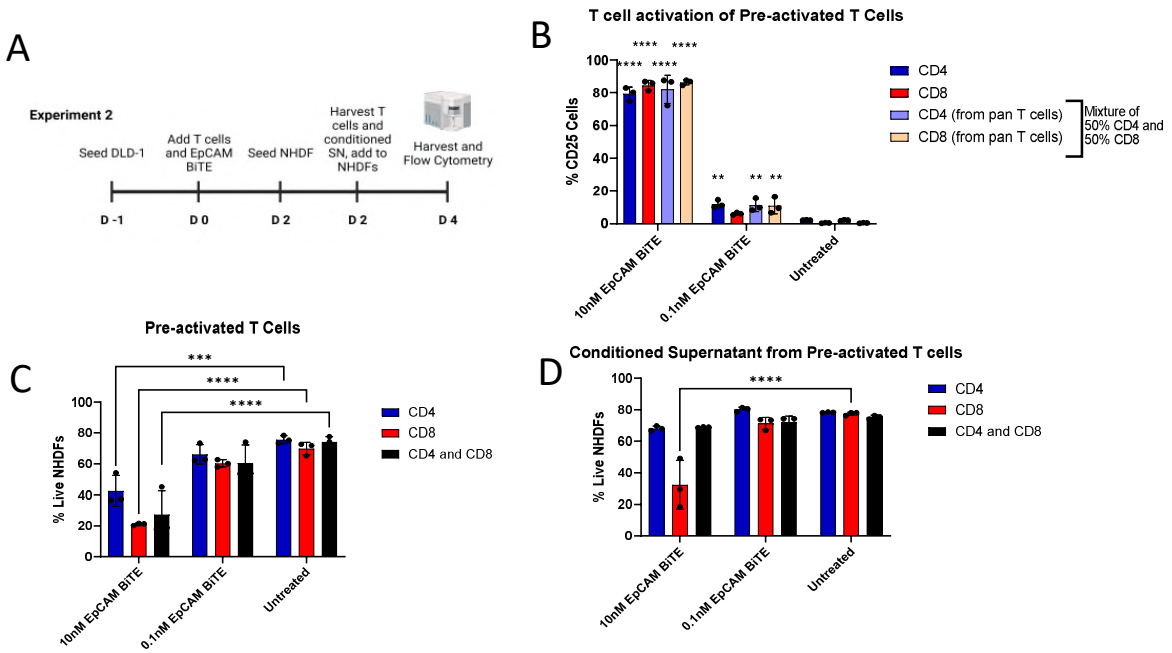

Figure 3.4: Bystander killing is mostly mediated via cell-cell contact whereby CD8 T cells in high concentrations can kill via soluble mediators *in vitro*. A: Depiction of the experimental set up. DLD-1 cells were seeded on D-1 and T cells and EpCAM BiTE were added on D0. NHDF cells were then seeded on D1 and on D2, the activated T cells and the conditioned supernatant from the T cells were separated from the DLD-1 cells and added to the NHDF cells. The experiment was then incubated for another 48h before harvesting and staining for flow cytometry. B: Graph representing the activation of T cells post DLD-1 incubation on D2, showing the activation levels of the three conditions as follows: CD4 T cells alone, CD8 T cells alone and a 50%/50% CD4/CD8 T cell mixture. n=3, two-way ANOVA with Dunnett's multiple comparisons test to untreated, p<0.05 *, p<0.01 **, p<0.001 ***, p<0.0001 ****. C: Cell viability of NHDF cells 48h post incubation with the T cells, therefore depicting the cytotoxic bystander capacity of the cellular fraction of activated T cells. n=3, two-way ANOVA with Tukey's multiple comparisons, p<0.05 *, p<0.01 **, p<0.001 ***, p<0.0001 ****. D: Graph showing the viability of NHDF cells after 48h incubation with the supernatant of activated T cells. n=3, two-way ANOVA with Tukey's multiple comparisons, p<0.05 *, p<0.01 **, p<0.001 ***, p<0.0001 ****.

activated CD8 T cells is non-linear and requires a certain threshold concentration before being observed.

3.4 Discussion

In this chapter, we have explored the implications of bystander killing occurring when T cells are activated either with an antigen-specific BiTE or non-specifically with CD3/CD28 Dynabeads *in vitro*. Although directed T cell therapies often claim to act only based on recognition of a specific antigen, bystander killing probably has contributed towards the success of these therapies.

In order to be able to measure bystander killing, an EpCAM-dependent experiment was established, including EpCAM positive DLD-1 cells and EpCAM negative NHDF cells. Upon co-culture of the two different cell lines together with T cells and either the EpCAM BiTE or CD3/CD28 Dynabeads as activators, cell viability of the cell lines after 48h could be assessed. In **Figure 3.2**, it can be seen that bystander cytotoxicity occurs, as EpCAM negative NHDF cells are also killed in the presence of the EpCAM BiTE and $EpCAM^+$ DLD-1, but not when DLD-1 cells are absent. Similarly, DLD-1 and NHDF cells are killed in the presence of Dynabeads and T cells, indicating antigen-independent bystander killing. Although many studies have observed the elimination of antigen-negative cells (Ross et al. 2015; Schietinger et al. 2010), it is interesting to note that T cells activated even in the complete absence of an antigen through CD3/CD28 Dynabeads are able to mediate bystander cytotoxicity, killing both DLD-1 cancer cells and NHDF fibroblasts *in vitro*.

Most studies investigating T cell mediated bystander killing either only involve CD8 T cells (Upadhyay et al. 2021) or analyse pan T cells (Ross et al. 2015), however they never distinguish between CD4 and CD8 T cells. The same is true for other studies looking at bystander T cell killing not necessarily in the context of cancer or BiTEs (Kim and Shin 2019; Shim et al. 2022). This then poses the question whether bystander killing is primarily the province of either both CD4 and CD8 T cells or, as expected from the literature, CD8 T cells

only (Upadhyay et al. 2021). As can be seen in **Figure 3.3**, our data show that both CD4 and CD8 T cells mediate bystander killing, although CD8 T cells show a higher potential to exert bystander cytotoxicity. Given the fact that CD8 T cells are generally considered to be far more cytotoxic than CD4 T cells, it is surprising to see that there is merely a 15% difference in the ability to kill via bystander cytotoxicity. This again indicates the importance of CD4 CTLs in directed T cell therapies such as BiTEs. Although there are a few studies looking into CD4 T cell-mediated cytotoxicity, none of them looks at their capacity to mediate bystander cytotoxicity (Knudson et al. 2021; Schietinger et al. 2010). One of the possible reasons for the lack of research might be that in physiology, CD4 CTLs are not primarily arising and migrating to sites of infection. When working with targeted immunotherapies such as BiTEs which target CD3ε without CD4 or CD8 discrimination, the topic of directed and local activation of tumour infiltrating CD4 T cells becomes more important.

To further investigate the observed bystander killing and to elucidate if bystander cytotoxicity is mediated by cell-cell contact or through soluble mediators, T cells were pre-activated with EpCAM BiTE on DLD-1 cells and pre-activated cells and conditioned supernatant were incubated with NHDF cells. As expected, much of the cytotoxicity is mediated through cell- cell contact as seen in **Figure 3.4** C. Again, CD4 T cells showed approximately a 15% reduced potency of cytotoxicity compared to CD8 T cells. Interestingly, when looking at the transferred supernatants, only CD8 T cells managed to mediate cytotoxicity at a high concentration of BiTE. CD4 T cells, however, did not mediate any cytotoxicity though conditioned supernatant. This could be a strong indication towards SMAPs, a recently described type of nano particle secreted by CD8 T cells and containing perforin and granzymes (Bálint et al. 2020). SMAPs have been shown to have the ability to kill independently and autonomous after secretion, which fits with the effect we can observe in **Figure 3.4** D. Additionally, SMAPs have not been observed to be produced by CD4 T cells (Bálint et al. 2020) and hence were also not able to mediate cytotoxicity via conditioned supernatant in this study.

Showing that even antigen-independently activated T cells can mediate cytotoxicity against neighbouring cells, immediately raises the question of whether the T cells will eliminate themselves by bystander killing. Because T cells harbour considerable quantities of granzyme B in secretory granules, they simultaneously express proteinase inhibitor 9 (PI-9 or SerpB9), which protects them against leaking granzyme B. Similarly, PI-9 might also protect T cells from cytotoxic attack by other T cells. In a study from 2007, Cunningham et al. have showed that a high induced expression of PI-9 in cells mediates resistance towards both granzyme B and Fas/FasL killing (Cunningham, Jiang, and Shapiro 2007). There are only three human serpins known to inhibit granzymes, SerpinA1, SerpinB9 (PI-9), and SerpinC1. However, the most relevant serpin is PI-9, showing high and stable expression in CD8 T cells, NK cells and APCs, but also in some endothelial and mesothelial cells (Buzza et al. 2001; Hirst et al. 2001, 2003). Some studies also suggest the upregulation of PI-9 in cancer could pose a way for the tumour to escape T cell cytotoxicity (Bladergroen et al. 2002; Bossard et al. 2007). As normal tissues and immune privileged tissues such as the placenta and testis also express PI-9 mainly as a protection mechanism for bystander cells to prevent excessive tissue damage, this might also be a contributing factor as to why T cells are not readily eliminating each other (Hirst et al. 2001). This is especially important in the scenario of bystander killing where T cells are activated in an antigen independent way (e.g. CD3/CD28 Dynabeads), as this could affect and potentially dampen the cytotoxic effect severely.

The results from this Chapter, however, do not allow for definitive predictions as to the total amount of bystander killing and antigen-specific killing towards T cell mediated cytotoxicity. However, it is clear also from other publications, that bystander cytotoxicity plays an important role in antigen-specific therapeutic strategies such as BiTEs (Ross et al. 2015; Upadhyay et al. 2021).

Bystander killing has probably been involved in the success of many T cell-based cancer therapies, without having been fully acknowledged nor accounted for. Our data suggest that bystander cytotoxicity can be of roughly comparable potency as direct antigen-mediated

cytotoxicity, and it may provide an important strategy to counter tumour immune evasion by antigen silencing. Given that bystander killing has also been observed *in vivo* (Ross et al. 2015), this unconventional way of antigen-independent T cell killing might pose a novel and potent strategy for cancer treatments based on local targeting of treatment, rather than the more conventional antigen-dependent approach.

4 Targeting extracellular glycosaminoglycans using positively charged bispecifics to elicit bystander cytotoxicity

4.1 Introduction

After having shown that bystander killing, independent of an antigen, can be elicited by CD4 and CD8 T cells activated by clustering of CD3 by anti-CD3 scFv or CD3/CD28 Dynabeads, we set out to determine how this phenomenon could be exploited in a therapeutic approach. Since bystander cytotoxicity could be induced solely by clustering of CD3, it now seemed likely this could result just from tethering anti-CD3 scFvs to non-cellular targets, such as the ECM. This approach would allow the decoration of the TME and a potentially prolonged functional timeframe for the tethered bispecific, independent of the death of any particular cell. Additionally, as ECM with fundamentally similar properties is present in most solid tumours, both within the same patient and in different patients, this approach should be able to deliver treatment effectively to a wide range of tumours without mediating a selective pressure on any tumour specific cell surface marker.

Not only does the ECM provide many different possible tethering targets, it is also a crucial player in maintaining local tumour immunosuppression. For example, it forms a reservoir for various immunosuppressive cytokines such as TGF-β, IL-10 and IL-6. TGF-β is deposited covalently on fibrillin and released upon direct integrin binding by an incoming cell, resulting in a targeted and localised effect on infiltrating immune cells, as described in Chapter 1.4. Additionally, IL-10 and IL-6 contain positively charged islands which interact with the abundant negative charges of the ECM, resulting in electrostatic retention within the tumour ECM (Gehrcke and Pisabarro 2015; Mummery and Rider 2000) and localised immunosuppression. In physiology, these molecular interactions play an important role in maintaining local immunosuppression around healing wounds, where potentially immunogenic tissue remodelling is occurring (Ghatak et al. 2015). However, tumour ECM can exploit these same

physiological mechanisms for creating and maintaining an immunosuppressive tumour microenvironment.

This ability to mediate immunosuppression makes targeting the ECM, to reverse immunosuppression, an even more attractive strategy. One option could be to exploit electrostatic tethering, similar to the mechanisms exploited by IL-6 and IL-10. As targets, proteoglycans and particularly their attached GAGs comprise the main source of negative charges in the ECM (Silva et al. 2019). GAGs are unbranched, highly negatively charged chains of repeating disaccharide sugars, discussed in more detail in Chapter 1.2.1.2. Several studies have previously explored the relationship between overexpression of GAGs and cancer biology (Kalathas et al. 2010, 2011; Momose, Yoshimura, and Harumiya 2016), perhaps most notably the binding of CD44 to hyaluronic acid (HA) which resulted in the HA-dependent proliferation and progression of tumours by CD44 engagement leading to Rho-associated kinase (ROK) and Tas signalling (Chaudhry et al. 2021). Additionally, the overexpression also correlated with an impaired delivery of chemotherapies and immunotherapies, which is hypothesised to be also mediated via HA-CD44 signalling. For example presence of excess HA was reported to decrease blood vessel function, which resulted in less drug reaching the tumour (Jacobetz et al. 2013).

Selective targeting of tumour ECM by systemic IV injection is practically not possible due to the presence of very similar ECM within healthy tissues and organs. Interestingly, some groups have targeted the fibronectin extra domain B (EDB FN), a splice variant of fibronectin and one of the few known specific markers of tumour ECM. It was previously targeted in order to provide a way of ECM-based imaging (Han and Lu 2016; Tijink et al. 2009) or using an antibody drug conjugate (ADC) as a therapeutic approach (Hooper et al. 2022). However, targeting only a splice variant of fibronectin significantly limits the amount of available target and does not exploit the high tethering capacity that could be achieved by targeting more abundant ECM binding sites.

Targeting a more abundant molecule in the ECM such as GAGs might pose a superior approach, with the potential for immobilisation of greater therapeutic payloads. Indeed, GAGs have already been explored for targeted cancer therapy using a range of strategies. Perhaps most notably synthetic or semi-synthetic heparan sulphates (HS) have been evaluated in ongoing clinical trials. Their main mechanism of action involves blocking heparinase (HPSE) and other GAG-binding partners including growth factors (Wieboldt and Läubli 2022). Pixatimod is one HS that has been shown to inhibit the activity of HPSE in this way and in addition to this has an effect on several immune cells, including the activation of NK cells and suppression of TAMs (Hammond et al. 2018).

Given the clinical interest and moderate success of current therapies to target GAGs, we chose to use the abundance of GAGs as an advantage to target and retain immunotherapeutics within the ECM and TME. Since the binding of negatively charged GAGs is mostly charge based, two positively charged motifs were explored as potential GAG anchors. Firstly, the Hubbell lab identified a 21 amino acid portion of the placental growth factor II (PlGF-2) by comparing binding of different growth factors to several ECM components, including PlGF-1 (Martino et al. 2014). PlGF-1 bound very poorly to all tested components, whereas PlGF-2 (which contains 21 additional amino acids) bound to most of the tested components, suggesting the increase in the binding affinity was due to those 21 amino acids. Another study used the same 21 amino acids and chemically attached them to PD-L1 and CTLA-4 antibodies in order to increase retention within the tumour (Ishihara et al. 2017). Secondly, a synthetic polyarginine-containing protein was designed, consisting of a six time repeat of arginine (R) in order to mimic a positively charged protein island. This chapter explored PlGF-2 and polyarginine (R) for GAG binding and induction of bystander cytotoxicity.

As therapeutic strategy, in this chapter we aim to harness bystander killing by using bispecific proteins consisting of an anti-CD3 scFv and a GAG binding domain, which should self-tether onto GAGs present in the ECM and also on the surfaces of the producer cell and nearby tumour or stromal cells. For geographic selectivity, the bispecific will ultimately be expressed

locally from an oncolytic virus, bypassing systemic exposure and the potential for tethering to GAGs in healthy locations and the possibility of off-tumour toxicities. Accordingly, bispecific fusion proteins were designed consisting of an anti-CD3 OKT3 scFv fused to a synthetic polyarginine or PlGF-2 (21 AA) motif and their activity has been validated *in vitro* in this chapter.

4.2 Hypothesis

We hypothesise that anchoring anti-CD3 motifs to GAGs in the ECM via synthetic polyarginine and PlGF-2 motifs, will lead to (1) T cell activation and (2) induction of antigen-independent bystander killing towards both cancer cells and stromal cells.

4.3 Results

4.3.1 Graphical abstract

The objective of this Chapter is to create a polyarginine- or PlGF-2-containing fusion protein with an anti-CD3 scFv as described in **Figure 4.1** below. Upon entering the ECM (1), these bispecific agents will bind to the available GAGs and therefore “decorate” the ECM with anti-CD3 motifs, leading to T cell binding and subsequently T cell activation (2). In step 3 and 4, the activated T cells will kill cancer cells and other cells in the vicinity via bystander cytotoxicity. Simultaneously, the bispecifics potentially will be able to remain bound to the ECM for a prolonged period and therefore increase and promote T cell surveillance after tumour cell elimination, and thereby inhibit tumour relapse.

4.3.2 Construct design and production in HEK293a cells

In total, two positively charged groups of motifs were fused to an anti-CD3 scFv, as seen in **Figure 4.2** A. Initially, six times arginines (polyarginines) were added in a three, two- or one-

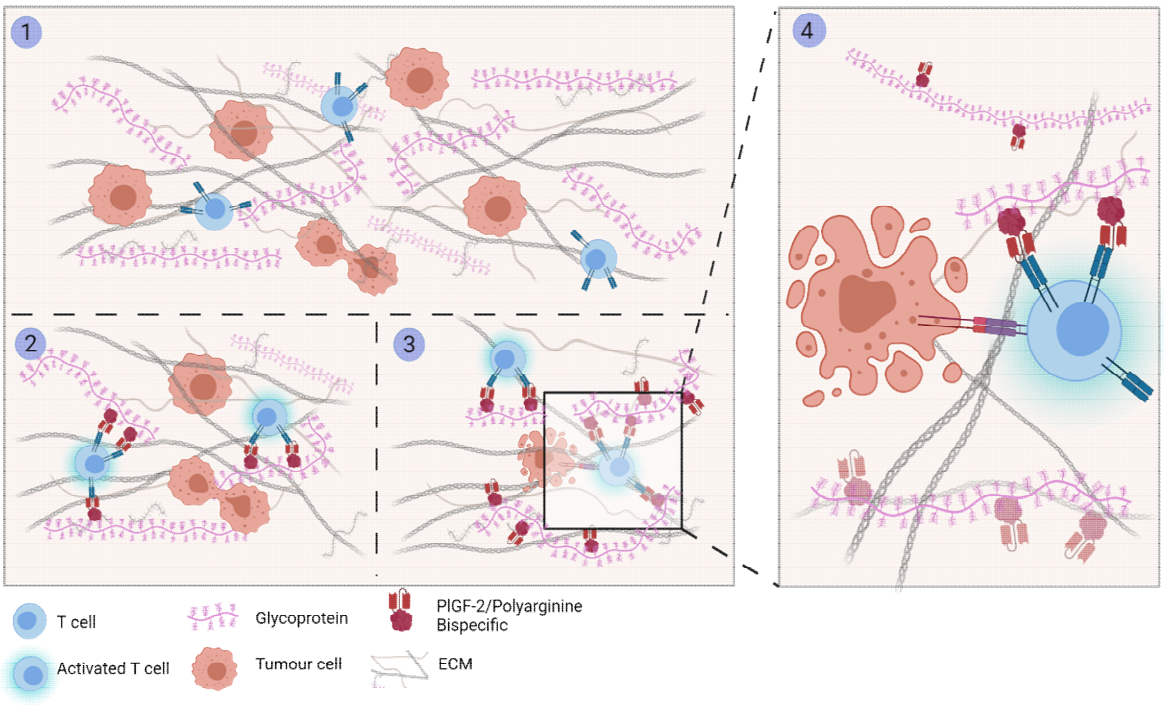

Figure 4.1: Positively charged bispecifics binding to the ECM and to CD3 on T cells can activate and prime T cells for bystander cytotoxicity. ECM and especially negatively charged GAGs are abundant in the tumour and therefore constitute and interesting target (1). The bispecifics bind to GAGs upon entering the tumour ECM and simultaneously activated T cells by anti-CD3 scFv clustering (2 and 3). Lastly, the activated T cells mediate bystander killing and eliminate neighbouring cells (4).

time repeat separated by a GGGGS linker to the anti-CD3 scFv, and subsequently 21 amino acids of PlGF-2 (amino acids 123-144, (Martino et al. 2014)) were added in a three, two or one time repeat with GGGGS linkers as separation to the scFv. As a control, an anti-CD3 scFv without a positively charged motif was used. All constructs were cloned into pSF plasmid under the control of a CMV promotor and tagged by an N-terminal FLAG tag to enable detection of the bispecifics. The constructs were expressed in HEK293a cells upon transfection, whereby the more positive constructs tended to remain in the cell lysate as seen in **Figure 4.2** A. Additionally, the anti-CD3 control scFv showed a very strong production and secretion into the supernatant.

Furthermore, **Figure 4.2** B shows the charge distribution of the constructs, visualising positive tails in the C-terminus with spikes for both groups of constructs. The bispecifics containing three of the respective positive tails are shown as representative graphs. Although the polyarginines show a higher positive value for each of the tails, the PlGF-2 motifs are slightly longer and therefore constituted for more distributed positive charges.

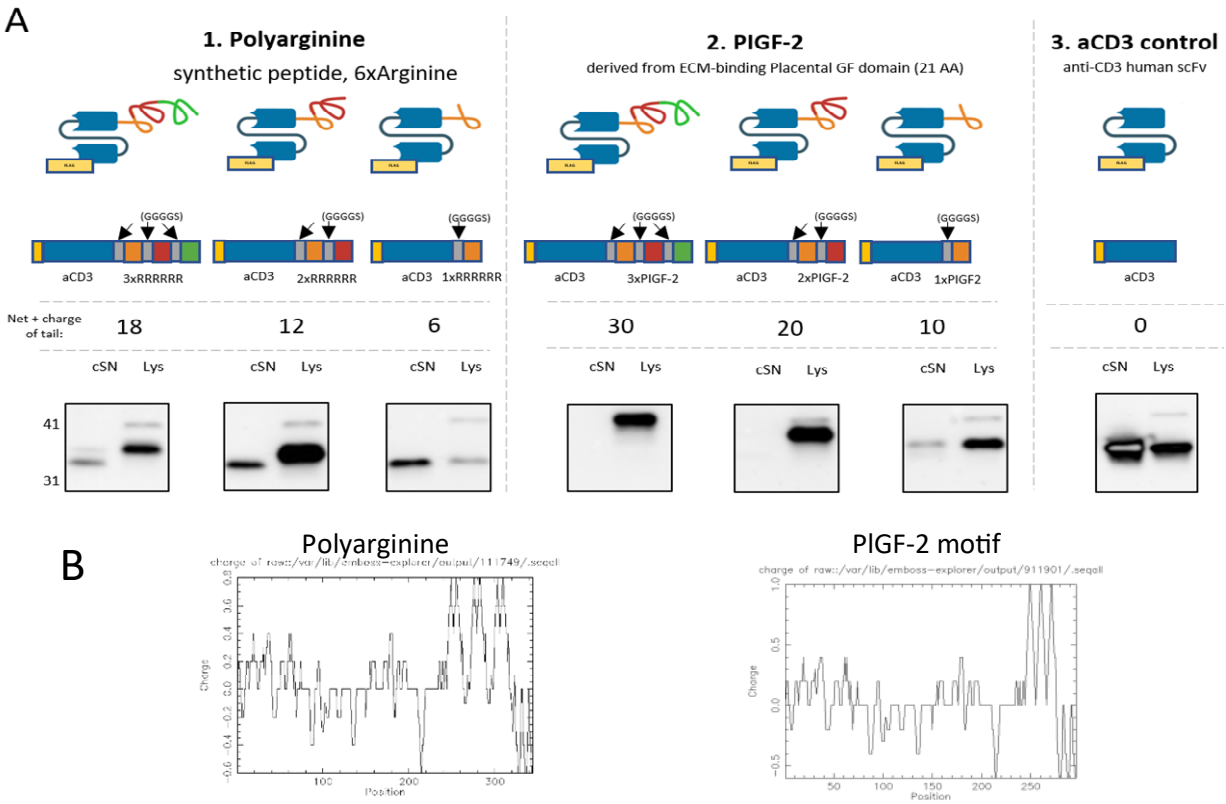

Figure 4.2: Design and expression of the bispecifics in HEK293a cells. A: The polyarginines and PIGF-2 constructs were all designed including an N-terminal FLAG Tag, followed by an anti-CD3 scFv and then the polyarginines or PIGF-2 motifs. Expression was assessed via western blot (WB) using an anti-FLAG HRP antibody. Cells and supernatant were collected 48h after transfection whereby the supernatant was concentrated approximately 20x before added to the WB. B: Online analysis of the charge profile of the polyaringine and PlGF-2 bispecifics, Reference: https://www.bioinformatics.nl/cgi-bin/emboss/charge, February 2020. This figure was created using BioRender.

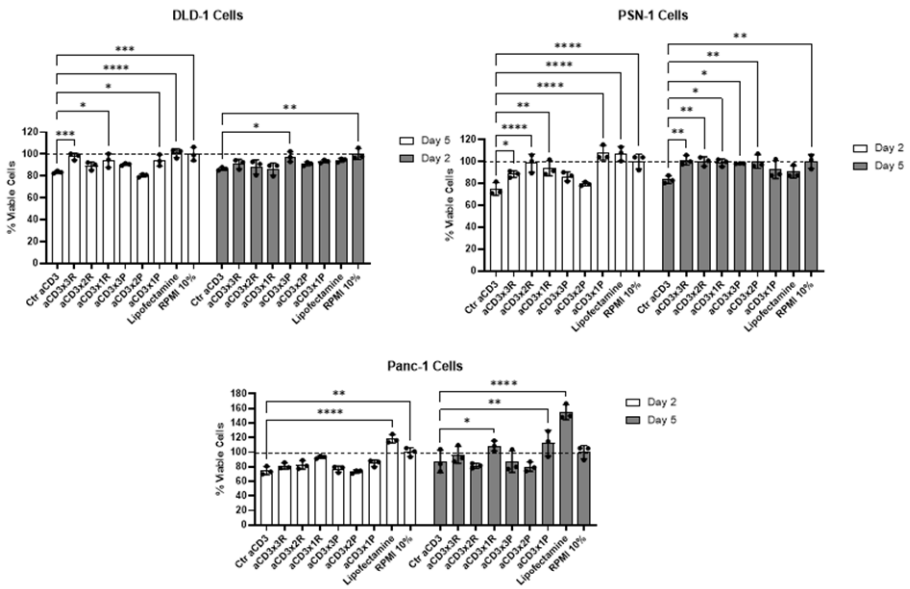

Figure 4.3: Constructs are not cytotoxic after transfection of host cells even at day five post transfection. Transfections were performed in a 96-well plate and cell viability was assessed 48h or 120h post transfection with an XTT cell viability kit. Absorbance at 450 nm was measured after 3-4h incubation with the solution in the cell incubator. n=3, two-way ANOVA with Dunnett's multiple comparisons test to anti-CD3 control, p<0.05 *, p<0.01 **, p<0.001 ***, p<0.0001 ****.

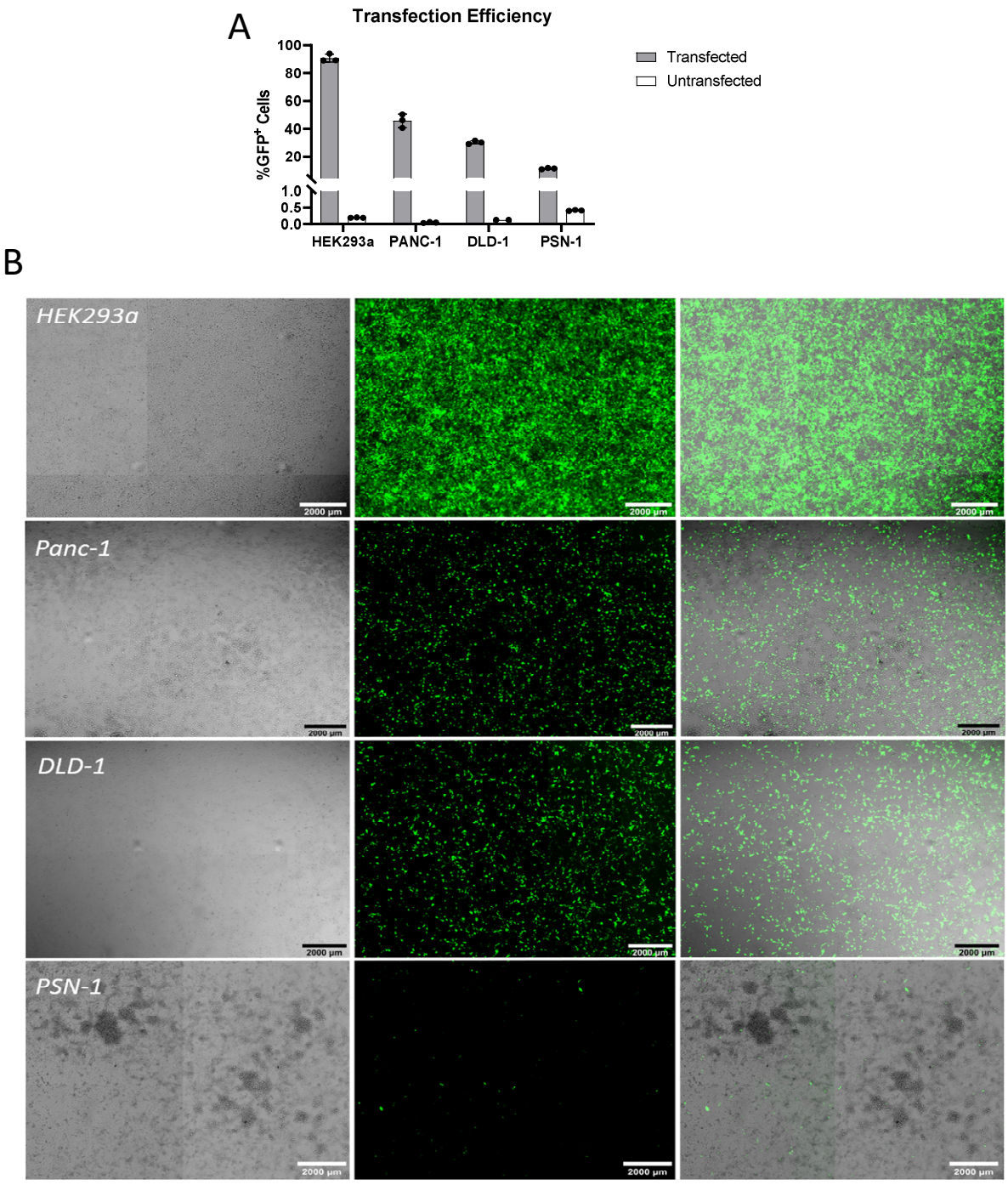

Figure 4.4: Transfection efficiency in HEK293a, Panc-1, DLD-1 and PSN-1 cells. A: Cells were transfected in a 96-well plate and harvested after 48h. Subsequently, cells were measured using a flow cytometer and then analysed. B: The same cells were imaged using the Celigo plate imager at 48h post transfection prior to flow cytometry analysis.

In order to assess whether the transfection of positively charged proteins affects cell viability of the producer cells, the cell viability of DLD-1, Panc-1 and PSN-1 cell lines after transfection was analysed using an XTT assay (**Figure 4.3**). For this, cell lines were transfected with the different constructs and viability was measured after two or five days. No decline in cell viability was observed compared to the anti-CD3 control or un-transfected control cells, and no

difference was observed between day two and day five. Viability in the graph was normalised to cells cultured in 10% FBS in DMEM or RPMI.

As transfection efficiency varies greatly between different types of cancer cell lines, it was important to measure and quantify the differences in transfectability of HEK293a, Panc-1, PSN-1 and DLD-1 cells. Therefore, all cell lines were seeded on a plate, then transfected with a CMV-GFP pSF plasmid the next day and incubated for 48h before harvesting and running on a flow cytometer. **Figure 4.4** A shows the different percentages of green cells, representing the transfected cells. HEK293a cells showed most positive cells (95%), followed by Panc-1 (50%), DLD-1 (40%) and PSN-1 (20%) cells. Furthermore, **Figure 4.4** B shows images taken by Celigo shortly before harvesting of the cells. A similar qualitative trend can be seen when looking at the pictures, however, DLD-1 and Panc-1 cells seem to be transfected to similar levels.

4.3.3 Binding of the constructs to cell lines and ECM-components

It is commonly known that GAGs are abundantly found on cell surfaces, which could lead to the binding of the bispecifics upon secretion (Naik et al. 2011). Therefore, we wanted to investigate whether high amounts of the bispecific found in the cell lysate of the western blot in **Figure 4.3** A was due to a problem in the secretion or due to the strong surface binding of the secreted bispecifics to the producer cells. Hence, HEK293, DLD-1, PSN-1 and Panc-1 cells were transfected with the different constructs and harvested after 48h. The cells were then surface stained with an anti-FLAG PE antibody and analysed using a flow cytometer. As seen in **Figure 4.5** A, the gMFI (white background) and percentage positive cells (grey background) were largely comparable within the same cell line, however, large differences between the cell lines could be observed. Overall, these data suggested that at least a proportion of the constructs were secreted and bound to the outside due to the surface staining performed. In accordance with the transfection efficiency (**Figure 4.4**), PSN-1 cells showed the least amount of signal (least percent transfected) and HEK293a showed the highest signal

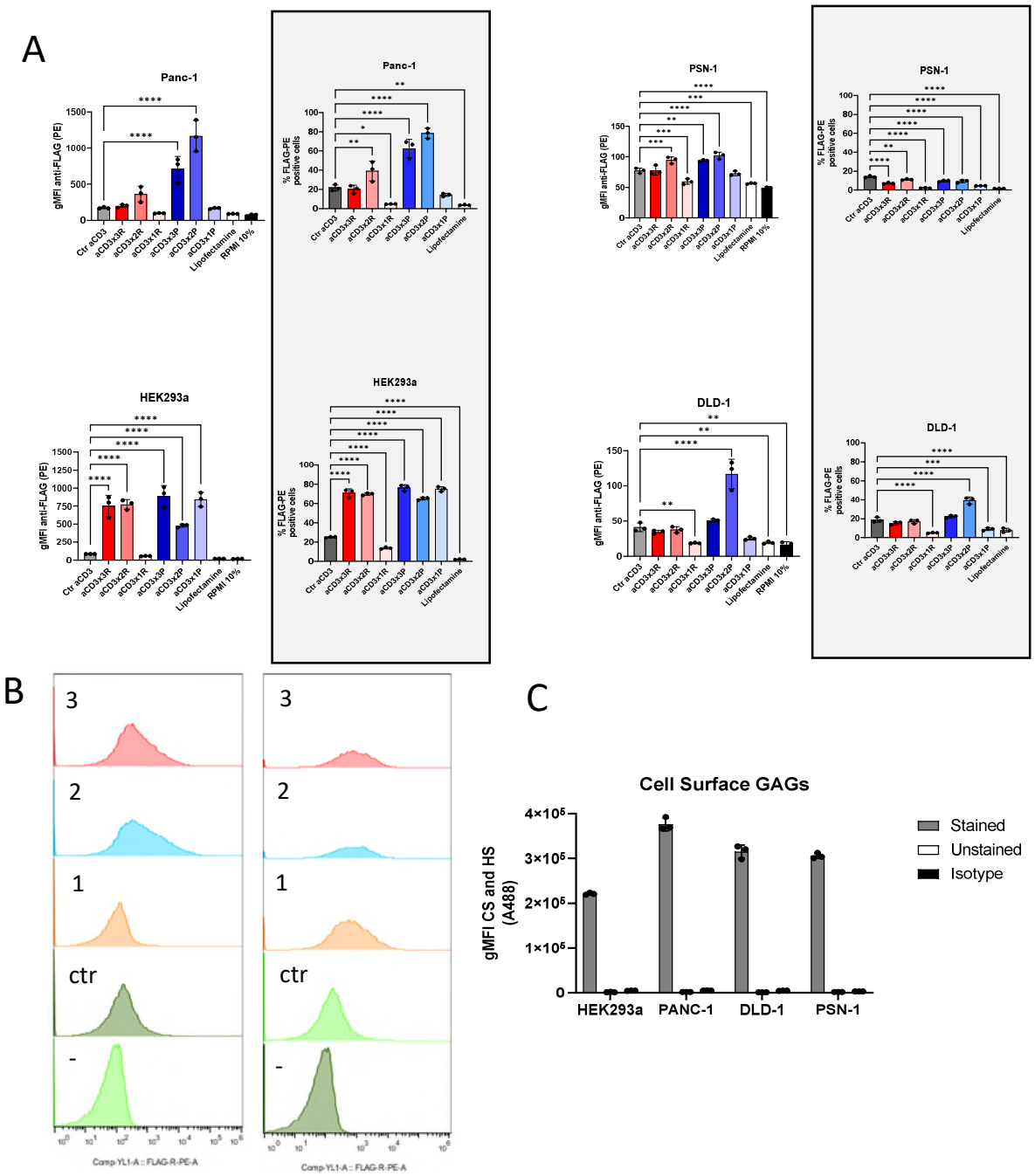

Figure 4.5: Binding of the bispecifics to different host cells after transfection. A: Graph depicting the cell lines 48h post transfection with the constructs. Cells were harvested and stained with an anti-FLAG PE antibody and subsequently run and analysed on a flow cytometer (surface stain). n=3, two-way ANOVA with Dunnett's multiple comparisons test to anti-CD3 control, p<0.05 *, p<0.01 **, p<0.001 ***, p<0.0001 ****. B: Representative histograms from A. C: Surface staining of different cell lines using an antibody against chondroitin sulphate (CS) and heparan sulphate (HS), measured by flow cytometry. n=3.

(highest percent of transfected cells). In all cell lines except for HEK293a, 2xPlGF-2 was the best at binding to the cell surface whereas in HEK293a, all constructs with exception of 1xPolyarginine gave a high signal. Generally, the constructs containing the PlGF-2 motifs seemed to bind overall better in Panc-1 and DLD-1 cells, whereas there is not a big difference between the two groups in PSN-1 and HEK293a cells. **Figure 4.5** B shows the corresponding

histograms, which are representative graphs showing construct binding for FLAG-PE in HEK293 cells. As can be appreciated, the PlGF-2 constructs showed a wider peak compared to the controls or polyarginines, suggesting that more construct was bound to the cells (as can also be seen in the graph in **Figure 4.5** A).

Figure 4.5 D shows the CS and HS GAGs on the different cell line surfaces. For this, the cell lines were cultured and harvested using a gentle harvesting buffer to preserve surface marker integrity. Afterwards, the cells were stained with the isotype controls and CS/HS antibodies, and measured using flow cytometry. As can be seen, HEK293a cells have the least amount of HS and CS, whereby Panc-1 cells have the highest amount. Additionally, DLD-1 and PSN-1 cells seem to have similar levels or surface HS and CS.

After showing that the bispecifics bound to the surface of the producer cells, the binding of the bispecifics to different ECM components was assessed. In particular, the binding to the most abundant proteins in the ECM, collagen I and fibronectin was analysed. On top of this, basement membrane component collagen IV was checked for construct binding. As seen in **Figure 4.6** B, 3xPolyarginine is the only polyarginine construct showing significant binding to all tested ECM components. For the PlGF-2 constructs, all of them show some binding the tested ECM proteins, with 2xPlGF2 performing best at binding when compared to the other

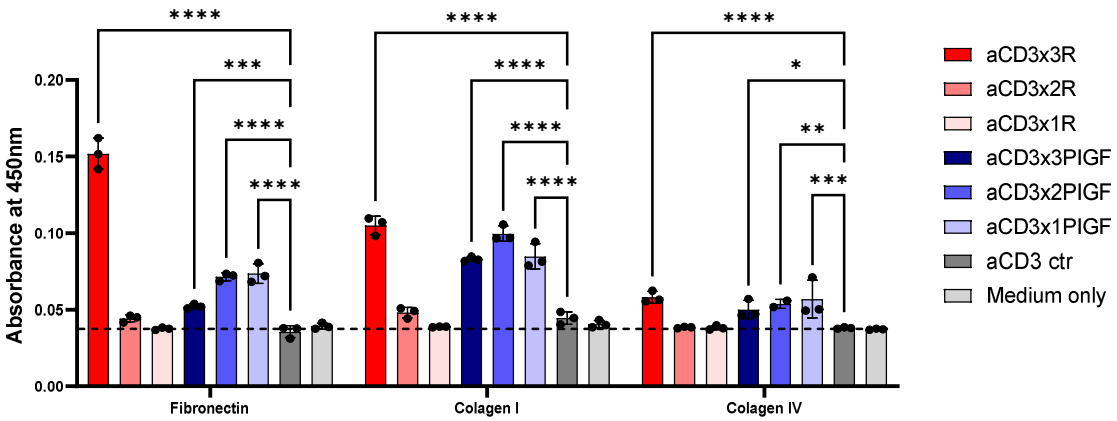

Figure 4.6: ECM binding capability of the different constructs. ELISA plates were coated with collagen I, collagen IV and fibronectin and subsequently challenged with the different constructs (100 nM). Absorbance was measured at 450 nm. n=3, two-way ANOVA with Dunnett's multiple comparisons test to anti-CD3 control, p<0.05 *, p<0.01 **, p<0.001 ***, p<0.0001 ****.

PlGF-2 constructs. There was no binding of the aCD3 scFv control to any of the tested ECM components.

4.3.4 Polarginine and PlGF-2 bispecific mediated T cell activation and bystander cytotoxicity

After showing that the constructs were indeed binding to the cell surface and were not wholly retained inside the cell, we sought to investigate the bispecific-mediated T cell activation and cytotoxic potential. Therefore, the different cell lines were seeded and transfected with the

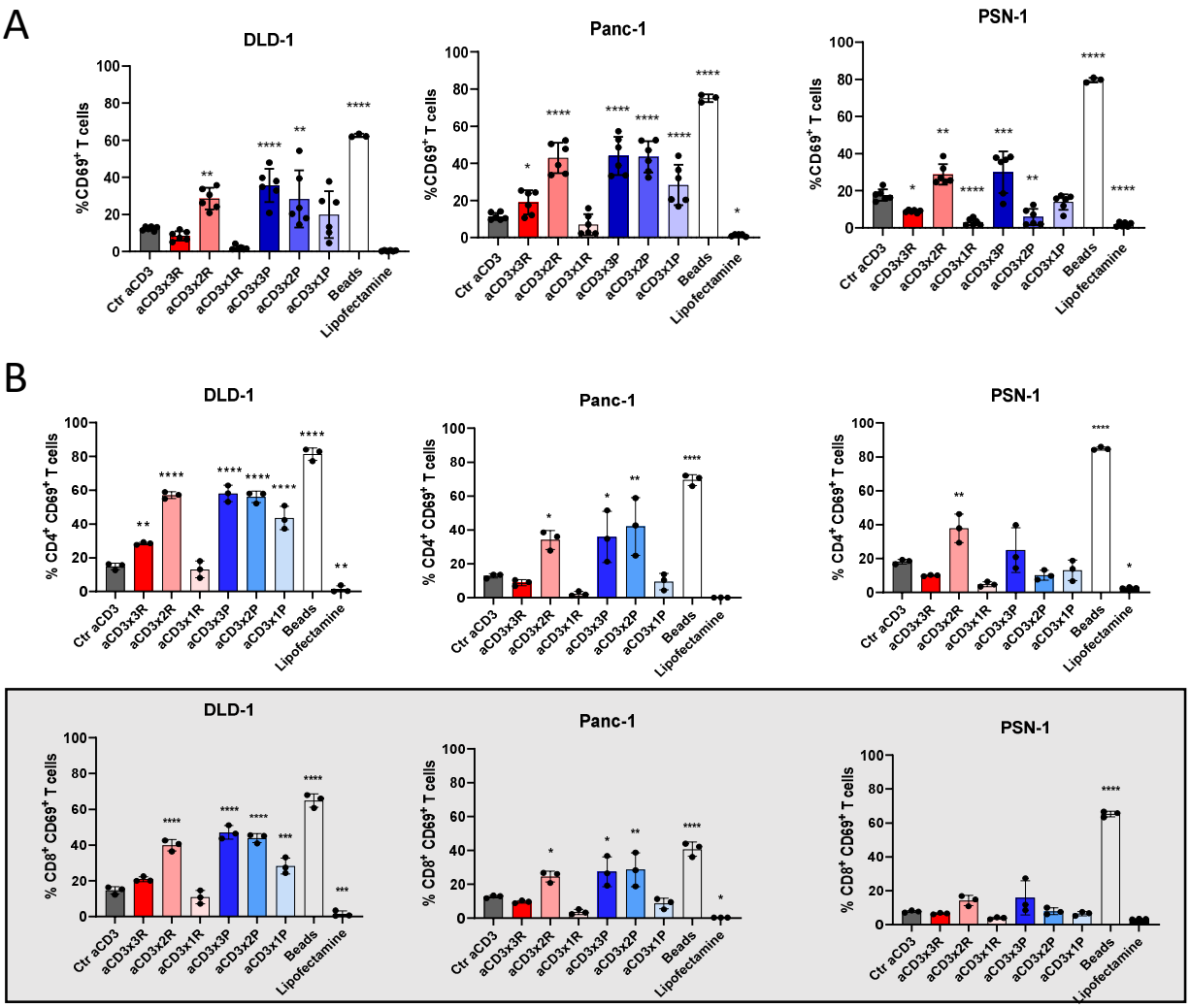

Figure 4.7: Human PBMC T cell activation 16h post transfection. A: DLD-1, PSN-1 and Panc-1 cells were transfected with the different constructs and human derived PBMC T cells were subsequently added to the cells. The T cells were harvested after 16h and stained for CD4, CD8, Live/Dead, CD69 and afterwards measured using a flow cytometer. n=6, two independent experiments, One-way ANOVA with Dunnett's multiple comparisons test to anti-CD3 control, p<0.05 *, p<0.01 **, p<0.001 ***, p<0.0001 ****. B: The same cells as shown in A but split into CD4 and CD8 T cells. n=6, two independent experiments, One-way ANOVA with Dunnett's multiple comparisons test to anti-CD3 control, p<0.05 *, p<0.01 **, p<0.001 ***, p<0.0001 ****.

constructs on day one and left to recover overnight. On day two, T cells were added to the cell lines and incubated for 24h before harvesting and staining for CD69 surface expression (T cell activation marker), followed by analysis using flow cytometry. In **Figure 4.7** A, the T cell activation measured by CD69 upregulation on total T cells is shown for DLD-1, PSN-1 and Panc-1, and **Figure 4.7** B shows the upregulation of CD69 on CD4 and CD8 T cells separately. As can be seen in the graphs, the PlGF-2 constructs showed some activation in all the three cell lines, whereas the 2xPolyarginine only showed T cell activation in DLD-1 and Panc-1 cells. 3xPolyarginine only showed CD69 activation in Panc-1 cells. Additionally, all constructs demonstrated only moderate activation compared to the Dynabeads control, with exception of the CD69 induction on T cells cultured with Panc-1 cells.

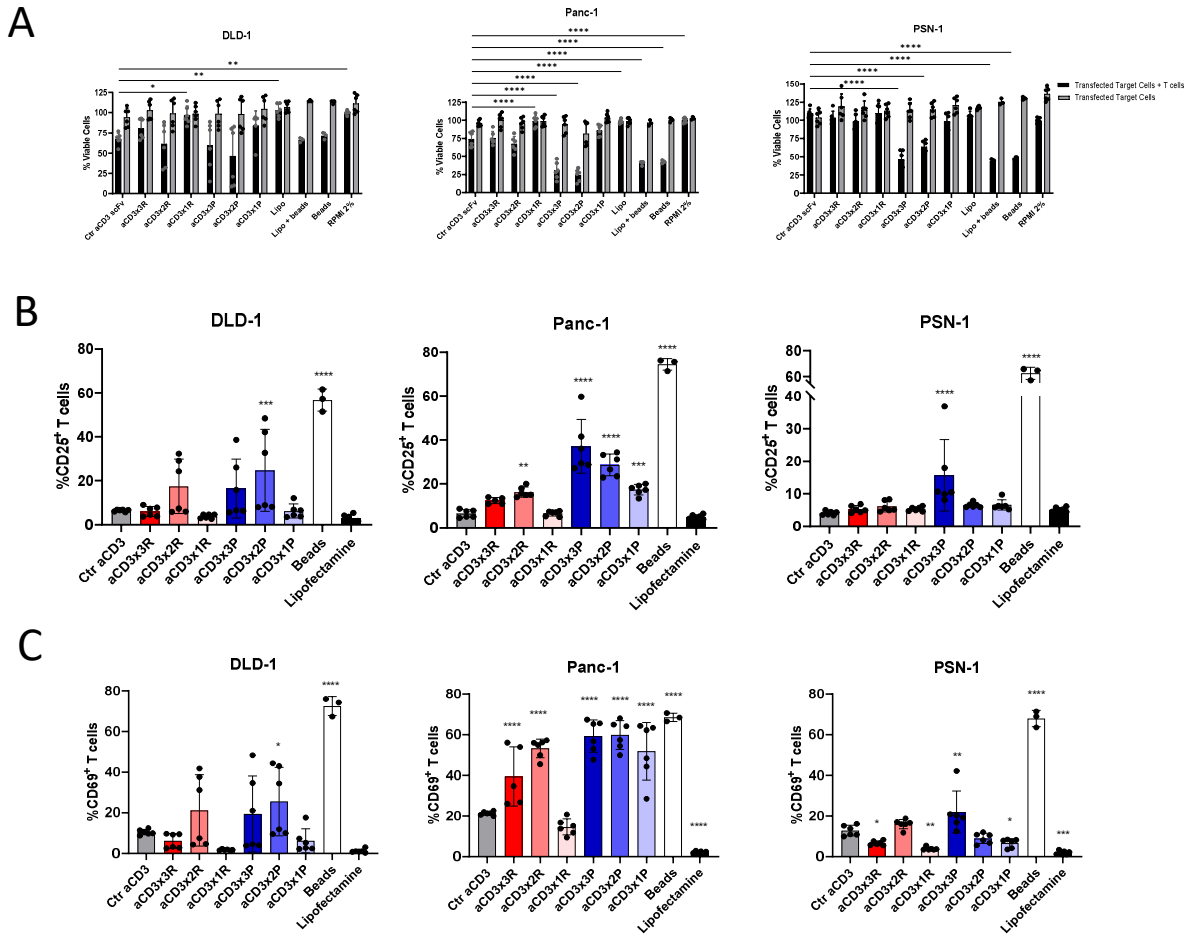

Figure 4.8: T cells mediated bystander cytotoxicity upon activation with positively charged bispecifics. A: Cells were transfected with the different construct and left to recover overnight. The next day, human PBMC T cells were added to the cells and incubated for 5 days before performing an XTT viability assay. Absorbance was measured at 450 nm. n=6, two independent experiments, Two-way ANOVA with Dunnett's multiple comparisons test to anti-CD3 control, p<0.05 *, p<0.01 **, p<0.001 ***, p<0.0001 ****. B and C: Corresponding T cell activation as measured by CD25 and CD69 expression to A. n=6, two independent experiments, One-way ANOVA with Dunnett's multiple comparisons test to anti-CD3 control, p<0.05 *, p<0.01 **, p<0.001 ***, p<0.0001 ****.

In addition to the 16h activation of T cells, their capacity to mediate cytotoxicity after a 5-day incubation was assessed. Therefore, Panc-1, DLD-1 and PSN-1 cells were transfected with the constructs and left overnight to recover. The next day, T cells were added to the cells and incubated for 5 days. On day 5, an XTT assay was performed to assess the percentage of living cells, whereby the values shown on the graph are blank corrected and normalised to Lipofectamine 2000 only control condition. Additionally, T cells were harvested and stained for CD25 and CD69 surface markers, indicating T cell activation. As can be seen in **Figure 4.8** A, there was only very little cytotoxicity mediated through the polyarginines across all the tested cell lines. The PlGF-2 motifs, however, showed comparable cytotoxicity to the Dynabead control and somewhat decreasing levels of cytotoxicity with decreasing repeats of the PlGF-2 motifs. Contrary to the activation levels of the T cells, the PIGF-2 constructs induced similar amounts or even more cytotoxicity in the tested cell lines when compared with the CD3/CD28 Dynabead control.

In **Figure 4.8** B and C, the T cell activation of the cytotoxicity experiment can be seen. Similar results to **Figure 4.7** can be observed, with the PlGF-2 construct performing well overall and very little reactivity shown by the polyarginine construct, except for Panc-1 cells.

4.3.5 Colorectal liver metastases slices show an increased IFN-γ production upon treatment with positively charged bispecifics

In order to test the feasibility of deploying the bispecifics in a more clinical setting, patient-derived human colorectal liver metastasis samples were sliced using a vibratome as shown in **Figure 4.9** A. In comparison to *in vitro* experiments, tumour slices present a more clinically relevant and impactful model to study and evaluate new therapeutics for cancer research, not at least due to the intact TME and ECM. Especially the intact ECM made this test system very relevant to validate the feasibility of the constructs used in this study. For this experiment, the tumour was collected from surgery and brought to pathology, where it was then taken to the laboratory before being processed and cut into 250 µM thin slices. The slices were then

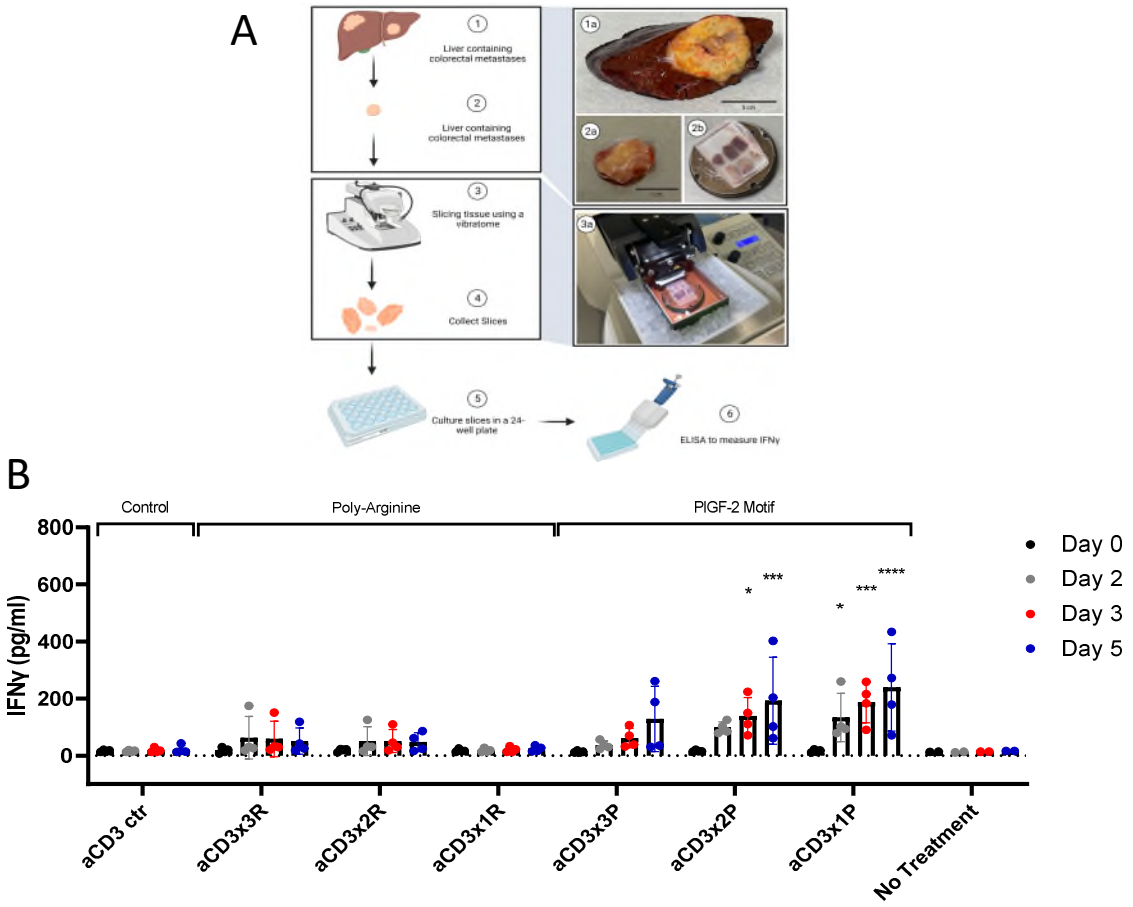

Figure 4.9: Treatment of colorectal liver metastasis slices with the different positively charged bispecifics leads to IFN-γ production. A: Graphical schematic of the tumour slicing process. The metastases were collected right after surgery and cut into 250 µm thick slices for the treatment. B: The slices were treated over five days with 100 nM of the different constructs, whereby medium for ELISA was taken at day 0, day 2, day 3 and on day 5. A total amount of two patients are shown with two slices per patient. Each line represents one separate slice. n=4, two different patients are shown, Two-way ANOVA with Dunnett's multiple comparisons test to anti-CD3 control, p<0.05 *, p<0.01 **, p<0.001 ***, p<0.0001 ****.

transferred into a 24-well plate and subsequently incubated in slice medium overnight to get a baseline reading, and then again with the treatment for five days. Supernatant samples for readings were taken on day two, day three and day five, and measured by ELISA to check for the amount of IFN-γ. IFN-γ is a cytokine predominantly produced by activated T cells, however, can also be produced by NK or NKT-cells. There are a total of four slices shown, in **Figure 4.9** B, deriving from two different patients. The greatest level of IFN-γ was induced by the PlGF-2 constructs, with some slices also producing low levels following incubation with 3x and 2xPolyarginine. This is clinically relevant evidence that ECM within clinical colorectal metastases can bind these agents to sufficiently high density to mediate the endogenous production of IFN-γ, validating the therapeutic concept. It seems that the levels of T cell

activation are higher with PlGF-2 than with polyarginine, although arguably both approaches show the potential for further development. In addition, while we have demonstrated the ability to activate T cells within tumours, bystander cytotoxicity within tumour biopsies has not been directly established, although it was clearly seen in the *in vitro* experimental systems.

4.4 Discussion

In this study, we investigated the *in vitro* feasibility of using non-specific T cell activation motifs tethered to GAGs in the ECM in order to mediate T cell activation and bystander cytotoxicity in the TME. This approach could be combined in the future with OVs for local and specific expression.

CD3/CD28 Dynabeads are one of the most commonly used controls for *in vitro* T cell activation, mainly because they can cluster CD3 and CD28 and thereby activate T cells non-specifically and in the absence of target cells. In the presence of target cells, however, Dynabead-activated T cells facilitate cytotoxicity via bystander killing as seen in the literature and in the previous chapter (Ross et al. 2015; Upadhyay et al. 2021).

Having the advantage of potentially exploiting local expression through an oncolytic virus to avoid unwanted off-tumour cytotoxicity, two classes of ECM-binding bispecifics were designed containing positively charged tails deriving from polyarginine repeats or 21 AA from PlGF-2. The PlGF-2 motif has already previously been used to retain antibodies in the TME after injection by Hubbell et al. (Ishihara et al. 2017). As a comparison to the PlGF-2 motif, a positively charged tail was created using six-time repeats of arginine, to investigate charge-mediated binding only. Despite having a similar number of positive charges on the constructs containing 3xPolyarginine (18 positive charges) and 2xPlGF-2 (20), the 2xPlGF-2 construct performs much better in terms of binding to cells and ECM components, it is also superior in functionally activating human PBMC T cells and in mediating bystander cytotoxicity. This suggests that the configuration of the positive charge plays an important role for the function of the bispecifics.

It was unclear from an initial western blot (**Figure 4.3** A), if the constructs were secreted or aberrantly remained inside the producer cells. Therefore, a cell surface staining was performed and showed that the bispecifics were secreted but remained attached to the cell surface. Although all the cell lines expressed abundant amounts of GAGs (HS and CS) on their surface (**Figure 4.5**), this was not the main determinator of the amount of bispecific retained on the cell surface, but rather the transfection efficiency of the different cell lines (**Figure 4.4** and **Figure 4.5**). Therefore, HEK293a, for example, show the least amount of surface GAGs, but simultaneously display the highest gMFI and percentages of bound bispecific. Additionally, a spread of the construct from cell to cell could be observed especially in Panc-1 cells, given that approximately 40-50% of the cells are transfected but 80% were measured to have the PlGF-2 construct bound to the cell surface.

Interestingly, Hubbell et al. showed a strong association of the PlGF-2 motif with ECM-GAGs, but they never accounted for the binding of PlGF-2 to the cell surface GAGs (Ishihara et al. 2017; Martino et al. 2014). Data in this chapter (**Figure 4.4** and **Figure 4.5**), however, suggests that the bulk of the retention of PlGF-2 is mediated by the cell surface GAGs and potentially not through ECM-GAGs.

Although the amount of T cell activation between the different constructs varies greatly and was only small compared to the activation achieved through the EpCAM BiTE or Dynabeads (**Figure 4.7** and **Figure 3.2**), the constructs were still able to mediate relatively high levels of cytotoxicity *in vitro*. In addition to this, it is important to note that the test systems as used in this chapter always involved the transfection and expression of the bispecifics by tumour cells, which contrasts with other bispecific experimental set ups, where the bispecifics are often produced and quantified in other cells and externally added to the experiments in a defined amount. As such, even cells lines with a relatively low level of transfected cells such as PSN-1 cells were still able to induce significant levels of T cell activation and mediated cytotoxicity. This could suggest a spread of the proteins to non-transfected cells or bystander killing.

Due to the high expression of GAGs in the ECM of healthy tissue and on normal cells, IV injection of these bispecific agents as simple proteins is likely to lead to unwanted side effects. Instead, tumour specificity could be achieved by expression of the bispecific from an oncolytic virus, as has been shown previously with different payloads (discussed in Chapter 1.6.2). Additionally, as this approach relies on GAG expression, it is applicable in most solid cancers when combined with local delivery or expression (Wieboldt and Läubli 2022).

Due to the lack of a comprehensive ECM in *in vitro* experimental settings, it has proven very difficult to assess the full potential of the bispecifics. Here, we used an *ex vivo* colorectal liver metastasis slice model. This model not only provides clinical relevance, but also contains an intact ECM as found in the patient TME. Additionally, no cells were added to the slices, meaning that all produced mediators stem from endogenous cells. As seen in **Figure 4.9** B, the constructs induced various amounts of IFN-γ release potentially relating to T cell activation (Runge et al. 2022). The PlGF-2 constructs also seem to induce higher IFN-γ levels compared to the Polyarginine constructs, which was to be expected from the other experiments. However, contrary to the previous data, 1xPlGF-2 construct induced higher levels of IFN-γ compared to 3xPlGF and 2xPlGF-2. This discrepancy with the data in **Figure 4.7** showing higher IFN-γ production with 2xPlGF-2, can perhaps be explained by a lower penetration of the more positively charged bispecifics which can be hindered by a dense and GAG-rich ECM as discussed in the introduction (Chapter 1.5.5.1). Therefore, positively charged bispecifics such as 3xPlGF-2 and 2xPlGF-2 will stick to the outer layers of the slice and hence cannot reach many T cells inside the slice. It is important to note that the production of IFN-γ is an indirect marker of T cell activation, as other producers of IFN-γ such as NKT-cells, NK cells or B cells could be prompted by activated T cells to produce IFN-γ themselves. This lack of differentiation of the IFN-γ producer cells represents a limitation of this assay. However, this experiment nevertheless shows that the bispecifics can induce significant IFN-γ production of endogenous cells (potentially T cells).

Overall, the PlGF-2 motif containing bispecifics performed better in terms of T cell activation and target cytotoxicity, demonstrating that the evolved PlGF-2 sequence displays a potentially more adapted and refined binding compared to the synthetic polyarginines. Additionally, the total number of charges plays a role *in vitro*, with 2x and 3xPlGF-2 outperforming 1xPlGF-2 in T cell activation and cytotoxicity. In *ex vivo* samples, however, the number of charges loses importance, as 1xPlGF-2 performs better compared to 2x and 3xPlGF-2, probably due to the reason discussed above. This is an issue which could be prevented by delivering the bispecifics with an OV, which can penetrate further into the tissue.

In conclusion, this study shows that tumour infiltrating T cells can be non-specifically activated by anti-CD3 motifs bound in the extracellular space and mediate local bystander cytotoxicity. This is the first-time bystander killing has been exploited in a therapeutic approach and shows that it is, given the specific delivery through a gene therapy vector or oncolytic virus, a potentially feasible immunotherapeutic approach.

One disadvantage of the approach described in this chapter is that a significant proportion of the encoded bispecific agents appear to tether to GAGs on the surface of the producer cells, or on other cancer cells. While this is sufficient to validate our T cell-activation hypothesis, it may mean that the bispecific agents are lost when those cancer cells die, limiting the overall duration of immunostimulation that can be achieved. Accordingly, in the next chapter we explore strategies to achieve ECM-tethering without the agents becoming bound to the outside of the cancer cells.

5 Targeting collagen I to harness bystander cytotoxicity using a LAIR-2xanti-CD3 bispecific

5.1 Introduction

The previous chapter demonstrated that anti-CD3 motifs bound to GAGs on the cell surface and ECM can activate T cells and mediate bystander killing *in vitro* and *ex vivo*. Although the immobilisation of bispecifics onto GAGs has proven to be somewhat effective, the non-specific nature of the interactions may lead to several unknown and hard to account for factors contributing to the binding of the bispecifics. Moreover, the bispecific could bind to other cells' surfaces and lead to the unwanted spread of the bispecific throughout the body. Therefore, we sought to explore different, abundant ECM targets with more specificity, including collagens.

Collagens are the most abundant proteins in the ECM and therefore display a vast number of potential binding sites. In particular, collagen type I is upregulated in many cancers such as hepatocellular carcinoma and lung adenocarcinoma, and collagen I mRNA levels are correlated with a poorer prognosis in many cancers (Shi et al. 2022). Additionally, collagen cross-linking enzymes such as LOX, responsible for mediating collagen stiffness, have also been shown to negatively impact on patient survival (Baker et al. 2013; W. Ma et al. 2019). Besides the myriad of factors contributing towards tumour growth (described in Chapter 1.2.1.1), collagen I is also involved in shaping the immune landscape of the tumour, especially in respect to tumour infiltrating T cells.

It has been demonstrated that T cells have a reduced capacity to migrate in tumours with higher collagen stiffness (Nicolas-Boluda et al. 2021; Tabdanov et al. 2021). Importantly, the reduction in migration was confirmed in another study to not be dependent on pore size but rather on the stiffness of the 3D network (Hörner et al. 2019). Furthermore, it has been observed that pre-activated T cells cultured in a high-density collagen network showed a

decrease in proliferation when compared to the same T cells cultured in a low-density collagen network (Kuczek et al. 2019), suggesting that collagen is able to alter T cell behaviour after activation. Other studies suggest that collagen impacts on the immune synapse formation between APCs and T cells, thereby potentially reducing antigen-specific T cell activation (Dustin and De Fougerolles 2001; Gunzer et al. 2000; Rømer, Thorseth, and Madsen 2021).

In terms of specific binding interactions, collagen I in particular plays an important role in engaging the immunosuppressive leukocyte-associated immunoglobulin-like receptor 1 (LAIR-1) on T cells. Accordingly, LAIR-1 has emerged as an ECM-mediated IC, with several studies showing that a LAIR-1 blockade could potentially have similar effects as IC therapy and, among other things, lead to a higher T cell activation *in vitro* and *in vivo* (Jansen et al. 2007; Park et al. 2020; Peng et al. 2020; Ramos et al. 2021). Upon collagen I engagement, the two intracellular ITIMs recruit SHP-1 and SHP-2, dephosphorylating key proteins in the TCR-activation pathway. Although LAIR-1 is expressed on a myriad of immune cells, most prominently on T cells, B cells, macrophages and NK cells (Meyaard et al. 1997; Xie et al. 2022), this chapter focusses on the effects of LAIR-1 on T cells. Generally, CD8 T cells show a higher LAIR-1 expression than CD4 T cells, and different studies have shown the involvement of the inhibitory capacity of the collagen I – LAIR-1 axis in the inhibition of CD8 T cell-mediated cytotoxicity (Saverino et al. 2002) and cytokine production induced by the TCR in T cell clones (Meyaard et al. 1999).

In contrast to LAIR-1, LAIR-2, which shares approximately 84% homology with LAIR-1, is regarded as a soluble competitor to LAIR-1, binding to the same epitope on collagen I with higher affinity compared to LAIR-1 (Lebbink et al. 2008). LAIR-2 is, for example, found in the synovial fluid of patients with Rheumatoid Arthritis (RA) and in patients suffering from autoimmune thyroid disease, whereby the degree of inflammation correlates with the amount of LAIR-2 which can be detected (Lebbink et al. 2008; Nordkamp, Van Roon, et al. 2011; Ramos et al. 2021; Simone et al. 2013).

The LAIR-1/-2 axis poses a simple yet potentially effective way to enhance current cancer therapies. A study by Xie et al. looked into using h219, an antagonistic LAIR-1 antibody as a potential new approach. They could observe *in vitro* an enhanced DC differentiation and resulting from this, also T cell proliferation and differentiation as well as cytokine secretion by macrophages. When administered *in vivo*, a delayed development of the tumour could be observed (Xie et al. 2022). In another study, Ramos et al. developed a fusion protein consisting of two LAIR-2 proteins fused to an Fc region, named NC410. Upon IP injections in mice, they observed a general increase of effector T cell numbers and increased T cell infiltration into the tumour. Taken together, the study suggests this approach should be considered as a supplemental therapy, and first clinical trials to assess safety are currently underway (NCT04408599, (Ramos et al. 2021)).

In conclusion, targeting collagen or the LAIR-1/-2 axis in cancer is very promising. One of the big problems to overcome is related to the omnipresence of collagen I, which implies a local delivery might have a stronger effect or might even be necessary for safety reasons. However, because the above mentioned approaches probably rely on IV delivery, it is possible that the full effect of targeting the axis might not yet have been exploited.

Therefore, we aim to design an immunotherapeutic strategy to target collagen I, disrupting the engagement with LAIR-1, and simultaneously decorating the ECM with an agonistic CD3 scFv. This should activate intratumoural T cells and prime them for bystander cytotoxicity of neighbouring cells.

5.2 Hypothesis

In this chapter, we hypothesise that a fusion protein of LAIR-2 with an immune stimulatory anti-CD3 scFv is able to (1) bind to collagen I *in vitro* and *ex vivo*, (2) form a durable reservoir of anti-CD3 scFvs on collagen I *in vitro*, (3) activate PBMC- and tumour-derived human T cells and (4) exhibit bystander cytotoxicity towards a multitude of different cell types (tumour cells but also the non-transformed tumour-supportive fibroblasts).

5.3 Results

5.3.1 Graphical abstract

Figure 5.1 shows a graphical representation of the hypothesis and aims laid out in the previous paragraph. Upon engagement of collagen I with the inhibitory receptor LAIR-1, the intracellular ITIMs of LAIR-1 recruit SHP-1/-2, which mediate the inhibition of different pathways within the T cells (**Figure 5.1**, 1). In order to interfere with this signal, we have designed a bispecific fusion protein consisting of LAIR-2 and an anti-CD3 scFv. On the one hand, the bispecific is designed to interrupt the LAIR-1 – collagen I interaction, and on the other, it can form a reservoir of agonistic anti-CD3 motifs in the tumour ECM and therefore locally activate T cells (**Figure 5.1**, 2). Both of these effects ultimately lead to the induction of T cell bystander killing.

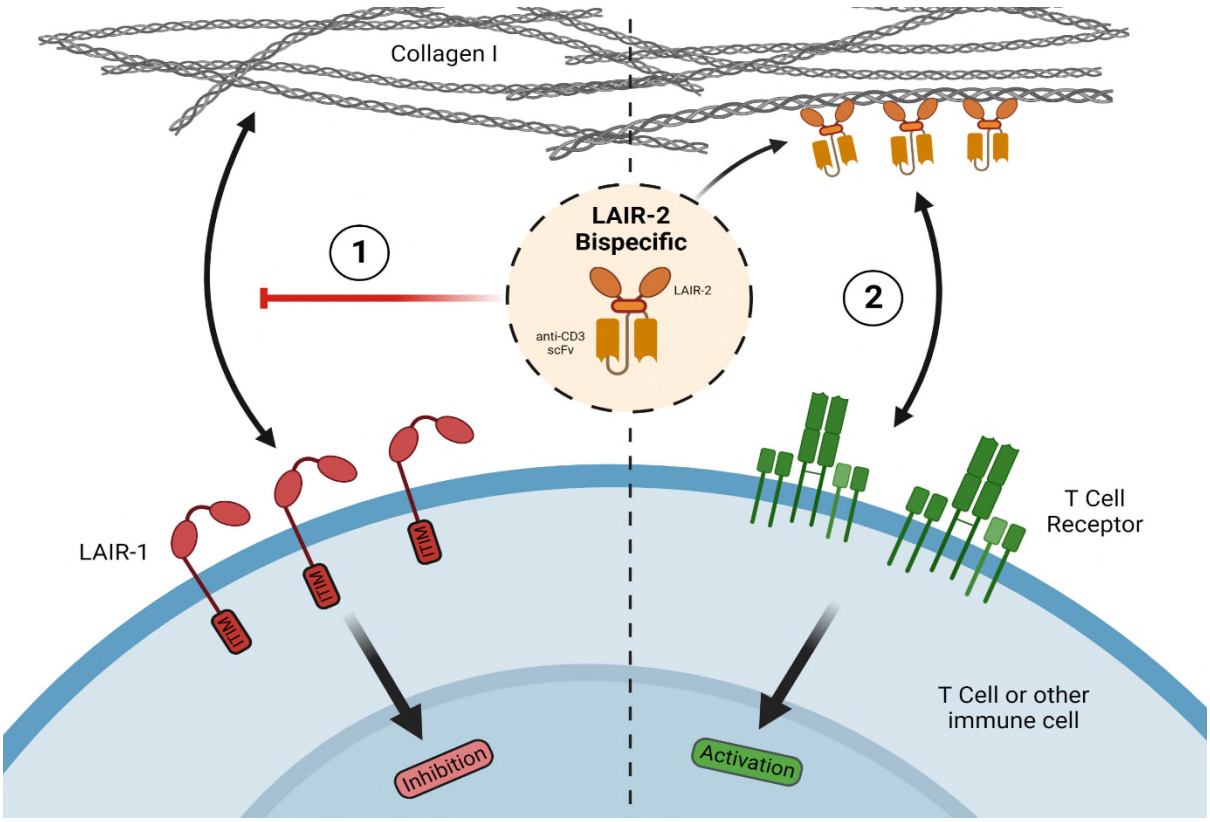

Figure 5.1: Graphical abstract for Chapter 5. The bispecific consisting of LAIR-2 and an anti-CD3 scFv (LAIR-2xaCD3) has a dual effect upon binding to collagen I in the TME: Firstly, binding to collagen I will mask the binding site for the ECM-mediated IC LAIR-1 receptor expressed on T cells (and other immune cells), preventing suppression of T cell activation (1). Secondly, upon collagen I binding of the bispecific, the ECM will be decorated with agonistic anti-CD3 motifs, capable of antigen-independently and locally activate T cells and evoke local bystander killing (2).

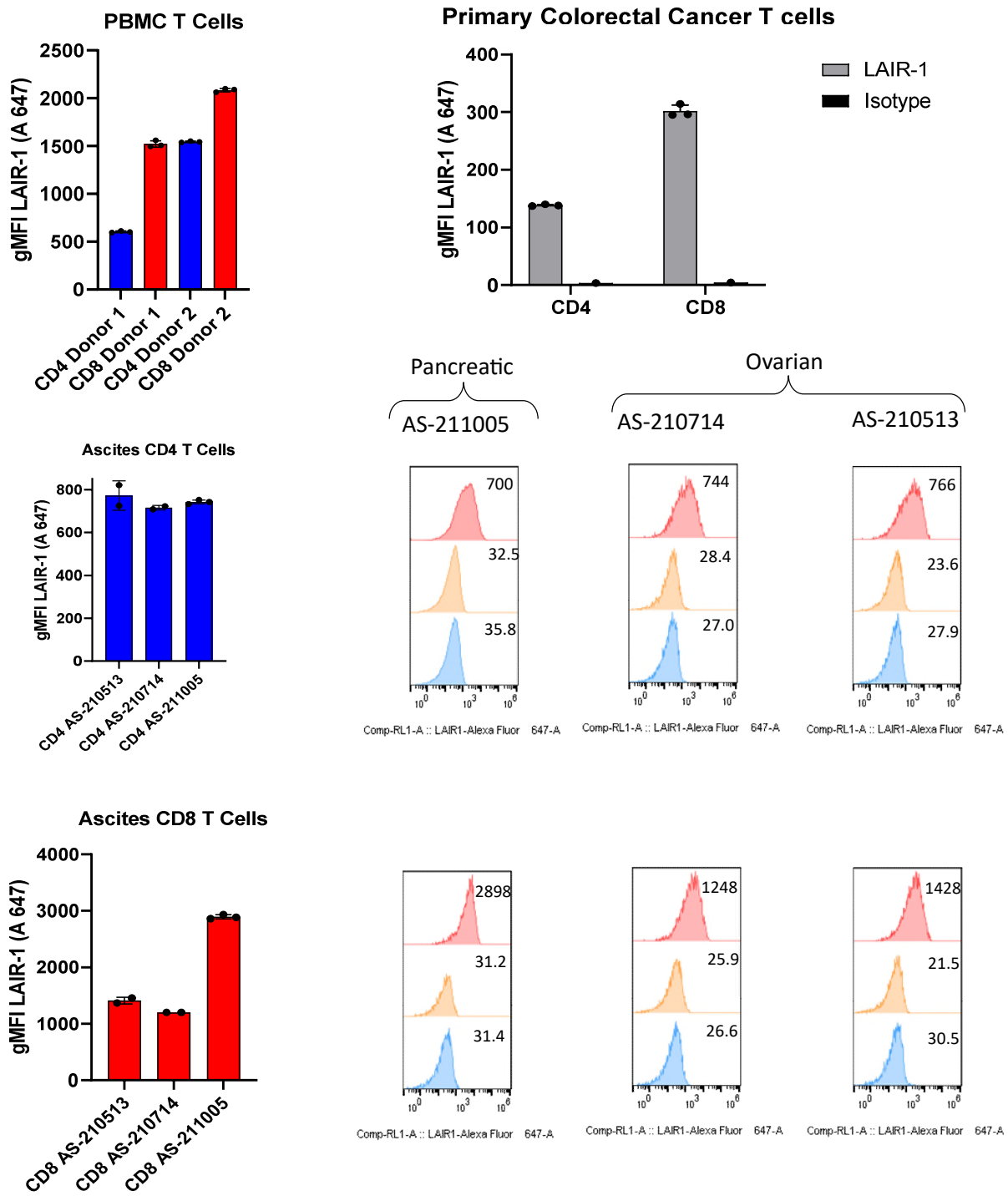

Figure 5.2: Patient-derived T cells from various model systems express LAIR-1. A: Expression of LAIR-1 on PBMC-T cells used in in vitro T cell activation assays, showing the expression on CD4 and CD8 T cells from two different donors. B: LAIR-1 expression on patient-derived primary colorectal cancer T cells used as *ex vivo* dissociated cells. C: LAIR-1 expression on ascites-derived T cells. Three different ascites patients (pancreatic and ovarian) are shown in this panel and divided into CD4 and CD8 T cells.

5.3.2 LAIR-1 Expression on T cells and construct design

According to the literature, LAIR-1 is highly expressed on many effector immune cells and especially on T cells (Meyaard et al. 1997). Therefore, all different types of T cells used in the subsequent experiments were stained for LAIR-1 expression and measured using flow cytometry. In **Figure 5.2** A, the expression of two different donors of PBMC-T cells can be seen, where the stark difference of the gMFI between the donors can be appreciated. CD4 T cells, however, show a lower LAIR-1 expression compared to CD8 T cells by approximately a factor of three. In **Figure 5.2** B, LAIR-1 expression on primary human colorectal cancer T cells was measured. Similar to **Figure 5.2** A, CD8 T cells express more LAIR-1 compared to CD4 T cells by approximately three times. As seen in **Figure 5.2** C, the LAIR-1 expression on ascites-derived T cells is similar as found on the other T cells, with CD4 T cells expressing less LAIR-1 compared to CD8 T cells, whereby the difference between CD4 and CD8 T cells is less pronounced.

After checking on the expression of LAIR-1 on different T cells, we have designed two bispecific proteins and two control constructs. Therefore, fusion proteins consisting of a LAIR-2 and an anti-CD3 scFv was designed in both orientations (**Figure 5.3** A). LAIR-2 was in this instance chosen over soluble LAIR-1 because of the higher affinity to the same epitope on

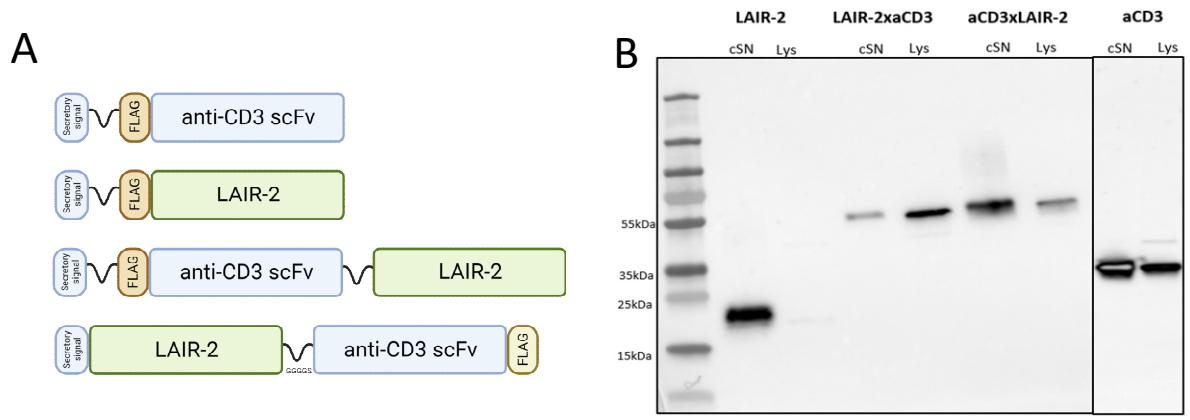

Figure 5.3: Design and expression of the different bispecifics and controls. A: An anti-CD3 scFv and a full-length LAIR-2 protein were designed as controls, and the bispecific consisting of a fusion protein of an anti-CD3 scFv and full length LAIR-2 protein were cloned in both possible confirmations. Additionally, all proteins were FLAG tagged and the domains were separated by a GGGGS linker (black line in the schematic). B: Western blot showing the supernatant (concentrated, approximately 40x) and the cell lysate for the different constructs, detected using an anti-FLAG HRP antibody.

collagen I and hence the competitive binding capability (Nordkamp, Roon, et al. 2011). As controls, a separate LAIR-2 only and anti-CD3 scFv only were cloned. All constructs were FLAG-tagged and the major domains were separated by a GGGGS linker, as can be seen in **Figure 5.3** A. In **Figure 5.3** B, HEK293a cells were transfected with the different constructs to confirm that the proteins could be secreted. Supernatant and lysate was harvested after 48h, run on a western blot and probed for FLAG. As seen in **Figure 5.3** B, all constructs were expressed and secreted, with the LAIR-2 only running at approximately 15 kDa, aCD3 control running at approximately 32 kDa and the fusion proteins running at approximately 47 kDa.

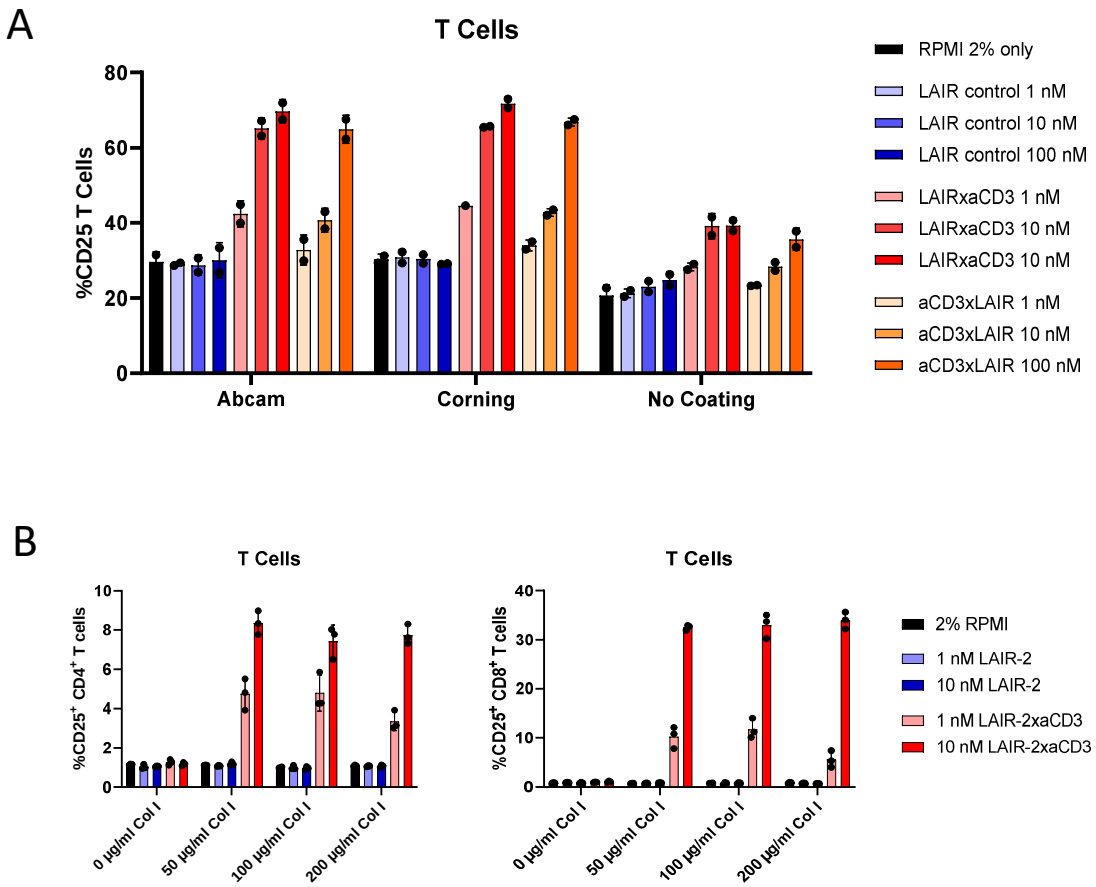

Figure 5.4: Preliminary data showing LAIR-2xaCD3 bispecific induced more potent T cell activation compared to the other orientation. Additionally, the Corning human collagen I at a concentration of 100 µg/ml was chosen to continue further experiments. A: T cells were pre-activated with 0.5 µl of Dynabeads (CD3/CD28) per well on a plate pre-coated with collagen I from different manufacturers and different amounts of the bispecifics and controls bound to the collagen I. n=2 shown from a biological replicate. B: T cell activation (CD4 and CD8) measured by CD25 on different amounts of Corning collagen I. n=3 shown from three biological replicates.

5.3.3 Preliminary results using LAIR-2xaCD3 show higher T cell activation compared to aCD3xLAIR-2

In order to assess if there was a difference between the two configurations of the LAIR-2 bispecifics, a 96-well plate was coated with collagen I from different manufacturers and at different concentrations, and then incubated with the different bispecifics for 1h. After 1x washing, T cells were added to the plate. In **Figure 5.4** A, the T cells were pre-activated with 0.5 µl of Dynabeads per well in order to assess any T cell inhibition mediated by the LAIR-1 – collagen I axis. T cells in **Figure 5.4** B were unstimulated. Cells were harvested after 48h, then stained and measured using a flow cytometer. As can be seen in **Figure 5.4** A, there was no difference between the brands of collagen I used. Due to shipping conditions and stability, it was decided to proceed with collagen I from Corning. Additionally, LAIR-2xaCD3 mediated higher T cell activation at lower concentrations compared to aCD3xLAIR-2, therefore omitting aCD3xLAIR-2 from testing in further studies.

In **Figure 5.4** B, the effect of different amounts of collagen I coated to a 96-well plate was assessed. As can be seen, even low amounts of collagen I mediated high T cell activation. Therefore, it was decided to proceed with 100 µg/ml for coating of tissue culture treated plates.

5.3.4 CD4 and CD8 T cells activation upon challenge with LAIR-2xaCD3

After establishing the optimal orientation of the bispecific and the conditions of the collagen I coating of plates, it was important to repeat the T cell activation assay and measure T cell activation more robustly. Therefore, 100 µg/ml of collagen I was coated for 1.5h at RT on a 96-well plate and subsequently challenged by the different proteins for 2h at 37°C, then washed and human-derived PBMC T cells were added to the plates. The T cells were harvested after 48h and the T cell activation was measured by looking at CD25 and CD69 upregulation using flow cytometry. As can be seen in **Figure 5.5** A, CD4 T cells can be activated by the bispecific only in the presence of collagen I, which can be seen by an upregulation of

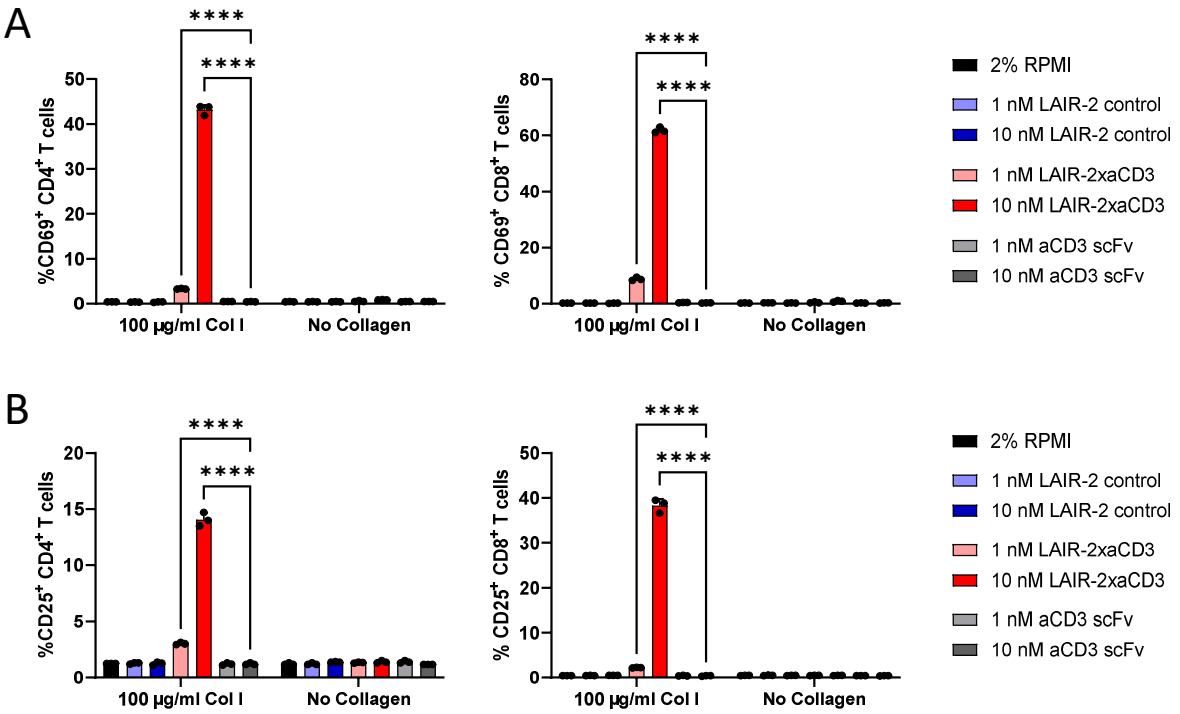

Figure 5.5: CD4 and CD8 T cell are activated upon interaction with bispecific bound to collagen I. Therefore, a plate was first coated with collagen I or left uncoated, followed by challenge with the bispecifics at 1 or 10 nM. Thereafter, the plate was washed and the T cells were added to the plate for 48h before harvesting and CD69 and CD25 expression analysis using flow cytometry. A: CD4 and CD8 T cell activation measured by CD69 upregulation. n=3, two-way ANOVA with Sidak's multiple comparisons test to anti-CD3 control (10 nM), p<0.05 *, p<0.01 **, p<0.001 ***, p<0.0001 ****. B: CD4 and CD8 T cell activation measured by CD25 upregulation. n=3, two-way ANOVA with Sidak's multiple comparisons test to anti-CD3 control, p<0.05 *, p<0.01 **, p<0.001 ***, p<0.0001 ****.

both CD25 and CD69. This T cell activation was additionally dose dependent, with 1 nM activating the T cells to a lesser extent. There was no noticeable upregulation of any of the tested markers for the controls or untreated conditions. In **Figure 5.5** B, CD8 T cell activation is shown. Results are very similar to CD4 T cell activation, however, the values are approximately 15-20% higher for both CD25 and CD69 upregulation compared to CD4 T cell activation. Again, there was no upregulation of the markers for any control, untreated condition or in the absence of collagen I. For all further experiments, it was decided to continue with 10 nM of the bispecifics as test concentration for the *in vitro* assays.

5.3.5 LAIR-2xaCD3 binds specifically and strongly to collagen I, however, not to fibronectin

As a next step, it was crucial to show the specific binding of the LAIR-2 bispecific to collagen I. Therefore, an ELISA plate was coated with 50 µg/ml collagen I or fibronectin for 1h and

subsequently challenged with the different constructs for 1h before adding an anti-FLAG detection antibody and TMB substrate. In **Figure 5.6** A, it can be seen that the constructs are unable to bind to fibronectin, however, the singular LAIR and LAIR-2xaCD3 bispecific are able to strongly bind to collagen I. Interestingly, LAIR-2 only shows a much higher binding to collagen I, which suggests that some of the binding potency is lost when an anti-CD3 scFv is fused to LAIR-2.

5.3.6 LAIR-2xaCD3 activated T cells mediate bystander cytotoxicity

After showing that T cells could be activated in the presence of collagen I and the bispecific, we sought to explore the cytotoxic potential of the activated T cells. Therefore, a 96-well plate was coated with collagen I and challenged with the bispecific or relevant controls. Afterwards, the wells were either washed prior to adding cells (**Figure 5.7** A) or the cells were added alongside the bispecifics for the duration of the experiment (**Figure 5.7** B). Subsequently, DLD-1 cells and PBMC-derived human T cells were added to the wells. The cells were then incubated for five days in an xCELLigence machine, tracking the cell viability by measuring impedance. As shown in **Figure 5.7** A, DLD-1 cells in presence of collagen I and the LAIR-2xaCD3 bispecific are killed after 24h, whereby the other conditions show no cytotoxic effect and the DLD-1 cells are able to grow and attach. This was also the case for the control wells containing CD3/CD28 Dynabeads. Furthermore, in **Figure 5.7** B, where no wash was performed after the incubation with the bispecific or controls, no difference in cytotoxicity can

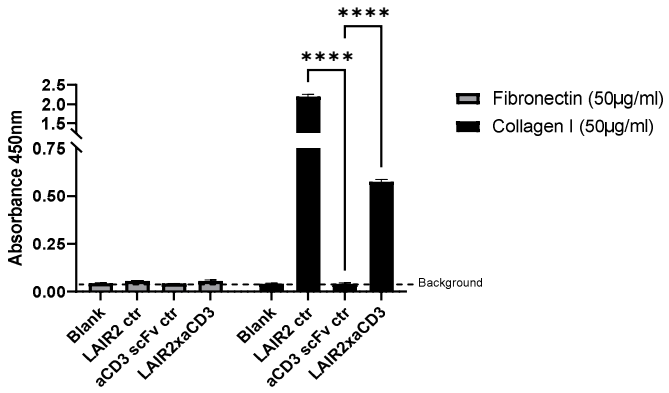

Figure 5.6: LAIR-2 containing constructs bind to human collagen I, however, not to fibronectin. ELISA plates were coated with fibronectin or collagen I and challenged with the produced constructs at 10 nM concentration. n=3, two-way ANOVA with Sidak's multiple comparisons test to anti-CD3 control, p<0.05 *, p<0.01 **, p<0.001 ***, p<0.0001 ****.

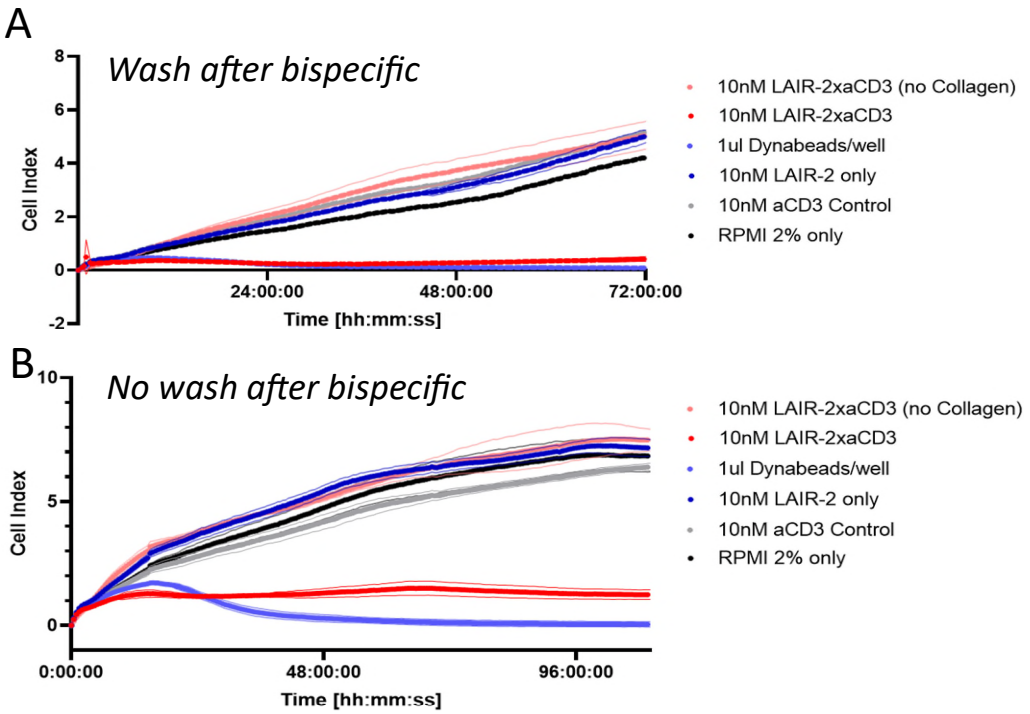

Figure 5.7: No difference in cytotoxic kinetics is seen when washing or not washing after challenge with the bispecific or control. For this experiment, a plate was coated with collagen I and then challenged with the bispecifics and controls. In A, the wells were washed after the challenged and all unbound proteins were removed before adding DLD-1 target cells and T cells, n=4. In B, T cells and DLD-1 cells were added in the presence of the bispecific and controls, n=4.

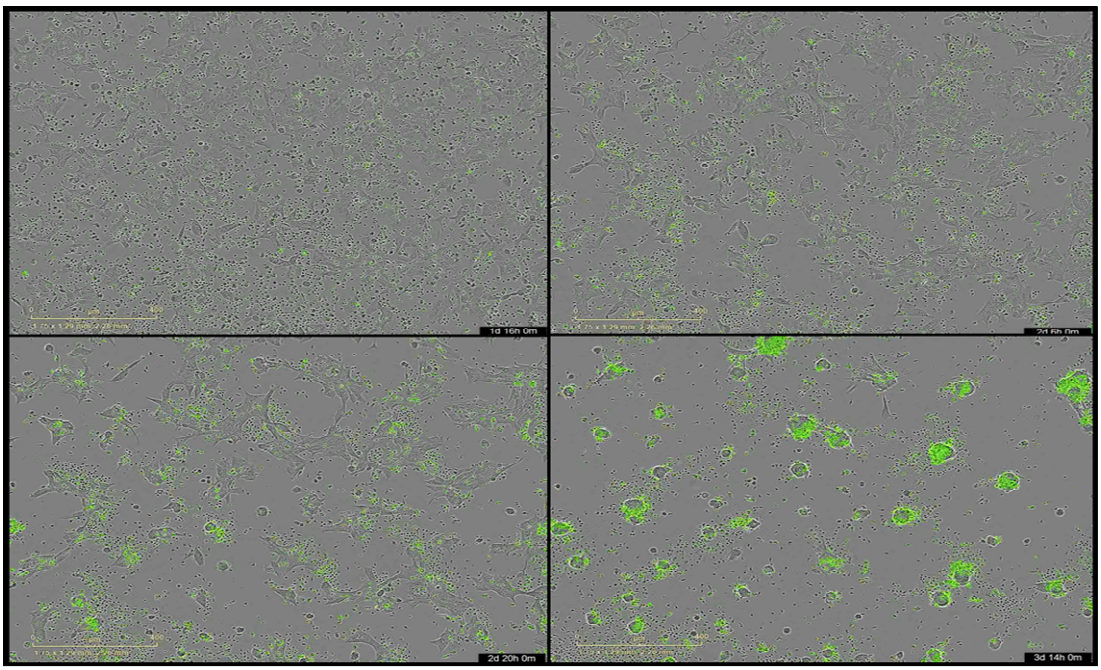

Figure 5.8: Visualisation of T cell-mediated cytotoxicity towards DLD-1 cells. A 24-well plate was coated with collagen I and bispecific/controls, before being washed once with PBS. Subsequently, a sub-confluent number of DLD-1 cells and 5:1 ratio of T cells: DLD-1 cells were added. Visualisation was shown by cell event green, activated upon caspase 3/7 cleavage. Pictures show different time-points, images were taken using an IncuCyte. Representative images are shown.

be observed. Therefore, it was decided to perform a wash after the initial incubation with the bispecific and controls prior to adding cells for the following experiments in this Chapter.

In order to visualise bystander killing mediated by the bispecific with microscopic images, a 24-well plate was coated with collagen I, challenged with the LAIR-2xaCD3 bispecific (10 nM) and washed with PBS before adding a sub-confluent number of DLD-1 cells and 1:5 ratio (target:effector) of PBMC-derived T cells. Additionally, a caspase-cleaved dye was added, leading to apoptotic cells producing a green compound. In **Figure 5.8**, it can be seen that the DLD-1 cells are surrounded by T cells in the early stages (top pictures), which subsequently start to mediate cytotoxicity and activation of caspase 3/7, as seen by the appearing green colour. Eventually, the DLD-1 cells detach and round up, a sign for the late stages of apoptosis.

After showing cytotoxicity against DLD-1 cells, cytotoxicity towards other cancer cell types and against fibroblasts was explored, since tumour-associated fibroblasts play a decisive role in enabling cancer growth (Joshi et al. 2021). Therefore, a similar experimental set up as used for **Figure 5.7** A, whereby the wells were washed after challenge with the bispecific and controls. Panc-1 or normal human dermal fibroblasts (NHDF) were added as target cells together with T cells, and the experiment was stopped after four days. Cytotoxicity was assessed either using an XTT (Panc-1) viability assay or using flow cytometry (NHDF cells), T cell activation was assessed using flow cytometry. As can be seen in **Figure 5.9** A, the bispecific is able to kill Panc-1 cells at a concentration of 10 nM. However, there is no cytotoxicity detectable at 1 nM concentration. The corresponding T cell activation (**Figure 5.9** B) shows a similar picture, with strong T cell activation at 10 nM and only slight T cell activation at 1 nM. **Figure 5.9** C shows the xCELLigence measurement of Panc-1 cells, where it is evident that the cells are only killed in the presence of collagen I. Additionally, this killing seems to be slightly slower compared to DLD-1 cells, as cytotoxicity only begins after 36h after incubation compared to 12h for DLD-1 cells.

Figure 5.10 A shows that NHDFs were also killed by the T cells (after four days), but only in the presence of collagen I. This is also reflected in the accompanying T cell activation graphs

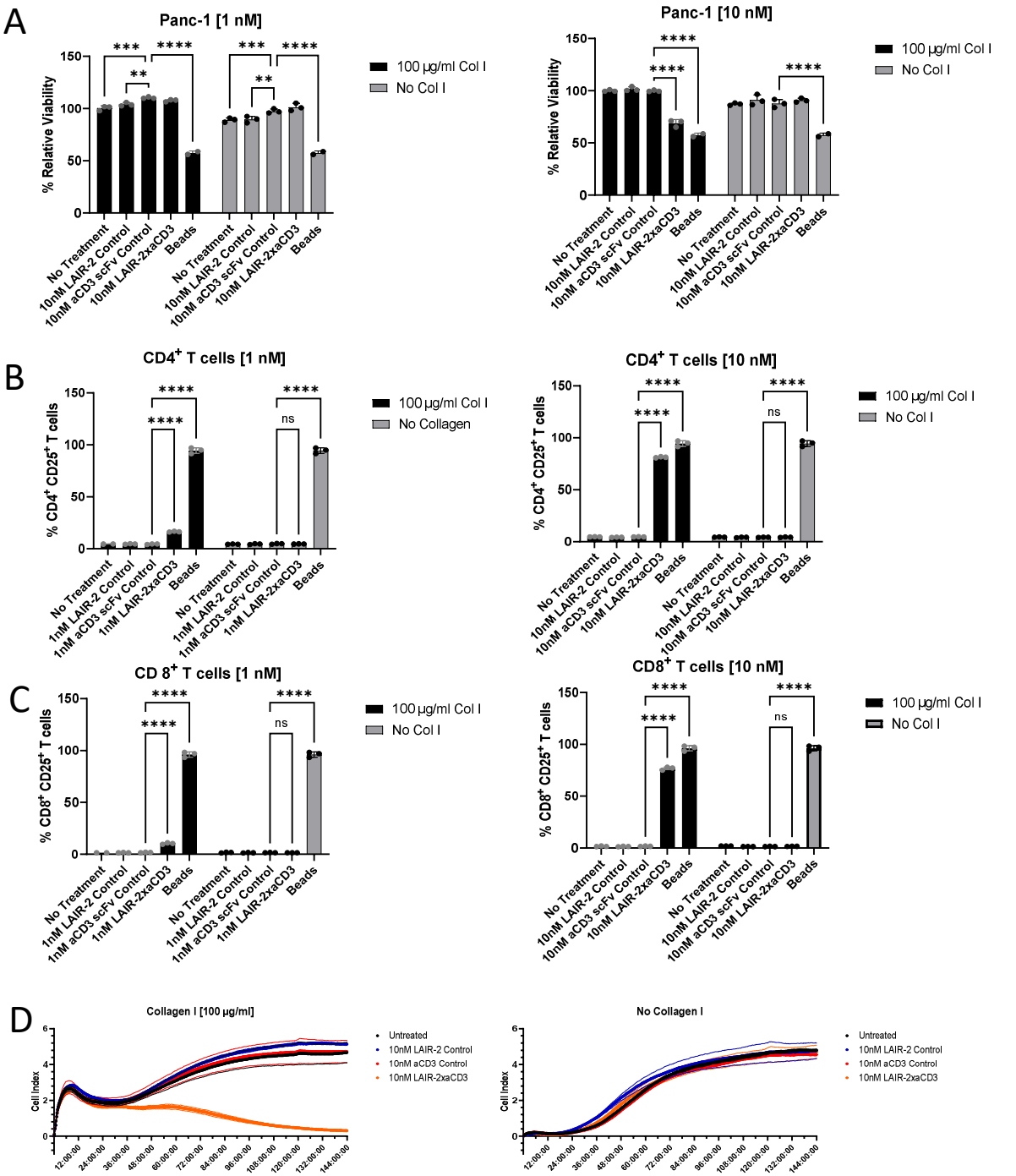

Figure 5.9: T cells exert strong bystander cytotoxicity towards Panc-1 cells upon incubation with LAIR-2xaCD3 bispecific. Panc-1 cells plated on collagen coated or uncoated plates and incubated with T cells (5:1 effector:target). T cell activation and cytotoxicity were assessed after 4 days using flow cytometry (analysing upregulation of CD25 on T cells) and XTT assay. A: Panc-1 viability after 4 days incubation with wither 1 nM or 10 nM of the LAIRxaCD3 bispecific. n=3, two-way ANOVA with Dunnett's multiple comparisons test to anti-CD3 control, p<0.05 *, p<0.01 **, p<0.001 ***, p<0.0001 ****. B: CD4 T cell and C: CD8 T cell activation measured by CD25 upregulation upon 4-day incubation. n=3, two-way ANOVA with Dunnett's multiple comparisons test to anti-CD3 control, p<0.05 *, p<0.01 **, p<0.001 ***, p<0.0001 ****. D: xCELLigence real time analysis of cytotoxicity with a collagen I coated and uncoated plate. n=3.

shown in **Figure 5.10** A. Significant CD4 and CD8 T cell activation (**Figure 5.10** B and C) could only be detected for the LAIR-2xaCD3 bispecific in the presence of collagen I and for the Dynabeads control.

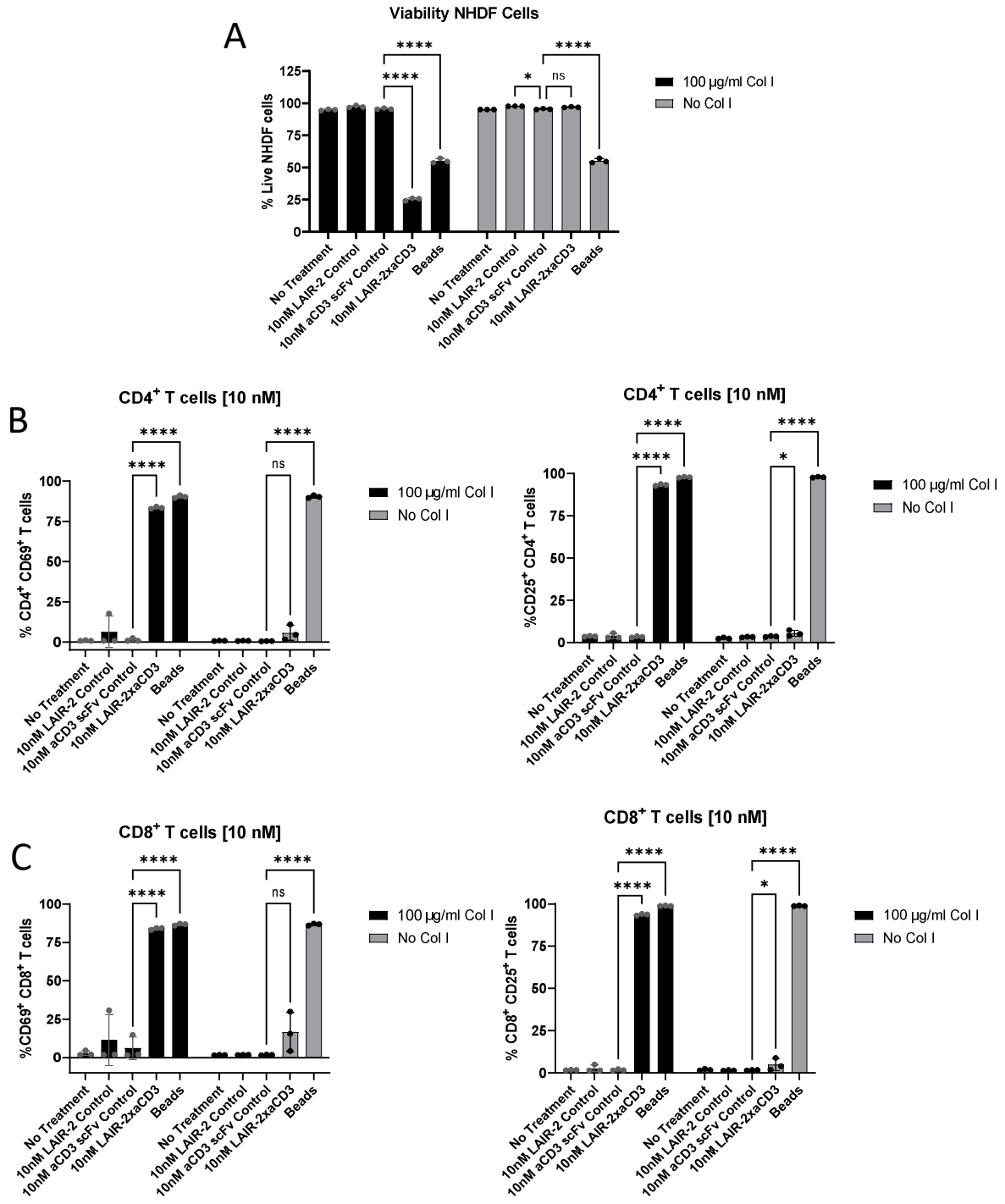

Figure 5.10: LAIR-2xaCD3 bispecific activated T cells exert bystander killing towards normal fibroblasts. NHDF cells were seeded on collagen coated or uncoated plates and incubated with T cells (5:1 effector:target). T cell activation and cytotoxicity was assessed after 4 days using flow cytometry (analysing upregulation of CD25 on T cells); cytotoxicity was assessed after 4 days using a live/dead dye and measured using a flow cytometer. A: NHDF viability after 4 days incubation with either 10 nM of the LAIR-2xaCD3 bispecific. n=3, two-way ANOVA with Dunnet's multiple comparisons test to anti-CD3 control, p<0.05 *, p<0.01 **, p<0.001 ***, p<0.0001 ****. B: CD4 T cell and C: CD8 T cell activation measured by CD25 upregulation upon 4-day incubation. n=3, two-way ANOVA with Dunnett's multiple comparisons test to anti-CD3 control, p<0.05 *, p<0.01 **, p<0.001 ***, p<0.0001 ****.

5.3.7 LAIR-2xaCD3 bound to collagen is durable in activating multiple generations of T cells

One possible advantage of tethering bispecifics to the ECM its the durability. In order to fully exploit this trait for the therapeutic approach chosen, it was important to explore the stability and robustness of the bispecific bound to collagen I over a period of time.

For this, a 96-well plate was coated with collagen I and then treated for 1.5h at 37°C with the bispecific. After this, the unbound bispecific was washed off and three subsequent generations of T cells were added each for 48h to the same wells, without re-applying the bispecific for the 6 day duration of the experiment. As a positive control, CD3/CD28 Dynabeads were used, which were re-applied with each new generation of T cells. Each generation was harvested after 48h and stained for surface expression of CD25 and CD69. As can be seen in **Figure 5.11** A, CD25 was upregulated to approximately 20% for all three generations, with only a very

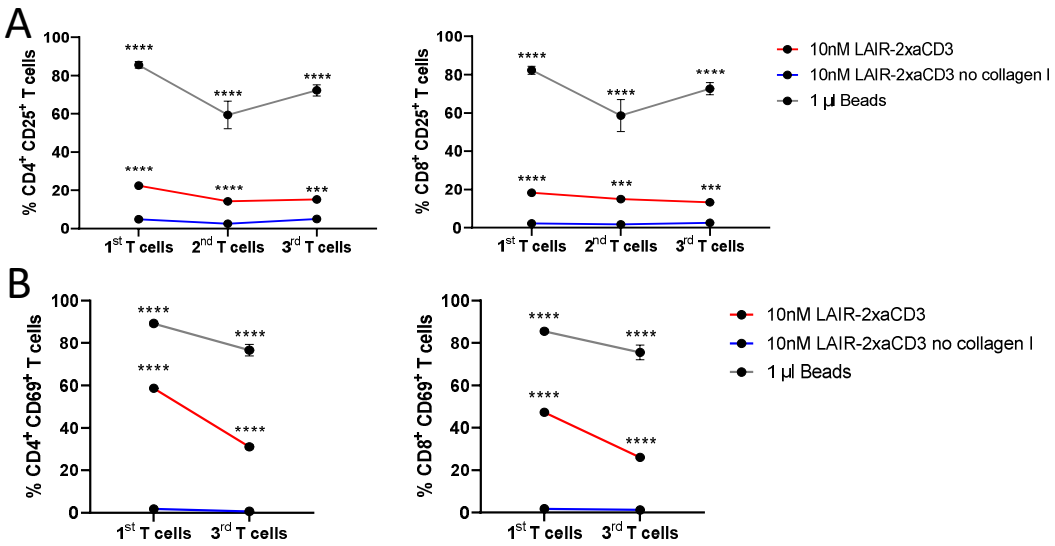

Figure 5.11: LAIR-2xaCD3 bispecific bound to collagen I activates multiple generations of T cells. A 96-well plate was coated with collagen I and challenged with the bispecific (day 0). Subsequently, the first round of T cells was isolated and added for 48h (day 2), before harvesting and measuring for CD25 and CD69 T cell activation markers via flow cytometry. At the same time, new T cells were isolated from the same patient and added to the plate without re-applying collagen I or the bispecific on day 2 and left for 48h to activate until day 4, before being harvested and analysed using flow cytometry. The third round of T cells (same donor as before) was freshly isolated and added on day 4 without re-applying collagen I or the bispecific. On day 6 after 48h, the cells were harvested and stained for analysis via flow cytometry. A: CD25 expression on CD4 and CD8 T cells, n=3, two-way ANOVA with Dunnett's multiple comparisons test to the no collagen control, p<0.05 *, p<0.01 **, p<0.001 ***, p<0.0001 ****. B: CD69 expression on CD4 and CD8 T cells. n=3, two-way ANOVA with Dunnett's multiple comparisons test to the no collagen control, p<0.05 *, p<0.01 **, p<0.001 ***, p<0.0001 ****.

small regression throughout the three sets of T cells. Additionally, both CD4 and CD8 T cells were activated to a similar extent.

In **Figure 5.11** B, the CD69 expression can be seen. Contrary to CD25, CD69 drops slightly with the third set of T cells, however, both CD8 and CD4 T cells still show a significant upregulation compared to the well without collagen I by the third set.

5.3.8 Exhausted T cells derived from human ascites fluid can be activated upon treatment with LAIR-2xaCD3

Given the *in vitro* effects of the bispecific, we aimed to test the bispecifics in more clinically relevant settings. As a first step, T cells derived from patient malignant ascites fluid drains were isolated. The samples used in the following experiments were from patients with primary ovarian cancers (AS210513 and AS210714) or pancreatic cancer (AS211005). Therefore, it was important to characterise these T cells in order to assess whether the T cells displayed

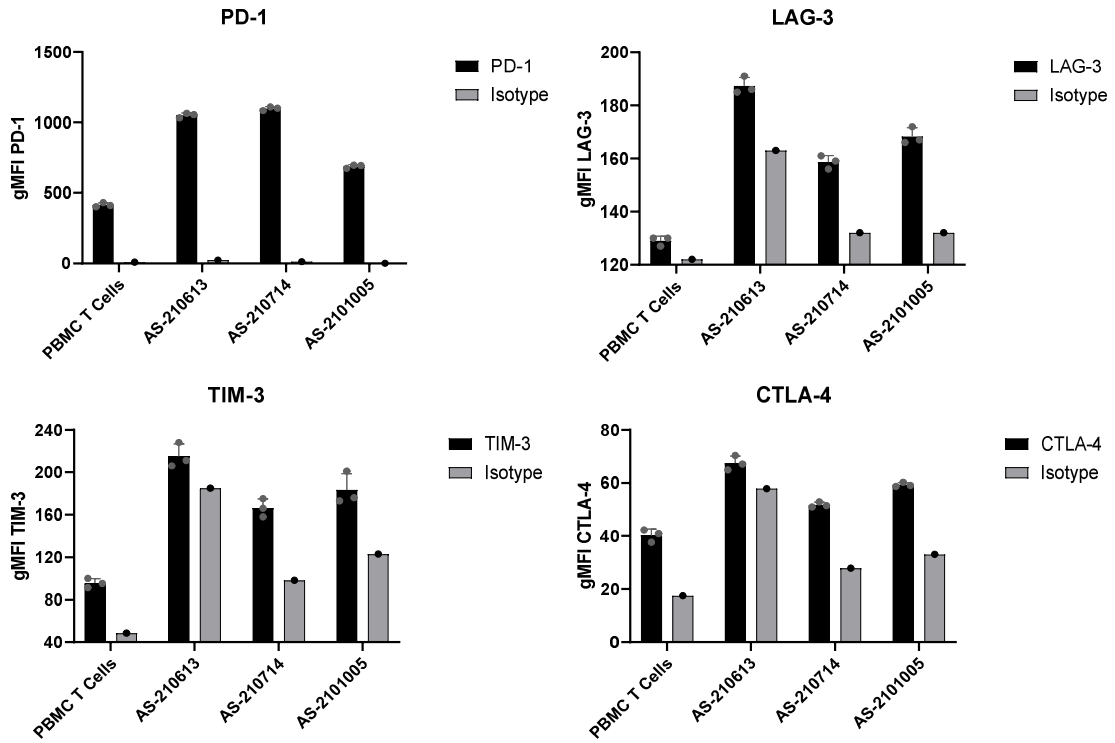

Figure 5.12: Ascites derived T cells show an exhausted phenotype, displayed an upregulation of several immune checkpoints. All cells were isolated from frozen ascites samples and subsequently stained (24h after reviving) for the indicated markers. n=3.

an exhausted phenotype. The cells were subsequently stained for PD-1, LAG-3. TIM-3 and CTLA-4 surface expression. As a control and to compare, PBMC-derived T cells were also included in the experiment, which should not exhibit and exhausted phenotype. As can be seen in **Figure 5.12**, PD-1 was expressed higher in all three tested ascites patient-derived T cells compared to PBMC-derived T cells. Additionally, there was an upregulation of LAG-3 (**Figure 5.12**), however, it was difficult to read from the data if there was an up- or downregulation of TIM-3 and CTLA-4 compared to the isotype controls.

After seeing that ascites-derived T cells in fact displayed an exhausted phenotype, the activation and cytotoxic potential of the T cells was further investigated. For the T cell activation, ascites T cells were isolated from the samples and similarly as described before, added to wells treated with collagen I and the bispecific together with DLD-1 cells. All cells were harvested after 4 days and measured using flow cytometry. As can be seen in **Figure**

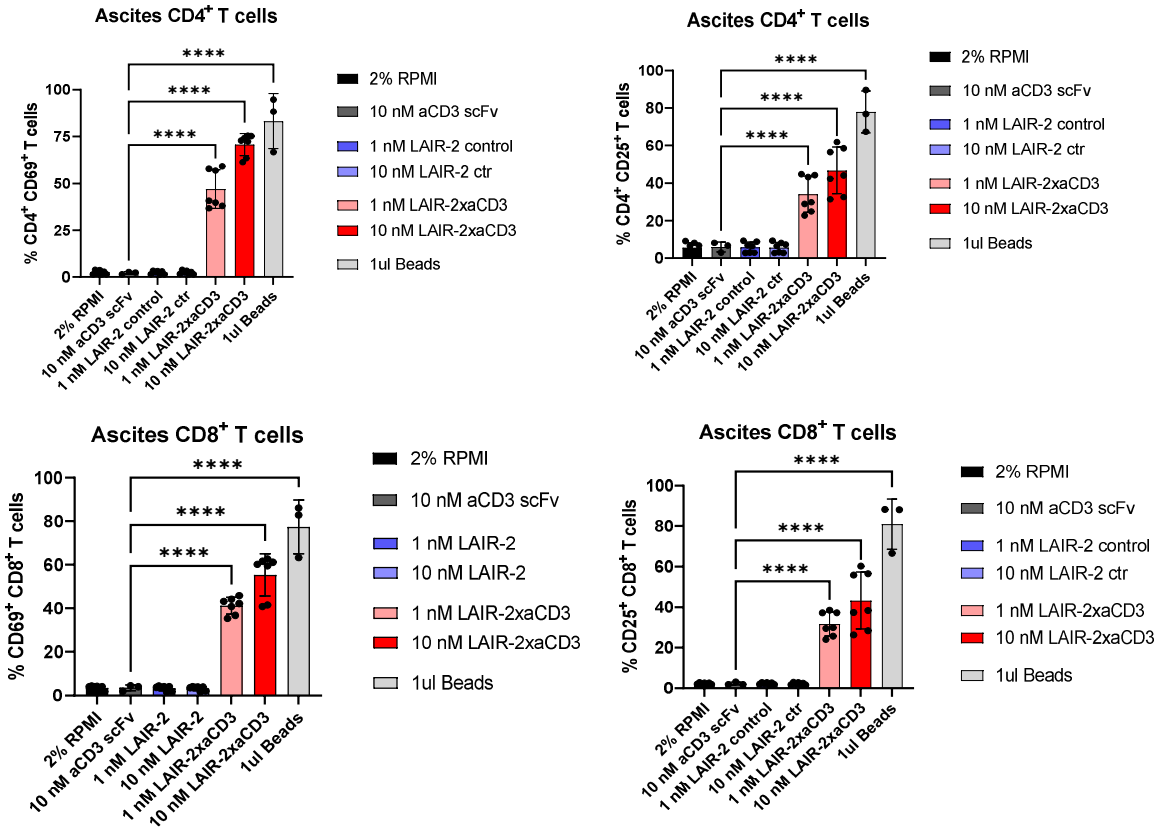

Figure 5.13: Ascites-derived T cells can be activated upon incubation with LAIR-2xaCD3 bispecific. The aforementioned ascites T cells have subsequently been incubated on a plate coated with collagen I and the bispecific or the controls, before harvesting after 48h and staining for flow cytometry analysis. CD4 and CD8 T cell activation is represented by CD25 upregulation. n=7 (total of three patients shown), two-way ANOVA with Dunnett's multiple comparisons test to anti-CD3 control, p<0.05 *, p<0.01 **, p<0.001 ***, p<0.0001 ****.

5.13, CD4 T cells derived from the three ascites samples reacted to the wells coated with collagen I and treated with the LAIR-2xaCD3 bispecific, whereby the activation was dose dependent. Both a CD25 and CD69 upregulation could still be detected after 4 days of incubation. Similar results can be seen in **Figure 5.13** B for CD8 T cells. There was no activation in the untreated or control wells.

In order to assess the cytotoxic potential of ascites-derived T cells activated with the bispecific, a similar experimental set up to

Figure 5.8 B was used and cell viability was tracked using the xCELLigence impedance measurement over 5 days. As seen in **Figure 5.14**, all three tested ascites samples contained T cells which were able to kill DLD-1 cells upon collagen I dependent activation with the LAIR-2xaCD3 bispecific. As a comparison, PBMC-derived T cells were used, however, no difference between the ascites-derived and PBMC T cells could be observed in the killing potency and speed. All cytotoxicity was dependent on the presence of collagen I in the plates.

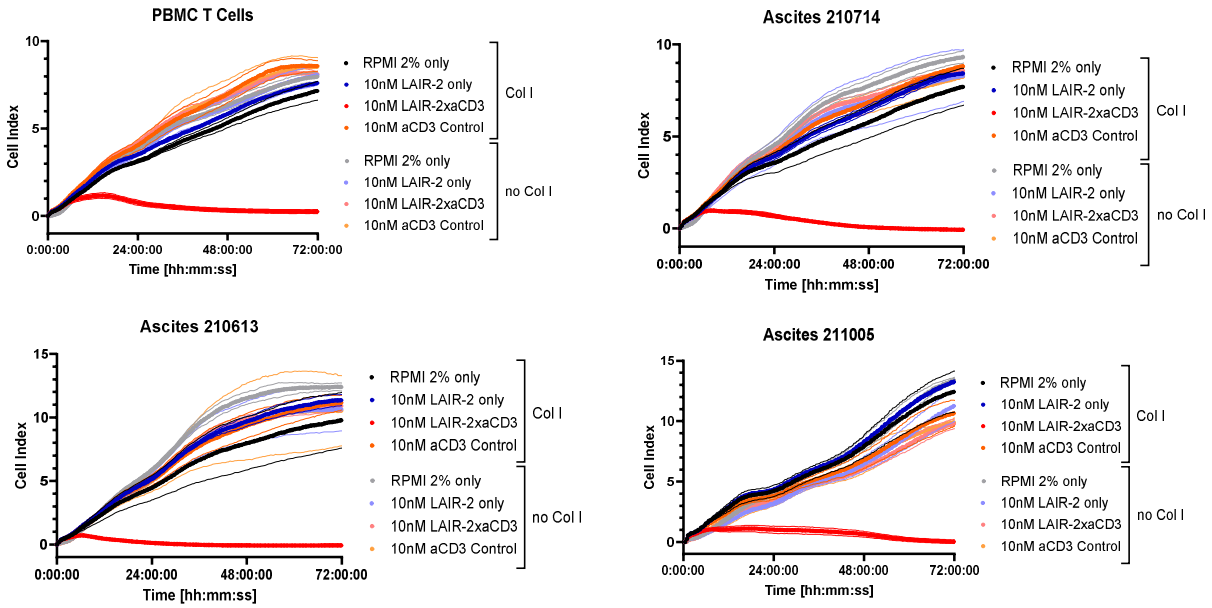

Figure 5.14: Exhausted ascites-derived T cells mediate collagen I dependent bystander killing of DLD-1 cells upon LAIR-2xaCD3 treatment. An xCELLigence 96-well plate was coated with collagen I and challenged with the bispecific and controls, before washing and seeding DLD-1 and isolated ascites-derived T cells. Cytotoxicity was measured using a xCELLigence machine. Each experiment shows an n=3.

5.3.9 Tumour infiltrating T cells from primary human colorectal tumours can be activated with LAIR-2xaCD3.

Similarly, we wanted to assess the ability of the bispecific to activate T cells deriving from a primary human tumour. For this, primary human colorectal tumours were received 30 minutes after surgery and washed extensively in PBS. Thereafter, the tumour was cut into small pieces and dissociated using the GentleMACS. This cell suspension was subsequently added to 96-well plates treated with collagen I and the bispecific. The cells were harvested after 5 days

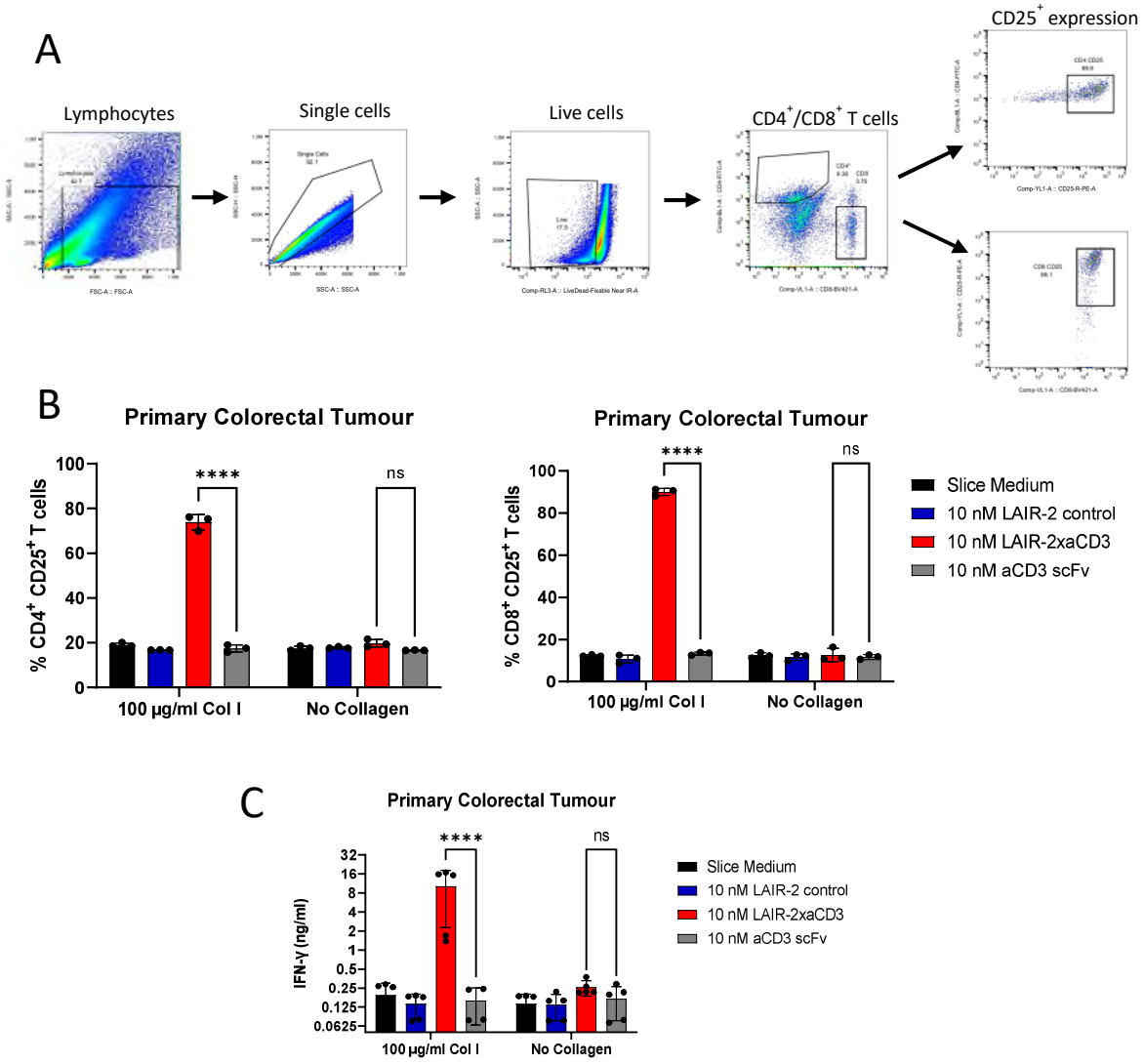

Figure 5.15: Primary colorectal tumour T cells can be activated by LAIR-2xaCD3 bispecific bound to a collagen I coated plate. The tumour was dissociated using the GentleMACS and subsequently incubated with the bispecific on collagen I coated plates for 5 days. A: Gating strategy used for analysis. B: CD4 and CD8 T cell activation displayed as %CD25 upregulation. n=3 (total of one patient shown), two-way ANOVA with Dunnett's multiple comparisons test to anti-CD3 control, $p<0.05$ *, $p<0.01$ **, $p<0.001$ ***, $p<0.0001$ ****. C: IFN-γ production by the T cells measured in the supernatant after 5 days incubation using an ELISA. n=5 (total of two patients shown), two-way ANOVA with Dunnett's multiple comparisons test to anti-CD3 control, $p<0.05$ *, $p<0.01$ **, $p<0.001$ ***, $p<0.0001$ ****.

and stained with a T cell panel to assess T cell activation using flow cytometry. Conditioned supernatant was also collected and the IFN-γ content was measured using ELISA. In **Figure 5.15** A, the gating strategy for the tumour samples is shown. In **Figure 5.15** B, the CD25 levels of tumour infiltrating T cells can be seen. There is only an upregulation in the presence of collagen I, whereby the controls and untreated wells remain low on surface CD25. Additionally, as already seen in previous Figures, CD8 T cells show a 15-20% higher level of activation compared to CD4 T cells. Generally, the levels of CD25 are for both CD4 and CD8 T cells well above 70% and 80%, which indicates a strong activation.

In **Figure 5.15** C, the IFN-γ production of the differently treated wells can be seen. It is clearly visible that there is only an IFN-γ production in wells treated with both collagen I and LAIR-2xaCD3, whereas the untreated and the control wells show very low levels of IFN-γ. This increase of IFN-γ lies between 20x-60x, which indicates a very strong T cell activation.

5.3.10 Endogenous immune cells in slices from colorectal liver metastases are activated and mediate cytotoxicity upon treatment with LAIR-2xaCD3

After having shown that T cells deriving from ascites fluids and endogenous T cells from primary human colorectal cancer can be activated, we sought to investigate whether LAIR-2xaCD3 is also able to potentially activate endogenous immune cells within slices from

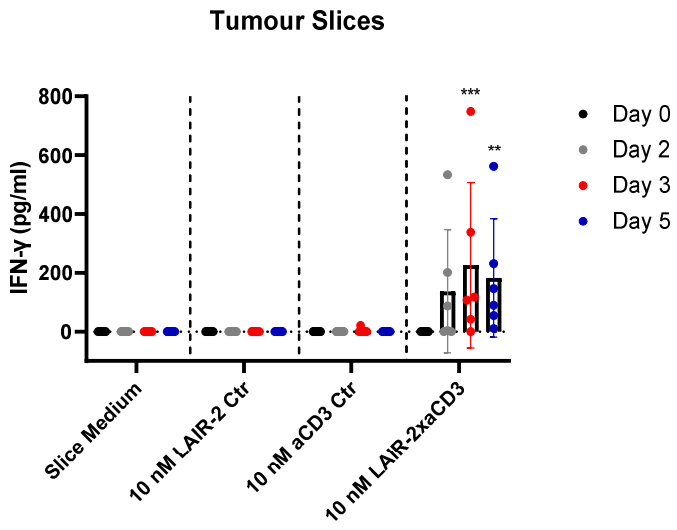

Figure 5.16: LAIR-2xaCD3 bispecific induces endogenous cell activation in colorectal liver metastases slices. Slices of colorectal liver metastases were incubated with the different controls and the bispecific for 5 days, whereby supernatant was collected on day 0, 2, 3 and 5 for ELISA quantification of produced IFN-γ. n=6 (total of two patients shown), two-way ANOVA with Dunnett's multiple comparisons test to anti-CD3 control, p<0.05 *, p<0.01 **, p<0.001 ***, p<0.0001 ****.

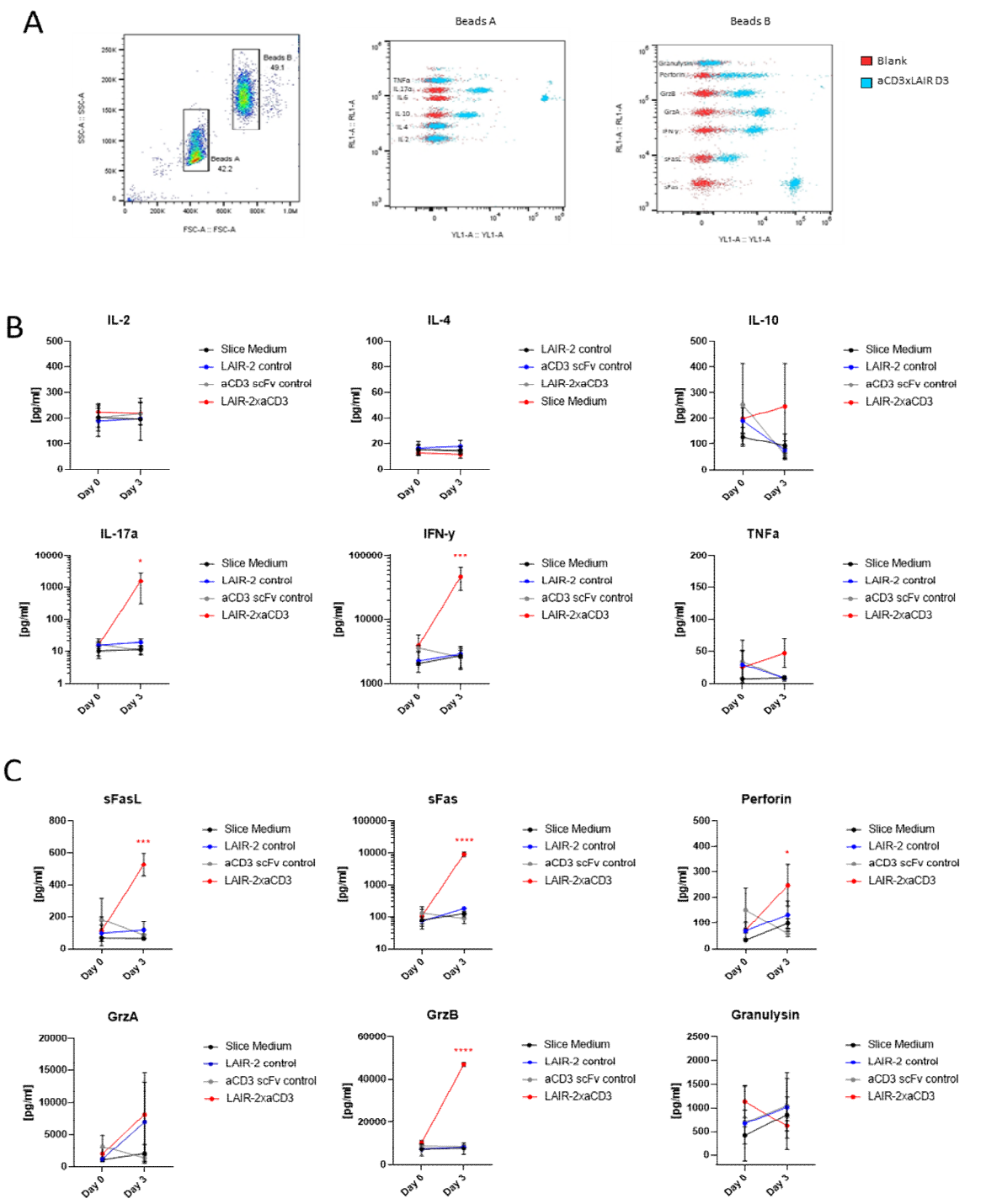

Figure 5.17: Endogenous T cells in colorectal liver metastases slices are robustly activated and exert cytotoxicity upon activation with the LAIR-2xaCD3 bispecific. A: Validation of the assay, showing the different populations of beads contained in the kit. B: Important inflammatory and anti-inflammatory cytokines are displayed in this panel. n=2 (total of two patients shown), two-way ANOVA with Dunnett's multiple comparisons test to anti-CD3 control, p<0.05 *, p<0.01 **, p<0.001 ***, p<0.0001 ****. C: Important cytotoxic mediators are shown in this panel. n=2 (total of two patients shown), two-way ANOVA with Dunnett's multiple comparisons test to anti-CD3 control, p<0.05 *, p<0.01 **, p<0.001 ***, p<0.0001 ****.

colorectal liver metastasis in the context of a native ECM. Liver metastasis in general is often linked with poor survival and, more importantly, induces specific resistance to immunotherapeutic approaches (Yu et al. 2021). For the following experiments, no exogenous

T cells were added to the slices and the measured IFN-γ is solely from cells present in the slices. This and the reason mentioned above, make liver metastasis slice cultures a very valuable and indicative experimental system.

To assess the IFN-γ production, the tumours were sliced to a thickness of 250 µm, kept overnight in slice medium (baseline) before changing the subsequent day into slice medium containing the treatments. The slice culture was then kept in the incubator for five days, whereas conditioned medium was taken on day two, three and five for ELISA measurements. As can be seen in **Figure 5.16**, only slices incubated with LAIR-2xaCD3 bispecific show an upregulation in IFN-γ production. These values vary starkly, depending on the tumour sample and region, from nearly no IFN-γ to 800 pg/mL.

In order to further investigate the nature of T cell activation and potential cytotoxicity, a LegendPlex assay using the collected supernatants was performed. As seen in **Figure 5.17** A, the LegendPlex assay is a quantitative, flow cytometry-based analysis method for multiple cytokines. As such, two population of beads are distinguished in size, which both contain beads of different fluorophore strength. In the end, PE-Streptavidin indicates binding of the mediator to the beads and when compared to a standard curve, the values can be interpolated. For this experiment, the CD8 and NK LegendPlex assay kit was used, which measured 13 different cytokines. The baseline on day 0 was compared to the conditioned supernatant from day three.

As can be seen in **Figure 5.17** B, there is a significant upregulation of IL-17a and IFN-γ, however, no changes can be observed for IL-2, IL-4, IL-10 and TNFα. All the controls and the untreated condition do not exceed the background signal of the slices. However, when looking at **Figure 5.17** C, a stark and significant upregulation of many mediators can be observed, such as sFasL/sFas, granzyme B and perforin. Especially the upregulation of granzyme B and perforin also infers the targeted cytotoxicity of activated T cells towards target cells. For the untreated and the controls, there was no significant upregulation of any mediators that could be observed within this assay.

5.4 Discussion

In this chapter, the possibility of creating a LAIR-2 fusion protein with an anti-CD3 scFv was explored. This could potentially lead to a double effect by interrupting the inhibitory LAIR-1-collagen I interaction and simultaneously anchor an anti-CD3 scFv within the tumour ECM for local a non-specific T cell activation and cytotoxicity.

According to several studies, the expression of LAIR-1 is mainly restricted to immune cells, and especially prominent on T cells and macrophages (Meyaard et al. 1997; Xie et al. 2022). As LAIR-1 has also been described as an ECM-mediated immune checkpoint, it was important to explore its expression on the multiple *in vitro* and *ex vivo* model systems used in this chapter. In the literature, the LAIR-1 expression seen on CD8 T cells is in general higher compared to CD4 T cells (Jansen et al. 2007). This also holds true for the observations made in **Figure 5.2**, whereby all T cells deriving from different systems show a higher CD8 LAIR-1 expression compared to CD4 with high inter-patient variability. This substantial difference in expression reflects the inter-patient variability in the clinics, and should be regarded as a strength of the ascites system since it appears to capture the diversity of patients who may eventually receive treatment. Although the inhibitory effect of LAIR-1 was very difficult to mimic *in vitro*, it is clear from other sources that it can have a great impact in terms of patient outcome (Ramos et al. 2021).

One important factor for this LAIR-1 – collagen I interruption is the ability of the LAIR-2xaCD3 bispecific to bind to collagen I with a high affinity. Although the bispecific could still bind to collagen I, it displayed a diminished binding capacity compared to LAIR-2 alone (**Figure 5.6**). However, binding was still very strong and appeared to remain specific, as there was no non-specific binding to fibronectin. This decrease in binding activity could potentially impact the bispecifics' ability to interrupt a LAIR-1 – collagen I interaction efficiently.

Further, as the ECM is a very durable structure, the possibility of the LAIR-2xaCD3 bispecific to create a durable reservoir within the TME was explored. As shown in **Figure 5.11**, a plate

coated with collagen I and with the LAIR2xaCD3 bispecific bound to it was capable of activating multiple rounds of T cells. Even after two sets of T cells, the third set, added four days after the bispecific was incubated with the collagen I coated plate, was able to achieve similar activation levels compared to the first set. This not only proved that the bispecific is able to activate multiple generations of T cells, but also suggests that part of it remains bound to collagen I, probably even after interaction with the CD3 on the T cells. Additionally, bispecific agents injected IV mostly face very short half-lives due to rapid renal clearance (Klinger et al. 2012). Therefore, the demonstrated prolonged binding and retention to collagen, should ensure that the bispecifics are not cleared rapidly and thereby extend their therapeutic half-life. However, further experiments, specifically also *in vivo* experiments, are needed to further investigate this point.

After having investigated bystander killing in detail in Chapter 3, we next sought to elucidate the potency of bystander cytotoxicity mediated by the LAIR-2xaCD3 bispecific. Therefore, it was demonstrated that not only could cell lines such as DLD-1 and Panc-1 be killed using the bispecific, but also NHDF fibroblasts (**Figure 5.7**-**Figure 5.10**). As other studies have shown and inherently implied, there are many different cell types responsible for the maintenance and growth of the tumour, particularly fibroblasts (Glabman, Choyke, and Sato 2022). Hence, it was decisive to show that the LAIR2xaCD3 bispecific is able to activate T cells sufficiently to kill multiple different cell types. Fibroblasts are also abundantly found next to capillaries, shielding the tumour cells, which are mostly found further away from the blood vessels, from any possible drug administered IV and entering the tumour through the blood flow (Smith et al. 2013). Although tumour architecture is an often-overlooked field of study, it plays a key role when assessing new therapeutic approaches, and potentially could be one of the many reasons why therapies fail in the clinical trials. Mouse models and *in vitro* models are important to achieve preliminary results, however, they often lack either all the different cell types, parts of the TME or tumour architecture in general, and should therefore not be the gold standard alone to allow compounds to be taken up for clinical studies. Therefore, *ex vivo* human tumour living biopsies represent the best available model of clinical cells and TME, and should

arguably be given more credit and paid greater attention. Although they often result in high inter-patient and even intra-patient variabilities, this should never be a reason to discount them, as they reflect the patient variability seen in the clinic, rather than a perfectly normalised and overly simplistic murine model system.

The contribution of the different T cell cytotoxicity pathways (Fas/FasL and granzyme/perforin pathways, or potentially MHC-independent killing) cannot conclusively be determined from these experiments. More experiments involving inhibitors of the respective pathways might shed some light on the mechanism behind the bystander cytotoxicity triggered by the LAIR-2xaCD3 bispecific.

In order to implement this here, the ability of the bispecifics to activate apparently exhausted human T cells within human tumour biopsies was extensively assessed. Exhausted T cells were on the one hand taken from ascites samples as shown in **Figure 5.12**-**Figure 5.14**, and on the other hand also from primary colorectal cancer slices, as shown in **Figure 5.15**. Although the main expressed checkpoint was PD-1, there was no difference between the activation, and importantly, cytotoxic potential of the exhausted T cells compared to normal PBMC-derived T cells. Ascites in particular is a platform to obtain and study suppressed T cells, especially because of the broad variety of primary tumours causing ascites to form. This system has already been well established and various publications have previously been made (Scott et al. 2020). Additionally, the exhausted T cells deriving from a primary colorectal biopsy were able to produce a significant amount of IFN-γ upon stimulation with the bispecific, which potentially indicates a strong and robust T cell activation (**Figure 5.15**).

As a last step, we also looked at the potency of the bispecifics in slice culture from colorectal liver metastases. As discussed prior, these slices not only contain a multitude of different cell types, but also contain an intact TME and ECM, which are both invaluable for these studies. Although there is ECM in mouse tumours, it is mostly co-injected or formed over a rather short period to time (2-5 weeks). In human tumours, however, the ECM is established and changed throughout several months up to years and therefore has plenty of time to evolve and mature

into a properly immunosuppressive environment. Additionally, it has been shown previously that metastasis occurring in the liver render any immunotherapy obsolete, as their proposed mechanism indicated the specific killing of tumour specific T cells through macrophages present in the normal liver tissue (Yu et al. 2021). Also, the liver is intrinsically a very immune cell-rich organ, including T cells and macrophages. Hence, a tumour forming in these circumstances is probably very immunosuppressive, as it would otherwise be eliminated before it has gotten time to establish. These reasons make this slice system especially valuable, as a successful activation of liver metastases is very promising for further investigation.

Upon treatment with the bispecific, we were able to demonstrate a strong upregulation of IL-17a and IFN-γ (**Figure 5.17**), two potent anti-tumour cytokines. On one hand, upregulation in IFN-γ has been established as a robust marker for T cell activation in clinical samples previously (Corthay et al. 2005; Matsushita et al. 2015). There are several different effects that IFN-γ can have on cancer and immune cells in tumours, including the activation and maintenance of the status of effector T cells (Bhat et al. 2017), upregulation of surface MHC II in antigen presenting cells boosting peptide-presentation to CD4 T cells (Corthay et al. 2005; Fazle Akbar, Inaba, and Onji 1996) and upregulation of HLA-1 molecules on tumour cells (Garrido et al. 2017; Hazini, Fisher, and Seymour 2021). Therefore, the strong upregulation of IFN-γ by the bispecific treatment potentially indicates a strong T lymphocyte activation.

On the other hand, IL-17a is considered a proinflammatory cytokine produced by CD4 and CD8 T cells (Simon et al. 2023) and has previously been shown to cause tissue destruction and autoimmunity if not controlled (Mcginley et al. 2020). In early stages of cancer, it has been shown that IL-17a can contribute towards the formation of cancer and metastases in pre-clinical models (probably attributed to the “wound that never heals” (Dvorak 1986)). However, in this instance, the induction of bystander killing is done on purpose and therefore the upregulation of IL-17a could indicate a successful induction of a potent anti-cancer cytotoxic response.

Intriguingly, soluble Fas and soluble FasL were both highly upregulated in the slices treated with the LAIR2xaCD3 bispecific. In the literature, the exact function of soluble Fas and soluble FasL is not fully elucidated. However, it has been shown before that sFasL is able to bind to membrane bound Fas without inducing apoptosis and acting as a decoy that suppresses membrane bound FasL to induce cell death (Suda, Hashimoto, and Tanaka 1997; Volpe et al. 2016). sFasL has also been shown to be shed from the cell surface by metalloproteinases (Kayagaki et al. 1995; Wallach-dayan et al. 2021). Similarly, sFas is also involved in the suppression of apoptosis (Cheng et al. 1994).

Given that there is a stark upregulation of anti-apoptotic sFas and sFasL upon LAIR-2xaCD3 bispecific treatment of tumour slices, this might hint towards a yet undiscovered mechanism for these soluble proteins in bystander killing. It has before been postulated that sFas and sFasL might be involved in preventing excessive tissue damage (Bohana-Kashtan et al. 2011). Together with the findings in Upadhyay et al. (Upadhyay et al. 2021) of the potential strong involvement of the Fas/FasL cytotoxicity axis in bystander killing, this might hint towards a novel, undiscovered role of sFas and sFasL in order to prevent uncontrollable tissue damage. However, there is still a significant upregulation in the perforin/granzyme B mediated cytotoxicity pathway with the bispecific treatment, indicating that cytotoxicity through this pathway would not be impacted by the upregulation of sFas and sFasL.

Additionally to sFasL and sFas, granzyme B was highly upregulated, indicating that the activated T cells were also cytotoxic and killing neighbouring cells through the granzyme/perforin pathway.

One of the only other approaches targeting the LAIR-1 – collagen I axis using LAIR-2 is currently in clinical trials under the name NC410. The main objective of this antibody is to block the inhibitory interaction in collagen rich regions, with promising results in xenograft and humanised mouse models (Ramos et al. 2021). However, there is a severe lack of testing of this approach in patient-derived *ex vivo* model systems, leaving this approach vulnerable to the conditions and variability faced in the clinical setting.

Although the LAIR-1 – collagen I axis is often described in the literature as an attractive and effective target (Peng et al. 2020; Ramos et al. 2021), the results in this section across the board show that LAIR-2 alone disrupting the LAIR-1 – collagen I axis is not very effective at enhancing T cell activation, especially in the slice model with a comprehensive ECM. This might indicate that LAIR-2 blockade alone potentially is not enough to elicit a potent enough induction of T cells. This has also been seen in Peng et al., where LAIR-2 overexpression alone did not lead to the reduction in tumour size in mice, but only in combination with an anti-PD-1 antibody (Peng et al. 2020).

Finally, successful activation by the LAIR2xaCD3 bispecific of T cells within human tumours slices shows there is a sufficient density of LAIR-binding sites within human tumours for tethered bispecifics to create activational synapses with endogenous T cells, clustering CD3 sufficiently to activate T cell cytotoxicity.

In conclusion, we demonstrated that a LAIR-2xaCD3 fusion protein has a big potential to serve as a novel immunotherapeutic approach. The bispecific was able to not only activate PBMC-derived T cells *in vitro* when bound to collagen coated on a plate, but was also able to activate apparently-exhausted T cells derived from *ex vivo* patient ascites fluid and primary human colorectal cancer slices. The activated T cells were then able to mediate bystander cytotoxicity against target cancer cells, but also against fibroblasts. On top of this, T cells could also be robustly activated in an *ex vivo* slice model derived from patients with colorectal liver metastases, indicating that the bispecific was able to bind to the present tumour ECM and not only activate T cells, but according to their secretory profile, also prime and induce cytotoxicity. Therefore, this approach together with the potential durability of the bispecific once bound to the ECM, could form a novel platform with a great potential for novel approaches, not only in cancer therapies, but also in the field of autoimmunity and rheumatoid arthritis.

6 Targeted expression of LAIR-2xaCD3 bispecific through the oncolytic adenovirus Enadenotucirev (EnAd)

6.1 Introduction

The previous chapter showed that the LAIR-2xaCD3 bispecific agent could exert potent T cell activation leading to bystander cytotoxicity. However recombinant LAIR-2 itself has two other relevant functions - apart from blocking T cell inactivation mediated by LAIR-1 binding to collagen in the tumour, LAIR-2 is known to bind to collagen-like domains of the complement proteins C1q and MBL (Mannose binding lectin). Given systemically, the LAIR-2 protein is likely to bind circulating complement proteins and may fail to access the tumour site. The bispecific developed here also contains anti-CD3, and this raises the possibility of off-target T cell activation by any immune complexes formed, potentially giving unwanted systemic toxicities. Accordingly in this chapter, we explored a strategy using an oncolytic virus to achieve *in situ* expression of the LAIR-2xaCD3 agonist in order to maximise anticancer efficacy and simultaneously minimise unwanted toxicity.

OVs have been engineered predominantly for their intrinsic anti-cancer effects, which include selective replication and lysis of tumour cells, while leaving normal cells relatively unharmed. In addition to their direct cytotoxicity, lysis of cancer cells releases PAMPs and DAMPs, creating a local proinflammatory environment that helps to stimulate the function of local phagocytes and dendritic cells.

In total, 408 clinical trials with OVs have been conducted (stand October 2021), whereby approximately 80% are phase 1 and phase 2 trials. The vast majority (>80%) include DNA viruses and the most popular viruses used are adenoviruses (approximately 40% of all OVs entered) (Li et al. 2022). Additionally, only 36% of the clinical trials investigated the use of OVs as monotherapies, as the majority of the trials focussed on OVs in combination with chemotherapy, immunotherapy or radiation (Li et al. 2022).

Arising from these clinical trials, there are currently three oncolytic virus therapies which have been licensed in parts of the world for treatment. The first one to be approved in October 2015 by the FDA was T-VEC, an OV based on the herpes simplex virus (oHSV) with deletions in ICP34.5 and ICP47, leading to loss of unwanted virulence in the brain and nervous system to improve biosafety (Rehman et al. 2016). Additionally, the sequence for GM-CSF was encoded within the virus, that upon expression in the cancer leads to a local recruitment of APCs (Ferrucci et al. 2021). The therapy was approved for the use in inoperable melanoma lesions given by IT injection and has seen reasonable success in treating patients thus far. It was also observed that some distal lesions, which were not injected directly with the virus, showed a decrease in size, suggesting an abscopal effect elicited either through a potential replication and spread of the virus, or the induction of a systemic immune response leading to primed immune cells migrating into the non-injected lesion (Kaufman et al. 2016). The other two approved therapies include Oncorine H101, a recombinant human type 5 adenovirus licensed by the Chinese SFDA in 2005 for treatment of nasopharyngeal cancer by direct IT injection (He and Lin 2017; Zhang et al. 2021) and G47Δ Delytact, a herpes virus-based OV that received conditional approval in Japan in 2021 for the treatment for glioblastoma through IT injection (Todo et al. 2022).

Besides the direct anti-tumour effects mediated by OV therapy, many OVs can accommodate encoded transgenes for selective expression and secretion *in situ*, acting as targeted vectors for gene therapy (Boagni, Ravirala, and Zhang 2021). This combination of virotherapy and gene therapy has three main advantages: Firstly, due to the selectivity of the OV, the transgene will only be expressed in cancer tissue and therefore not in normal tissue. This minimises side effects that would normally occur when the transgene is administered systemically IV. Secondly, the OV replication and spread within the tumour simultaneously leads to an amplification of the transgene expression. Lastly, as the virus hijacks the tumour cell and repurposes the cellular machinery for over-production of viral proteins, it will also induce a strong expression of the encoded transgene protein, resulting in a high local concentration of the transgene.

In this study, the oncolytic adenovirus Enadenotucirev (EnAd) was chosen as gene therapy vector. EnAd has been created by directed evolution and is a highly carcinoma-selective virus chimera of isoforms (Ad11/Ad3) that have not been encountered by most human immune systems (Kuhn et al. 2008b). Due to its various deletions, EnAd conveniently allows to encode relatively large transgenes without approaching its packaging limit (approximately 2000-3000 base pairs).

Eleven different phase I and phase I/II clinical trials have been conducted using EnAd, with four ongoing, including a collaborative study with the University of Oxford and CRUK. Initial trials focussed on the investigation of IV delivery in patients, viral delivery, spread and finding the maximum tolerated dose and a suitable schedule for multiple IV virus injections, involving a total of 116 participants (NCT02053220, NCT02028442 and NCT02028117). Later trials assessed the combination of EnAd with checkpoint inhibitors, mainly to explore adverse effects and the tolerability of these combination therapies, or with chemoradiation (Capecitabine and radiotherapy) as a neoadjuvant to surgery in patients with resectable rectal cancer. Finally, trials are ongoing exploring EnAd ‘armed’ with an anti-CD40 super agonist antibody (NCT03852511), or with a fibroblast-targeting BiTE (NCT05043714).

EnAd has previously proven to be an attractive vector for transgene delivery and expression *in situ* (Freedman et al. 2018; Scott et al. 2019). Therefore, we aim to clone the different transgenes tested in Chapter 5 within EnAd constructs under transcriptional control of a CMV promotor. The rescued viruses will then be produced and validated to ensure controlled and efficient expression of all proteins. On top of this, the functionality of the virus and the transgene proteins expressed by the virus will be assessed *in vitro,* and finally T cell activation and T cell cytotoxicity will be analysed in more clinically relevant models, including *ex vivo* slice cultures of freshly resected human colorectal tumour metastases.

6.2 Hypothesis

In this chapter, we hypothesise that encoding the LAIR-2 bispecifics as tested in chapter 5 within the oncolytic adenovirus EnAd leads to (1) a high local expression of the bispecifics by the virus in various tumour cells and secretion into the ECM, (2) strong binding of the expressed bispecifics to collagen I and (3) activation of endogenous T cells and induction of cytokine production.

6.3 Results

6.3.1 Graphical abstract

Figure 6.1 shows a schematic representation of the hypothesis and aims of this chapter. In a first step, the OV encoding the bispecific is administered IV and reaches the tumour via the blood stream (2). Subsequently, the virus infects tumour cells and replicates selectively within the tumour, releasing DAMPs, PAMPs together with the expressed bispecific. The produced bispecific can then bind to the surrounding collagen I, blocking the LAIR-1 – collagen I

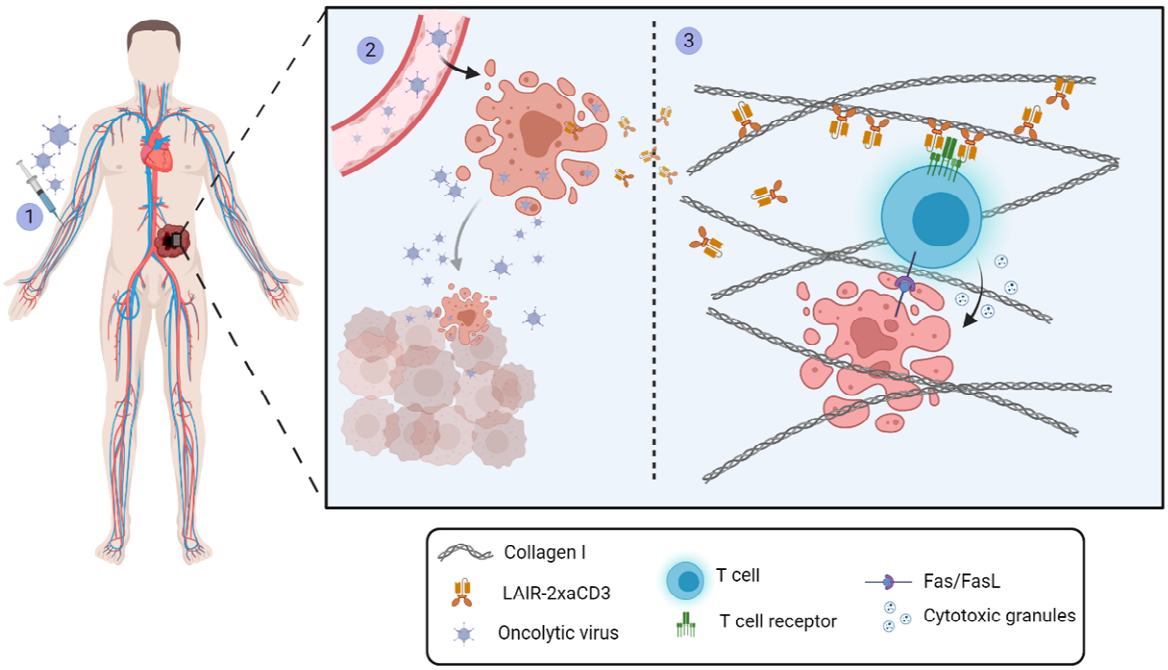

Figure 6.1: Graphical abstract of the aims in Chapter 6. The IV delivered OV infects and replicates within the tumour, producing the LAIR-2xaCD3 bispecific, which in turn coats the available collagen I. This leads to an inhibition of the LAIR-1 - collagen I axis and to the direct activation of T cell-mediated bystander killing.

inhibitory axis and simultaneously induce T cell activation mediated via the anti-CD3 scFvs (3). The locally activated T cells will then exert bystander killing, eliminating the tumour cells.

6.3.2 Cloning, validation and titrating of EnAd encoding the LAIR-3xaCD3 bispecific agent

The EnAd plasmid cloning strategy has been used many times before and is therefore well established. The insert was cloned into the backbone using Gibson assembly between E4 and Fiber, whereby the gene of interest was placed under a CMV promotor (**Figure 6.2** A). The next step after assembly involved the validation that the insert was in fact within the backbone by doing a test digest. Therefore, **Figure 6.2** B shows the digest with ApaLI, which leads to a specific band pattern that is distinguishable between parental EnAd and EnAd containing a payload. It can clearly be seen that the three constructs show a higher second band from above than the parental EnAd, indicating that the DNA is correct and the insert is present.

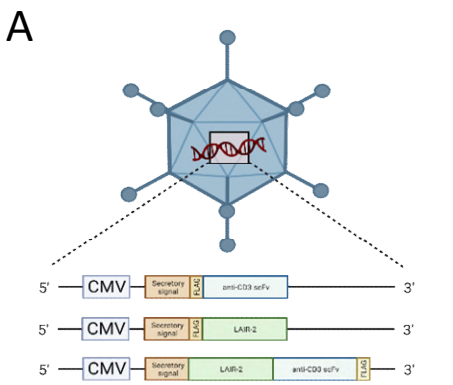

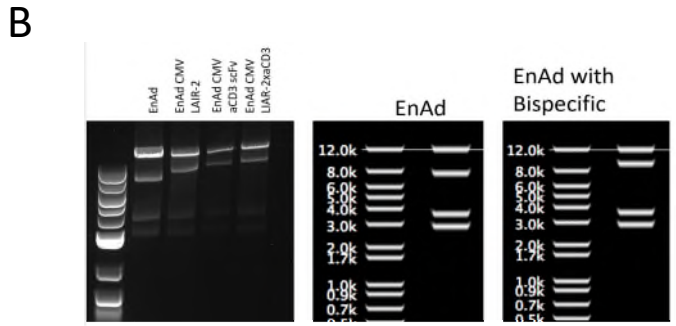

C

Name	Promotor	Insert	TCID50 (MOI, A549)	VP/ml
EnAd Parental	CMV	-	$1.27x10^{9}$	-
EnAd CMV LAIR-2	CMV	LAIR-2	$3.94x10^{9}$	-
EnAd CMV aCD3 scFv	CMV	anti-CD3 scFv	$1.2x10^{9}$	-
EnAd CMV LAIR-2xaCD3	CMV	LAIR-2xaCD3	$5.74x10^{8}$	-
EnAd CMV GFP	CMV	GFP	$5.15x10^{9}$	-
EnAd E1A UnaG x SA mCherry	CMV SA (MLP)	UnaG, mCherry	-	$6.27x10^{12}$

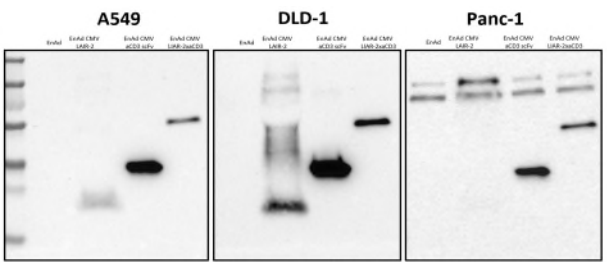

Figure 6.2: Validation and characterisation of parental EnAd, EnAd encoding LAIR-2 only, anti-CD3 scFv only and LAIR-2xaCD3 bispecific. A: Plasmid maps depicting the different insertions. B: Test digest to confirm the correct insertion of the backbone, as can be seen by the second band from the top. C: Titres as calculated by $TCID_{50}$ in A549 cells. D: Western blot analysis of protein expression in different tumour cell lines. Due to low expression, loading was LAIR-2 only was 4x higher compared to the other lanes to confirm the presence of the protein and the correct size. A549 and DLD-1 cells were infected with an MOI of 0.1, Panc-1 cells were infected with an MOI of 5. This figure was created using BioRender.

Thereafter, the backbone DNA was linearised, transfected into HEK293a cells and rescued after plaquing had occurred 7-14 days post infection. Subsequently, the viral supernatants underwent two rounds of clonal selection before one clone was picked and titred (the process is described in more detail in Chapter 2.5).

Titrating was performed by $TCID_{50}$ on A549 cells in duplicates and repeated twice and showed that all the constructs had an approximate viral concentration of between 10^{-8} to 10^{-9} MOI/mL (**Figure 6.2** C). Additionally, parental EnAd and CMV-GFP EnAd used in this study were generated in the same way by Emma Page and kindly gifted to be utilised. The parental virus was re-titrated using the same strategy as described above.

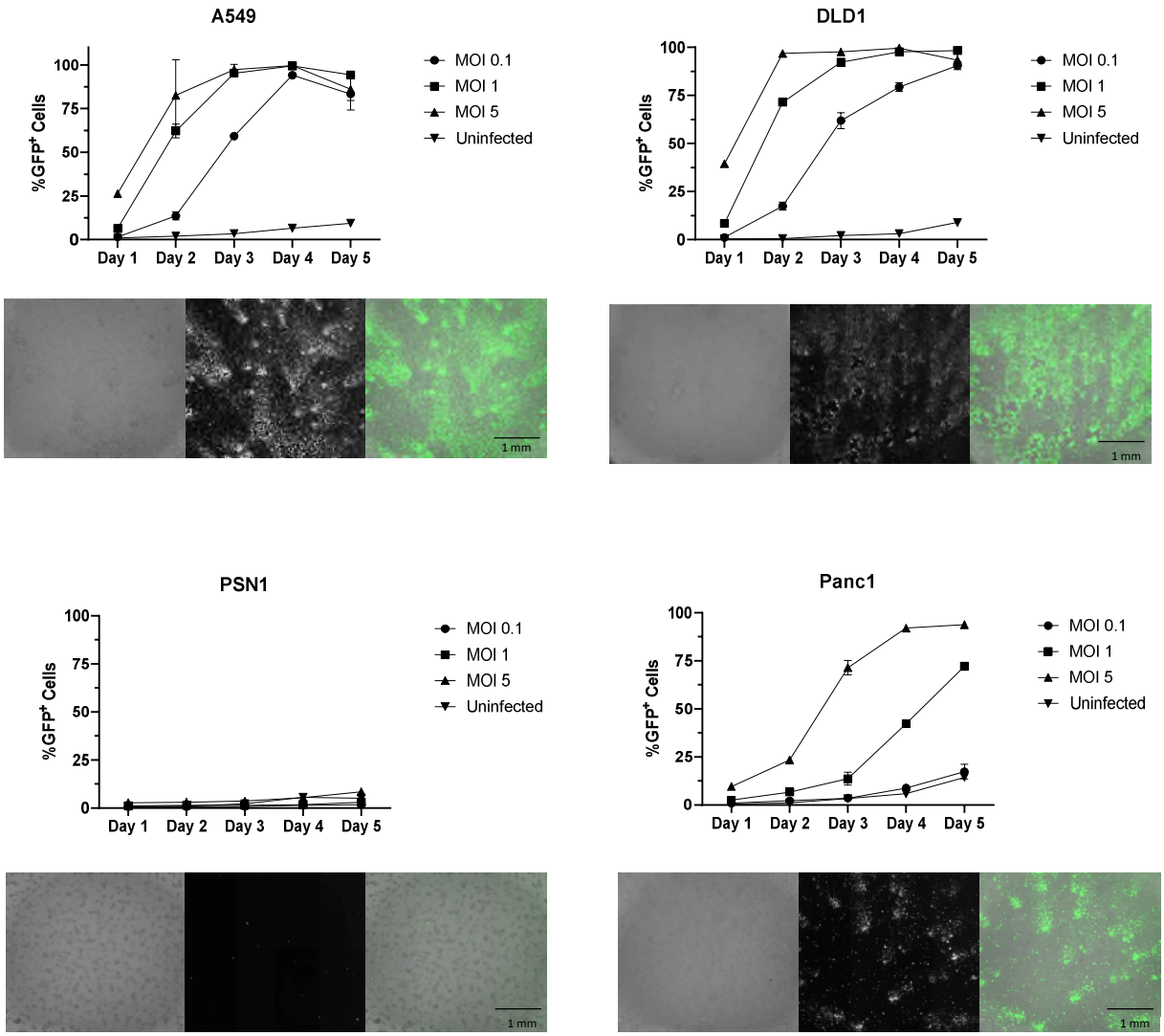

Figure 6.3: MOI comparison between A549, DLD-1, PSN1 and Panc-1 using a CMV-GFP EnAd (kindly provided by Emma Page). All infections were carried out in a 96-well plate and harvested in triplicates on the indicated day and immediately run on flow cytometry. Images below are from day 3 post infection, taken with a Celigo microscope.

As a last step in the EnAd validation process, it was checked that the produced transgene proteins were fully expressed and secreted. Therefore, the supernatant of infected A549 (MOI 0.1), DLD-1 (MOI 0.1) and Panc-1 (MOI 5) cells was collected and run on a western blot as seen in **Figure 6.2** D. Interestingly, LAIR-2 only was weakly expressed in all the tested cell lines, but could nevertheless be detected when adding 4x the amount of supernatant. Additionally, the proteins ran at the expected sizes of 16 kDa for LAIR-2, 32 kDa for aCD3 control and 48 kDa for the bispecific.

Given that the viruses were able to infect and reproduce as well as express the transgenes of interest, we aimed to standardise the MOIs between A549 and the other cell lines used in the study. Therefore, MOI 0.1, 1 and 5 of EnAd encoding GFP under a CMV promotor was added to A549, DLD-1, PSN-1 and Panc-1 cells. Efficiency of cell infection was measured using flow cytometry and a picture was taken with Celigo on five consecutive days. As seen in **Figure 6.3**, A549 and DLD-1 were both very permissive to EnAd, whereas Panc-1 cells were somewhat permissive. PSN-1, however, were not permissive to EnAd in the tested MOIs, although some singular GFP positive cells could be observed at day five for high MOIs. Therefore, PSN-1 cells were omitted for the rest of the experiments. However, MOI 0.1 in A549 and DLD-1 and MOI 5 for Panc-1 showed very similar GFP infection with time and this MOI ratio was therefore chosen for the following experiments. A picture showing the representative infection with MOI 0.1 or 5 respectively on day three is shown below the different graphs.

As the genetic insertion of a payload could potentially impact on the oncolytic effect due to the increased genome size and added expression of the transgene, a cell viability measurement using the xCELLigence machine was set up in order to compare parental EnAd to payload containing EnAd viruses. Infections were studied at MOI 0.2 and MOI 10 for DLD-1 and Panc-1 cells over five days using the xCELLigence. As can be seen in **Figure 6.4** A, all three transgene-containing viruses actually showed increased oncolytic potency, starting to kill DLD-1 cells after approximately 30h, whereas killing by the parental EnAd was not observed until

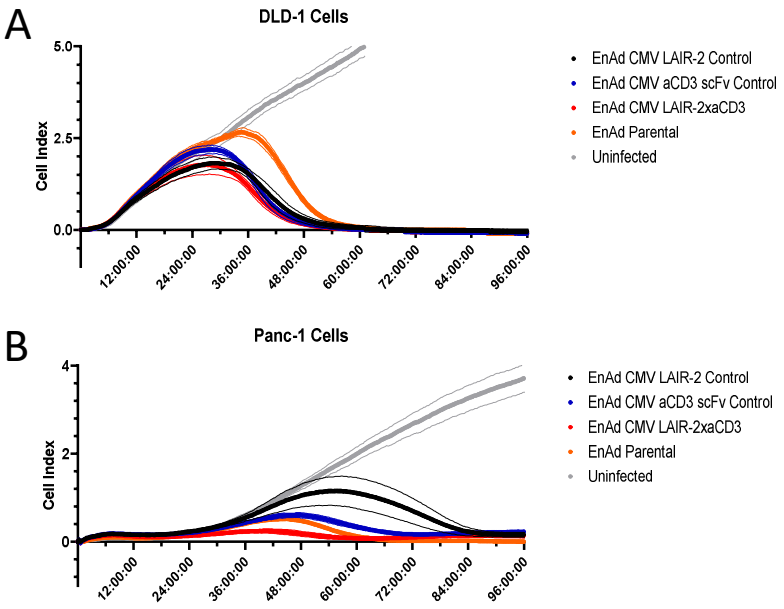

Figure 6.4: DLD-1 and Panc-1 killing potency of parental EnAd and EnAd encoding the different constructs. Therefore, an xCELLigence plate was seeded with the corresponding cell line and the virus was added at the same time (DLD MOI 0.2, Panc-1 MOI 10). Cell viability was measured using impedance for the following days. A: DLD-1 cells and B: Panc-1 cells are shown. n=4 within one experiment.

36-40h post infection. In the less permissive Panc-1 cells (**Figure 6.4** B), the various constructs showed some variability. Although viruses armed with LAIR-2xaCD3, and aCD3 scFv, together with the parental EnAd, showed similar rates of cytotoxicity, visible at around 40-48h, the virus armed with LAIR-2 only exhibited cytotoxicity approximately 12h slower.

6.3.3 EnAd encoding LAIR-2xaCD3 activates T cells and mediates cytotoxicity

Seeing that the viruses were able to produce and secrete the bispecifics, and after exploring the kinetics of viral infection and replication, we investigated the functionality of the expressed bispecifics with an *in vitro* T cell assay. Accordingly a 96-well plate was coated with collagen I (100 µg/ml), followed by the addition of DLD-1 or Panc-1 cells together with T cells and the EnAd viruses at MOI 0.2 or MOI 10 for DLD-1 and Panc-1 respectively. As seen in **Figure 6.5** A, both CD4 and CD8 T cells showed an upregulation in CD25 after three days with the LAIR-2xaCD3 expressing virus in the presence of collagen I and DLD-1 or Panc-1 cells respectively. Unexpectedly, there was also a slightly smaller increase of CD25 expression on T cells in the absence of collagen I, suggesting a partial T cell activation. Activation for both cell lines in the presence of collagen I ranged between 55-80% CD25 expression, whereas only 15-35% of T cells showed an upregulation of CD25 in the absence of collagen I.

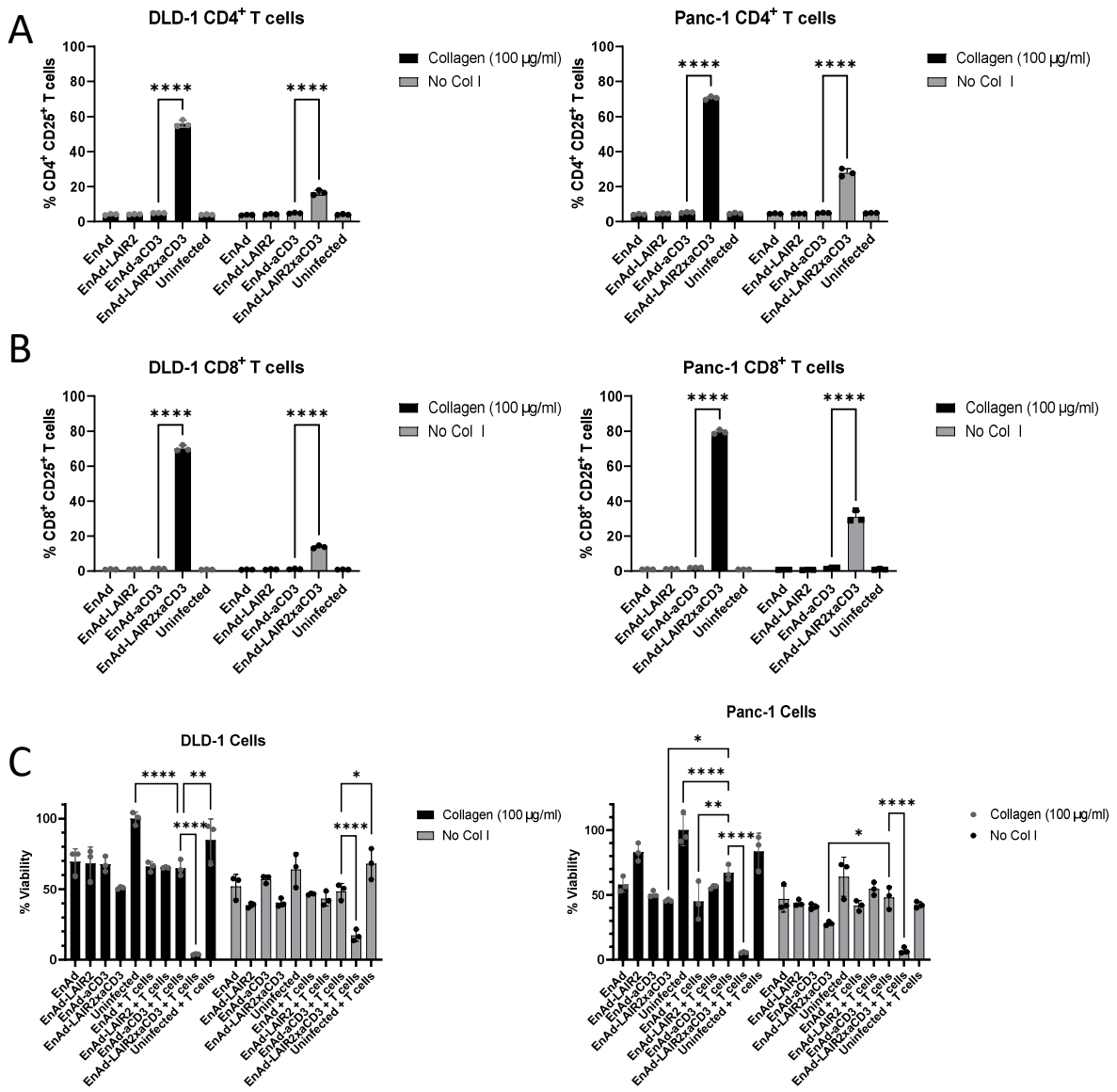

Figure 6.5: Oncolytic adenovirus encoding LAIR-2xaCD3 activates T cells and mediates cytotoxicity but shows less collagen-dependency. A 96-well plate was coated with collagen I or left uncoated, then challenged with 10 nM of the bispecifics and controls. After 1x wash, 10'000 target cells and 50'000 human PBMC T cells were added to the well and incubated for 3 days before T cells were harvested for flow cytometry and an XTT-assay was performed on the cells. A: CD4 T cell activation measured by CD25 upregulation, n=3, two-way ANOVA with Šídák's multiple comparisons test to EnAd expressing anti-CD3 control, p<0.05 *, p<0.01 **, p<0.001 ***, p<0.0001 ****. B: CD8 T cell activation measured by CD25 upregulation, n=3, two-way ANOVA with Šídák's multiple comparisons test to EnAd expressing anti-CD3 control, p<0.05 *, p<0.01 **, p<0.001 ***, p<0.0001 ****. C: Normalised XTT viability values to uninfected, n=3, two-way ANOVA with Dunnett's multiple comparisons test to EnAd expressing anti-CD3 control, p<0.05 *, p<0.01 **, p<0.001 ***, p<0.0001 ****.

In addition to T cell activation, the cytotoxic capacity of the activated T cells was explored. **Figure 6.5** E and F both showed that DLD-1 and Panc-1 cells were both killed after three days with the LAIR-2xaCD3 virus in the presence or absence of collagen I, although the cytotoxicity was slightly less pronounced if the T cells were activated in the absence of collagen I.

6.3.4 T cells can be robustly activated upon stimulation with EnAd encoding LAIR-2xaCD3

Even though some residual T cell activation could be observed after infection with LAIR-2xaCD3 when collagen I was absent, the next step involved checking for key cytotoxicity markers within T cells upon EnAd LAIR-2xaCD3 stimulation. Therefore, the same experimental set up was used as before for Panc-1 cells (**Figure 6.5**), whereby the T cells were this time stained for extracellular CD25, CD69 and CD107a, and intracellularly for IFN-γ, perforin and granzyme B. As can be seen in **Figure 6.6** A, there was a highly significant upregulation of all tested markers in the presence of collagen I compared to EnAd encoding an anti-CD3 scFv control on CD8 T cells. In the absence of collagen I, there was a smaller but

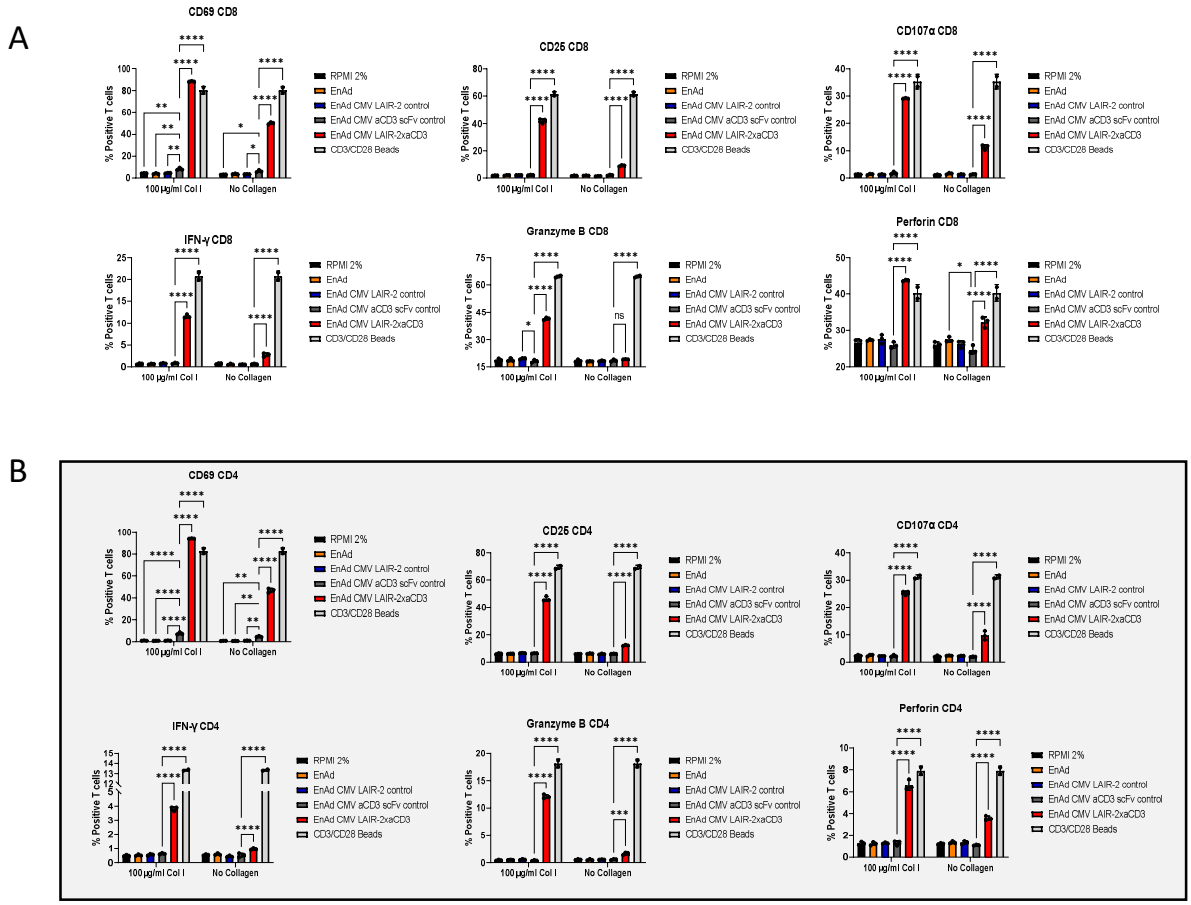

Figure 6.6: LAIR-2xaCD3 expressing OV is able to induce several activation and cytotoxicity markers in CD4 and CD8 T cells upon infection of target cells. For this experiment, Panc-1 cells were seeded on a collagen I coated plate, infected the subsequent day with the various viruses. T cells were also added at a 5:1 ratio to target cells at the same time as the virus infection. Cells were harvested on day 2 and stained extracellularly and intracellularly for the indicated markers and measured via flow cytometry. A: Activation and cytotoxicity makers on CD8 T cells, B: Activation and cytotoxicity markers on CD4 T cells. For all graphs: n=3, two-way ANOVA with Dunnett's multiple comparisons test to EnAd expressing anti-CD3 control, $p<0.05$ *, $p<0.01$ **, $p<0.001$ ***, $p<0.0001$ ****.

still significant upregulation of the markers (except for granzyme B). For perforin and CD69, the upregulation was greater compared to the stimulation with anti-CD3/CD28 beads. In **Figure 6.6** B, the same can be seen for CD4 T cells. Again, in the presence of collagen I, there was a highly significant upregulation of all the tested markers, including perforin and granzyme B. Although the upregulation in the absence of collagen I was also significant, it was in all cases at least 2x or lower compared to when collagen I was present. Overall, IFN-γ, perforin and granzyme B were highly upregulated in CD8 T cells compared to CD4, whereas surface activation markers such as CD25 and CD69 were highly upregulated in both in the presence of collagen I. In the absence of collagen I, the levels of all tested markers were reduced.

Given the collagen I independent cytotoxicity shown by EnAd CMV LAIR-2 xaCD3, the kinetics of the killing were explored in more detail. Panc-1 cells were seeded in an xCELLigence plate either coated with collagen I or without collagen I, and additionally either incubated with or without T cells. At the same time, the different viruses were added at an MOI of 10 to all the

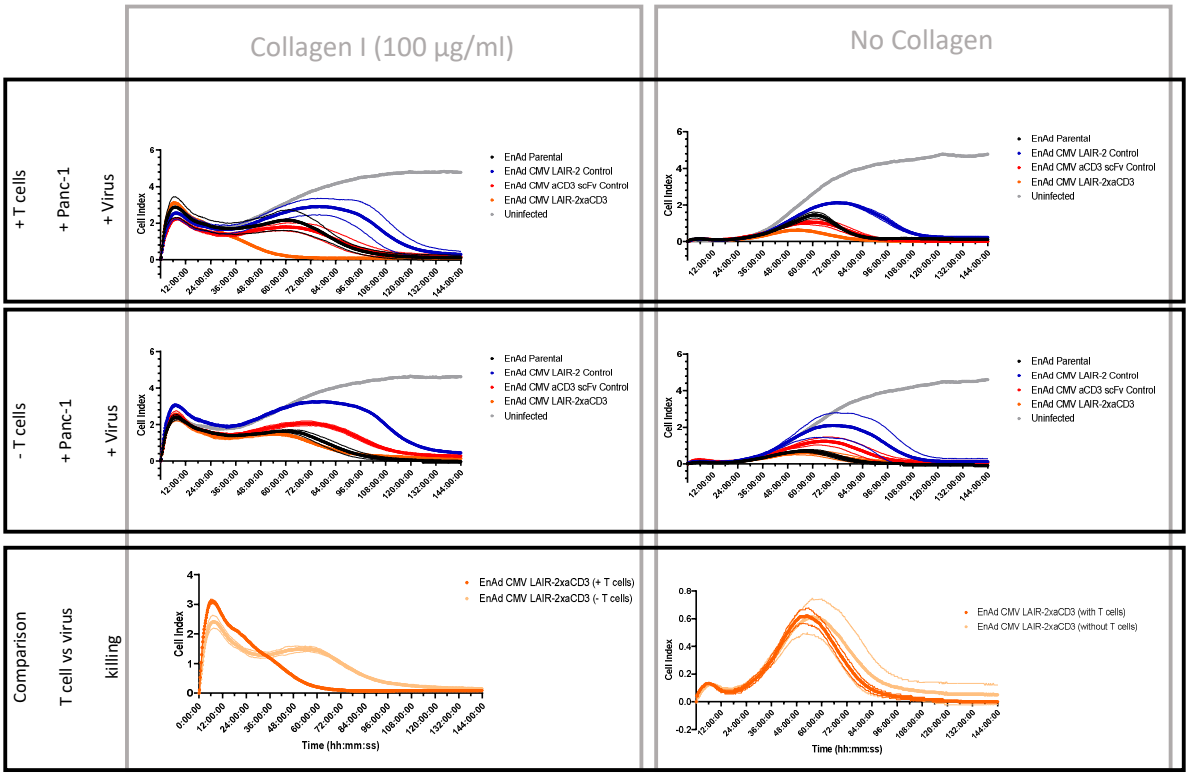

Figure 6.7: T cell-dependent and collagen I dependent killing of Panc-1 cells upon LAIR-2xaCD3 EnAd infection can be seen. Panc-1 cells were seeded on a collagen I coated plate, and subsequently infected with the virus and incubated with T cells (1:5 ratio). Top graphs represent conditions containing T cells, target cell (Panc-1) and OVs. The middle graphs show the same conditions as above, but with no T cells present. The bottom graphs show the LAIR-2xaCD3 bispecific data from the two diagrams above, facilitating the comparison of T cell dependent cell killing (n=3).

wells and incubated for the time of the experiment. Interestingly, initial Panc-1 adhesion happened within 8-12h on collagen I coated plates, as can be seen in **Figure 6.7** A and B, whereas on non-coated plates, it took nearly 36h for the cells to properly attach and start growing. When looking at the collagen I coated plates without T cells, it can be seen that the parental virus alone starts killing after approximately 60h (**Figure 6.7** B) whereas EnAd encoding LAIR-2 shows slower cytotoxicity (approximately 72h; also seen in **Figure 6.4** B). The wells containing T cells from **Figure 6.7** A show no difference in the time of killing, except for the ones infected with the LAIR-2xaCD3 virus, which display bispecific-mediated killing 30h after infection (dark orange line in **Figure 6.7** A). In **Figure 6.7** C, only the wells with LAIR-2xaCD3 virus on collagen I coated plates from **Figure 6.7** A and B are shown for comparison, highlighting the T cell-dependent killing in the dark orange, whereas the LAIR-2xaCD3 shows virus only killing (no T cells) in light orange. The T cell-mediated killing constitutes approximately a 30h shift in killing Panc-1 faster than the virus alone.

However, when looking at the plates which were not coated with collagen I, there is no noticeable difference between virus-mediated killing and LAIR-2xaCD3-mediated killing, as can be seen in **Figure 6.7** F.

6.3.5 "Traffic light" EnAd can be used to study *in vivo* and *ex vivo* infection and replication

Although *in vitro* experiments are crucial for initial validation, it is especially important to validate translational approaches such as armed OVs in clinically relevant samples. In order to better predict whether specific samples were susceptible for EnAd, a traffic light EnAd was engineered by Egon Jacobus and kindly gifted for the use in this study. This virus expresses an early E1A-UnaG fusion protein under control of a CMV promoter, which will turn the cells green upon infection and early gene transcription and translation. Additionally, the virus encodes an mCherry under the major late promotor, which is transcribed and translated when the virus enters the late stage of infection. Therefore, infected cells should first turn green,

followed by yellow depicting the transition between early and late, and finally move towards red as the cell starts to translate preferentially mRNA containing the tripartite leader sequence (resembling a traffic light).

The virus was initially validated in A549 cells using an IncuCyte imager. A549 cells were seeded in 24-well plate and infected with 10 vp/cell (approximately MOI of 0.1), before overlaying the well with agarose and incubation in the IncuCyte. The wells were monitored over a total of 5 days, and a representative plaque can be seen in **Figure 6.8**. In the picture on the top left a single cell at a late stage of infection can be seen, made evident by the mCherry expression and the rounded morphology. In the picture on the top left, the previous cell has burst and infected the surrounding cells, as seen by the neighbouring cells expressing UnaG. In the bottom left picture, it can be seen that the plaque is slowly expanding, accompanied by the rounding of some of the infected cells and the transition of them into late gene expression. Finally, the bottom right picture shows a mature plaque, with many red and yellow cells towards the middle and newly infected cells on the edges.

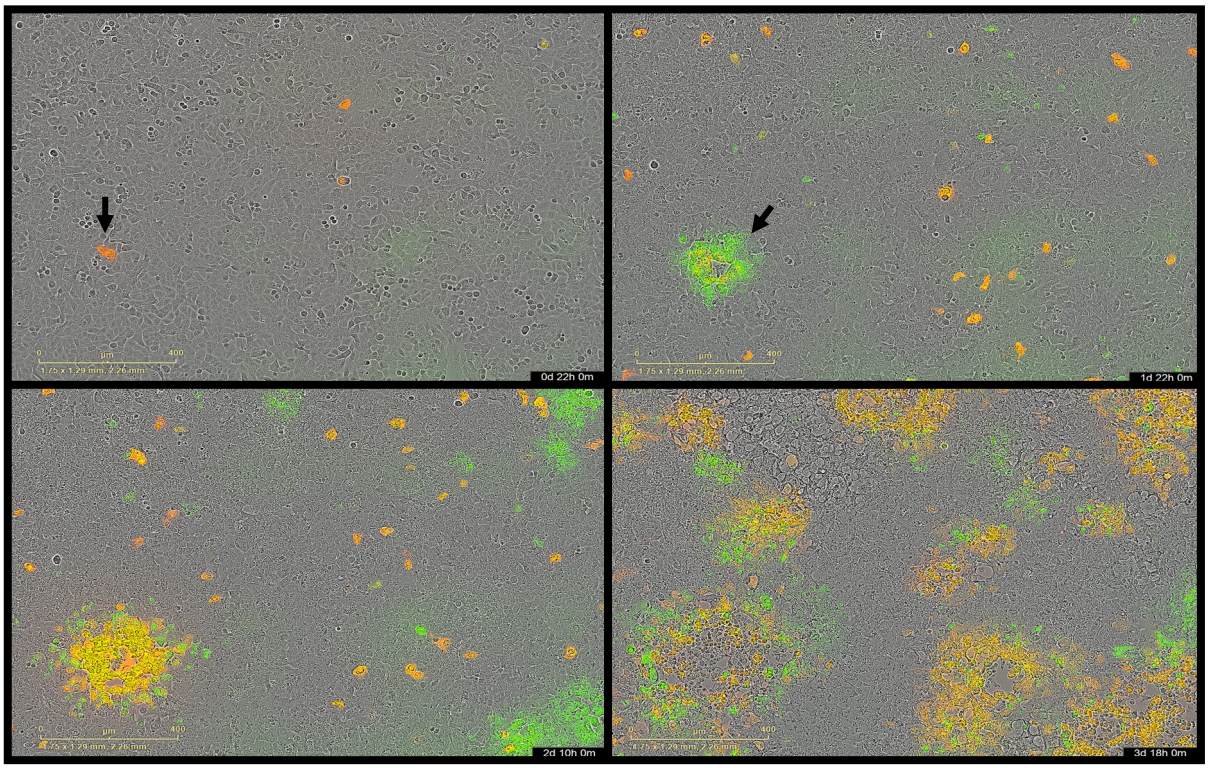

Figure 6.8: Plaque formation using EnAd encoding an UnaG tagged E1A (early genes, infection) and an mCherry (late genes, major late promotor SA). A549 cells were seeded in a 24-well plate and infected with the virus at 10 virus particles per cell (corresponding to an MOI of 0.1). The infection was left on for 5h, before the cells were overlayed with agarose and placed in the IncuCyte machine for analysis. Pictures shown are representation images of plaques seen in the experiment over time.

In order to validate and confirm the permissivity of EnAd in cancer patients, the traffic light EnAd virus was tested in *ex vivo* colorectal liver metastases slices deriving from patient samples. It was assumed that each slice contained roughly 1 million cells, which were then infected with the equivalent of an MOI of 10 as measured in A549 or 1000 vp/cell.

In **Figure 6.9** A, the tumour slices and some normal adjacent liver slices were infected with the same traffic light virus. As can be seen in **Figure 6.9** A, day three and day five post infection were imaged on a confocal microscope and shown as a maximum projection. In the tumour panels (left), an increase in signal from day three to day five can clearly be seen, and comparatively, there are more orange or red cells in the merged picture, which indicates viral replication and late stage of gene expression. When looking at the normal liver samples in the right panel, it is evident that there are less plaques on day three and day five compared to the tumour slices. Furthermore, the colours in the normal liver slices do not always co-localise, with certain cells only expressing red colour and relatively few orange/yellow plaques, potentially indicating background autofluorescence or non-specific fluorescence. However, there are a few spots in the liver slices which have gone into late stage of the EnAd life cycle, although there is still a large difference in size and incidence when comparing to the tumour slices.

A similar experiment has also been conducted with a CMV GFP expressing EnAd in **Figure 6.9** B corresponding to a closer comparison to the EnAd containing the bispecific due to the same expression promoter. In this instance, the ability to distinguish between early and late viral gene expression was lost, however, the GFP signal was easier to detect on the microscope for a prolonged period of time compared to UnaG. Results were very similar to **Figure 6.9** A, meaning that there were more and bigger plaques in the tumour panels compared to the normal liver. Nevertheless, there was still a considerable amount of infection in the normal liver cells as would be expected since the GFP reads out early stages of infection and not the full virus life cycle.

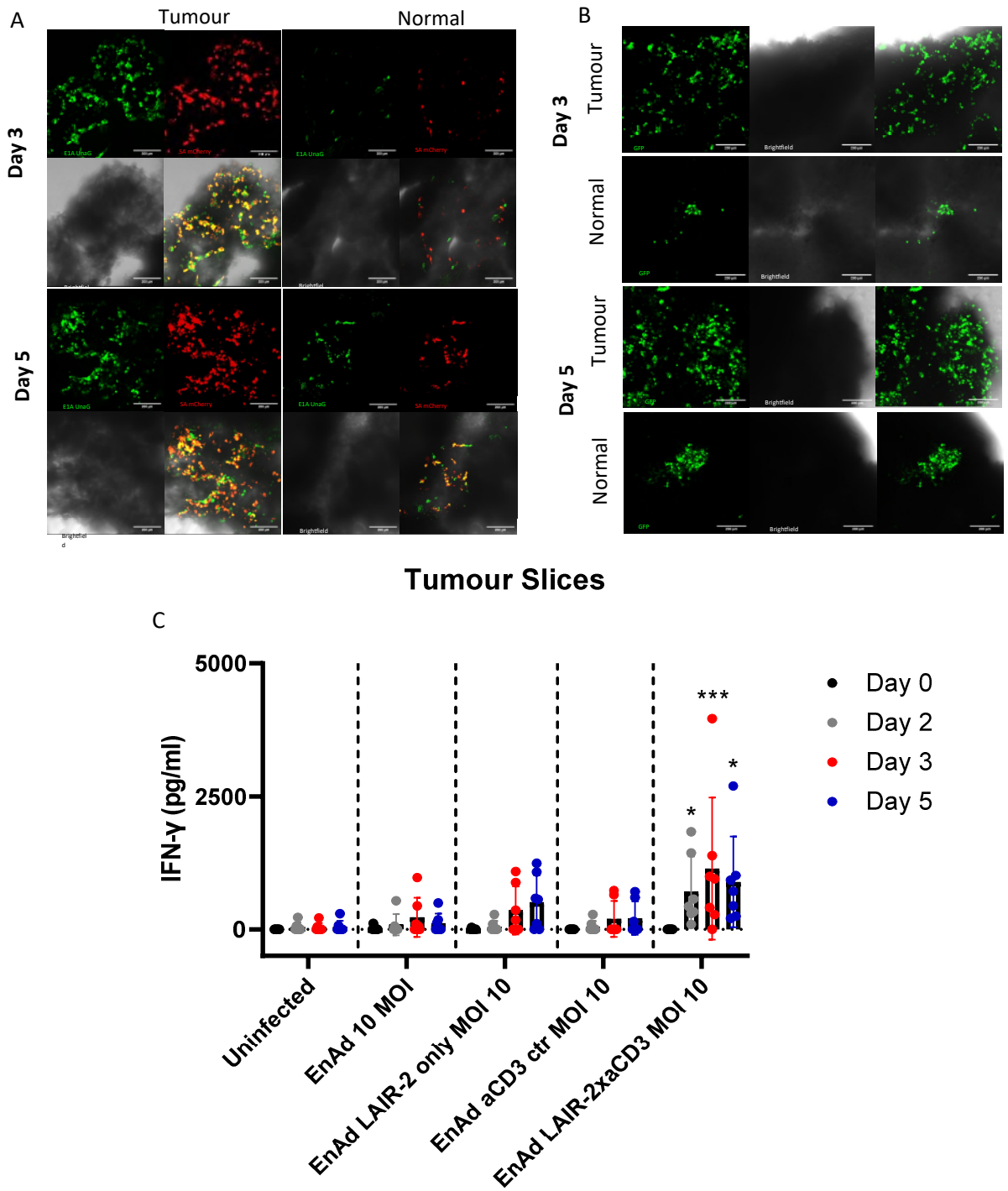

Figure 6.9: Colorectal liver metastases slices can be infected with EnAd and show upregulated IFN-γ production when infected with EnAd expressing LAIR-2xaCD3 bispecific. Tumour pieces were cut in 250 µm thick slices and incubated for 5 days with the different treatments. Supernatant was taken on the indicated days and measured using an IFN-γ ELISA. A: Tumour (left) and normal liver (right) slices infected with the EnAd traffic light virus, showing infection in green and replication in red. Top panel shows slices three days post infection, bottom panel shows slices five days post infection. B: EnAd expressing GFP under a CMV promotor three (top panel) and five (bottom panel) days after infection. Top row shows tumour slices whereas the bottom row represents the normal liver slices. Representative images are shown in all the panels from A and B. C: IFN-γ ELISA measured from the supernatant at the indicated days post infection. n=two patients with 3 and 4 slices respectively, two-way ANOVA with Dunnett's multiple comparisons test to EnAd expressing anti-CD3 control, $p<0.05$ *, $p<0.01$ **, $p<0.001$ ***, $p<0.0001$ ****.

6.3.6 EnAd encoding LAIR-2xaCD3 bispecific potentially activates endogenous T cells in human biopsies and primes them for bystander killing

After establishing that tumour cells in the slices could be infected with EnAd and that the virus could replicate in the tumour, we proceeded to add the viruses encoding the bispecifics to the slices. Similarly to the other chapters, supernatant was taken on day 0, day 2, day 3 and day 5 and measured for IFN-γ content using ELISA. It was estimated that each slice contained roughly 1 million cells, which were then infected with the equivalent of an MOI of 10 as measured in A549. It can be seen (**Figure 6.9** C), that some of the slices exhibit a background activity, however, only the LAIR-2xaCD3 EnAd treated wells show a significant production of IFN-γ compared to the anti-CD3 scFv control virus. Intriguingly, EnAd alone and EnAd with aCD3 only show some upregulation compared to uninfected. Nevertheless, EnAd encoding LAIR-2 alone shows a greater upregulation, especially on day 3 and on day 5. Overall, two patients with a total of 7 slices from different tumour regions are shown.

In order to further investigate these differences, a LegendPlex cytokine quantification assay was run. The principles of the assay are described in **Figure 6.10** A. In short, there are two populations of beads of different sizes, which again are subdivided in beads with a different content of APC fluorophore and can hence be separated as such. Each of these populations binds to a predefined cytokine. The amount of cytokine bound to each bead was detected by streptavidin PE and then quantified using a standard curve. The different plots and the labels for each cytokine are depicted with two samples to exemplify in **Figure 6.10** A.

In **Figure 6.10** B, the main cytokines involved in a T cell response are shown at different timepoints after supernatant collected from the infected tumour slices was incubated with the LegendPlex beads. Interestingly, there was not a big difference in which mediators were induced, but rather in the level of the induction between the responders and non-responders. IL-10 and IL-2 and TNFα, for example, seem to be upregulated to a higher extent in responders, whereas the other cytokines remained at the same level for all the conditions.

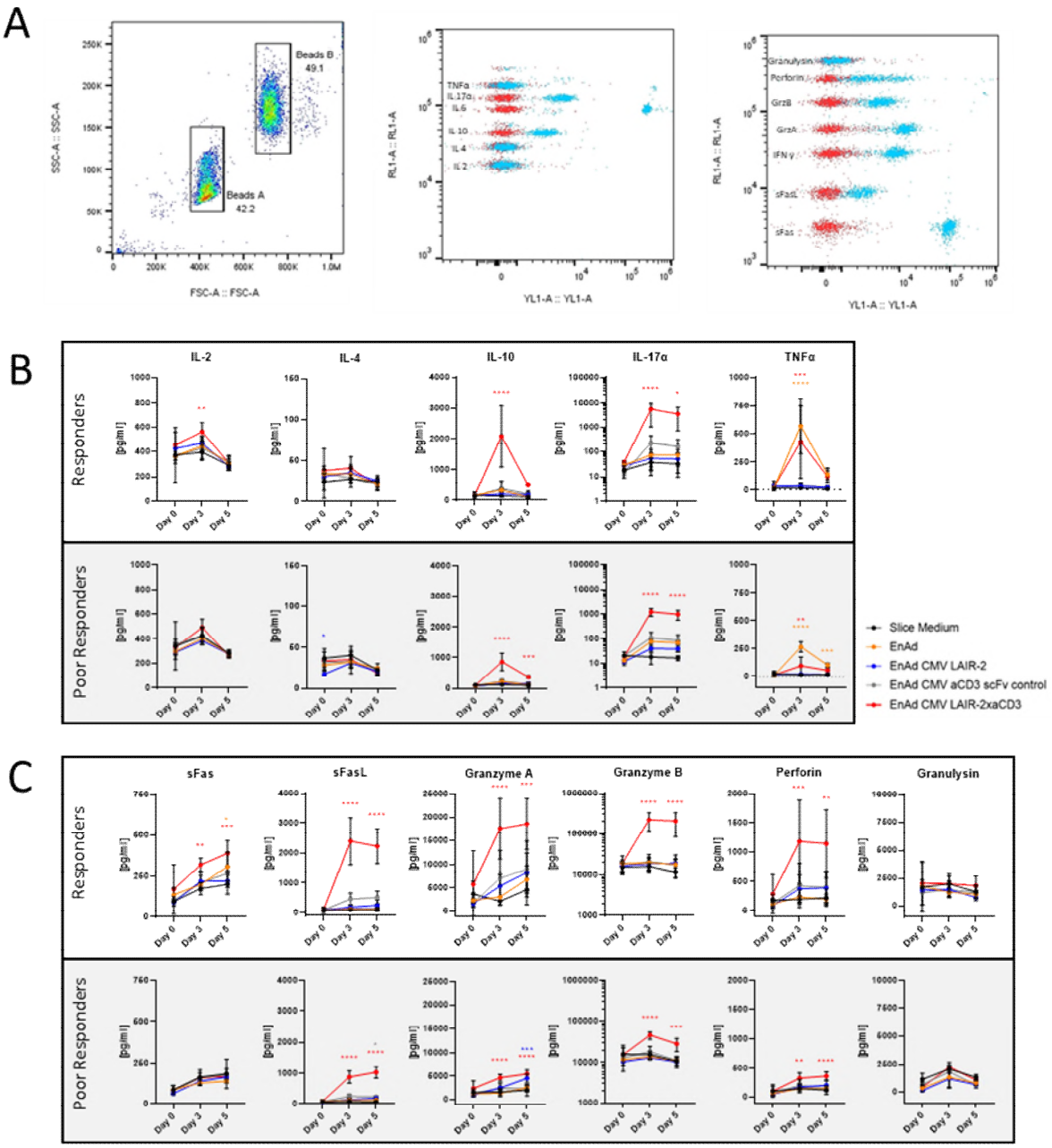

Figure 6.10: Responders and poor-responder colorectal liver metastases slices show signs of endogenous T cell activation and cytotoxicity upon infection with LAIR-2xaCD3 expressing EnAd. For this experiment, one responder and one poor-responder slice per patient (two slices in total) were selected after IFN-γ ELISA for the LegendPlex assay. A: Validation of the LegendPlex cytokine quantification assay. B: Cytokines important in cytotoxic T cell responses are depicted in this panel, with responders in the top row and poor-responders in the bottom row. C: Mediators important for cytotoxicity and activation are depicted in this panel. Statistics for B and C: n=2 slices with 2 technical replicates for each datapoint, two-way ANOVA with Dunnett's multiple comparisons test to EnAd expressing anti-CD3 control, $p<0.05$ *, $p<0.01$ **, $p<0.001$ ***, $p<0.0001$ ****.

Parental EnAd virus also evoked a TNFα response, however, not when a payload is encoded except for the LAIR-2xaCD3 bispecific. There was additionally a big spike in IL-10 on day 3, which subsided by day 5 in both responders and poor responders.

In **Figure 6.10** C, the mediators involved in T cell-mediated cytotoxicity are displayed. In general, it can be seen that cytotoxicity is taking place within the slices, as all the main indicators such as perforin and granzymes are upregulated. Additionally, there is a strong difference between responders and non-responders, as non-responders show a mild induction of sFasL, granzyme A/B and perforin, whereas high levels of the mediators can be detected in responders. Granulysin, however, shows no upregulation in any conditions over the period of five days.

6.4 Discussion

In this Chapter, the feasibility and functionality of encoding the LAIR-2xaCD3 bispecific from Chapter 5 into the oncolytic adenovirus EnAd was explored.

Production of the EnAd expressing the bispecific agent under the CMV promotor (**Figure 6.2**) shows that multiple tested cancer cell lines are able to express and secrete the bispecific. Expression under the major late promotor (SA) was also explored but did not succeed. However, for all the tested cell lines, LAIR-2 only was the least well-expressed protein, which can have multiple reasons. One possible explanation could be that the protein might be stuck inside the cell and not get secreted.

After two rounds of clonal selection, one protein expressing virus per construct was grown in a T25 and a stock was created. Due to time constraints, no further purification could be performed. However, as the titres were relatively high and all the viral constructs showed roughly similar MOIs for their cell preps, meaning that the amount added to the cells was small and consistent for all constructs. Without banding, it was also not possible to determine the number of virus particles. Therefore, a $TCID_{50}$ in A549 cells was performed. Subsequently, all used cell lines for the experiment were infected with MOIs relating to A549 cells in order to optimise which dose of virus would be similar between cell lines and allow for a fair comparison. DLD-1 and A549 cells were very susceptible to the virus and therefore an MOI of 0.1 or 0.2 respectively, was enough to achieve a strong infection. Panc-1 and PSN-1 on the

other hand, were difficult to infect, whereas Panc-1 cells could still be infected with an MOI of 5 or 10 respectively, which was comparable to the MOI 0.1/0.2 in A549 and DLD-1 (**Figure 6.3**). Therefore, the previously stated MOI ratio was kept for the subsequent experiments in DLD-1 and Panc-1 cell lines. The difference in susceptibility (e.g. infectivity measured by GFP expression) to infection could reflect multiple factors, for example the main entry receptor CD46 or secondary receptor desmoglein 2 could be expressed to a lesser extent and therefore allow less uptake of the virus into the cells.

On the other hand, Dyer et al have previously shown the impact of glucose and glutamine supply on EnAd in a permissive (A549) and non permissive (SK-OV-3) cell line for EnAd, underlining the importance of metabolism in OV therapy (Dyer et al. 2019). They were able to show that glutamine but not glucose metabolism played a crucial role, and that EnAd reproduced to a higher extent in cells which relied on glutamine uptake and reductive carboxylation. This indicates that part of the tumour-selectivity of EnAd might be a loss of control of host cell metabolism. This means that EnAd replicates far more efficiently in cells already displaying aberrant metabolism (such as the Warburg effect which is a key hallmark of cancer) than in normal cells with coupled respiration (Dyer et al. 2019).

After establishing all parameters and validating the viral properties, the functionality of the bispecific and controls were assessed and confirmed. The T cell activation and cytotoxicity, however, seemed to lose some of the collagen I specificity displayed in chapter 5. This could mean that the virus infection changes the cells' surface, which could result in the bispecific binding to it and hence inducing a residual activation. Alternatively, the virus infection could also upregulate membrane bound collagen such as collagen 17, which is also known to bind to LAIR-1 and therefore potentially also to LAIR-2 (Lebbink et al. 2006). A third option could also be, that virus infection changes the properties of the cell surface through for example GAG upregulation, which could lead to non-specific binding of the bispecific to the cell surface. However, more experiments to further investigate this are necessary to evaluate what the cause is and especially also to validate if this phenomenon could be an *in vitro* artefact only.

However, this residual T cell activation and cytotoxicity in the absence of collagen I does not pose a problem for the further development of this therapeutic, as there is always collagen I present *in vivo*, making the no collagen I scenario irrelevant for further investigative steps. Additionally, this activation is not close to as robust as the activation in the presence of collagen I. It is also important to note that the anti-CD3 motifs do only activate T cells when clustered on the T cell surface. Especially the findings of T cell activation from the liver metastasis slices shows, that collagen I has sufficiently close binding sites for LAIR-2 to ensure clustering of the anti-CD3 motifs and thus induce T cell activation. This might also pose another safety mechanism, ensuring that small amounts leaking out of the tumour will not activate T cells systemically if there is not enough bispecific for clustering.

To investigate the potency of the armed OV, we sought to use the slice model used in Chapters 4 and 5 to investigate further into the potency of the virus. Slice cultures have already been used in virus models such as VSV infection studies, as they allow the observation of viral spread in conditions very close to human tumours (Runge et al. 2022). Infectivity and replication were confirmed with the traffic light EnAd and GFP expressing EnAd in **Figure 6.9**.

It was also evident that some of the cells in the adjacent liver tissue were infected and could even express late-stage proteins. Similarly, it was seen with the CMV GFP expressing EnAd that adjacent tissue could be infected. Qualitatively, the areas of infection within the liver tissue seem to be very contained and only show very few plaques of infection, whereas the areas of infection within the tumour slices showed higher numbers of plaques and also showed a greater area. This rather high unexpected infection of normal liver tissue can potentially also be explained by the high density of Kupffer cells (macrophages), that are inevitably taking up the virus particles and hence there could be a slight leakage with the macrophages expressing the target and virus proteins (Tao et al. 2001; Xu et al. 2008). However, it is also possible that the signal is arising from hepatocytes, which would potentially explain the ability of the virus to go late in these cells. Hence, in high doses, EnAd might not be 100% cancer selective and might still replicate in small amounts in normal cells such as hepatocytes.

Apart from imaging and spread, slice models have also been used to characterise therapeutics *ex vivo*. Recently published studies by Runge et al. and Roelants et al. looked at head and neck tumour slice cultures as pre-clinical predictive models using a VSV (Roelants et al. 2020; Runge et al. 2022). EnAd has also previously been tested on tissue slices derived from prostate cancer, whereby they were treated with EnAd encoding a FAP-bispecific (Freedman et al. 2018).

When looking at the IFN-γ production of the slices upon infection with the viruses, there is more IFN-γ production when looking at parental EnAd infection compared to the uninfected control. Interestingly, EnAd encoding anti-CD3 does not show more IFN-γ production compared to the slices infected with parental EnAd. This shows that an expressed anti-CD3 scFv alone does not activate T cells *in situ,* presumably because there is no mechanism for it to cluster CD3 on the T cell surface. When looking at EnAd expressing LAIR-2 only, a slight upregulation of IFN-γ can be observed, especially later on in the timepoints (day 3 and day 5). This later on-set of the potential effect on T cells might be due to the many available collagen I binding sites, which can only be depleted by the accumulation of LAIR-2 *in situ*. This accumulation therefore potentially reaches an effective threshold after day 3 - day 5. Finally, it is clearly visible that the virus expressing the LAIR-2xaCD3 bispecific has a strong and fast response, which lasts up to day 5. This is significant when compared to the values of the virus expressing the anti-CD3 scFv alone. Similar to our findings, the induced IFN-γ production lies in a comparable level in other studies, whereby they also observe a high variability between the different types of cancer (Runge et al. 2022).

As there are great differences of slices that respond and do not respond coming from the same patient but from a different region within the slice, we decided to analyse further cytokines to elucidate the reason for these differences. Especially when looking at the main cytotoxic T cell mediators shown in **Figure 6.9** B, there is no change observed for IL-4 levels, whereas all other measured cytokines show a change. This is a phenomenon not seen in the graphs where free LAIR-2xaCD3 bispecific was used in **Figure 5.10** B and therefore could most likely stem from

the combination of the LAIR-2xaCD3 and EnAd, as parental EnAd alone or with the controls encoded does not lead to a significant change in most of the tested mediators. Interestingly, the inhibitory cytokine IL-10 is upregulated shortly after activation and then depleted again by day 5, with responders showing a higher IL-10 production compared to the poor responders. This IL-10 is most probably produced by activated cytotoxic T cells, as this is a known phenomenon and has already been shown before (Oft 2014; Trandem et al. 2008). IL-10 is especially important in physiology in order to minimise tissue damage and contain the T cell response (Smith et al. 2018; Trinchieri 2007). Therefore, it is not surprising to see that the virus alone or the controls alone did not induce a spike in IL-10, as we would not expect any T cell activation. Additionally, IL-17a production spiked in both responders and poor responders, principally upon LAIR-2xaCD3 treatment and parental EnAd only. In general, IL-17a has been shown to be involved in anti-viral immunity by promoting CTL-mediated target cell clearance (Acharya et al. 2017). On a different note, IL-17a has been shown to negatively impact on CD8 T cell recruitment in colorectal cancer mouse models, promoting cancer growth (Chen et al. 2019). These conflicting views make for a difficult assessment of the data and more experiments would have to be performed in order to decide if IL-17a is beneficial or detrimental in this case.

Also, there was a temporary spike of TNFα at day three for both responders and poor responders, whereby the spike especially with the LAIR-2xaCD3 virus was less in the poor responders. The response elicited by the parental EnAd is very interesting, as a similar response is seen with the LAIR-2xaCD3 virus, but not with EnAd encoding the two controls respectively.

As the LAIR-2xaCD3 bispecific kills via bystander killing, especially the induction of cytokines such as IFN-γ and TNFα are important as shown in infected slices depicted in **Figure 6.9** B. A recent study has shown that both cytokines have the ability to specifically upregulate molecules such as Fas and ICAM1 on neighbouring cells and therefore potentiate bystander killing (Upadhyay et al. 2021). As a strong induction can be seen with the virus, this suggests

a potentiation of the bystander killing effect and further underlines the potential of harnessing antigen-independent cancer cell killing.

Furthermore, when looking at T cell effector mediators in **Figure 6.9** C, the upregulation in all cytotoxic markers is relatively stark (with the exception of granylysin). There was also a depletion in levels when comparing responders to poor-responders, which was to be expected. Given the results from Chapter 3, this also confirms the strong involvement of both the Fas/FasL as well as the granzyme/perforin pathway in bystander killing. For this graph, the strong upregulation is mostly seen in EnAd encoding the LAIR-2xaCD3 bispecific, whereby the other viruses did not amount to a similar level of response, especially not in the responders.

In conclusion, we have shown in this chapter that, through encoding the bispecific LAIR-2xaCD3 in EnAd, delivering and expressing it *in situ* leads to a strong T cell activation as well as an anti-viral response of the tumour and immune system present. Although the experiments in Chapter 5 using the free proteins show similar results, there is a stark potentiation of the T cell activation through the viral delivery of the bispecifics, seen by the upregulation of many key cytokines and mediators. This additionally shows that harnessing bystander killing by decorating collagen I with anti-CD3 scFvs delivered through an OV is enough to robustly activate T cells *in situ* and therefore induce an antigen-independent cytotoxicity.

7 Final discussion

7.1 CD4 and CD8 involvement in bystander cytotoxicity

Bystander killing has been reported to occur in several different contexts, including with T cell therapies such as CAR T cells and BiTEs (Ross et al. 2015; Upadhyay et al. 2021). Intriguingly, bystander killing is a physiological phenomenon which is reported to occur upon T cell activation, and cell types such as epithelial and mesothelial cells (at immune privileged sites) have naturally heightened expression of serpins (PI-9), which likely inhibit cytotoxic pathways mediated via granzymes, and (at higher concentration) Fas/FasL cytotoxicity (Cunningham et al. 2007). As epithelial cells are often localised at effector sides of CTLs, the heightened PI-9 content could be a mechanism to control excessive bystander killing and minimise tissue damage (Buzza et al. 2001). The exact mechanism behind bystander killing is not yet fully understood, and the extent of the involvement of CD4 and CD8 T cells or the perforin/granzyme and Fas/FasL pathways have still not been determined.

Publications generally focus on CD8 T cells as archetypal cytotoxic T cells, however, we have seen that CD4 T cells are also able to mediate cytotoxicity to a high extent upon cell-cell contact (Chapter 3.3.4). Interestingly, only CD8 T cells were able to mediate bystander cytotoxicity via soluble mediators, suggesting potentially that the perforin/granzyme pathway is a preferred mechanism of killing for CD8 T cells which might involve killing via SMAPs (Bálint et al. 2020), whereas other cytotoxic pathways such as Fas/FasL could be more involved in CD4 T cell mediated bystander killing. This was further exemplified by the findings of **Figure 6.6**, demonstrating that CD4 and CD8 T cells were showing similar levels of activation after virus infection of co-cultured tumour cells on collagen I-coated plates, wherein a startling difference in their upregulation of several intracellular mediators could be observed. The IFN-γ production of CD4 T cells was approximately halved when compared to CD8 T cells and the intracellular levels of perforin and granzyme were both only expressed by a third compared to

CD8 T cells, strongly hinting towards CD8 T cells preferring the perforin/granzyme pathway to exert bystander killing. Additionally, the stark reduction of key cytotoxic mediators in CD4 T cells while maintaining a comparatively high level of cytotoxicity as seen in **Figure 3.4**, strongly suggests that receptor-mediated killing pathway is involved in CD4 T cell-mediated cytotoxicity.

The exact involvement of Fas and FasL in bystander killing is not yet known, but it is suggested that it plays an important role besides the traditional perforin/granzyme pathway (Smyth, Krasovskis, and Johnstone 1998; Upadhyay et al. 2021). This is further exemplified by the LegendPlex data from Chapter 5 and 6 (**Figure 5.17**, **Figure 6.10**), showing a strong upregulation of sFas and sFasL. Especially sFasL could be an indication that Fas-mediated killing is occurring, given that membrane bound FasL co-localises with granzyme B, is upregulated following T cell activation (Blott et al. 2001; Kassahn et al. 2009) and cleaved off the surface in order to produce sFasL (Matsuno et al. 2001). However, further experiments need to be conducted in order to definitively elucidate the role of Fas and CD4 T cells in bystander cytotoxicity.

Another important point to address regarding bystander killing is the possibility of T cells targeting other T cells or immune cells in a process of fratricide. In addition to many epithelial cells showing upregulated PI-9, T cells also show high levels or PI-9 expression (Classen, Bird, and Debatin 2006). The expression of PI-9 is especially strong in cytotoxic T cells as a self defence against potential leaking of granzymes from secretory granules (Ko et al. 2007). Therefore, this prevents other activated T cells to eliminate themselves during an immune response. In addition to this, a reduction in T cell numbers in the wells with activated T cells was not observed.

7.2 Potentiation of bystander killing

Potentiation of bystander killing has been reported in Upadhyay et al. and in Ross et al. (Ross et al. 2015; Upadhyay et al. 2021), and proven to be mainly mediated by IFN-γ and TNFα as

described above. However, it has also been reported that the use of PD-1 blocking antibody enhanced bystander killing (Upadhyay et al. 2021). This might hint towards a possible synergy, whereby activated T cells primed to mediate bystander killing upregulate exhaustion markers, which can be counteracted using IC inhibitors, thereby increasing their cytotoxicity. This also suggests that exhausted cells can be rescued by IC inhibitors and can further exert antigen-independent bystander killing. However, further experiments in this area are needed and different IC inhibitors would have to be tested in order to define optimal treatment strategies.

On another note, approaches such as CAR T cells have over the years been refined by adding co-stimulatory signals to the intracellular tail of the chimeric receptor, making the CAR T cell activation more stable and robust (Subklewe and Bergwelt-baildon 2019). Especially when trying to harness bystander killing, the inclusion of a co-stimulatory agonistic anti-CD28 alongside the anti-CD3 signal could be a feasible approach to mediate greater bystander killing and induce a more robust T cell activation. Furthermore, Dynabeads are often used in this thesis as an analogy to the main hypothesis, as they also contain both anti-CD3 and anti-CD28 motifs. This idea has partly already been explored before by Scott et al. with Bi- and Trispecifics (BiTE, TriTE), where the anti-CD28-containing TriTE caused non-specific T cell activation (Scott et al. 2019). However, the T cell activation levels (in terms of CD25 expression and IFN-γ production) achieved by Scott et al. were comparable to those achieved using an anti-CD3 (OKT3) alone, rendering the inclusion of an anti-CD28 in this system superfluous. This is further supported by the reduced cytotoxic ability exhibited by CD3/CD28 Dynabeads compared to the LAIR-2xaCD3 bispecific (**Figure 5.10**). However, it should be noted that the maximum activation threshold in these *in vitro* experiments might have been exhausted by the anti-CD3 only, showing no further potentiation by anti-CD28 inclusion. Therefore, clinically relevant systems such as tumour slices might pose a better way to detect potential synergies.

7.3 Clinically relevant cancer model systems

Every novel therapeutic is thoroughly tested and validated *in vitro* to determine feasibility and the potential to proceed to the next step towards development. For subsequent steps, *in vivo* experiments in mice are generally the gold standard, conducted to gain more impactful data and assess whether the approach could be taken further into clinical trials. It is only then when therapeutics are faced for the first time with the “reality” of human cancer, whereby many thoroughly pre-clinically tested approaches demonstrate little in patient efficacy and struggle to generate enough strong data to justify the continuation (Fernandez-Moure 2016). By this stage, considerable money has already been invested into one or multiple costly clinical trials. A recent publication estimated that approximately 40-50% of costs incur during pre-clinical research, whereas the other half of the costs are linked to clinical trials and clinical development (Simoens and Huys 2021).

One strategy to minimise the costly attrition rate of therapeutic candidates at the clinical trial stage is the early assessment of this therapeutic in clinically relevant models, including *ex vivo* primary tumour cell culture or slice models. Although these models often show high variability and need a large amount of optimisation, they ultimately represent the reality that therapeutics encounter within patients. Especially when working with tumour stroma and ECM, which are difficult to accurately replicate in mice and in *in vitro* conditions, it is important to make use of human *ex vivo* samples. Additionally, not all patient samples will react the same way to a treatment and some might not respond at all, which can lead to data with large confidence intervals and low statistical power, which are often not appreciated by editors and therefore potentially not published in high impact journals. However, these data are pivotal in representing a fraction of the real patient situation and therefore should be used as predictors for the potential success of the novel therapeutic in a clinical setting. Furthermore, attempts to try to quantify and account for the high variability seen in clinical samples have been done before, but a general effort to tackle this issue is needed in the future (Alic, Niessen, and Veenland 2014).

Suitable *ex vivo* models for testing of immunotherapies are difficult to source, mainly because slice models lack an intact immune system, which are crucial in testing cancer vaccines in order to assess efficacy and immune responses. In the case of effector-based approaches such as BiTEs or CAR T cells, however, the endogenous immune cells within the TME as found in tumour slices may be enough to predict if a patient would respond to a treatment, and therefore might also indicate how many patients could potentially respond to a given approach, provided the therapeutic reaches the tumour site in a sufficiently high concentration.

The three clinical systems used in this thesis can illustrate the different levels of clinical relevance. Firstly, T cells derived from ascites fluids (as used in Chapter 5.3.8) proved the concept that exhausted T cells can indeed be re-directed towards cancer cells, with the experimental set up consisting of a controlled number of T cells and cancer cell lines as target cells. Secondly, dissociated primary colorectal human tumours were used to demonstrate that TILs could be activated, without the possibility to control how many T cells are in the sample and without the addition of more T cells. Thirdly, the colorectal liver metastasis slices (as used in Chapters 4.3.5, 5.3.10 and 6.3.6) represent a nearly intact piece of human tumour, including all the constituent cell types and ECM. Therefore, if a response can be detected within tumour slices, this may be a strong indication towards a potential clinical success of the therapeutic. One limitation of the slice model used in this thesis is the lack of a viability control, in order to prove that the cells within the slices indeed stay alive for the duration of the experiment. This could, for example, be measured using an ATP assay.

Finally, it is important to stress that mouse experiments are still crucial for pre-clinical study assessment, including indications of the biodistribution of the therapeutic. However, they should not serve as the only gold-standard to decide whether a therapeutic should or should not go into clinical trials or warrant high impact publications, but rather be used in combination with more clinically relevant *ex vivo* models derived directly from patient samples. Of course they become even less relevant when the therapeutic being tested is human-specific, which is often the case with oncolytic viruses and also with many forms of immunotherapy.

7.4 Exploiting the ECM for a long-term anchoring of therapeutic

Approaches to therapeutically target the ECM have thus far been relatively scarce or conservative in their execution. Most approaches target tumour ECM specific components such as tenascin C (Deligne et al. 2020), EDB fibronectin (Hooper et al. 2022) or dysregulated enzymes modifying the ECM such as MMPs (Almutairi et al. 2023) or heparanases (Coombe and Gandhi 2019). The latter groups often induce harsh side effects, mainly because these enzymes still perform functions within the normal tissue and systemic administration might not be the optimal means of drug delivery (Sainio and Järveläinen 2020). Thus, existing therapeutic approaches to target the ECM had to be within a certain level of tolerable side effects, setting them up for a likely failure in clinical trials.

In order to allow for a more targeted agonistic approach, we have explored the possibility of delivering an ECM targeting bispecific using an oncolytic virus (EnAd). The OV delivery allows for tumour-selective and local expression of the bispecific, which could then subsequently bind to the available ECM in the TME. Therefore, we can directly target commonly occurring proteins and molecules in the ECM such as collagen I and glycosaminoglycans, as cancer selectivity is achieved by the OV itself. Additionally, cancer-selective expression in combination with the instant retention via the ECM-binding motif allows for the more radical approach of locally harnessing bystander killing using an anti-CD3 scFvs. Importantly, this strategy would never be feasible by conventional means of direct systemic delivery due to the high risk of non-specific T cell activation and subsequent induction of a cytokine storm.

Multiple studies have already explored the spread and the behaviour of OVs *in vivo*, indicating that once the virus reaches the tumour, it can potentially survive for several infection rounds (Bommareddy et al. 2017; Jogler et al. 2006; Jung et al. 2019). Therapeutic strategies using BiTEs are often limited by BiTE retention within the TME due to their small size (Warnders et al. 2016); meanwhile, the LAIR-2 and polyarginine/PlGF-2 bispecifics can directly bind to the ECM upon expression and therefore be retained in the TME for a potentially longer period of

time. The LAIR-2xaCD3 bispecific has been shown (**Figure 5.11**) to bind over a long period of time to collagen I without losing the ability to activate newly added T cells. This, coupled with potential multiple rounds of tumour cell infection by the OV, might lead to an extended and highly targeted therapy, minimising off-target effects and maximising therapeutic efficacy within the tumour.

Although the immobilisation by LAIR-2 on the ECM is very directed and the binding site is well studied, non-specific immobilisation to GAGs in TME (as explored in Chapter 4) is an alternative option. IFN-γ production was assessed in human-derived colorectal liver metastasis slices and showed promising results with aCD3x2PlGF/2 and aCD3x1PlGE-2 constructs. However, in order to fully understand the binding kinetics of the positively charged bispecifics in tumour slices, delivery with a virus is crucial in order to study diffusion and retention time within the TME. Additionally, due to the better studied LAIR-2 and mapped single binding site on collagen, this method provides more security for the further developments of the technique.

7.5 Harnessing bystander killing as novel approach

Thus far, immunotherapies directly harnessing T cells, such as BiTEs or CAR T cells, have focussed on the antigen-dependent cytotoxicity and, thus, the safety of exclusive cytotoxicity towards tumour cells and not normal cells. Bystander killing has often unintentionally also been a part of these therapies and potentially helped with their success (Ross et al. 2015). Harnessing and exploiting bystander killing only as a form of cancer treatment, however, is a novel approach which was validated in this thesis.

For robust BiTE-mediated T cell activation, it is essential to have sufficient clustering of CD3 on the cell surface, via interactions with the BiTE. Hence, it was important to show that there were enough binding sites on collagen I or GAGs to demonstrate that T cells can be sufficiently activated to mediate cytotoxicity (Chapters 4.3.4, 5.3.6, 5.3.10 and 6.3.6).

A further challenge to overcome in cancer therapy is the intra-tumoural and intra-patient heterogeneity, whereby it has previously been shown that tumours consist of many different cancer cells, which are genetically very heterogeneous (Proietto et al. 2023). Therefore, harnessing bystander killing will ensure that all cells, regardless of their antigenic status, will be killed locally, including potential cancer associated stromal cells such as fibroblasts. When working with BiTEs, one singular target antigen is often chosen, which not only limits the types of cancer cells which can be targeted within a tumour, but potentially also limits the types of tumours which can be treated. Additionally, most solid human tumours express ECM and could therefore be targeted, and thus this may provide an attractive pan-cancer therapeutic approach.

7.6 Future challenges

Although harnessing bystander killing could have great potential, several challenges persist and need to be addressed. Firstly, when working with a T cell agonist rather than more passive approaches, such as IC inhibitors, a highly cancer-specific delivery vector is required. Additionally, the agonist should be expressed under a tumour-specific or late viral promotor, in order to further increase safety of the therapy. Poor cancer selectivity could lead to severe side effects as previously seen in clinical trials involving agonists, including cytokine storms and excessive tissue damage (Suntharalingam et al. 2006). Hence, a mouse model or relevant clinical model, such as liver perfusions, might help to address this issue.

Secondly, it is important to check the *in vivo* distribution and kinetics of the LAIR-2xaCD3 and PlGF-2/polyarginine bispecifics. Tumour retention is an important feature of this approach and therefore needs careful examination in order to progress with this project. Leakage into normal tissues could result to similar problems as mentioned above. This could be checked with a mouse model and direct IT injections of a luciferase-tagged bispecific.

Thirdly, as this approach relies on the presence of tumour infiltrating lymphocytes (TILs), this therapeutic is limited by the abundance of T lymphocytes present in the TME. This limitation can already be seen to a certain extent in the colorectal liver metastases slices, where some tumour regions of a patient respond strongly, whereas others only respond poorly (**Figure 6.9**). This could potentially also have other causes, such as the presence of immunosuppressive cells. However, it is important to note that even the slices which responded poorly to the OV encoding LAIR-2xaCD3 bispecific still demonstrated a degree of response compared to the anti-CD3 only control. Additionally, each patient had at least one tested tumour region which responded well, which in turn may direct the activated T cells to migrate towards other tumour regions and exert cytotoxicity.

Lastly, it is not clear yet if this approach could be used in all tumours or only in tumours containing high levels of collagen I/GAGs. For example, thus far, LAIR-2 has been used in

glioblastoma, suggesting that even cancers with a potentially low collagen I can be targeted by this approach (Ramos et al. 2021). However, more testing on patient samples is required to determine what types of cancers could be suitable targets for this approach**.**

7.7 Future directions

Future validation requires the use of a mouse model to evaluate the kinetics and duration of local retention of the ECM-binders. This includes the delivery via EnAd in a xenograft, as well as the binding of the bispecifics in syngeneic models. Additionally, by using luciferase-tagged constructs, the retention time and local accumulation of the bispecifics can be assessed.

Secondly, not only collagens and/or GAGs should be considered as viable ECM anchoring proteins, but also fibronectin and other abundant proteins. The nature of these proteins might change how the immune system reacts to the anchored therapeutic and might change the set of tumours which can be targeted.

Thirdly, more clinical samples should be collected and added to the existing graphs in order to give a more comprehensive overview over the effect of the LAIR-2xaCD3 bispecific in a clinical setting. In line with this, a viability assay should be performed specifically on the tumour slice model (such as an ATP assay).

Fourthly, the bispecifics were so far driven by a CMV promoter in EnAd, however, for additional safety, the proteins should be under control of the splice acceptor (SA) promoter, which is only active once the virus is producing structural proteins late in the EnAd life cycle and therefore garners enhanced targeted expression due to the cancer-selective replication of the virus.

Lastly, this approach is not limited to anchoring of anti-CD3 motifs to the ECM. Therefore, other proteins such as enzymes, cytokines or agents used in imaging could be interesting proteins to be tethered on the ECM and should be explored in further research.

7.8 Concluding remarks

In conclusion, conventional cancer therapies generally target specific pathways in cancer cells to induce cytotoxicity, which can often lead to the establishment of resistant populations that re-populate the tumour, resulting in recurrence and relapse of cancer.

Therefore, the results in this thesis suggest that (1) bystander killing can be exploited and may provide a novel therapeutic approach to eliminate cancer and cancer-associated cells, (2) ECM-anchoring of anti-CD3 scFvs via LAIR-2 or PlGF-2/polyarginines induces potent bystander killing mediated by CD4 and CD8 T cells and that (3) the bispecifics can be encoded and delivered via the oncolytic virus EnAd.

Hence, it is crucial to further assess the feasibility of such an approach using *in vivo* models and to explore the possibility of combination therapies that could ultimately not only lead to the elimination of the tumour, but also ensure a long-lasting presence of the therapeutic within the tumour and thus prevent the relapse of the tumour.

Bibliography

Abdollahi, Amir, David W. Griggs, Heike Zieher, Alexandra Roth, Kenneth E. Lipson, Rainer Saffrich, Hermann-josef Gro, Dennis E. Hallahan, Ralph A. Reisfeld, Juergen Debus, Andreas G. Niethammer, and Peter E. Huber. 2005. “Cancer Therapy : Preclinical Inhibition of A v B 3 Integrin Survival Signaling Enhances Antiangiogenic and Antitumor Effects of Radiotherapy.” *CancerTherapy: Preclinical* 11(17):6270–79.

Acharya, D., C. Penghua Wang, b, D. Amber M. Paul, a Jianfeng Dai, b, E. David Gate, F. Jordan E. Lowery, a Dobrivoje S. Stokic, F. A. Arturo Leis, H. Richard A. Flavell, g, H. Terrence Town, e Erol Fikrig, b, and Fengwei Baia. 2017. “Interleukin-17A Promotes CD8ɲ T Cell Cytotoxicity To Facilitate West Nile Virus Clearance.” *Journal of Virology* 91(1):1–22.

Alic, Lejla, Wiro J. Niessen, and Jifke F. Veenland. 2014. “Quantification of Heterogeneity as a Biomarker in Tumor Imaging : A Systematic Review.” *PLoS ONE* 9(10):1–15.

Almutairi, Shriefa, Hanin Moh’d Kalloush, Nour A. Manoon, and Sanaa K. Bardaweel. 2023. “Matrix Metalloproteinases Inhibitors in Cancer Treatment: An Updated Review (2013–2023).” *Molecules*.

Altun, İnsaf and Alper Sonkaya. 2018. “Letter to the Editor The Most Common Side Effects Experienced by Patients Were Receiving First Cycle of Chemotherapy.” *Iran J Public Health* 47(8):1218–19.

Andrin, Christi, Michael J. Pinkoski, Kimberly Burns, Eric A. Atkinson, Olivier Krahenbuhl, Dorothy Hudig, Stephanie A. Fraser, Urlike Winkler, Michal Opas, R. Chris Bleackley, and Marek Michalak. 1998. “Interaction between a Ca 2 + -Binding Protein Calreticulin and Perforin , a Component of the Cytotoxic T-Cell Granules †.” *Biochemistry* 2960(98):10386–94.

Artym, Vira V, Stephen Swatkoski, Kazue Matsumoto, Catherine B. Campbell, Ryan J. Petrie, Emilios K. Dimitriadis, Xin Li, Susette C. Mueller, Thomas H. Bugge, Marjan Gucek, and Kenneth M. Yamada. 2015. “Dense Fibrillar Collagen Is a Potent Inducer of Invadopodia via a Specific Signaling Network.” *J. Cell Biol* 208(3):331–50.

Auvinen, Paivi, Raija Tammi, Jyrki Parkkinen, Markku Tammi, Ulla Ågren, Risto Johansson, Pasi Hirvikoski, and Matti Eskelinen. 2000. “Hyaluronan in Peritumoral Stroma and Malignant Cells Associates with Breast Cancer Spreading and Predicts Survival.” *American Journal of Pathology* 156(2):529–36.

Baker, A. M., D. Bird, G. Lang, T. R. Cox, and J. T. Erler. 2013. “Lysyl Oxidase Enzymatic Function Increases Stiffness to Drive Colorectal Cancer Progression through FAK.” *Oncogene* 32(14):1863–68.

Bálint, S. Müller, R. Fischer, B. M. Kessler, M. Harkiolaki, S. Valitutti, and M. L. Dustin. 2020. “Supramolecular Attack Particles Are Autonomous Killing Entities Released from Cytotoxic T Cells.” *Science* 368(6493):897–901.

Barry, Michele and R. Chris Bleackley. 2002. “Cytotoxic T Lymphocytes: All Roads Lead to Death.” *Nature Reviews Immunology* 2(June):1–9.

Baskar, Rajamanickam, Kuo Ann Lee, Richard Yeo, and Kheng-wei Yeoh. 2012. “Cancer and Radiation Therapy : Current Advances and Future Directions.” *Int. J. Med. Sci.*

Bates, Adam and Christine A. Power. 2019. “David vs . Goliath : The Structure, Function, and Clinical Prospects of Antibody Fragments.” *Antibodies*.

Beckenlehner, Karin, Silke Bannke, Thilo Spru, Giinther Bernhardt, Helmut SchOnenberger, and Wilfried Schiess. 1992. “Hyaluronidase Enhances the Activity of Adriamycin in Breast Cancer Models in Vitro and in Vivo.” *J Cancer Res Clin Onco*.

Bełdowski, Piotr, Adam Mazurkiewicz, Tomasz Topolinski, and Tomasz Małek. 2019. “Hydrogen and Water Bonding between Glycosaminoglycans and Phospholipids in the

Synovial Fluid : Molecular Dynamics Study.” *Materials*.

Benmebarek, Mohamed-reda, Clara Helke Karches, Bruno Loureiro Cadilha, Stefanie Lesch, Stefan Endres, and Sebastian Kobold. 2019. “Killing Mechanisms of Chimeric Antigen Receptor.” *Int Journal of Molec Sciences*.

Berardi, G. Spitaleri R. and C. Pierantoni T. De Pas. 2013. “Phase I / II Study of the Tumour-Targeting Human Monoclonal Antibody – Cytokine Fusion Protein L19-TNF in Patients with Advanced Solid Tumours.” *J Cancer Res Clin Oncol.* 447–55.

Bergers, Gabriele, Rolf Brekken, Gerald Mcmahon, Thiennu H. Vu, Takeshi Itoh, Kazuhiko Tamaki, Kazuhiko Tanzawa, Philip Thorpe, Shigeyoshi Itohara, and Douglas Hanahan. 2000. “Matrix Metalloproteinase-9 Triggers the Angiogenic Switch during Carcinogenesis.” *Nat Cell Biol* 2(10):737–44.

Bertrand, Florie, Sabina Müller, Kyung Ho Roh, Camille Laurent, Loïc Dupré, and Salvatore Valitutti. 2013. “An Initial and Rapid Step of Lytic Granule Secretion Precedes Microtubule Organizing Center Polarization at the Cytotoxic T Lymphocyte/Target Cell Synapse.” *Proceedings of the National Academy of Sciences of the United States of America* 110(15):6073–78.

Bhat, Purnima, Graham Leggatt, Nigel Waterhouse, and Ian H. Frazer. 2017. “Interferon-γ Derived from Cytotoxic Lymphocytes Directly Enhances Their Motility and Cytotoxicity.” *Cell Death and Disease* 8(6):1–11.

Bladergroen, Bellinda A., Chris J. L. M. Meijer, Rosita L. Ten Berge, C. Erik Hack, Jettie J. F. Muris, Danny F. Dukers, Andreas Chott, Yoshiaki Kazama, Joost J. Oudejans, Oskar Van Berkum, and J. Alain Kummer. 2002. “Expression of the Granzyme B Inhibitor, Protease Inhibitor 9, by Tumor Cells in Patients with Non-Hodgkin and Hodgkin Lymphoma: A Novel Protective Mechanism for Tumor Cells to Circumvent the Immune System?” *Blood* 99(1):232–37.

Blott, Emma J., Giovanna Bossi, Richard Clark, Marketa Zvelebil, and Gillian M. Griffiths.

2001. “Fas Ligand Is Targeted to Secretory Lysosomes via a Proline-Rich Domain in Its Cytoplasmic Tail.” *Journal of Cell Science*.

Boagni, Drew Ashton, Divya Ravirala, and Shaun Xiaoliu Zhang. 2021. “Current Strategies in Engaging Oncolytic Viruses with Antitumor Immunity.” *Molecular Therapy - Oncolytics* 22(September):98–113.

Bochet, Ludivine, Camille Lehuede, Stephanie Dauvillie, Yuan Yuan Wang, Beatrice Dirat, Victor Laurent, Cedric Dray, Romain Guiet, Isabelle Maridonneau-Parini, Sophie Le Gonidec, Bettina Couderc, Ghislaine Escourrou, Philippe Valet, and Catherine Muller. 2013. “Adipocyte-Derived Fibroblasts Promote Tumor Progression and Contribute to the Desmoplastic Reaction in Breast Cancer.” (17):5657–68.

Boehm, Heike. 2017. “A Trickster in Disguise : Hyaluronan ’ s Ambivalent Roles in the Matrix.” 7(October).

Bohana-Kashtan, Osnat, Sebastien Morisot, Richard Hildreth, Cory Brayton, I. Hyam, and Curt I. Civin. 2011. “Selective Reduction of Graft-versus-Host Disease-Mediating Human T Cells by Ex Vivo Treatment with Soluble Fas Ligand.” *J Immunol.* 183(1):696–705.

Boivin, Wendy Anne, Dawn Michelle Cooper, Paul Ryan Hiebert, and David James Granville. 2009. “PATHOBIOLOGY IN FOCUS Intracellular versus Extracellular Granzyme B in Immunity and Disease : Challenging the Dogma.” *Laboratory Investigation* 89(November):1195–1220.

Bommareddy, Praveen K., Anand Patel, Saamia Hossain, and Howard L. Kaufman. 2017. “Talimogene Laherparepvec (T-VEC) and Other Oncolytic Viruses for the Treatment of Melanoma.” *American Journal of Clinical Dermatology* 18(1):1–15.

Bossard, Céline, Karim Belhadj, Felix Reyes, Nadine Martin-Garcia, Françoise Berger, Jean Alain Kummer, Josette Brière, Anne Catherine Baglin, Stéphane Cheze, Jacques Bosq, Vincent Ribrag, Christian Gisselbrecht, Nicolas Mounier, and Philippe Gaulard. 2007.

"Expression of the Granzyme B Inhibitor PI9 Predicts Outcome in Nasal NK/T-Cell Lymphoma: Results of a Western Series of 48 Patients Treated with First-Line Polychemotherapy within the Groupe d'Etude Des Lymphomes de l'Adulte (GELA) Trials." *Blood* 109(5):2183–89.

Branton, Philip E. and Diana E. Roopchand. 2001. "The Role of Adenovirus E4orf4 Protein in Viral Replication and Cell Killing." *Oncogene*.

Brett, Elizabeth A., Matthias A. Sauter, Hans-günther Machens, and Dominik Duscher. 2020. "Tumor-Associated Collagen Signatures : Pushing Tumor Boundaries." *Cancer & Metabolism* 1–5.

Broder, Claudia, Philipp Arnold, Sandrine Vadon-le Goff, Moritz A. Konerding, Kerstin Bahr, Stefan Müller, Catherine Moali, and Christoph Becker-pauly. 2013. "Metalloproteases Meprin α and Meprin β Are C- and N-Procollagen Proteinases Important for Collagen Assembly and Tensile Strength." *PNAS* (35).

Brooks, Michael, Qianxing Mo, Ross Krasnow, Philip Levy Ho, Jing Xiao, Antonina Kurtova, Seth Lerner, Gui Godoy, Weiguo Jian, Patricia Castro, Fengju Chen, David Rowley, Michael Ittmann, and Keith Syson. 2016. "Positive Association of Collagen Type I with Non-Muscle Invasive Bladder Cancer Progression." 7(50):82609–19.

Burnet, Macfarlane. 1957. "CANCER-A BIOLOGICAL APPROACH." *British Medical Journal*.

Buscemi, Lara, David Ramonet, Franco Klingberg, Aurélie Formey, Josiane Smith-Clerc, Jean Jacques Meister, and Boris Hinz. 2011. "The Single-Molecule Mechanics of the Latent TGF-B1 Complex." *Current Biology* 21(24):2046–54.

Buzza, Marguerite S., Claire E. Hirst, Catherina H. Bird, Patrick Hosking, Joseph McKendrick, and Phillip I. Bird. 2001. "The Granzyme B Inhibitor, PI-9, Is Present in Endothelial and Mesothelial Cells, Suggesting That It Protects Bystander Cells during Immune Responses." *Cellular Immunology* 210(1):21–29.

Cancer Research UK (CRUK). 2023. “Cancer Statistics for the UK.” *Retrieved on 12.08.2023*. Retrieved (https://www.cancerresearchuk.org/health-professional/cancer-statistics-for-the-uk).

Canty, Elizabeth G. and Karl E. Kadler. 2005. “Procollagen Trafficking, Processing and Fibrillogenesis.” *Journal of Cell Science*.

Cao, Qizhi, Aili Fu, Shude Yang, Xiaoli He, Yue Wang, Xiaoshu Zhang, Jiadi Zhou, Xiying Luan, Wenzheng Yu, and Jiangnan Xue. 2015. “Biochemical and Biophysical Research Communications Leukocyte-Associated Immunoglobulin-like Receptor-1 Expressed in Epithelial Ovarian Cancer Cells and Involved in Cell Proliferation and Invasion.” *Biochemical and Biophysical Research Communications* 458(2):399–404.

Cappellesso, Rocco, Renato Millioni, Giorgio Arrigoni, and Francesca Simonato. 2015. “Lumican Is Overexpressed in Lung Adenocarcinoma Pleural Effusions.” *PLoS ONE* 1–13.

Carew, John F., David A. Kooby, Marc W. Halterman, Se-heon Kim, Howard J. Federoff, and Yuman Fong. 2001. “A Novel Approach to Cancer Therapy Using an Oncolytic Herpes Virus to Package Amplicons Containing Cytokine Genes.” *Molecular Therapy* 4(3):250–56.

Carnemolla, Barbara, Enrica Baiza, Annalisa Siri, Lucia. n. Zardi, Mafia Rita Nicotra, Aldo Bigotti, and Pier Giorgio Natali. 1989. “A Tumor-Associated Fibronectin Isoform Generated by Alternative Splicing of Messenger RNA Precursors.” *The Journal of Cell Biology* 108(March).

Castellani, P., G. Viale, A. Dorcaratto, G. Nicolo, J. Kaczmarek, G. Querze, and L. Zardi. 1994. “The Fibronectin Isoform Containing the ED-B Oncofetal Domain: A Marker of Angiogenesis.” *Int J Cancer* 1;59(5):61.

Charman, Matthew, Christin Herrmann, and Matthew D. Weitzman. 2020. “Viral and Cellular Interactions During Adenovirus DNA Replication.” *FEBS Lett* 593(24):3531–50.

Chaudhry, Gul-e-saba, Abdah Akim, Muhammad Naveed Zafar, Naila Safdar, and Yeong Yik Sung. 2021. “Understanding Hyaluronan Receptor (CD44) Interaction , HA-CD44 Activated Potential Targets in Cancer Therapeutics.” *Tabriz University of Medical Sciences* 11(3):426–38.

Chen, Daniel S. and Ira Mellman. 2013. “Oncology Meets Immunology: The Cancer-Immunity Cycle.” *Immunity* 39(1):1–10.

Chen, Robert, Pier Luigi Zinzani, Hun Ju Lee, Philippe Armand, Nathalie A. Johnson, Pauline Brice, John Radford, Vincent Ribrag, Daniel Molin, Theodoros P. Vassilakopoulos, Akihiro Tomita, Bastian Von Tresckow, Margaret A. Shipp, Jianxin Lin, and Eunhee Kim. 2019. “Pembrolizumab in Relapsed or Refractory Hodgkin Lymphoma : 2-Year Follow-up of KEYNOTE-087.” *Blood* 134(14):1144–53.

Chen, Xiaoyang Ye, Elise Pitmon, Mengqian Lu, Jun Wan, Evan R. Jellison, Adam J. Adler, Anthony T. Vella, and Kepeng Wang. 2019. “IL-17 Inhibits CXCL9 / 10-Mediated Recruitment of CD8 + Cytotoxic T Cells and Regulatory T Cells to Colorectal Tumors.” 1–13.

Chen, Yuying, Zhanxiang Wang, Pingan Chang, Liuxin Xiang, Feng Pan, Jianjun Li, and Jinyan Jiang. 2010. “The Effect of Focal Adhesion Kinase Gene Silencing on 5-Fluorouracil Chemosensitivity Involves an Akt / NF- j B Signaling Pathway in Colorectal Carcinomas.” *Int J Cancer*.

Chen, Zhengshan, Seyedmehdi Shojaee, Maike Buchner, Huimin Geng, Jae Woong, Elisabeth Paietta, Stephen P. Hunger, Cheryl L. Willman, and Ari Melnick. 2015. “Signaling Thresholds and Negative B Cell Selection in Acute Lymphoblastic Leukemia.” *Nature* 521(7552):357–61.

Cheng, Jianhua, Tong Zhou, Changdan Liu, John P. Shapiro, Matthew J. Brauer, Michael C. Kiefer, Philip J. Barr, and John D. Mountz. 1994. “Protection from Fas-Mediated Apoptosis by a Soluble Form of the Fas Molecule.” *Science* 263(March):6–10.

Classen, C. F., P. I. Bird, and K. M. Debatin. 2006. “Modulation of the Granzyme B Inhibitor Proteinase Inhibitor 9 (PI- 9) by Activation of Lymphocytes and Monocytes in Vitro and by Epstein – Barr Virus and Bacterial Infection.” *Clinical and Experimental Immunology* 9:534–42.

Colak, Selcuk and Peter ten Dijke. 2017. “Targeting TGF-β Signaling in Cancer.” *Trends in Cancer* 3(1):56–71.

Conklin, Matthew W., Jens C. Eickhoff, Kristin M. Riching, Carolyn A. Pehlke, Kevin W. Eliceiri, Paolo P. Provenzano, Andreas Friedl, and Patricia J. Keely. 2011. “Aligned Collagen Is a Prognostic Signature for Survival in Human Breast Carcinoma.” *The American Journal OfPathology* 178(3):1221–32.

Coombe, Deirdre R. and Neha S. Gandhi. 2019. “Heparanase : A Challenging Cancer Drug Target.” *Frontiers in Oncology* 9(November).

Cordes, N. and C. Beinke. 2004. “Fibronectin Alters Cell Survival and Intracellular Signaling of Confluent A549 Cultures After Irradiation.” *Cancer Biology & Therapy* (February).

Corthay, Alexandre, Dag K. Skovseth, Katrin U. Lundin, Egil Røsjø, Hilde Omholt, Peter O. Hofgaard, Guttorm Haraldsen, and Bjarne Bogen. 2005. “Primary Antitumor Immune Response Mediated by CD4+ T Cells.” *Immunity* 22(3):371–83.

Cowman, Mary K., Hong-gee Lee, Kathryn L. Schwertfeger, and James B. Mccarthy. 2015. “The Content and Size of Hyaluronan In.” 6(June):1–8.

Cunningham, Thomas D., Xinguo Jiang, and David J. Shapiro. 2007. “Expression of High Levels of Human Proteinase Inhibitor 9 Blocks Both Perforin/Granzyme and Fas/Fas Ligand-Mediated Cytotoxicity.” *Cell Immunol.* 245(1):32–41.

D’Ambrosio, B. Y. E., N. D. E. L. Grosso, A. Chicca, M. Midulla, and Viale Regina Elena. 1982. “Neutralizing Antibodies against 33 Human Adenoviruses in Normal Children in Rome.” *J Hyg Camb*.

Dakhel, Sheila, Tiziano Ongaro, Baptiste Gouyou, Mattia Matasci, Dario Neri, and Samuele Cazzamalli. 2019. “Targeted Enhancement of the Therapeutic Window of L19-TNF by Transient and Selective Inhibition of RIPK1-Signaling Cascade.” *Oncotarget* 10(62):6678–90.

Davenport, Alexander J., Misty R. Jenkins, Ryan S. Cross, Carmen S. Yong, H. Miles Prince, David S. Ritchie, Joseph A. Trapani, Michael H. Kershaw, Phillip K. Darcy, and Paul J. Neeson. 2018. “CAR-T Cells In Fl Ict Sequential Killing of Multiple Tumor Target Cells.” *Cancer Immunology Research* 483–94.

Decaprio, James A. 2009. “How the Rb Tumor Suppressor Structure and Function Was Revealed by the Study of Adenovirus and SV40.” *Virology* 384(2):274–84.

Deligne, Claire, Devadarssen Murdamoothoo, Anis N. Gammage, Martha Gschwandtner, William Erne, Thomas Loustau, Anna M. Marzeda, Raphael Carapito, Nicodème Paul, Inés Velazquez-quesada, Imogen Mazzier, Zhen Sun, Gertraud Orend, and S. Kim. 2020. “Matrix-Targeting Immunotherapy Controls Tumor Growth and Spread by Switching Macrophage Phenotype.” *Cancer Immunol Res.* 8(3):368–82.

Dewhirst, Mark W., Timothy W. Secomb, and North Carolina. 2019. “Transport of Drugs from Blood Vessels to Tumour Tissue.” *Nat Rev Cancer* 17(12):738–50.

Dirkx, Anita, Mirjam Oude Egbrink, Marijke J. E. Kuijpers, Sandra T. van der Niet, Viviane V. T. Heijnen, Jessica C. A. Bouma-ter Steege, John Wagstaff, and Arjan W. Griffioen. 2003. “Tumor Angiogenesis Modulates Leukocyte-Vessel Wall Interactions in Vivo by Reducing Endothelial Adhesion Molecule Expression.” *Cancer Res* 63(9):2322–29.

Du, T., G. Shi, Y. M. Li, J. F. Zhang, H. W. Tian, Y. Q. Wei, H. Deng, and D. C. Yu. 2014. “Tumor-Specific Oncolytic Adenoviruses Expressing Granulocyte Macrophage Colony-Stimulating Factor or Anti-CTLA4 Antibody for the Treatment of Cancers.” *Cancer Gene Therapy* (1):340–48.

Dunn, Gavin P., Allen T. Bruce, Hiroaki Ikeda, Lloyd J. Old, and Robert D. Schreiber. 2002.

"Cancer Immunoediting : From Immuno- Surveillance to Tumor Escape." *Nature Immunology* 3(11):991–98.

Dunn, Gavin P., Lloyd J. Old, Robert D. Schreiber, St Louis, F. Macfarlane Burnet, and Lewis Thomas. 2004. "The Immunobiology of Cancer Immunosurveillance and Immunoediting." *Immunity* 21:137–48.

Dustin, Michael L. and Antonin R. De Fougerolles. 2001. "Reprograming T Cells: The Role of Extracellular Matrix in Coordination of T Cell Activation and Migration." *Current Opinion in Immunology* 13(3):286–90.

Dustin, Michael L. and Eric O. Long. 2011. "Cytotoxic Immunological Synapses." *Immunol Rev.* 235(1):24–34.

Dvorak, Harold F. 1986. "Tumors: Wounds That Do Not Heal." *The New England Journal of Medicine* 315:1650-1.

Dyer, Arthur, Benjamin Schoeps, Sally Frost, Philip Jakeman, Eleanor M. Scott, Joshua Freedman, Egon J. Jacobus, and Leonard W. Seymour. 2019. "Antagonism of Glycolysis and Reductive Carboxylation of Glutamine Potentiates Activity of Oncolytic Adenoviruses in Cancer Cells." *Cancer Research* 79(2):331–45.

Ebbinghaus, Christina, Roberto Ronca, Manuela Kaspar, Dragan Grabulovski, Alexander Berndt, Hartwig Kosmehl, Luciano Zardi, and Dario Neri. 2005. "Engineered Vascular-Targeting Antibody-Interferon- c Fusion Protein for Cancer Therapy." *Int. J. Cancer*.

Eke, Iris, Katja Storch, Mechthild Krause, and Nils Cordes. 2013. "Cetuximab Attenuates Its Cytotoxic and Radiosensitizing Potential by Inducing Fibronectin Biosynthesis." *Cancer Research* 5869–79.

Erdogan, Begum, Mingfang Ao, Lauren M. White, Anna L. Means, Bryson M. Brewer, Lijie Yang, M. Kay Washington, Chanjuan Shi, Omar E. Franco, Alissa M. Weaver, Simon W. Hayward, Deyu Li, and Donna J. Webb. 2017. "Cancer-Associated Fibroblasts

Promote Directional Cancer Cell Migration by Aligning Fibronectin." *J. Cell Biol.* 216(11):3799–3816.

Fajardo, Carlos Alberto, Sonia Guedan, Luis Alfonso Rojas, Rafael Moreno, Marcel Arias-badia, Jana De Sostoa, Carl H. June, and Ramon Alemany. 2017. "Oncolytic Adenoviral Delivery of an EGFR-Targeting T-Cell Engager Improves Antitumor Efficacy." *Therapeutics, Targets, and Chemical Biology Oncolytic* 77(15):2052–63.

Fazle Akbar, S. M., K. Inaba, and M. Onji. 1996. "Upregulation of MHC Class II Antigen on Dendritic Cells from Hepatitis B Virus Transgenic Mice by Interferon-γ: Abrogation of Immune Response Defect to a T-Cell-Dependent Antigen." *Immunology* 87(4):519–27.

Fernandez-Moure, Joseph S. 2016. "Lost in Translation : The Gap in Scientific Advancements and Clinical Application." *Frontiers in Bioenginering and Biotechnology* 4(June):1–6.

Ferrucci, Pier Francesco, Laura Pala, Fabio Conforti, and Emilia Cocorocchio. 2021. "Talimogene Laherparepvec (T-vec): An Intralesional Cancer Immunotherapy for Advanced Melanoma." *Cancers* 13(6):1–14.

Fessler, Michael, Michael B. Rudel, Lawrence L., and Brown Mark. 2014. "TGFβ in T Cell Biology and Tumor Immunity: Angel or Devil? Eric." *Bone* 23(1):1–7.

Ford, Kirsty, Christopher J. Hanley, Massimiliano Mellone, Cedric Szyndralewiez, Freddy Heitz, Philippe Wiesel, Oliver Wood, Maria Machado, Maria-antoinette Lopez, Anusha-preethi Ganesan, Chuan Wang, Ankur Chakravarthy, Tim R. Fenton, V. Emma, Pandurangan Vijayanand, Christian H. Ottensmeier, Aymen Al-shamkhani, Natalia Savelyeva, and Gareth J. Thomas. 2021. "Europe PMC Funders Group NOX4 Inhibition Potentiates Immunotherapy by Overcoming Cancer-Associated Fibroblast-Mediated CD8 T-Cell Exclusion from Tumors." *Cancer Res.* 80(9):1846–60.

Franquiz, Miguel J. and Nicholas J. Short. 2020. "Blinatumomab for the Treatment of Adult B-Cell Acute Lymphoblastic Leukemia : Toward a New Era of Targeted

Immunotherapy.” *Biologics: Targets and Therapy* 23–34.

Freedman, Joshua D., Margaret R. Duffy, Janet Lei-Rossmann, Alice Muntzer, Eleanor M. Scott, Joachim Hagel, Leticia Campo, Richard J. Bryant, Clare Verrill, Adam Lambert, Paul Miller, Brian R. Champion, Leonard W. Seymour, and Kerry D. Fisher. 2018. “An Oncolytic Virus Expressing a T-Cell Engager Simultaneously Targets Cancer and Immunosuppressive Stromal Cells.” *Cancer Research* 78(24):6852–65.

Freedman, Joshua D., Joachim Hagel, Eleanor M. Scott, Ioannis Psallidas, Avinash Gupta, Laura Spiers, Paul Miller, Nikolaos Kanellakis, Rebecca Ashfield, Kerry D. Fisher, Margaret R. Duffy, and Leonard W. Seymour. 2017. “Oncolytic Adenovirus Expressing Bispecific Antibody Targets T-cell Cytotoxicity in Cancer Biopsies.” *EMBO Molecular Medicine*.

Frisch, Steven M. and Joe S. Mymryk. 2002. “Adenovirus-5 E1A: Paradox and Paradigm.” *Nature Reviews Molecular Cell Biology* 3(June).

Galon, Jérôme. 2019. “Approaches to Treat Immune Hot , Altered and Cold Tumours with Combination Immunotherapies.” *Nature Reviews Drug Discovery* 18(March):10–13.

Ganusov, Vitaly V. and Rob J. De Boer. 2008. “Estimating In Vivo Death Rates of Targets Due to CD8 T-Cell-Mediated Killing.” *Journal of Virology* 82(23):11749–57.

García-suárez, Olivia, Beatriz García, Iván Fernández-vega, Aurora Astudillo, and Luis M. Quirós. 2014. “Neuroendocrine Tumors Show Altered Expression of Chondroitin Sulfate , Glypican 1 , Glypican 5 , and Syndecan 2 Depending on Their Differentiation Grade.” *Frontiers in Oncology* 4(February):1–16.

Garrido, Greta, Ailem Rabasa, Cristina Garrido, Lisset Chao, Federico Garrido, ángel M. García-Lora, and Belinda Sánchez-Ramírez. 2017. “Upregulation of HLA Class I Expression on Tumor Cells by the Anti-EGFR Antibody Nimotuzumab.” *Frontiers in Pharmacology* 8(OCT):1–11.

Garrison, Carly M., Jean E. Schwarzbauer, and Valerie Marie Weaver. 2021. “Fibronectin Fibril Alignment Is Established upon Initiation of Extracellular Matrix Assembly.” *MBoC* 32:739–52.

Gehrcke, Jan Philip and M. Teresa Pisabarro. 2015. “Identification and Characterization of a Glycosaminoglycan Binding Site on Interleukin-10 via Molecular Simulation Methods.” *Journal of Molecular Graphics and Modelling* 62:97–104.

Ghatak, Shibnath, Edward V Maytin, Judith A. Mack, Vincent C. Hascall, Ilia Atanelishvili, Ricardo Moreno Rodriguez, Roger R. Markwald, and Suniti Misra. 2015. “Roles of Proteoglycans and Glycosaminoglycans in Wound Healing and Fibrosis.” *International Journal of Cell Biology* 2015.

Ghosh, Sue, Lina Albitar, Richard Lebaron, William R. Welch, Goli Samimi, J. Michael, Ross S. Berkowitz, and Samuel C. Mok. 2011. “Up-Regulation of Stromal Versican Expression in Advanced Stage Serous Ovarian Cancer.” *Gynecol Oncol.* 119(1):114–20.

Glabman, Raisa A., Peter L. Choyke, and Noriko Sato. 2022. “Cancer-Associated Fibroblasts: Tumorigenicity and Targeting for Cancer Therapy.” *Cancers* 14(16):1–21.

Gong, Jun, Alexander Chehrazi-raffle, Srikanth Reddi, and Ravi Salgia. 2018. “Development of PD-1 and PD-L1 Inhibitors as a Form of Cancer Immunotherapy : A Comprehensive Review of Registration Trials and Future Considerations.” *Journal for ImmunoTherapy of Cancer* 1–18.

Graaf, J. F. De, L. De Vor, R. A. M. Fouchier, and B. G. Van Den Hoogen. 2020. “Armed Oncolytic Viruses: A Kick-Start for Anti-Tumor Immunity.” *Cytokine and Growth Factor Reviews* (January).

Greber, UF, Melanie Willetts, Paul Webster, and Ari Helenius. 1993. “Stepwise Dismantling of Adenovirus 2 Durhg Entry into Cell.” *Cell* 75:477–86.

Grindel, B. J., J. R. Martinez, C. L. Pennington, M. Muldoon, J. Stave, L. W. Chung, and M. C. Farach-Carson. 2014. “Matrilysin/Matrix Metalloproteinase-7(MMP7) Cleavage of Perlecan/HSPG2 Creates A Molecular Switch to Alter Prostate Cancer Cell Behavior.” *Matrix Biol* (713):64–76.

Gruen, Michael, Æ. Kurt Bommert, Æ. Ralf C. Bargou, and Immunotherapy Æ. Perforin Æ. T. 2004. “T-Cell-Mediated Lysis of B Cells Induced by a CD19xCD3 Bispecific Single-Chain Antibody Is Perforin Dependent and Death Receptor Independent.” *Cancer Immunol Immunother.* 625–32.

Guedan, Sonia, Juan José Rojas, Alena Gros, Elena Mercade, Manel Cascallo, and Ramon Alemany. 2009. “Hyaluronidase Expression by an Oncolytic Adenovirus Enhances Its Intratumoral Spread and Suppresses Tumor Growth.” *Molecular Therapy* 18(7):1275–83.

Gunzer, Matthias, Angelika Schäfer, Stefan Borgmann, Stephan Grabbe, Kurt S. Zänker, Eva Bettina Bröcker, Eckhart Kämpgen, and Peter Friedl. 2000. “Antigen Presentation in Extracellular Matrix: Interactions of T Cells with Dendritic Cells Are Dynamic, Short Lived, and Sequential.” *Immunity* 13(3):323–32.

Guo, Na, Kui Zhang, Xingchun Gao, Minghua Lv, Jing Luan, Zhifang Hu, Ailian Li, and Xingchun Gou. 2020. “ScienceDirect Role and Mechanism of LAIR-1 in the Development of Autoimmune Diseases , Tumors , and Malaria : A Review.” *Current Research in Translational Medicine* 68(3):119–24.

Hakim, Nausheen, Rajvi Patel, Craig Devoe, and Muhammad W. Saif. 2020. “Why HALO 301 Failed and Implications for Treatment of Pancreatic Cancer.” *Pancreas* 3(1):1–7.

Halle, Stephan, Kirsten Anja Keyser, Felix Rolf Stahl, Andreas Busche, Anja Marquardt, Xiang Zheng, Melanie Galla, Vigo Heissmeyer, Katrin Heller, Jasmin Boelter, Karen Wagner, Yvonne Bischoff, Rieke Martens, Asolina Braun, Kathrin Werth, Alexey Uvarovskii, Harald Kempf, Michael Meyer-Hermann, Ramon Arens, Melanie Kremer,

Gerd Sutter, Martin Messerle, and Reinhold Förster. 2016. “In Vivo Killing Capacity of Cytotoxic T Cells Is Limited and Involves Dynamic Interactions and T Cell Cooperativity.” *Immunity* 44(2):233–45.

Hammond, Edward, Nicole M. Haynes, Carleen Cullinane, Todd V Brennan, Darryn Bampton, Paul Handley, Tomislav Karoli, Fleur Lanksheer, Liwen Lin, Yiping Yang, and Keith Dredge. 2018. “Immunomodulatory Activities of Pixatimod : Emerging Nonclinical and Clinical Data , and Its Potential Utility in Combination with PD- 1 Inhibitors.” *Journal for ImmunoTherapy of Cancer* 1–13.

Han, Zheng and Zheng-Rong Lu. 2016. “Targeting Fibronectin for Cancer Imaging and Therapy.” *J Mater Chem B Mater Biol Med.* 25(3):289–313.

Hanahan, D. and R. A. Weinberg. 2011. “Hallmarks of Cancer: The Next Generation.” *Cell* 144:646–74.

Hanahan, Douglas and Robert A. Weinberg. 2000. “The Hallmarks of Cancer.” *Cell* 100:57–70.

Hanley, Christopher J. and Gareth J. Thomas. 2021. “Targeting Cancer Associated Fibroblasts to Enhance Immunotherapy : Emerging Strategies and Future Perspectives.” *Oncotarget* 12(14):1427–33.

Hastings, Jordan F., Joanna N. Skhinas, Dirk Fey, David R. Croucher, and Thomas R. Cox. 2019. “The Extracellular Matrix as a Key Regulator of Intracellular Signalling Networks.” *British Journal of Pharmacology*.

Havunen, Riikka, João M. Santos, Suvi Sorsa, Tommi Rantapero, Dave Lumen, Mikko Siurala, Anu J. Airaksinen, Victor Cervera-carrascon, Siri Tähtinen, Anna Kanerva, and Akseli Hemminki. 2018. “Abscopal Effect in Non-Injected Tumors Achieved with Cytokine-Armed Oncolytic Adenovirus.” *Molecular Therapy: Oncolytics* 11(December):109–21.

Hazini, Ahmet, Kerry Fisher, and Len Seymour. 2021. “Deregulation of HLA- - I in Cancer and Its Central Importance for Immunotherapy.” *Journal for ImmunoTherapy of Cancer* 1–17.

He, Chao-bin and Xiao-jun Lin. 2017. “Inflammation Scores Predict the Survival of Patients with Hepatocellular Carcinoma Who Were Treated with Transarterial Chemoembolization and Recombinant Human Type-5 Adenovirus H101.” *PLoS ONE* 1–16.

He, Yingying, Tao Liu, Shuang Dai, Zihan Xu, Li Wang, and Feng Luo. 2021. “Tumor-Associated Extracellular Matrix : How to Be a Potential Aide to Anti-Tumor Immunotherapy ?” *Frontiers in Cell and Developmental Biology* 9(October):1–15.

Hebert, Jess D., Samuel A. Myers, Alexandra Naba, Genevieve Abbruzzese, John M. Lamar, Steven A. Carr, and Richard O. Hynes. 2020. “Proteomic Profiling of the ECM of Xenograft Breast Cancer Metastases in Different Organs Reveals Distinct Metastatic Niches.” *CANCER RESEARCH* 1475–85.

Henke, Erik, Rajender Nandigama, and Süleyman Ergün. 2020. “Extracellular Matrix in the Tumor Microenvironment and Its Impact on Cancer Therapy.” *Frontiers in Molecular Biosciences* 6(January):1–24.

Hirst, Claire E., Marguerite S. Buzza, Catherina H. Bird, Hilary S. Warren, Paul U. Cameron, Manling Zhang, Philip G. Ashton-Rickardt, and Phillip I. Bird. 2003. “The Intracellular Granzyme B Inhibitor, Proteinase Inhibitor 9, Is Up-Regulated During Accessory Cell Maturation and Effector Cell Degranulation, and Its Overexpression Enhances CTL Potency.” *The Journal of Immunology* 170(2):805–15.

Hirst, Claire E., Marguerite S. Buzza, Vivien R. Sutton, Joseph A. Trapani, Kate L. Loveland, and Phillip I. Bird. 2001. “Perforin-Independent Expression of Granzyme B and Proteinase Inhibitor 9 in Human Testis and Placenta Suggests a Role for Granzyme B-Mediated Proteolysis in Reproduction.” *Molecular Human Reproduction* 7(12):1133–42.

Holthaus, Lisa, Daniel Lamp, Anita Gavrisan, Virag Sharma, and Anette-gabriele Ziegler. 2018. “CD4 + T Cell Activation , Function , and Metabolism Are Inhibited by Low Concentrations of DMSO.” *Journal of Immunological Methods* 463(June):54–60.

Hongu, Tsunaki, Maren Pein, Jacob Insua-rodríguez, Ewgenija Gutjahr, Greta Mattavelli, Jasmin Meier, Kristin Decker, Arnaud Descot, Matthias Bozza, Richard Harbottle, Andreas Trumpp, Hans-peter Sinn, Angela Riedel, and Thordur Oskarsson. 2022. “Activation of Macrophages and Endothelial Cells the Lungs.” 3(April).

Hooper, Andrea T., Kimberly Marquette, Chao-pei Betty Chang, Jonathon Golas, Sadhana Jain, My-hanh Lam, Magali Guffroy, Mauricio Leal, Hadi Falahatpisheh, Divya Mathur, Ting Chen, Kerry Kelleher, Kiran Khandke, Elwira Muszynska, Frank Loganzo, Edward Rosfjord, Judy Lucas, Zhengyan Kan, Chakrapani Subramanyam, Christopher O. Donnell, Dario Neri, Hans-peter Gerber, Chad May, and Puja Sapra. 2022. “Anti-Extra Domain B Splice Variant of Fibronectin Antibody – Drug Conjugate Eliminates Tumors with Enhanced Ef Fi Cacy When Combined with Checkpoint Blockade.” *Molecular Cancer Therapeutics* 1462–72.

Hörner, Maximilian, Katrin Raute, Barbara Hummel, Josef Madl, Guido Creusen, Oliver S. Thomas, Erik H. Christen, Natascha Hotz, Raphael J. Gübeli, Raphael Engesser, Balder Rebmann, Jasmin Lauer, Bernd Rolauffs, Jens Timmer, Wolfgang W. A. Schamel, Jan Pruszak, Winfried Römer, Matias D. Zurbriggen, Christian Friedrich, Andreas Walther, Susana Minguet, Ritwick Sawarkar, and Wilfried Weber. 2019. “Phytochrome-Based Extracellular Matrix with Reversibly Tunable Mechanical Properties.” *Advanced Materials* 31(12):1–11.

Hou, Lingjie, Tie Lin, Yicun Wang, Bao Liu, and Meng Wang. 2021. “Collagen Type 1 Alpha 1 Chain Is a Novel Predictive Biomarker of Poor Progression-Free Survival and Chemoresistance in Metastatic Lung Cancer.” *Journal of Cancer* 12.

Hussell, Tracy, Sylvia Lui, Christopher Jagger, David Morgan, and Oliver Brand. 2018. “The

Consequence of Matrix Dysfunction on Lung Immunity and the Microbiome in COPD." *Eur Respir Rev*.

Ishihara, Jun, Kazuto Fukunaga, Ako Ishihara, Hans M. Larsson, Lambert Potin, Peyman Hosseinchi, Gabriele Galliverti, Melody A. Swartz, and Jeffrey A. Hubbell. 2017. "Matrix-Binding Checkpoint Immunotherapies Enhance Antitumor Efficacy and Reduce Adverse Events." *Sci. Transl. Med* 4(November).

Ishihara, Jun, Ako Ishihara, Koichi Sasaki, Steve Seung-young Lee, John-michael Williford, Mariko Yasui, Hiroyuki Abe, Lambert Potin, Peyman Hosseinchi, Kazuto Fukunaga, Michal M. Raczy, Laura T. Gray, Aslan Mansurov, Kiyomitsu Katsumata, Masashi Fukayama, Stephen J. Kron, Melody A. Swartz, and Jeffrey A. Hubbell. 2019. "Targeted Antibody and Cytokine Cancer Immunotherapies through Collagen Affinity." *Science Translational Medicine*.

Jacobetz, Michael A., Derek S. Chan, Albrecht Neesse, Tashinga E. Bapiro, Natalie Cook, Kristopher K. Frese, Christine Feig, Tomoaki Nakagawa, Meredith E. Caldwell, Heather I. Zecchini, Martijn P. Lolkema, Ping Jiang, Anne Kultti, Curtis B. Thompson, Daniel C. Maneval, Duncan I. Jodrell, Gregory I. Frost, H. M. Shepard, Jeremy N. Skepper, and David A. Tuveson. 2013. "Hyaluronan Impairs Vascular Function and Drug Delivery in a Mouse Model of Pancreatic Cancer." *Pancreas* 112–20.

Jansen, Christine A., Carin W. A. Cruijsen, Talitha de Ruiter, Nening Nanlohy, Neeltje Willems, Pirkko Liisa Janssens-Korpela, and Linde Meyaard. 2007. "Regulated Expression of the Inhibitory Receptor LAIR-1 on Human Peripheral T Cells during T Cell Activation and Differentiation." *European Journal of Immunology* 37(4):914–24.

Jansson, Andreas, Eleanor Barnes, Paul Klenerman, Mikael Harle, Poul Sørensen, Simon J. Davis, and Patric Nilsson. 2020. "A Theoretical Framework for Quantitative Analysis of the Molecular Basis of Costimulation." *Journal of Immunology*.

Jogler, Christian, Dennis Hoffmann, Dirk Theegarten, Thomas Grunwald, Oliver Wildner, U.

Klaus, Ruhr-university Bochum, Medical Virology, and D. Bochum. 2006. “Replication Properties of Human Adenovirus In Vivo and in Cultures of Primary Cells from Different Animal Species.” *Journal of Virology* 80(7):3549–58.

Joseph, Chitra, Mansour A. Alsaleem, Michael S. Toss, Yousif A. Kariri, Maryam Althobiti, Sami Alsaeed, Abrar I. Aljohani, Pavan L. Narasimha, Nigel P. Mongan, Andrew R. Green, and Emad A. Rakha. 2021. “The ITIM-Containing Receptor : Leukocyte-Associated Carcinoma.” *Cancers* 1:1–19.

Joshi, Rushikesh S., Samanvi S. Kanugula, Sweta Sudhir, Matheus P. Pereira, Saket Jain, and Manish K. Aghi. 2021. “The Role of Cancer-Associated Fibroblasts in Tumor Progression.” *Cancers* 1–26.

Ju, Fei, Yong Luo, Chaolong Lin, Xian Jia, Zilong Xu, Rui Tian, Yanhua Lin, Min Zhao, Yating Chang, Xiaoxuan Huang, Shaopeng Li, Wenfeng Ren, Yaning Qin, Mengqin Yu, Jizong Jia, Jinle Han, Wenxin Luo, Jun Zhang, Guo Fu, Xiangzhong Ye, Chenghao Huang, and Ningshao Xia. 2022. “Oncolytic Virus Expressing PD-1 Inhibitors Activates a Collaborative Intratumoral Immune Response to Control Tumor and Synergizes with CTLA-4 or TIM-3 Blockade.” *Journal for ImmunoTherapy of Cancer* 10(6):1–17.

Jung, Mi-yeon, Chetan P. Offord, Matthew K. Ennis, Iris Kemler, Claudia Neuhauser, David Dingli, Mayo Clinic, Twin Cities, Computational Biology Program, and Mayo Clinic. 2019. “In Vivo Estimation of Oncolytic Virus Populations within Tumors.” *Cancer Res.* 78(20):5992–6000.

Kaczmarek, Janusz, Patrizia Castellani, and Guido Nicolo. 1994. “Distribution of Oncofetal Fibronectin Isoforms in Normal, Hyperplastic and Neoplastic Human Breast Tissues.” *Int. J. Cancer* 58:11–16.

Kägi, David, Birgit Ledermann, Kurt Bürki, Peter Seiler, Bernhard Odermatt, Kristin J. Olsen, Eckhard R. Podack, Rolf M. Zinkernagel, and Hans Hengartner. 1994. “Cytotoxicity Mediated by T Cells and Natural Killer Cells Is Greatly Impaired in Perforin-Deficient

Mice.” *Nature* 369(6475):31–37.

Kalathas, Dimitrios, Dimitrios A. Theocharis, Dimitrios Bounias, Dora Kyriakopoulou, Nikoletta Papageorgakopoulou, Michael S. Stavropoulos, and Demitrios H. Vynios. 2011. “Chondroitin Synthases I , II , III and Chondroitin Sulfate Glucuronyltransferase Expression in Colorectal Cancer.” *Molecular Medicine Reports* 363–68.

Kalathas, Dimitrios, Irene-eva Triantaphyllidou, Nicholas S. Mastronikolis, Panos D. Goumas, Thoedore A. Papadas, Gabriel Tsiropoulos, and Demitrios H. Vynios. 2010. “The Chondroitin / Dermatan Sulfate Synthesizing and Modifying Enzymes in Laryngeal Cancer : Expressional and Epigenetic Studies.” *Head & Neck Oncology* 2(1):27.

Kang, Xunlei, Zhigang Lu, Changhao Cui, Mi Deng, Yuqi Fan, Baijun Dong, Xin Han, Fuchun Xie, Jeffrey W. Tyner, John E. Coligan, Robert H. Collins, Xiangshu Xiao, and M. James You. 2015. “The ITIM-Containing Receptor LAIR1 Is Essential for Acute Myeloid Leukaemia Development.” *Nature Cell Biology* 17(5).

Kassahn, D., U. Nachbur, S. Conus, O. Micheau, P. Schneider, H-u Simon, and T. Brunner. 2009. “Distinct Requirements for Activation-Induced Cell Surface Expression of Preformed Fas / CD95 Ligand and Cytolytic Granule Markers in T Cells.” 115–24.

Kaufman, Howard L., Thomas Amatruda, Tony Reid, Rene Gonzalez, John Glaspy, Eric Whitman, Kevin Harrington, John Nemunaitis, Andrew Zloza, Michael Wolf, and Neil N. Senzer. 2016. “Systemic versus Local Responses in Melanoma Patients Treated with Talimogene Laherparepvec from a Multi-Institutional Phase II Study.” *Journal for ImmunoTherapy of Cancer* 1–8.

Kayagaki, By Nobuhiko, Akemi Kawasaki, Tomohiko Ebata, Hiroshi Ohmoto, and Ko Okumura. 1995. “Metalloproteinase-Mediated Release of Human Fas Ligand.” *J . Exp . Med* 182(December).

Khalique, Hena, Richard Baugh, Arthur Dyer, Eleanor M. Scott, Leonard W. Seymour, Sally Frost, Sarah Larkin, and Janet Lei-. 2021. “Oncolytic Herpesvirus Expressing PD- -

BiTE for Cancer Therapy : Exploiting Tumor Immune Suppression as an Opportunity for Targeted Immunotherapy." *Journal for ImmunoTherapy of Cancer* 1–14.

Kim, Ryungsa, Manabu Emi, and Kazuaki Tanabe. 2007. "Cancer Immunoediting from Immune Surveillance to Immune Escape." *Immunology* 1–14.

Kim, Seong Keun and Sun Wook Cho. 2022. "The Evasion Mechanisms of Cancer Immunity and Drug Intervention in the Tumor Microenvironment." *Frontiers in Pharmacology* 13(May):1–16.

Kim, Tae-shin and Eui-cheol Shin. 2019. "The Activation of Bystander CD8 + T Cells and Their Roles in Viral Infection." *Experimental & Molecular Medicine* 1–9.

Kleinberger, Tamar. 2015. "Mechanisms of Cancer Cell Killing by the Adenovirus E4orf4 Protein." *Viruses* 2334–57.

Klinger, Matthias, Christian Brandl, Gerhard Zugmaier, Youssef Hijazi, Ralf C. Bargou, Max S. Topp, Nicola Go, Svenja Neumann, Mariele Goebeler, Andreas Viardot, Matthias Stelljes, Monika Bru, Dieter Hoelzer, Evelyn Degenhard, Dirk Nagorsen, Patrick A. Baeuerle, Andreas Wolf, and Peter Kufer. 2012. "Immunopharmacologic Response of Patients with B-Lineage Acute Lymphoblastic Leukemia to Continuous Infusion of T Cell – Engaging CD19 / CD3-Bispecific BiTE Antibody Blinatumomab." *Clinical Trials and Observations* 119(26):6226–33.

Knudson, Cory J., Maria Férez, Pedro Alves-peixoto, and Dan A. Erkes. 2021. "Mechanisms of Antiviral Cytotoxic CD4 T Cell Differentiation." *Journal of Virology*.

Ko, Young-hyeh, Sanghui Park, Heekyung Jin, Heesook Woo, Hyunseop Lee, Chaewha Park, and Kihyun Kim. 2007. "Granzyme B Leakage-Induced Apoptosis Is a Crucial Mechanism of Cell Death in Nasal-Type NK / T-Cell Lymphoma." *Laboratory Investigation* 87(June 2006):241–50.

Kobayashi, Yoshie, Seung-oe Lim, and Hirohito Yamaguchi. 2020. "Oncogenic Signaling

Pathways Associated with Immune Evasion and Resistance to Immune Checkpoint Inhibitors in Cancer.” *Seminars in Cancer Biology* 65(September 2019):51–64.

Kohli, Aditya G., Saul Kivimäe, Matthew R. Tiffany, and Francis C. Szoka. 2014. “Improving the Distribution of Doxil® in the Tumor Matrix by Depletion of Tumor Hyaluronan.” *J Control Release* 105–14.

Kuang, Dong-ming, Yan Wu, Nini Chen, Jiasen Cheng, Shi-mei Zhuang, and Limin Zheng. 2007. “Tumor-Derived Hyaluronan Induces Formation of Immunosuppressive Macrophages through Transient Early Activation of Monocytes.” 110(2):587–95.

Kuczek, Dorota E., Anne Mette H. Larsen, Marie Louise Thorseth, Marco Carretta, Adrija Kalvisa, Majken S. Siersbæk, Ana Micaela C. Simões, Anne Roslind, Lars H. Engelholm, Elfriede Noessner, Marco Donia, Inge Marie Svane, Per Thor Straten, Lars Grøntved, and Daniel H. Madsen. 2019. “Collagen Density Regulates the Activity of Tumor-Infiltrating T Cells.” *Journal for ImmunoTherapy of Cancer* 7(1):1–15.

Kuhn, Irene, Paul Harden, Maxine Bauzon, Cecile Chartier, Julie Nye, Steve Thorne, Tony Reid, Shaoheng Ni, Andre Lieber, Kerry Fisher, Len Seymour, Gabor M. Rubanyi, Richard N. Harkins, and Terry W. Hermiston. 2008a. “Directed Evolution Generates a Novel Oncolytic Virus for the Treatment of Colon Cancer.” *PLoS ONE*.

Kuhn, Irene, Paul Harden, Maxine Bauzon, Cecile Chartier, Julie Nye, Steve Thorne, Tony Reid, Shaoheng Ni, Andre Lieber, Kerry Fisher, Len Seymour, Gabor M. Rubanyi, Richard N. Harkins, and Terry W. Hermiston. 2008b. “Directed Evolution Generates a Novel Oncolytic Virus for the Treatment of Colon Cancer.” *PLoS ONE* 3(6):1–11.

Kuryk, Lukasz and Anne Sophie W. Møller. 2019. “Abscopal Effect When Combining Oncolytic Adenovirus and Checkpoint Inhibitor in a Humanized NOG Mouse Model of Melanoma.” *Journal of Medical Virology* 91(9):1702–6.

Van Laethem, François, Lucie Donaty, Emmanuelle Tchernonog, Vanessa Lacheretz-Szablewski, Jennifer Russello, Delphine Buthiau, Marion Almeras, Jérôme Moreaux,

and Caroline Bret. 2022. “LAIR1, an ITIM-Containing Receptor Involved in Immune Disorders and in Hematological Neoplasms.” *International Journal of Molecular Sciences* 23(24):1–16.

Lebbink, Robert Jan, Maaike C. W. Van Den Berg, Talitha De Ruiter, Nicolas Raynal, Joel A. G. Van Roon, Peter J. Lenting, Boquan Jin, and Linde Meyaard. 2008. “The Soluble Leukocyte-Associated Ig-Like Receptor (LAIR)-2 Antagonizes the Collagen/LAIR-1 Inhibitory Immune Interaction.” *The Journal of Immunology* 2–9.

Lebbink, Robert Jan, Talitha De Ruiter, Jelle Adelmeijer, Arjan B. Brenkman, Joop M. Van Helvoort, Manuel Koch, Richard W. Farndale, Ton Lisman, Arnoud Sonnenberg, Peter J. Lenting, and Linde Meyaard. 2006. “Collagens Are Functional, High Affinity Ligands for the Inhibitory Immune Receptor LAIR-1.” *Journal of Experimental Medicine* 203(6):1419–25.

Leiphrakpam, Premila D., Prathamesh P. Patil, Neeley Remmers, Benjamin Swanson, Paul M. Grandgenett, Fang Qiu, Fang Yu, and Prakash Radhakrishnan. 2019. “Role of Keratan Sulfate Expression in Human Pancreatic Cancer Malignancy.” *Scientific Reports* (June):1–10.

Li, Ke, Yalong Zhao, Xiaocong Hu, Jiao Jiao, Wei Wang, and Hongtao Yao. 2022. “Advances in the Clinical Development of Oncolytic Viruses.” *American Journal of Translational Research* 14(6):4192–4206.

Li, Zhe, Ben-fillippo Krippendorff, Sharad Sharma, Antje C. Walz, and Thierry Lav. 2016. “Influence of Molecular Size on Tissue Distribution of Antibody Fragments.” *Monoclonals Antibodies* (January):113–19.

Lichtenstein, Drew L., Karoly Toth, Konstantin Doronin, E. Ann, William S. M. Wold, William S. M. Wold Functions, Mechanisms Of, and Action Of. 2009. “International Reviews of Immunology FUNCTIONS AND MECHANISMS OF ACTION OF THE ADENOVIRUS E3 PROTEINS.” *International Reviews of Immunology* 0185.

Lin, Wen, Varan Singh, Raynel Springer, Gabrielle Choonoo, Namita Gupta, Aditi Patel, Davor Frleta, Jun Zhong, Tomasz Owczarek, Corinne Decker, Lynn Macdonald, Andrew Murphy, Gavin Thurston, Markus Mohrs, Ella Ioffe, and Yi-fen Lu. 2023. “Human CD4 Cytotoxic T Lymphocytes Mediate Potent Tumor Control in Humanized Immune System Mice.” *Communications Biology*.

Lion, Thomas. 2014. “Adenovirus Infections in Immunocompetent and Immunocompromised Patients.” *Clinical Microbiology Reviews* 27(3):441–62.

Liu, B. L., M. Robinson, Z. Q. Han, R. H. Branston, C. English, P. Reay, Y. McGrath, S. K. Thomas, M. Thornton, P. Bullock, C. A. Love, and R. S. Coffin. 2003. “ICP34.5 Deleted Herpes Simplex Virus with Enhanced Oncolytic, Immune Stimulating, and Anti-Tumour Properties.” *Gene Therapy* 10(4):292–303.

Liu, Xinjun, Jian Zhao, Xiaopeng Li, Fengxue Lao, and Min Fang. 2022. “Design Strategies and Precautions for Using Vaccinia Virus in Tumor Virotherapy.” *Vaccines MDPI* 1–20.

Lockhart-Cairns, Michael P., Stuart A. Cain, Rana Dajani, and Ruth Steer. 2022. “Latent TGF b Complexes Are Transglutaminase Cross-Linked to Fi Brillin to Facilitate TGF b Activation.” *Matrix Biology* 24–39.

Ma, Hon-ping, Hang-lung Chang, Oluwaseun Adebayo Bamodu, Shin-han Tsai, and Wei-hwa Lee. 2019. “Collagen 1A1 (COL1A1) Is a Reliable Biomarker and Putative Therapeutic Target for Hepatocellular Carcinogenesis and Metastasis.” *Cancers* 1.

Ma, Weidong, Ting Li, Si Wu, Jian Li, Xiuchao Wang, and Hui Li. 2019. “LOX and ACSL5 as Potential Relapse Markers for Pancreatic Cancer Patients.” *Cancer Biology and Therapy* 20(6):787–98.

Maali, Amirhosein, Monireh Gholizadeh, and Seyedeh Sheila Seyed-motahari. 2023. “Nanobodies in Cell-Mediated Immunotherapy : On the Road to Fi Ght Cancer.” *Frontiers in Immunology* (January):1–19.

Maasho, Kerima, Madhan Masilamani, Robert Valas, Simana Basu, John E. Coligan, and Francisco Borrego. 2005. “The Inhibitory Leukocyte-Associated Ig-like Receptor-1 (LAIR-1) Is Expressed at High Levels by Human Naive T Cells and Inhibits TCR Mediated Activation.” *Molecular Immunology* 42:1521–30.

Malyshkina, Anna, Elisabeth Littwitz-salomon, Kathrin Sutter, Gennadiy Zelinskyy, Sonja Windmann, Simone Schimmer, Annette Paschen, Hendrik Streeck, and J. Kim. 2017. “Fas Ligand-Mediated Cytotoxicity of CD4 + T Cells during Chronic Retrovirus Infection.” *Scientific Reports* (May):1–10.

Maroun, Justin, Miguel Muñoz-Alía, Arun Ammayappan, Autumn Schulze, Kah Whye Peng, and Stephen Russell. 2017. “Designing and Building Oncolytic Viruses.” *Future Virology* 12(4):193–213.

Martino, Mikaël M., Priscilla S. Briquez, Esra Güç, Federico Tortelli, Witold W. Kilarski, Stephanie Metzger, Jeffrey J. Rice, Gisela A. Kuhn, Ralph Müller, Melody A. Swartz, and Jeffrey A. Hubbell. 2014. “Growth Factors Engineered for Super-Affinity to the Extracellular Matrix Enhance Tissue Healing.” *Science* 343(February):885–89.

Matsuno, Hiroaki, Kazuo Yudoh, Yasuhiro Watanabe, Fujio Nakazawa, and Hiroyuki Aono. 2001. “Stromelysin-1 (MMP-3) in Synovial Fluid of Patients with Rheumatoid Arthritis Has Potential to Cleave Membrane Bound Fas Ligand.” *The Journal of Rheumatology* 1:22–28.

Matsushita, Hirokazu, Akihiro Hosoi, Satoshi Ueha, Jun Abe, Nao Fujieda, Michio Tomura, Ryuji Maekawa, Kouji Matsushima, Osamu Ohara, and Kazuhiro Kakimi. 2015. “Cytotoxic T Lymphocytes Block Tumor Growth Both by Lytic Activity and IFNγ-Dependent Cell-Cycle Arrest.” *Cancer Immunology Research* 3(1):26–36.

Mayya, Viveka, Edward Judokusumo, Enas Abu Shah, Chris H. Wiggins, Lance C. Kam, Michael L. Dustin, Viveka Mayya, Edward Judokusumo, Enas Abu Shah, Christopher G. Peel, Willie Neiswanger, and David Depoil. 2018. “Durable Interactions of T Cells

with T Cell Receptor Stimuli in the Absence of a Stable Immunological Report Durable Interactions of T Cells with T Cell Receptor Stimuli in the Absence of a Stable Immunological Synapse." *CellReports* 22(2):340–49.

Mcginley, Aoife M., Caroline E. Sutton, Sarah C. Edwards, Louis Boon, Nabil Djouder, Kingston H. G. Mills, Aoife M. Mcginley, Caroline E. Sutton, Sarah C. Edwards, Charlotte M. Leane, Joseph Decourcey, and Ana Teijeiro. 2020. "Interleukin-17A Serves a Priming Role in Autoimmunity by Recruiting IL-1 b -Producing Myeloid Cells That Promote Pathogenic T Cells Article Interleukin-17A Serves a Priming Role in Autoimmunity by Recruiting IL-1 b -Producing Myeloid Cells That Promote Pa." *Immunity* 52(2):342-356.e6.

Mcintosh, Stuart A., Fareeha Alam, Laura Adams, Ian S. Boon, Jonathan Callaghan, Isabella Conti, Ellen Copson, Victoria Carson, Mitchell Davidson, Helen Fitzgerald, Ashram Gautam, Christopher M. Jones, Saffron Kargbo, Gokul Lakshmipathy, Hannah Maguire, Kathryn Mcferran, Amatta Mirandari, Natasha Moore, Ross Moore, Aidan Murray, Lydia Newman, Stephen D. Robinson, and Ashvina Segaran. 2023. "Global Funding for Cancer Research between 2016 and 2020 : A Content Analysis of Public and Philanthropic Investments." *Lancet Oncology* 24(6):636–45.

Mcsharry, Brian P., Hans-gerhard Burgert, Douglas P. Owen, Richard J. Stanton, Virginie Prod, Martina Sester, Katja Koebernick, Veronika Groh, Thomas Spies, Steven Cox, Ann-margaret Little, Eddie C. Y. Wang, Peter Tomasec, and Gavin W. G. Wilkinson. 2008. "Adenovirus E3 / 19K Promotes Evasion of NK Cell Recognition by Intracellular Sequestration of the NKG2D Ligands Major Histocompatibility Complex Class I Chain-Related Proteins A and B □." *Journal of Virology* 82(9):4585–94.

Mecham, Robert P. 2012. "Overview of Extracellular Matrix." *Current Protocols in Cell Biology*.

Mekapogu, Alpha R., Srinivasa P. Pothula, Romano C. Pirola, Jeremy S. Wilson, and Minoti

V Apte. 2019. “Multifunctional Role of Pancreatic Stellate Cells in Pancreatic Cancer.” *Ann Pancreat Cancer* (9).

Meyaard, Linde. 2008. “The Inhibitory Collagen Receptor LAIR-1 (CD305).” *J Leukoc Biol* Apr;83(4):799–803.

Meyaard, Linde, Gosse J. Adema, Chiwen Chang, Erica Woollatt, Grant R. Sutherland, Lewis L. Lanier, and Joseph H. Phillips. 1997. “LAIR-1, a Novel Inhibitory Receptor Expressed on Human Mononuclear Leukocytes.” *Immunity* 7(2):283–90.

Meyaard, Linde, Jolanda Hurenkamp, Hans Clevers, Lewis L. Lanier, and Joseph H. Phillips. 1999. “Leukocyte-Associated Ig-Like Receptor-1 Functions as an Inhibitory Receptor on Cytotoxic T Cells.” *The Journal of Immunology* 162(10):5800–5804.

Misra, Suniti and Shibnath Ghatak. 2015. “Interactions between Hyaluronan and Its Receptors (CD44 , RHAMM) Regulate the Activities Of.” *Frontiers in Immunology* 6(May).

Mitra, AK, K. Sawada, P. Tiwari, K. Mui, K. Gwin, and E. Lengyel. 2011. “Ligand Independent Activation of C-Met by Fibronectin and A5 B1 - Integrin Regulates Ovarian Cancer Invasion and Metastasis.” *Oncogene.* 30(13):1566–76.

Miyamoto, Tsutomu, Keiko Ishii, Ryouichi Asaka, Akihisa Suzuki, Akiko Takatsu, Hiroyasu Kashima, and Tanri Shiozawa. 2011. “Immunohistochemical Expression of Keratan Sulfate : A Possible Diagnostic Marker for Carcinomas of the Female Genital Tract.” *J Clin Pathol* 64:1058e10.

Miyatake, Shin-ichi, A. N. U. Iyer, and Robert L. Martuza. 1997. “Transcriptional Targeting of Herpes Simplex Virus for Cell-Specific Replication.” *Journal of Virology* 71(7):5124–32.

Momose, Takashige, Yasuo Yoshimura, and Satoru Harumiya. 2016. “Chondroitin Sulfate Synthase 1 Expression Is Associated with Malignant Potential of Soft Tissue Sarcomas with Myxoid Substance ☆ , ☆☆.” *Human Pathology* 50:15–23.

Mueller, Barbara M., Ingrid U. Schraufstatter, Valentina Goncharova, Tatiana Povaliy, Richard Discipio, and Sophia K. Khaldoyanidi. 2011. “NIH Public Access.” 9(11):3024–32.

Mummery, Rosemary S. and Christopher C. Rider. 2000. “Characterization of the Heparin-Binding Properties of IL-6.” *The Journal of Immunology* 165(10):5671–79.

Mysiak, Monika E., P. Elly Holthuizen, and Peter C. Van Der Vliet. 2004. “The Adenovirus Priming Protein PTP Contributes to the Kinetics of Initiation of DNA Replication.” *Nucleic Acids Research* 32(13):3913–20.

Naik, Rangeetha J., Pallavi Chandra, Anita Mann, and Munia Ganguli. 2011. “Exogenous and Cell Surface Glycosaminoglycans Alter DNA Delivery Efficiency of Arginine and Lysine Homopeptides in Distinctly Different Ways * □.” *Journal of Biological Chemistry* 286(21):18982–93.

Naveen, Mehta, Kavya Rakhra, Kristan Meetze, Irina Shapiro, Karl Wittrup, Patrick Baeuerle, and Jennifer Michaelson. 2022. “CLN-617 Is an Intratumourally Injected Abd Kicakkt Retaubed Fusion of IL-2 and IL-12 That Drives Systemic Anti-Tumor Activity.” *Abstract, J Immunother Cancer* 2022.

Necula, Laura, Lilia Matei, Denisa Dragu, Ioana Pitica, Ana Neagu, Coralia Bleotu, Carmen C. Diaconu, and Mihaela Chivu-economescu. 2022. “Collagen Family as Promising Biomarkers and Therapeutic Targets in Cancer.” *International Journal of Molecular Sciences*.

Nevins, Joseph R., Harold S. Ginsberg, J. Blanchard, Michael C. Wilson, and James E. Darnell. 1979. “Regulation of the Primary Expression of the Early Adenovirus Transcription Units.” *Journal of Virology* 32(3):727–33.

Nicolas-Boluda, Alba, Javier Vaquero, Lene Vimeux, Thomas Guilbert, Sarah Barrin, Chahrazade Kantari-Mimoun, Matteo Ponzo, Gilles Renault, Piotr Deptula, Katarzyna Pogoda, Robert Bucki, Ilaria Cascone, José Courty, Laura Fouassier, Florence

Gazeau, and Emmanuel Donnadieu. 2021. “Tumor Stiffening Reversion through Collagen Crosslinking Inhibition Improves t Cell Migration and Anti-Pd-1 Treatment.” *ELife* 10:1–29.

Nikitovic, Dragana, Antonis Papoutsidakis, Nikos K. Karamanos, and George N. Tzanakakis. 2014. “Lumican Affects Tumor Cell Functions , Tumor – ECM Interactions , Angiogenesis and in Fl Ammatory Response.” *Matrix Biology* 35:206–14.

Niu, Zeshan, Fuliang Bai, D. Ph, Tian Sun, Hui Tian, Dan Yu, Jiechao Yin, D. Ph, Siming Li, D. Ph, Tianhe Li, D. Ph, Hongwei Cao, D. Ph, Qingzhong Yu, D. Ph, Yunzhou Wu, D. Ph, Guiping Ren, and D. Ph. 2015. “Recombinant Newcastle Disease Virus Expressing IL15 Demonstrates Promising Antitumor Efficiency in Melanoma Model.” *Technology in Cancer Research and Treatment* 14(5).

Noël, Agnès, Ana Gutiérrez-fernández, Nor Eddine Sounni, Niels Behrendt, Erik Maquoi, Ida K. Lund, Santiago Cal, Gunilla Hoyer-hansen, and Carlos López-otín. 2012. “New and Paradoxical Roles of Matrix Metalloproteinases in the Tumor Microenvironment.” *Frontiers in Pharmacology* 3(July):1–9.

Nordkamp, Marloes, Peter Boross, Cafer Yildiz, Marco Jansen, Jeanette HW Leusen, Rolf T. Urbanus, Diana Wouters, C. Erik Hack, and Linde Meyaard. 2014. “Inhibition of the Classical and Lectin Pathway of the Complement System by Recombinant LAIR-2.” *Innate Immunity* 284–92.

Nordkamp, Marloes, A. G. Van Roon, Max Douwes, Talitha De Ruiter, Rolf T. Urbanus, and Linde Meyaard. 2011. “Enhanced Secretion of and Soluble LAIR-1 in Rheumatoid Arthritis LAIR-2 Is a More Efficient Antagonist of the LAIR-1 – Collagen Inhibitory Interaction Than Is Soluble LAIR-1.” *Arthritis and Rheumatism* 63(12):3749–57.

Nordkamp, Marloes, Joël A. G. Van Roon, Max Douwes, Talitha De Ruiter, Rolf T. Urbanus, and Linde Meyaard. 2011. “Enhanced Secretion of Leukocyte-Associated Immunoglobulin-like Receptor 2 (LAIR-2) and Soluble LAIR-1 in Rheumatoid Arthritis:

LAIR-2 Is a More Efficient Antagonist of the LAIR-1-Collagen Inhibitory Interaction than Is Soluble LAIR-1.” *Arthritis and Rheumatism* 63(12):3749–57.

Oft, Martin. 2014. “IL-10: Master Switch from Tumor-Promoting Inflammation to Antitumor Immunity.” *Cancer Immunology Research* 2(3):194–99.

Omiya, Ryusuke, Hidehiko Narazaki, Yukimi Sakoda, Atsuo Kuramasu, Youn Kim, Haiying Xu, Gefeng Zhu, and Koji Tamada. 2009. “Leucocyte-Associated Immunoglobulin-like Receptor- 1 Is an Inhibitory Regulator of Contact Hypersensitivity.” *Immunology* 543–55.

Ongaro, Tiziano, Mattia Matasci, Samuele Cazzamalli, Baptiste Gouyou, Roberto De Luca, Dario Neri, and Alessandra Villa. 2019. “A Novel Anti-Cancer L19-Interleukin-12 Fusion Protein with an Optimized Peptide Linker Efficiently Localizes in Vivo at the Site of Tumors.” *Journal of Biotechnology* 291(August 2018):17–25.

Onoda, J. M., M. P. Piechocki, and K. V Honn. 1992. “Radiation-Induced Increase in Expression of the Alpha IIb Beta 3 Integrin in Melanoma Cells: Effects on Metastatic Potential.” *Radiat Res*.

Osińska, Iwona, Katarzyna Popko, and Urszula Demkow. 2014. “Perforin : An Important Player in Immune Response.” *Central European Journal of Immunology* 39(1):109–15.

Oskarsson, Thordur, Swarnali Acharyya, Xiang H-f Zhang, Sakari Vanharanta, Sohail F. Tavazoie, Patrick G. Morris, Robert J. Downey, Katia Manova-todorova, Edi Brogi, and Joan Massagué. 2011. “Breast Cancer Cells Produce Tenascin C as a Metastatic Niche Component to Colonize the Lungs.” 17(7).

Oyama, F., S. Hirohashi, Y. Shimosato, K. Titani, and K. Sekiguchi. 1990. “Oncodevelopmental Regulation of the Alternative Splicing of Fibronectin Pre-Messenger RNA in Human Lung Tissues.” *Cancer Res* 5;50(4):10.

Oyama, Fumitaka, Setuso Hirohashi, Yukio Shimosato, Koiti Titani, and Kiyotoshi Sekiguchi.

1989. “Deregulation of Alternative Splicing of Fibronectin Pre-MRNA in Malignant Human Liver Tumors*.” *Journal of Biological Chemistry*.

Park, Jeoung Eun, David D. Brand, Edward F. Rosloniec, Ae Kyung Yi, John M. Stuart, Andrew H. Kang, and Linda K. Myers. 2020. “Leukocyte-Associated Immunoglobulin-like Receptor 1 Inhibits T-Cell Signaling by Decreasing Protein Phosphorylation in the T-Cell Signaling Pathway.” *Journal of Biological Chemistry* 295(8):2239–47.

Parry, Richard V, Jens M. Chemnitz, Kenneth A. Frauwirth, Anthony R. Lanfranco, Inbal Braunstein, Sumire V Kobayashi, Peter S. Linsley, Craig B. Thompson, and James L. Riley. 2005. “CTLA-4 and PD-1 Receptors Inhibit T-Cell Activation by Distinct Mechanisms †.” *Molecular and Cellular Biology* 25(21):9543–53.

Peng, David H., Bertha Leticia Rodriguez, Lixia Diao, Limo Chen, Jing Wang, Lauren A. Byers, Ying Wei, Harold A. Chapman, Mitsuo Yamauchi, Carmen Behrens, Gabriela Raso, Luisa Maren Solis Soto, Edwin Roger Parra Cuentes, Ignacio I. Wistuba, Jonathan M. Kurie, and Don L. Gibbons. 2020. “Collagen Promotes Anti-PD-1/PD-L1 Resistance in Cancer through LAIR1-Dependent CD8+ T Cell Exhaustion.” *Nature Communications* 11(1):1–18.

Perbellini, Omar, Erika Falisi, Ilaria Giaretta, Elisa Boscaro, Elisabetta Novella, Monica Facco, Stefania Fortuna, Silvia Finotto, Eliana Amati, Francesco Maniscalco, Anna Montaldi, Alberta Alghisi, Fiorenza Aprili, Laura Bonaldi, Rossella Paolini, Maria Teresa Scupoli, Livio Trentin, Achille Ambrosetti, Gianpietro Semenzato, Giovanni Pizzolo, Francesco Rodeghiero, and Carlo Visco. 2014. “A Rticles Clinical Significance of LAIR1 (CD305) as Assessed by Flow Cytometry in a Prospective Series of Patients with Chronic Lymphocytic Leukemia.” *Chronic Lymphocytic Leukemia* 1(5):881–87.

Pirinen, Risto, Raija Tammi, Markku Tammi, Pasi HIRVIKOSKI, Jyrki J. PARKKINEN, Risto JOHANSSON, Jan BOHM, Sinikka HOLLMEN, and Veli-Matti. 2001. “Prognostic Value of Hyaluronan Expression in Non-Small-Cell Lung Cancer: Increased Stromal

Expression Indicates Unfavorable Outcome in Patients with Adenocarcinoma.” *Int. J. Cancer* 95:12–17.

Pisibon, C., Amira Ouertani, Corine Bertolotto, Robert Ballotti, and Yann Cheli. 2021. “Immune Checkpoints in Cancers : From Signaling to the Clinic.” *Cancers*.

Poggi, A., S. Catellani, A. Bruzzone, and M. Gobbi. 2008. “Lack of the Leukocyte-Associated Ig-like Receptor-1 Expression in High-Risk Chronic Lymphocytic Leukaemia Results in the Absence of a Negative Signal Regulating Kinase Activation and Cell Division.” *Leukemia* 980–88.

Popova, Nadezhda V and Manfred Jücker. 2022. “The Functional Role of Extracellular Matrix Proteins in Cancer.” *Cancers*.

Price, Zoe K., Noor A. Lokman, and Carmela Ricciardelli. 2018. “Differing Roles of Hyaluronan Molecular Weight on Cancer Cell Behavior and Chemotherapy Resistance.”

Proietto, Marco, Martina Crippa, Chiara Damiani, Valentina Pasquale, Elena Sacco, Marco Vanoni, and Mara Gilardi. 2023. “Tumor Heterogeneity : Preclinical Models , Emerging Technologies , and Future Applications.” *Frontiers in Oncology* (April):1–24.

Provenzano, Paolo P., Kevin W. Eliceiri, Jay M. Campbell, David R. Inman, John G. White, and Patricia J. Keely. 2006. “Collagen Reorganization at the Tumor-Stromal Interface Facilitates Local Invasion.” *BMC Medicine* 16:1–15.

Pujuguet, Philippe, Arlette Hammann, Monique Moutet, Jane Lyse Samuel, Franois Martin, and Monique Martin. 1996. “Expression of Fibronectin ED-A+ and ED-B+ Isoforms by Human and Experimental Colorectal Cancer Contribution of Cancer Cells and Tumor-Associated Myofibroblasts.” *American Jouirnal OfPathology* 148(2):579–92.

Quintero-fabián, Saray, Rodrigo Arreola, Enrique Becerril-villanueva, Mario Alberto Ramírez-camacho, and María Elizbeth Alvarez-sánchez. 2019. “Role of Matrix

Metalloproteinases in Angiogenesis and Cancer." *Frontiers in Oncology* 9(December):1–21.

Ramos, M. Ines Pascoal, Linjie Tian, Emma J. de Ruiter, Chang Song, Ana Paucarmayta, Akashdip Singh, Eline Elshof, Saskia V. Vijver, Jahangheer Shaik, Jason Bosiacki, Zachary Cusumano, Christina Jensen, Nicholas Willumsen, Morten A. Karsdal, Linda Liu, Sol Langermann, Stefan Willems, Dallas Flies, and Linde Meyaard. 2021. "Cancer Immunotherapy by Nc410, a Lair-2 Fc Protein Blocking Human Lair-Collagen Interaction." *ELife* 10:1–29.

Rawstron, A. .., Shingles J. De Tute, R. Bennett, F. Jack, A.S., and P. Hillmen. 2010. "Chronic Lymphocytic Leukaemia (CLL) and CLL-Type Monoclonal B-Cell Lymphocytosis (MBL) Show Differential Expression of Molecules Involved in Lymphoid Tissue Homing." *Cytometry Part B - Clinical Cytometry* 10.1002/cy:20534.

Ray, Arja, Mackenzie K. Callaway, Nelson J. Rodríguez-merced, Alexandra L. Crampton, Marjorie Carlson, Kenneth B. Emme, Ethan A. Ensminger, Alexander A. Kinne, Jonathan H. Schrope, Haley R. Rasmussen, Hong Jiang, David G. Denardo, David K. Wood, and Paolo P. Provenzano. 2022. "Stromal Architecture Directs Early Dissemination in Pancreatic Ductal Adenocarcinoma." *JCI Insight* 7(3):1–17.

Rehman, Hasan, Ann W. Silk, Michael P. Kane, and Howard L. Kaufman. 2016. "Into the Clinic : Talimogene Laherparepvec (T-VEC), a First-in-Class Intratumoral Oncolytic Viral Therapy." *Journal for ImmunoTherapy of Cancer* 1–8.

Rekers, Nicolle H., Veronica Olivo, Ala Yaromina, Natasja G. Lieuwes, Rianne Biemans, and Philippe Lambin. 2018. "The Immunocytokine L19-IL2 : An Interplay between Radiotherapy and Long-Lasting Systemic Anti-Tumour Immune Responses." *OncoImmunologyy* 7(4).

Ricard-blum, Sylvie. 2011. "The Collagen Family." *CSH* 1–19.

Rishikof, David C., Dennis A. Ricupero, Hanqiao Liu, and Ronald H. Goldstein. 2004.

"Phenylbutyrate Decreases Type I Collagen Production in Human Lung Fibroblasts." *Journal of Cellular Biochemistry* 748:740–48.

Robertson, Ian B., Masahito Horiguchi, Lior Zilberberg, Branka Dabovic, Krassimira Hadjiolova, and Daniel B. Rifkin. 2016. "Latent TGF-β-Binding Proteins." *Physiology & Behavior* 176(1):139–48.

Robertson, Ian B. and Daniel B. Rifkin. 2016. "And TGF- b -Related Proteins." 1–25.

Rodriguez-Rocha, Humberto, Jorge G. Gomez-Gutierreza, Aracely Garcia-Garciaa, Xiao-Mei Raob, Lan Chena, Kelly M. McMastersa, and Heshan Sam Zhoua. 2011. "Adenoviruses Induce Autophagy to Promote Virus Replication and Oncolysis." *Virology* 416(502):9–15.

Roelants, Caroline, Catherine Pillet, Quentin Franquet, Clément Sarrazin, Nicolas Peilleron, Sofia Giacosa, Laurent Guyon, Amina Fontanell, Gaëlle Fiard, Jean Alexandre Long, Jean Luc Descotes, Claude Cochet, and Odile Filhol. 2020. "Ex-Vivo Treatment of Tumor Tissue Slices as a Predictive Preclinical Method to Evaluate Targeted Therapies for Patients with Renal Carcinoma." *Cancers* 12(1):1–18.

Rømer, Anne Mette Askehøj, Marie Louise Thorseth, and Daniel Hargbøl Madsen. 2021. "Immune Modulatory Properties of Collagen in Cancer." *Frontiers in Immunology* 12(December):1–15.

Ross, Sandra L., Marika Mulen, Patricia L. McElroy, Julie Lofgren, Gordon Moody, Patrick A. Baeuerle, Angela Coxon, and Tara L. Arvedson. 2015. "BiTE Antibody Constructs Can Mediate Bystander Tumor Cell Killing." *Cancer Research* 75(15_Supplement):LB-232-LB-232.

Roy, Dominic Guy, Theresa Falls, Kwame Twumasi-boateng, Lauren Elizabeth St-germain, Monique Marguerie, Vanessa Garcia, Mohammed Selman, Victoria Ann Jennings, Jessica Pettigrew, Sally Amos, Jean-simon Diallo, Brad Nelson, and John Cameron Bell. 2016. "Oncolytic Vesicular Stomatitis Virus Expressing Interferon- γ Has Enhanced

Therapeutic Activity.” *Molecular Therapy — Oncolytics* (December 2015):1–11.

Rudman, S. M., M. B. Jameson, M. J. Mckeage, P. Savage, D. I. Jodrell, M. Harries, and G. Acton. 2012. “Europe PMC Funders Group Europe PMC Funders Author Manuscripts A Phase 1 Study of AS1409 , a Novel Antibody-Cytokine Fusion Protein , in Patients with Malignant Melanoma or Renal Cell Carcinoma.” 17(7):1998–2005.

Ruley, H. Earl. 1983. “Adenovirus Early Region LA Enables Viral and Cellular Transforming Genes to Transform Primary Cells in Culture.” *Nature* (July):7–11.

Runge, Annette, Melissa Mayr, Theresa Schwaiger, Susanne Sprung, Paolo Chetta, Timo Gottfried, Jozsef Dudas, Maria C. Greier, Marlies C. Glatz, Johannes Haybaeck, Knut Elbers, Herbert Riechelmann, Patrik Erlmann, and Monika Petersson. 2022. “Patient-Derived Head and Neck Tumor Slice Cultures: A Versatile Tool to Study Oncolytic Virus Action.” *Scientific Reports* 12(1):1–14.

Saatci, Ozge, Aysegul Kaymak, Umar Raza, Pelin G. Ersan, Ozge Akbulut, Carolyn E. Banister, Vitali Sikirzhytski, Unal Metin Tokat, Gamze Aykut, Suhail A. Ansari, Hayriye Tatli Dogan, Mehmet Dogan, Pouria Jandaghi, Aynur Isik, Fatma Gundogdu, Kemal Kosemehmetoglu, Omer Dizdar, Sercan Aksoy, Aytekin Akyol, Aysegul Uner, Phillip J. Buckhaults, Yasser Riazalhosseini, and Ozgur Sahin. 2020. “Targeting Lysyl Oxidase (LOX) Overcomes Chemotherapy Resistance in Triple Negative Breast Cancer.” *Nature Communications* 1–17.

Sainio, A. and H. Järveläinen. 2020. “Extracellular Matrix-Cell Interactions: Focus on Therapeutic Applications.” *Cellular Signalling* 66(September 2019):109487.

Saito, Fumiji, Kouyuki Hirayasu, Takeshi Satoh, W. Christian, John Lusingu, Takao Arimori, Kyoko Shida, Nirianne Marie Q. Palacpac, Sawako Itagaki, Shiroh Iwanaga, Eizo Takashima, Takafumi Tsuboi, Masako Kohyama, Tadahiro Suenaga, Marco Colonna, Junichi Takagi, Thomas Lavstsen, Toshihiro Horii, and Hisashi Arase. 2017. “Immune Evasion of Plasmodium Falciparum by RIFIN via Inhibitory Receptors.” *Nature*

Publishing Group.

Sarkar, Aurijit and Umesh R. Desai. 2015. “A Simple Method for Discovering Druggable , Specific Glycosaminoglycan-Protein Systems . Elucidation of Key Principles from Heparin / Heparan Sulfate-Binding Proteins.” *PLoS ONE* 1–18.

Saverino, Daniele, Marina Fabbi, Andrea Merlo, Giambattista Ravera, Carlo E. Grossi, and Ermanno Ciccone. 2002. “Surface Density Expression of the Leukocyte-Associated Ig-like Receptor-1 Is Directly Related to Inhibition of Human T-Cell Functions.” *Human Immunology* 63(7):534–46.

Schietinger, Andrea, Mary Philip, Rebecca B. Liu, Karin Schreiber, and Hans Schreiber. 2010. “Bystander Killing of Cancer Requires the Cooperation of CD4+ and CD8+ T Cells during the Effector Phase.” *Journal of Experimental Medicine* 207(11):2469–77.

Schneider, Helga, K. V. S. Prasad, Steven E. Shoelson, and E. S. Christopher. 1995. “CTLA-4 Binding to the Lipid Kinase Phosphatidy!~nositol 3-Kinase in T Cells.” *J. Exp. Med.* 181(January):3–7.

Schro, Michael, Janos Peli, Michael Hahne, È. Tschopp, and Ernst Reichmann. 2000. “Fas-Dependent Tissue Turnover Is Implicated in Tumor Cell Clearance.” *Oncogene* 1794–1800.

Scott, Eleanor M., Sally Frost, Hena Khalique, Joshua D. Freedman, Len W. Seymour, and Janet Lei-rossmann. 2020. “Use of Liquid Patient Ascites Fluids as a Preclinical Model for Oncolytic Virus Activity.” 2058:261–70.

Scott, Eleanor M., Egon J. Jacobus, Brian Lyons, Sally Frost, Joshua D. Freedman, Arthur Dyer, Hena Khalique, William K. Taverner, Alison Carr, Brian R. Champion, Kerry D. Fisher, Len W. Seymour, and Margaret R. Duffy. 2019. “Bi- and Tri-Valent T Cell Engagers Deplete Tumour-Associated Macrophages in Cancer Patient Samples.” *Journal for ImmunoTherapy of Cancer* 6:1–18.

Sewell-loftin, Mary Kathryn, Samantha Van Hove Bayer, Elizabeth Crist, Taylor Hughe, Sofia M. Joison, Gregory D. Longmore, and Steven C. George. 2017. “Cancer-Associated Fibroblasts Support Vascular Growth through Mechanical Force.” *Scientific Reports* 1–12.

Seymour, Leonard W. and Kerry D. Fisher. 2016. “Oncolytic Viruses: Finally Delivering.” *British Journal of Cancer*.

Sheppard, Kelly-ann, Lori J. Fitz, Julie M. Lee, Christina Benander, Judith A. George, Joe Wooters, Yongchang Qiu, Jason M. Jussif, Laura L. Carter, Clive R. Wood, and Divya Chaudhary. 2004. “PD-1 Inhibits T-Cell Receptor Induced Phosphorylation of the ZAP70 / CD3 f Signalosome and Downstream Signaling to PKC H.” *FEBS Letters* 574:37–41.

Shi, Minlong, Jianghai Zhu, Rui Wang, Xing Chen, Lizhi Mi, Thomas Walz, and Timothy A. Springer. 2011. “Latent TGF-β Structure and Activation.” *Nature* 474(7351):343–51.

Shi, Run, Zhe Zhang, Ankai Zhu, Xingxing Xiong, Jie Zhang, Jiang Xu, Man Sun Sy, and Chaoyang Li. 2022. “Targeting Type I Collagen for Cancer Treatment.” *International Journal of Cancer* 151(5):665–83.

Shim, Chae-hyeon, Sookyung Cho, Young-mi Shin, and Je-min Choi. 2022. “Emerging Role of Bystander T Cell Activation in Autoimmune Diseases.” *BMB Rep.* 55(2):57–64.

Silva, João C., Marta S. Carvalho, Xiaorui Han, Ke Xia, Paiyz E. Mikael, Joaquim M. S. Cabral, Frederico Castelo Ferreira, and Robert J. Linhardt. 2019. “Compositional and Structural Analysis of Glycosaminoglycans in Cell-Derived Extracellular Matrices.” *Glycoconj J.* 36(2):141–54.

Simoens, Steven and Isabelle Huys. 2021. “R&D Costs of New Medicines: A Landscape Analysis.” *Frontiers in Medicine* 8(October):1–6.

Simon, Felix, Ruben Picard, Veronika Lutz, Anna Brichkina, Felix Neuhaus, Teresa

Ruckenbrod, Anna Hupfer, Hartmann Raifer, Matthias Klein, Tobias Bopp, Petra Ina Pfefferle, Rajkumar Savai, Immo Prinz, Dong Chang, Stefan Heinrich, Ari Waisman, Sonja Moos, Detlef K. Bartsch, Malte Buchholz, Shiv Singh, Mengyu Tu, Lukas Klein, Christian Bauer, Robert Liefke, Andreas Burchert, Ryun Chung, Philipp Mayer, Thomas M. Gress, Matthias Lauth, Matthias Gaida, and Magdalena Huber. 2023. “IL- - 17A- - Producing CD8 + T Cells Promote PDAC via Induction of Inflammatory Cancer- - Associated Fibroblasts.” *Pancreas* 1–13.

Simone, Rita, Giampaola Pesce, Princey Antola, Domenico F. Merlo, Marcello Bagnasco, and Daniele Saverino. 2013. “Serum LAIR-2 Is Increased in Autoimmune Thyroid Diseases.” *PLoS ONE* 8(5).

Simpson, Melanie A. and Vinata B. Lokeshwar. 2009. “Hyaluronan and Hyaluronidase in Genitourinary Tumors Melanie.” *Front Biosci* 5664–80.

Singh, Purva, Cara Carraher, and Jean E. Schwarzenbauer. 2010. “Assembly of Fibronectin Extracellular Matrix Purva.” *Annu Rev Cell Dev Biol.* 397–419.

Smith, Logan K., Giselle M. Boukhaled, Stephanie A. Condotta, Sabrina Mazouz, Jenna J. Guthmiller, Rahul Vijay, Noah S. Butler, Julie Bruneau, Naglaa H. Shoukry, Connie M. Krawczyk, and Martin J. Richer. 2018. “Interleukin-10 Directly Inhibits CD8+ T Cell Function by Enhancing N-Glycan Branching to Decrease Antigen Sensitivity.” *Immunity* 48(2):299-312.e5.

Smith, Neil R., Dawn Baker, Matthew Farren, Aurelien Pommier, Ruth Swann, Xin Wang, Sunita Mistry, Karen Mcdaid, Jane Kendrew, Chris Womack, Stephen R. Wedge, and Simon T. Barry. 2013. “Tumor Stromal Architecture Can De Fi Ne the Intrinsic Tumor Response to VEGF-Targeted Therapy.” *Predictive Biomarkers and Personalized Medicine* (8):6943–56.

Smyth, Mark J., Erika Krasovskis, and Ricky W. Johnstone. 1998. “Fas Ligand-Mediated Lysis of Self Bystander Targets by Human Papillomavirus-Specific CD8 2 Cytotoxic T

Lymphocytes.” *Journal of Virology* 72(7):5948–54.

Somersalo, Kristina, Nadja Anikeeva, Tasha N. Sims, V. Kaye Thomas, Roland K. Strong, Thomas Spies, Tatiana Lebedeva, Yuri Sykulev, and Michael L. Dustin. 2004. “Cytotoxic T Lymphocytes Form an Antigen-Independent Ring Junction.” *The Journal of Clinical Investigation* 113(1):49–57.

Son, Myoungsun, Frances Santiago-schwarz, Yousef Al-abed, and Betty Diamond. 2012. “C1q Limits Dendritic Cell Differentiation and Activation by Engaging LAIR-1.” *PNAS* 109(46).

Stone, Daniel, Shaoheng Ni, Zong-yi Li, Anuj Gaggar, Nelson Dipaolo, Qinghua Feng, and Volker Sandig. 2005. “Development and Assessment of Human Adenovirus Type 11 as a Gene Transfer Vector.” *Journal of Virology* 79(8):5090–5104.

Subklewe, Marion and Michael Von Bergwelt-baildon. 2019. “Chimeric Antigen Receptor T Cells : A Race to Revolutionize Cancer Therapy.” *Transfus Med Hemother* 15–24.

Suda, By Takashi, Hideo Hashimoto, and Masato Tanaka. 1997. “Membrane Fas Ligand Kills Human Peripheral Blood T Lymphocytes, and Soluble Fas Ligand Blocks the Killing.” *J. Exp. Med.* 186(12):2045–50.

Sun, Hui, Yufeng Wang, Shentao Wang, Yikui Xie, Kun Sun, Shuai Li, Weitong Cui, and Kai Wang. 2023. “The Involvement of Collagen Family Genes in Tumor Enlargement of Gastric Cancer.” *Scientific Reports* (0123456789):1–11.

Sun, Xionghua, Xinjian Cui, Xihua Chen, and Xiaogang Jiang. 2020. “Biomedicine & Pharmacotherapy Baicalein Alleviated TGF β 1-Induced Type I Collagen Production in Lung Fibroblasts via Downregulation of Connective Tissue Growth Factor.” *Biomedicine & Pharmacotherapy* 131:110744.

Sung, Hyuna, Jacques Ferlay, Rebecca L. Siegel, Mathieu Laversanne, Isabelle Soerjomataram, Ahmedin Jemal, and Freddie Bray. 2021. “Global Cancer Statistics

2020 : GLOBOCAN Estimates of Incidence and Mortality Worldwide for 36 Cancers in 185 Countries." *Ca Cancers J Clin* 71(3):209–49.

Suntharalingam, G., Meghan R. Perry, Stephen Ward, Stephen J. Brett, Andrew Castello-Cortes, Michael D. Brunner, and Nicki Panoskaltsis. 2006. "Cytokine Storm in a Phase 1 Trial of the Anti-CD28 Monoclonal Antibody TGN1412." *New England Journal of Medicine* 1018–28.

Tabdanov, Erdem D., Nelson J. Rodríguez-Merced, Alexander X. Cartagena-Rivera, Vikram V. Puram, Mackenzie K. Callaway, Ethan A. Ensminger, Emily J. Pomeroy, Kenta Yamamoto, Walker S. Lahr, Beau R. Webber, Branden S. Moriarity, Alexander S. Zhovmer, and Paolo P. Provenzano. 2021. "Engineering T Cells to Enhance 3D Migration through Structurally and Mechanically Complex Tumor Microenvironments." *Nature Communications* 12(1):1–17.

Tao, Nianjun, Guang Ping Gao, Michael Parr, Julie Johnston, Timothy Baradet, James M. Wilson, James Barsoum, and Stephen E. Fawell. 2001. "Sequestration of Adenoviral Vector by Kupffer Cells Leads to a Nonlinear Dose Response of Transduction in Liver." *Molecular Therapy* 3(1):28–35.

Tavianatou, Anastasia G., Ilaria Caon, Marco Franchi, Zoi Piperigkou, and Devis Galesso. 2019. "Hyaluronan : Molecular Size-Dependent Signaling and Biological Functions in Inflammation and Cancer." 286:2883–2908.

Tenti, Paolo and Luca Vannucci. 2020. "Lysyl Oxidases : Linking Structures and Immunity in the Tumor Microenvironment." *Cancer Immunology, Immunotherapy* 69(2):223–35.

Thomas, Dori A. and Joan Massagué. 2005. "TGF-β Directly Targets Cytotoxic T Cell Functions during Tumor Evasion of Immune Surveillance." *Cancer Cell* 8(5):369–80.

Tian, Xiao, Jorge Azpurua, Christopher Hine, Amita Vaidya, Max Myakishev-rempel, Julia Ablaeva, and Zhiyong Mao. 2013. "High-Molecular-Mass Hyaluronan Mediates the Cancer Resistance of the Naked Mole Rat." 1–6.

Tijink, Bernard M., Lars R. Perk, Marianne Budde, and Marijke Stigter-van Walsum. 2009. “I-L19-SIP for Immuno-PET Imaging of Tumour Vasculature and Guidance of 131 I-L19-SIP Radioimmunotherapy.” *Eur J Nucl Med Mol Imaging* 1235–44.

To, Wing S. and Kim S. Midwood. 2011. “Plasma and Cellular Fibronectin : Distinct and Independent Functions during Tissue Repair.” *Fibrogenesis and Tissue Repair* 1–17.

Todo, Tomoki, Hirotaka Ito, Yasushi Ino, Hiroshi Ohtsu, Yasunori Ota, Junji Shibahara, and Minoru Tanaka. 2022. “Residual or Recurrent Glioblastoma : A Phase 2 Trial.” *Nature Medicine* 28(August).

Trandem, Kathryn, Jingxian Zhao, Erica Fleming, and Stanley Perlman. 2008. “Highly Activated Cytotoxic CD8 T Cells Express Protective IL-10 At The Peak Of Coronavirus-Induced Encephalitis.” *Bone* 23(1):1–7.

Trinchieri, Giorgio. 2007. “Interleukin-10 Production by Effector T Cells: Th1 Cells Show Self Control.” *Journal of Experimental Medicine* 204(2):239–43.

Tsukuda, Kazunori, Rainer Wiewrodt, Katherine Molnar-Kimber, Vuk P. Jovanovic, and Kunjlata Manibhai Amin. 2002. “An E2F-Responsive Replication-Selective Adenovirus Targeted to the Defective Cell Cycle in Cancer Cells : Potent Antitumoral Efficacy but No Toxicity To.” *Cancer Research* 62:3438–47.

Ucakturk, Ebru, Orkun Akman, Xiaojun Sun, and Dilek Ertoy Baydar. 2016. “Changes in Composition and Sulfation Patterns of Glycoaminoglycans in Renal Cell Carcinoma.” *Glycoconj J.* 103–12.

Upadhyay, Ranjan, Jonathan A. Boiarsky, Gvantsa Pantsulaia, Judit Svensson-, Matthew J. Lin, Aleksandra Wroblewska, Sherry Bhalla, Adrian Bot, John M. Rossi, Norah Sadek, Samir Parekh, Miriam Merad, Brian D. Brown, and Joshua D. Brody. 2021. “A Critical Role for Fas-Mediated off-Target Tumor Killing in T Cell Immunotherapy.” *Cancer Discov* 11(3):599–613.

Vaidya, Amita, Helen Wang, Victoria Qian, Hannah Gilmore, and Zheng-rong Lu. 2020. “Overexpression of Extradomain-B Fibronectin Is Associated with Invasion of Breast Cancer Cells.” *Cells* 1–19.

Verbrugge, Annelies, Talitha De Ruiter, Hans Clevers, and Linde Meyaard. 2003. “Differential Contribution of the Immunoreceptor Tyrosine-Based Inhibitory Motifs of Human Leukocyte-Associated Ig-like Receptor-1 to Inhibitory Function and Phosphatase Recruitment.” *International Immunology* 15(11).

Vigetti, Davide, Eugenia Karousou, Manuela Viola, Sara Deleonibus, Giancarlo De Luca, and Alberto Passi. 2014. “Biochimica et Biophysica Acta Hyaluronan : Biosynthesis and Signaling ☆.” *Biochimica et Biophysica Acta* 1840(8):2452–59.

Vijver, Saskia V, Akashdip Singh, Eline T. A. M. Mommers-elshof, and Jan Meeldijk. 2021. “Collagen Fragments Produced in Cancer Mediate T Cell Suppression Through Leukocyte-Associated Immunoglobulin-Like Receptor 1.” *Frontiers in Immunology* 12(October):1–13.

Volpe, Elisabetta, Manolo Sambucci, Luca Battistini, and Giovanna Borsellino. 2016. “Fas – Fas Ligand : Checkpoint of T Cell Functions in Multiple Sclerosis.” *Frontiers in Immunology* 7(September):1–9.

Wallach-dayan, Shulamit B., Dmytro Petukhov, Ronit Ahdut-hacohen, and Mark Richter-dayan. 2021. “SFasL — The Key to a Riddle : Immune Responses in Aging Lung and Disease.” *International Journal of Molecular Sciences*.

Wan, Peter Kok-Ting, Ricardo A. Fernandes, and Leonard W. Seymour. 2023. “Oncolytic Viruses and Antibodies : Are They More Successful When Delivered Separately or When Engineered as a Single Agent ?” *Journal for ImmunoTherapy of Cancer*.

Wang, Zhen, Bin Yu, Baoming Wang, Jingyi Yan, Xiao Feng, Zixuan Wang, Lizheng Wang, Haihong Zhang, Hui Wu, Jiaxin Wu, Wei Kong, and Xianghui Yu. 2016. “A Novel Capsid-Modified Oncolytic Recombinant Adenovirus Type 5 for Tumor-Targeting Gene

Therapy by Intravenous Route.” *Oncotarget* 7(30).

Warnders, Frank J., Stijn J. H. Waaijer, Martin Pool, Marjolijn N. Lub De Hooge, Matthias Friedrich, Anton G. T. Terwisscha Van Scheltinga, Petra Deegen, Sabine K. Stienen, Peter C. Pieslor, H. Kam Cheung, Jos G. W. Kosterink, and Elisabeth G. E. De Vries. 2016. “Biodistribution and PET Imaging of Labeled Bispecific T Cell – Engaging Antibody Targeting EpCAM.” *The Journal of Nuclear Medicine* 57(5):812–17.

Wei, Min, Shuguang Zuo, Zhimin Chen, Peng Qian, Yenan Zhang, Lingkai Kong, Honglan Gao, and Jiwu Wei. 2022. “Oncolytic Vaccinia Virus Expressing a Bispeci Fi c T-Cell Engager Enhances Immune Responses in EpCAM Positive Solid Tumors.” *Frontiers in Immunology* (November):1–14.

Wieboldt, Ronja and Heinz Läubli. 2022. “Glycosaminoglycans in Cancer Therapy.” *Invited Review for the American Journal of Physiology – Cell Physiology*.

Winer, Arthur, Sylvia Adams, and Paolo Mignatti. 2019. “Past Failures into Future Successes.” *Mol Cancer Ther.* 17(6):1147–55.

Wipff, Pierre Jean, Daniel B. Rifkin, Jean Jacques Meister, and Boris Hinz. 2007. “Myofibroblast Contraction Activates Latent TGF-B1 from the Extracellular Matrix.” *Journal of Cell Biology* 179(6):1311–23.

Wodrich, Harald. 2019. “Imaging the Adenovirus Infection Cycle.” *FEBS Letters* 593:3419–48.

Wu, Xiaojie, Leyan Zhang, Jiadi Zhou, Luying Liu, Qiang Fu, and Jiangnan Xue. 2019. “Clinicopathologic Significance of LAIR-1 Expression in Hepatocellular Carcinoma.” *Current Problems in Cancer* 43(1):18–26.

Xie, Jingjing, Xun Gui, Mi Deng, Heyu Chen, Yuanzhi Chen, Xiaoye Liu, Zhiqiang Ku, Lingxiao Tan, Ryan Huang, Yubo He, Bruce Zhang, Cheryl Lewis, Kenian Chen, Lin Xu, Jian Xu, Tao Huang, X. Charlene Liao, Ningyan Zhang, Zhiqiang An, and Cheng

Cheng Zhang. 2022. “Blocking LAIR1 Signaling in Immune Cells Inhibits Tumor Development.” *Frontiers in Immunology* 13(September):1–14.

Xie, Ying, Akgül Akpinarli, Charles Maris, Edward L. Hipkiss, Malcolm Lane, Eun-kyung M. Kwon, Pawel Muranski, Nicholas P. Restifo, and Paul Andrew Antony. 2010. “Naive Tumor-Specific CD4 + T Cells Differentiated in Vivo Eradicate Established Melanoma.” *JEM* 207(3):651–67.

Xu, Zhili, Jie Tian, Jeffrey S. Smith, and Andrew P. Byrnes. 2008. “Clearance of Adenovirus by Kupffer Cells Is Mediated by Scavenger Receptors, Natural Antibodies, and Complement.” *Journal of Virology* 82(23):11705–13.

Yan, Kin-ming Lo, Lan Scott, Lauder Jinyang, Beatrice Brunkhorst, Guozhong Qin, Rakesh Verma, and Nigel Courtenay-luck Stephen D. Gillies. 2007. “HuBC1-IL12 , an Immunocytokine Which Targets EDB-Containing Oncofetal W Bronectin in Tumors and Tumor Vasculature , Shows Potent Anti-Tumor Activity in Human Tumor Models.” *Cancer Immunol Immunother* 447–57.

Yang, Lei-lei, Meng-jie Zhang Dds, Lei Wu, Liang Mao, Lei Chen, Guang-tao Yu Wei-wei Deng, and Wen-feng Zhang Dds. 2019. “LAIR-1 Overexpression and Correlation with Advanced Pathological Grade and Immune Suppressive Status in Oral Squamous Cell Carcinoma.” *Head & Neck* (August 2018):1080–86.

Yoon, Hyunho, Chih-min Tang, Sudeep Banerjee, Antonio L. Delgado, Mayra Yebra, Jacob Davis, and Jason K. Sicklick. 2021. “TGF- β 1-Mediated Transition of Resident Fi Broblasts to Cancer-Associated Fi Broblasts Promotes Cancer Metastasis in Gastrointestinal Stromal Tumor.” *Oncogenesis*.

Yoon, Sang-oh, Sejeong Shin, Florian A. Karreth, Gwen R. Buel, and P. Mark. 2017. “Focal Adhesion- and IGF1R-Dependent Survival and Migratory Pathways Mediate Tumor Resistance to MTORC1/2 Inhibition.” *Mol Cell* 67(3):512–27.

Yoshinaga, Keiji, Hiroto Obata, Vladimir Jurukovski, Roberta Mazzieri, Yan Chen, Lior

Zilberberg, David Huso, Jonathan Melamed, Petra Prijatelj, Vesna Todorovic, Branka Dabovic, and Daniel B. Rifkin. 2008. “Perturbation of Transforming Growth Factor (TGF)-B1 Association with Latent TGF-β Binding Protein Yields Inflammation and Tumors.” *Proceedings of the National Academy of Sciences of the United States of America* 105(48):18758–63.

Youngnak, Pornpan, Yuko Kozono, Haruo Kozono, Hideyuki Iwai, Noriko Otsuki, Hisayo Jin, Ken Omura, Hideo Yagita, Drew M.Pardoll, Lieping Chen, and Miyuki Azuma. 2003. “Differential Binding Properties of B7-H1 and B7-DC to Programmed Death-1.” *Biochemical and Biophysical Research Communications* 307:672–77.

Yu, Bin, Yan Zhou, Hao Wu, Zhen Wang, Yang Zhan, Xiao Feng, Ranshen Geng, Yongge Wu, Wei Kong, and Xianghui Yu. 2012. “Seroprevalence of Neutralizing Antibodies to Human Adenovirus Type 5 in Healthy Adults in China.” *Journal of Medical Virology*.

Yu, Jiali, Michael D. Green, Shasha Li, Yilun Sun, Sara N. Journey, Jae Eun Choi, Syed Monem Rizvi, Angel Qin, Jessica J. Waninger, Xueting Lang, Zoey Chopra, Issam El Naqa, Jiajia Zhou, Yingjie Bian, Long Jiang, Alangoya Tezel, Jeremy Skvarce, Rohan K. Achar, Merna Sitto, Benjamin S. Rosen, Fengyun Su, Sathiya P. Narayanan, Xuhong Cao, Shuang Wei, Wojciech Szeliga, Linda Vatan, Charles Mayo, Meredith A. Morgan, Caitlin A. Schonewolf, Kyle Cuneo, Ilona Kryczek, Vincent T. Ma, Christopher D. Lao, Theodore S. Lawrence, Nithya Ramnath, Fei Wen, Arul M. Chinnaiyan, Marcin Cieslik, Ajjai Alva, and Weiping Zou. 2021. “Liver Metastasis Restrains Immunotherapy Efficacy via Macrophage-Mediated T Cell Elimination.” *Nature Medicine* 27(1):152–64.

Yue, Beatrice. 2014. “Biology of the Extracellular Matrix: An Overview Beatrice.” *J Glaucoma* S20–S23.

Zeine, Rana, Helen R. Salwen, Radhika Peddinti, Yufeng Tian, Lisa Guerrero, Qiwei Yang, Alexandre Chlenski, and Susan L. Cohn. 2009. “Presence Of Cancer-Associated Fibroblasts Inversely Correlates With Schwannian Stroma In Neuroblastoma Tumors.”

Mod Pathol 22(7):950–58.

Zeisberg, Elisabeth M., Scott Potenta, Liang Xie, Michael Zeisberg, and Raghu Kalluri. 2007. “Discovery of Endothelial to Mesenchymal Transition as a Source for Carcinoma-Associated Fibroblasts.” (21):10123–28.

Zhang, Guoliang, Lin Guo, Cuixia Yang, Yiwen Liu, Yiqing He, Yan Du, Wenjuan Wang, and Feng Gao. 2016. “ORIGINAL RESEARCH A Novel Role of Breast Cancer-Derived Hyaluronan on Inducement of M2-like Tumor- Associated Macrophages Formation.” *OncoImmunology* 5(6):1–13.

Zhang, Qian-ning, Yan Li, Qi Zhao, and Mi Tian. 2021. “Recombinant Human Adenovirus Type 5 (Oncorine) Reverses Resistance to Immune Checkpoint Inhibitor in a Patient with Recurrent Non-Small Cell Lung Cancer : A Case Report.” *Thorac Cancer* 5(February):1617–19.

Zou, Weiping, Jedd D. Wolchok, and Lieping Chen. 2016. “PD-L1 (B7-H1) and PD-1 Pathway Blockade for Cancer Therapy: Mechanisms, Response Biomarkers and Combinations.” *Sci Transl Med* 8(328).

Appendix

DNA sequences

LAIR-2 control

ATGGGATGGAGCTGCATCATCCTATTCCTCGTGGCGACGGCCACTGGAGTGCA
TAGCGGTGGTGGTGGTTCTGATTATAAAGATGATGATGATAAACAGGAAGGCG
CACTCCCCAGACCATCCATCTCCGCTGAACCCGGCACAGTCATCTCCCCTGGC
AGCCATGTGACATTTATGTGTAGAGGACCTGTGGGCGTGCAAACCTTCCGGCT
CGAAAGGGAGGACAGAGCCAAATATAAGGATAGCTACAACGTGTTTAGACTGG
GACCAAGCGAAAGCGAAGCCAGGTTTCACATCGACTCTGTCTCTGAAGGCAAT
GCCGGCCTCTACAGATGCCTCTATTATAAGCCCCCTGGCTGGAGCGAACACAG
CGACTTTCTGGAACTGCTCGTGAAAGAGAGCAGCGGCGGCCCCGACAGCCCC
GATACCGAACCCGGATCCTCCGCCGGAACAGTGCCAGGCACAGAAGCCAGCG
GCTTCGATGCCCCTTGA

LAIR2xaCD3 Bispecific

ATGGGATGGAGCTGCATCATCCTATTCCTCGTGGCGACGGCCACTGGAGTGCA
TAGCCAGGAAGGCGCACTCCCCAGACCATCCATCTCCGCTGAACCCGGCACAG
TCATCTCCCCTGGCAGCCATGTGACATTTATGTGTAGAGGACCTGTGGGCGTG
CAAACCTTCCGGCTCGAAAGGGAGGACAGAGCCAAATATAAGGATAGCTACAA
CGTGTTTAGACTGGGACCAAGCGAAAGCGAAGCCAGGTTTCACATCGACTCTG
TCTCTGAAGGCAATGCCGGCCTCTACAGATGCCTCTATTATAAGCCCCCTGGCT
GGAGCGAACACAGCGACTTTCTGGAACTGCTCGTGAAAGAGAGCAGCGGCGG
CCCCGACAGCCCCGATACCGAACCCGGATCCTCCGCCGGAACAGTGCCAGGC
ACAGAAGCCAGCGGCTTCGATGCCCCTGGCGGAGGGGGATCCGATATCAAAC
TGCAGCAGTCAGGGGCTGAACTGGCAAGACCTGGGGCCTCAGTGAAGATGTC
CTGCAAGACTTCTGGCTACACCTTTACTAGGTACACGATGCACTGGGTAAAACA
GAGGCCTGGACAGGGTCTGGAATGGATTGGATACATTAATCCTAGCCGTGGTT
ATACTAATTACAATCAGAAGTTCAAGGACAAGGCCACATTGACTACAGACAAAT
CCTCCAGCACAGCCTACATGCAACTGAGCAGCCTGACATCTGAGGACTCTGCA
GTCTATTACTGTGCAAGATATTATGATGATCATTACTGCCTTGACTACTGGGGCC
AAGGCACCACTCTCACAGTCTCCTCAGTCGAAGGTGGAAGTGGAGGTTCTGGT
GGAAGTGGAGGTTCAGGTGGAGTCGACGACATTCAGCTGACCCAGTCTCCAGC
AATCATGTCTGCATCTCCAGGGGAGAAGGTCACCATGACCTGCAGAGCCAGTT
CAAGTGTAAGTTACATGAACTGGTACCAGCAGAAGTCAGGCACCTCCCCCAAAA
GATGGATTTATGACACATCCAAAGTGGCTTCTGGAGTCCCTTATCGCTTCAGTG
GCAGTGGGTCTGGGACCTCATACTCTCTCACAATCAGCAGCATGGAGGCTGAA
GATGCTGCCACTTATTACTGCCAACAGTGGAGTAGTAACCCGCTCACGTTCGGT
GCTGGGACCAAGCTGGAGCTGAAAGATTATAAAGATGATGATGATAAATGA

aCD3 control

ATGGGATGGAGCTGCATCATCCTATTCCTCGTGGCGACGGCCACTGGAGTGCA
TAGCGGTGGTGGTGGTTCTGATTATAAAGATGATGATGATAAAGATATCAAACT

GCAGCAGTCAGGGGCTGAACTGGCAAGACCTGGGGCCTCAGTGAAGATGTCC
TGCAAGACTTCTGGCTACACCTTTACTAGGTACACGATGCACTGGGTAAAACAG
AGGCCTGGACAGGGTCTGGAATGGATTGGATACATTAATCCTAGCCGTGGTTAT
ACTAATTACAATCAGAAGTTCAAGGACAAGGCCACATTGACTACAGACAAATCC
TCCAGCACAGCCTACATGCAACTGAGCAGCCTGACATCTGAGGACTCTGCAGT
CTATTACTGTGCAAGATATTATGATGATCATTACTGCCTTGACTACTGGGGCCAA
GGCACCACTCTCACAGTCTCCTCAGTCGAAGGTGGAAGTGGAGGTTCTGGTGG
AAGTGGAGGTTCAGGTGGAGTCGACGACATTCAGCTGACCCAGTCTCCAGCAA
TCATGTCTGCATCTCCAGGGGAGAAGGTCACCATGACCTGCAGAGCCAGTTCA
AGTGTAAGTTACATGAACTGGTACCAGCAGAAGTCAGGCACCTCCCCCAAAAG
ATGGATTTATGACACATCCAAAGTGGCTTCTGGAGTCCCTTATCGCTTCAGTGG
CAGTGGGTCTGGGACCTCATACTCTCTCACAATCAGCAGCATGGAGGCTGAAG
ATGCTGCCACTTATTACTGCCAACAGTGGAGTAGTAACCCGCTCACGTTCGGTG
CTGGGACCAAGCTGGAGCTGAAATGA

3xPlGF

ATGGGATGGAGCTGCATCATCCTATTCCTCGTGGCGACGGCCACTGGAGTGCA
TAGCGGTGGTGGTGGTTCTGATTATAAAGATGATGATGATAAAGATATCAAACT
GCAGCAGTCAGGGGCTGAACTGGCAAGACCTGGGGCCTCAGTGAAGATGTCC
TGCAAGACTTCTGGCTACACCTTTACTAGGTACACGATGCACTGGGTAAAACAG
AGGCCTGGACAGGGTCTGGAATGGATTGGATACATTAATCCTAGCCGTGGTTAT
ACTAATTACAATCAGAAGTTCAAGGACAAGGCCACATTGACTACAGACAAATCC
TCCAGCACAGCCTACATGCAACTGAGCAGCCTGACATCTGAGGACTCTGCAGT
CTATTACTGTGCAAGATATTATGATGATCATTACTGCCTTGACTACTGGGGCCAA
GGCACCACTCTCACAGTCTCCTCAGTCGAAGGTGGAAGTGGAGGTTCTGGTGG
AAGTGGAGGTTCAGGTGGAGTCGACGACATTCAGCTGACCCAGTCTCCAGCAA
TCATGTCTGCATCTCCAGGGGAGAAGGTCACCATGACCTGCAGAGCCAGTTCA
AGTGTAAGTTACATGAACTGGTACCAGCAGAAGTCAGGCACCTCCCCCAAAAG
ATGGATTTATGACACATCCAAAGTGGCTTCTGGAGTCCCTTATCGCTTCAGTGG
CAGTGGGTCTGGGACCTCATACTCTCTCACAATCAGCAGCATGGAGGCTGAAG
ATGCTGCCACTTATTACTGCCAACAGTGGAGTAGTAACCCGCTCACGTTCGGTG
CTGGGACCAAGCTGGAGCTGAAAGGCGGAGGAGGATCACGCAGACGGCCAAA
GGGTCGAGGAAAAAGACGGAGAGAAAAGCAACGCCCCACAGACTGTCATCTTG
GTGGCGGGGGATCAAGGAGGCGCCCGAAAGGTAGGGGCAAACGGCGCCGGG
AAAAACAGCGACCCACTGACTGCCATTTGGGGGGTGGTGGATCACGACGCAG
GCCCAAAGGTAGAGGGAAGAGAAGGCGCGAGAAGCAGAGACCCACAGATTGC
CACTTGTGA

2xPlGF

ATGGGATGGAGCTGCATCATCCTATTCCTCGTGGCGACGGCCACTGGAGTGCA
TAGCGGTGGTGGTGGTTCTGATTATAAAGATGATGATGATAAAGATATCAAACT
GCAGCAGTCAGGGGCTGAACTGGCAAGACCTGGGGCCTCAGTGAAGATGTCC
TGCAAGACTTCTGGCTACACCTTTACTAGGTACACGATGCACTGGGTAAAACAG
AGGCCTGGACAGGGTCTGGAATGGATTGGATACATTAATCCTAGCCGTGGTTAT
ACTAATTACAATCAGAAGTTCAAGGACAAGGCCACATTGACTACAGACAAATCC
TCCAGCACAGCCTACATGCAACTGAGCAGCCTGACATCTGAGGACTCTGCAGT
CTATTACTGTGCAAGATATTATGATGATCATTACTGCCTTGACTACTGGGGCCAA
GGCACCACTCTCACAGTCTCCTCAGTCGAAGGTGGAAGTGGAGGTTCTGGTGG
AAGTGGAGGTTCAGGTGGAGTCGACGACATTCAGCTGACCCAGTCTCCAGCAA

TCATGTCTGCATCTCCAGGGGAGAAGGTCACCATGACCTGCAGAGCCAGTTCA
AGTGTAAGTTACATGAACTGGTACCAGCAGAAGTCAGGCACCTCCCCCAAAAG
ATGGATTTATGACACATCCAAAGTGGCTTCTGGAGTCCCTTATCGCTTCAGTGG
CAGTGGGTCTGGGACCTCATACTCTCTCACAATCAGCAGCATGGAGGCTGAAG
ATGCTGCCACTTATTACTGCCAACAGTGGAGTAGTAACCCGCTCACGTTCGGTG
CTGGGACCAAGCTGGAGCTGAAAGGCGGAGGAGGATCACGCAGACGGCCAAA
GGGTCGAGGAAAAAGACGGAGAGAAAAGCAACGCCCCACAGACTGTCATCTTG
GTGGCGGGGGATCAAGGAGGCGCCCGAAAGGTAGGGGCAAACGGCGCCGGG
AAAAACAGCGACCCACTGACTGCCATTTGTGA

1xPlGF

ATGGGATGGAGCTGCATCATCCTATTCCTCGTGGCGACGGCCACTGGAGTGCA
TAGCGGTGGTGGTGGTTCTGATTATAAAGATGATGATGATAAAGATATCAAACT
GCAGCAGTCAGGGGCTGAACTGGCAAGACCTGGGGCCTCAGTGAAGATGTCC
TGCAAGACTTCTGGCTACACCTTTACTAGGTACACGATGCACTGGGTAAAACAG
AGGCCTGGACAGGGTCTGGAATGGATTGGATACATTAATCCTAGCCGTGGTTAT
ACTAATTACAATCAGAAGTTCAAGGACAAGGCCACATTGACTACAGACAAATCC
TCCAGCACAGCCTACATGCAACTGAGCAGCCTGACATCTGAGGACTCTGCAGT
CTATTACTGTGCAAGATATTATGATGATCATTACTGCCTTGACTACTGGGGCCAA
GGCACCACTCTCACAGTCTCCTCAGTCGAAGGTGGAAGTGGAGGTTCTGGTGG
AAGTGGAGGTTCAGGTGGAGTCGACGACATTCAGCTGACCCAGTCTCCAGCAA
TCATGTCTGCATCTCCAGGGGAGAAGGTCACCATGACCTGCAGAGCCAGTTCA
AGTGTAAGTTACATGAACTGGTACCAGCAGAAGTCAGGCACCTCCCCCAAAAG
ATGGATTTATGACACATCCAAAGTGGCTTCTGGAGTCCCTTATCGCTTCAGTGG
CAGTGGGTCTGGGACCTCATACTCTCTCACAATCAGCAGCATGGAGGCTGAAG
ATGCTGCCACTTATTACTGCCAACAGTGGAGTAGTAACCCGCTCACGTTCGGTG
CTGGGACCAAGCTGGAGCTGAAAGGCGGAGGAGGATCACGCAGACGGCCAAA
GGGTCGAGGAAAAAGACGGAGAGAAAAGCAACGCCCCACAGACTGTCATCTTT
GA

3xR

ATGGGATGGAGCTGCATCATCCTATTCCTCGTGGCGACGGCCACTGGAGTGCA
TAGCGGTGGTGGTGGTTCTGATTATAAAGATGATGATGATAAAGATATCAAACT
GCAGCAGTCAGGGGCTGAACTGGCAAGACCTGGGGCCTCAGTGAAGATGTCC
TGCAAGACTTCTGGCTACACCTTTACTAGGTACACGATGCACTGGGTAAAACAG
AGGCCTGGACAGGGTCTGGAATGGATTGGATACATTAATCCTAGCCGTGGTTAT
ACTAATTACAATCAGAAGTTCAAGGACAAGGCCACATTGACTACAGACAAATCC
TCCAGCACAGCCTACATGCAACTGAGCAGCCTGACATCTGAGGACTCTGCAGT
CTATTACTGTGCAAGATATTATGATGATCATTACTGCCTTGACTACTGGGGCCAA
GGCACCACTCTCACAGTCTCCTCAGTCGAAGGTGGAAGTGGAGGTTCTGGTGG
AAGTGGAGGTTCAGGTGGAGTCGACGACATTCAGCTGACCCAGTCTCCAGCAA
TCATGTCTGCATCTCCAGGGGAGAAGGTCACCATGACCTGCAGAGCCAGTTCA
AGTGTAAGTTACATGAACTGGTACCAGCAGAAGTCAGGCACCTCCCCCAAAAG
ATGGATTTATGACACATCCAAAGTGGCTTCTGGAGTCCCTTATCGCTTCAGTGG
CAGTGGGTCTGGGACCTCATACTCTCTCACAATCAGCAGCATGGAGGCTGAAG
ATGCTGCCACTTATTACTGCCAACAGTGGAGTAGTAACCCGCTCACGTTCGGTG
CTGGGACCAAGCTGGAGCTGAAAGGCGGAGGGGGATCCAGAAGGAGACGGA
GGAGGGGAGGAGGCGGTAGTCGACGAAGAAGACGAAGGGGCGGGGGCGGGT
CAAGACGAAGGAGAAGAAGGTAG

2xR

ATGGGATGGAGCTGCATCATCCTATTCCTCGTGGCGACGGCCACTGGAGTGCA
TAGCGGTGGTGGTGGTTCTGATTATAAAGATGATGATGATAAAGATATCAAACT
GCAGCAGTCAGGGGCTGAACTGGCAAGACCTGGGGCCTCAGTGAAGATGTCC
TGCAAGACTTCTGGCTACACCTTTACTAGGTACACGATGCACTGGGTAAAACAG
AGGCCTGGACAGGGTCTGGAATGGATTGGATACATTAATCCTAGCCGTGGTTAT
ACTAATTACAATCAGAAGTTCAAGGACAAGGCCACATTGACTACAGACAAATCC
TCCAGCACAGCCTACATGCAACTGAGCAGCCTGACATCTGAGGACTCTGCAGT
CTATTACTGTGCAAGATATTATGATGATCATTACTGCCTTGACTACTGGGGCCAA
GGCACCACTCTCACAGTCTCCTCAGTCGAAGGTGGAAGTGGAGGTTCTGGTGG
AAGTGGAGGTTCAGGTGGAGTCGACGACATTCAGCTGACCCAGTCTCCAGCAA
TCATGTCTGCATCTCCAGGGGAGAAGGTCACCATGACCTGCAGAGCCAGTTCA
AGTGTAAGTTACATGAACTGGTACCAGCAGAAGTCAGGCACCTCCCCCAAAAG
ATGGATTTATGACACATCCAAAGTGGCTTCTGGAGTCCCTTATCGCTTCAGTGG
CAGTGGGTCTGGGACCTCATACTCTCTCACAATCAGCAGCATGGAGGCTGAAG
ATGCTGCCACTTATTACTGCCAACAGTGGAGTAGTAACCCGCTCACGTTCGGTG
CTGGGACCAAGCTGGAGCTGAAAGGCGGAGGGGGATCCAGAAGGAGACGGA
GGAGGGGAGGAGGCGGTAGTCGACGAAGAAGACGAAGGTAG

1xR

ATGGGATGGAGCTGCATCATCCTATTCCTCGTGGCGACGGCCACTGGAGTGCA
TAGCGGTGGTGGTGGTTCTGATTATAAAGATGATGATGATAAAGATATCAAACT
GCAGCAGTCAGGGGCTGAACTGGCAAGACCTGGGGCCTCAGTGAAGATGTCC
TGCAAGACTTCTGGCTACACCTTTACTAGGTACACGATGCACTGGGTAAAACAG
AGGCCTGGACAGGGTCTGGAATGGATTGGATACATTAATCCTAGCCGTGGTTAT
ACTAATTACAATCAGAAGTTCAAGGACAAGGCCACATTGACTACAGACAAATCC
TCCAGCACAGCCTACATGCAACTGAGCAGCCTGACATCTGAGGACTCTGCAGT
CTATTACTGTGCAAGATATTATGATGATCATTACTGCCTTGACTACTGGGGCCAA
GGCACCACTCTCACAGTCTCCTCAGTCGAAGGTGGAAGTGGAGGTTCTGGTGG
AAGTGGAGGTTCAGGTGGAGTCGACGACATTCAGCTGACCCAGTCTCCAGCAA
TCATGTCTGCATCTCCAGGGGAGAAGGTCACCATGACCTGCAGAGCCAGTTCA
AGTGTAAGTTACATGAACTGGTACCAGCAGAAGTCAGGCACCTCCCCCAAAAG
ATGGATTTATGACACATCCAAAGTGGCTTCTGGAGTCCCTTATCGCTTCAGTGG
CAGTGGGTCTGGGACCTCATACTCTCTCACAATCAGCAGCATGGAGGCTGAAG
ATGCTGCCACTTATTACTGCCAACAGTGGAGTAGTAACCCGCTCACGTTCGGTG
CTGGGACCAAGCTGGAGCTGAAAGGCGGAGGGGGATCCAGAAGGAGACGGA
GGAGGTAG

Antibody list

Antibodies were all purchased from BioLegend (USA), unless stated otherwise.

Name	Number	Application/Dilution
CD4 APC	317416	Flow: 1:200
CD4 PE	317410	Flow: 1:200
CD4 FITC	317408	Flow: 1:200
CD8a BV421	301036	Flow: 1:200
CD8a APC	300912	Flow: 1:200
CD69 BV605	310938	Flow: 1:200
CD25 PE/Cy7	302612	Flow: 1:200
CD25 PE	302606	Flow: 1:200
IFN-y FITC	502506	Flow: 1:100
Grz B Pacific blue	515408	Flow: 1:100
CD107 PE/Cy7	328618	Flow: 1:100
Perforin PE	353304	Flow: 1:100
LAIR-1 AF647	342802	Flow: 1:100
FLAG PE	637310	Flow: 1:100
EpCAM APC	324208	Flow: 1:100
FLAG HRP	637311	ELISA/WB: 1:15'0000
Anti-Mouse IgG/IgM AF488	A10680 (Thermo Fisher Sc.)	Flow: 1/250
HS	370255-S (Amsbio)	1/100
CS	ab11570 (Abcam)	1/100

Buffer list

Buffer	Protocol
TAE buffer (50x)	242 g Tris, 57.1 mL Glacial Acetic Acid, 100 mL 0.5 M ethylenediaminetetraacetic acid (EDTA) in 1 L of ddH_2O
SDS Running buffer (10x)	19.8 g Tris, 86.4 g Glycine, 6 g SDS, 1 L ddH_2O
MACS buffer	0.5% Bovine Serum Albumin, 2 mM EDTA in Phosphate Buffered Saline (PBS)
Blocking buffer ELISA	0.5% Bovine Serum Albumin in PBS